CENTER FOR TRANSPORTATION RESEARCH
THE UNIVERSITY OF TEXAS AT AUSTIN

THE LONG-TERM PERFORMANCE OF A DRILLED SHAFT RETAINING WALL IN AN EXPANSIVE CLAY

Andrew C. Brown
Gregory F. Dellinger
Chadi El-Mohtar
Jorge G. Zornberg
Robert B. Gilbert

CENTER FOR TRANSPORTATION RESEARCH
BUREAU OF ENGINEERING RESEARCH
THE UNIVERSITY OF TEXAS AT AUSTIN

Technical Report Documentation Page

1. Report No. FHWA/TX-13/0-6603-2	2. Government Accession No.	3. Recipient's Catalog No.
4. Title and Subtitle The Long-Term Performance of a Drilled Shaft Retaining Wall in an Expansive Clay		5. Report Date October 2013; Published January 2014
		6. Performing Organization Code
7. Author(s) Andrew C. Brown, Gregory F. Dellinger, Jorge G. Zornberg, Chadi El-Mohtar, Robert B. Gilbert		8. Performing Organization Report No. 0-6603-2
9. Performing Organization Name and Address Center for Transportation Research The University of Texas at Austin 1616 Guadalupe Street, Suite 4.202 Austin, TX 78701		10. Work Unit No. (TRAIS)
		11. Contract or Grant No. 0-6603
12. Sponsoring Agency Name and Address Texas Department of Transportation Research and Technology Implementation Office P.O. Box 5080 Austin, TX 78763-5080		13. Type of Report and Period Covered Technical Report September 2009–August 2013
		14. Sponsoring Agency Code
15. Supplementary Notes Project performed in cooperation with the Texas Department of Transportation and the Federal Highway Administration.		
16. Abstract The purpose of this research is to advance the understanding of the behavior of drilled shaft retaining walls installed through expansive clay. The primary source of information for this study is data from a full-scale instrumented test wall, which was installed through highly overconsolidated, expansive clay in Manor, Texas, and monitored for a period of 4 years. This study includes a summary of existing research, technical information on the design and construction of the instrumented test wall, an analysis of the relationship between soil behavior and wall deformation during the 4-year monitoring period, and preliminary recommendations on how to account for the effects of expansive soil in design of drilled shaft retaining walls.		
17. Key Words Drilled shaft, retaining wall, expansive clay, lateral earth pressure, p-y curve, design		18. Distribution Statement No restrictions. This document is available to the public through the National Technical Information Service, Springfield, Virginia 22161; www.ntis.gov.
19. Security Classif. (of report) Unclassified	20. Security Classif. (of this page) Unclassified	21. No. of pages 202 (Main Report) 22. Price

Form DOT F 1700.7 (8-72) Reproduction of completed page authorized

The Long-Term Performance of a Drilled Shaft Retaining Wall in an Expansive Clay

Andrew C. Brown
Gregory F. Dellinger
Chadi El-Mohtar
Jorge G. Zornberg
Robert B. Gilbert

Disclaimers

Acknowledgments

Table of Contents

List of Figures

xxi

List of Tables

CHAPTER 1: INTRODUCTION

1.1: Introduction

The design of drilled shaft retaining walls in non-expansive soils is well established. In expansive soils, however, there is no consensus on the correct way to model the effects of soil expansion on wall behavior during cycles of wetting and drying. Based on the range of design assumptions currently in practice, existing walls could be substantially over- or under-designed. The purpose of this research is to advance the understanding of the behavior of drilled shaft retaining walls installed through expansive clay. The primary source of information for this study will be data from a full-scale instrumented test wall, which was installed through highly overconsolidated, expansive clay in Manor, Texas, and monitored for a period of 4 years. This study includes a summary of existing research, technical information on the design and construction of the instrumented test wall, an analysis of the relationship between soil behavior and wall deformation during the 3-year monitoring period, and recommendations on how to account for the effects of expansive soil in design. The analysis of test wall response includes summaries of behavior before excavation, during excavation, during long-term moisture fluctuations that included an extreme drought, and during controlled inundation testing that provided the retained soil unlimited access to water until the wall deflections reached equilibrium.

1.2: Research Objectives

The goal of this research is to advance our understanding of the long-term behavior of retaining structures in expansive clays. The observed performance and instrumentation data from our test wall will be used to address the following objectives:

1. Identify and analyze the processes responsible for wall loading and deformation.

2. Evaluate how these processes change with time and moisture cycles.

3. Provide guidance for design practice to account for these processes and ensure adequate wall performance.

1.3: Research Methodology

The objectives of this research study will be accomplished according to the following methodology:

1. Design and construct a full-scale instrumented test wall through expansive clay.

2. Monitor the performance of the test wall during construction, excavation, natural seasonal moisture fluctuations, and controlled inundation testing that provides the expansive clay with unlimited access to water.

3. Analyze test wall performance data using standard of practice design methods.

4. Develop guidance for design practice based on results of analyses.

This study is primarily based on data from the Lymon C. Reese research wall in Manor. While the Taylor clay at the research site is typical of an overconsolidated, high plasticity, stiff-

1

fissured clay in Texas, the behavior of other expansive soil deposits may deviate from the behavior presented in this study.

1.4: Organization of Report

This report is organized into six chapters and ten appendices. Chapter 1 presents the introduction material. Chapter 2 presents the background information. An assessment of three existing TxDOT walls is discussed in Chapter 3. The design and construction of the full-scale instrumented test wall and the test wall performance and data analysis are presented in Chapters 4 and 5, respectively. Chapter 6 discusses the development of design guidelines and the conclusions and recommendations are presented in Chapter 7.

The wall design memo, site piezometric data, site moisture content data, the site and vicinity meteorological data, wall construction and installation of instrumentation, field inclinometer data, strain gauge data, p-y curves, finite element analysis, and the finite difference analysis are presented in Appendices A, B, C, D, E, F, G, H, I, and J respectively. Appendix K presents the student M.S. theses and Ph.D. dissertation associated with this project.

CHAPTER 2: BACKGROUND INFORMATION

2.1: The Design and Use of Drilled Shaft Retaining Walls in Texas

2.1.1: DRILLED SHAFT WALLS IN TEXAS

Cantilever drilled shaft retaining walls are common earth-retaining structures in Texas. They are well suited for use in urban environments where noise, space, and damage to adjacent structures are major considerations (Wang and Reese 1986). Additionally, because of the prevalence of drilled shaft foundations in Texas, experienced contractors are readily available. The design of drilled shaft retaining walls has changed over time. While initial design methods were based on limit equilibrium calculations, more refined p-y analyses based on soil-structure interaction have been developed and are currently in use by TxDOT (Wang and Reese 1986; TxDOT 2009).

2.1.2: ESTIMATION OF LATERAL EARTH PRESSURES

There is uncertainty in how to account for lateral earth pressures acting on drilled shaft walls installed through expansive clay. In Texas, some of the most problematic expansive clay deposits are also highly overconsolidated. For this reason, an examination of retaining wall design procedures for stiff, overconsolidated clay can provide a reference point for the design of walls in expansive clay deposits.

Commonly, the earth pressure on walls in stiff, overconsolidated clay is estimated using Coulomb active earth pressures with drained properties (Wang and Reese 1986). The TxDOT design procedure for cantilever drilled shaft walls employs this method with a recommended friction angle of 30° for "medium to stiff clays" (TxDOT 2009). For clays common in Texas, this approach results in earth pressures that correspond to an equivalent fluid unit weight of approximately 35 to 40 pounds per cubic foot (pcf).

2.1.3: SUMMARY OF CURRENT TxDOT DESIGN PROCEDURE FOR STIFF CLAYS (AFTER TxDOT, 2009)

In the current TxDOT design procedure, drilled shaft size and spacing is based on moment capacity. The following section presents a shortened version of the procedure that appears in TxDOT (2009). More detailed design information can be found in TxDOT (2012).

1. Determine earth pressures to be applied as loads using a Coulomb analysis with cohesion equal to zero.
    a. For stiff clays, use a friction angle of 30°. Assume angle of wall friction is equal to two-thirds the soil friction angle.
    b. Assume no water behind the wall.
    c. Include soil or traffic surcharge loads where appropriate.

2. Estimate maximum moment in shaft.
    a. Compute groundline moment from earth pressure distribution.
    b. Increase groundline moment by 50 percent to estimate the maximum earth pressure below the excavation line, i.e., $M_{max} = 1.5 \cdot M_{GL}$ (Figure 2.1).

3. Choose trial drilled shaft size and spacing based on moment capacity.
    a. Use load factor of 1.7 for earth pressure to compute ultimate moment (M_u)

b. Use nominal moment (M_n) from shaft properties, then check that the factored moment capacity ($\phi \cdot M_n$) exceeds M_u with $\phi = 0.9$.

4. Determine properties of the soil below the finished groundline.
   a. Use ultimate soil strengths for p-y curves.
   b. Reduce soil strengths from 0 to 5 feet below the excavation line by 50 percent to account for loss of strength after excavation.

5. Run p-y analysis using COM624 or LPILE.
   a. Reduce soil strengths to account for close shaft spacing based on Figure 2.2.
   b. Use uncracked section properties for the shaft.
   c. Ensure bending moments and deflections are within allowable values. Limit deflections to 1 percent of the cantilever height.

6. Determine depth of shaft fixity based on several embedment values.
   a. Determine depth of fixity where top-of-wall deflection is no longer affected by embedment depth.
   b. Determine final embedment depth by multiplying depth of fixity by 1.33.

| Equivalent Groundline Moment Calculated from Lateral Earth Pressure Distribution | Maximum Moment in Shaft Estimated from Computed Groundline Moment |
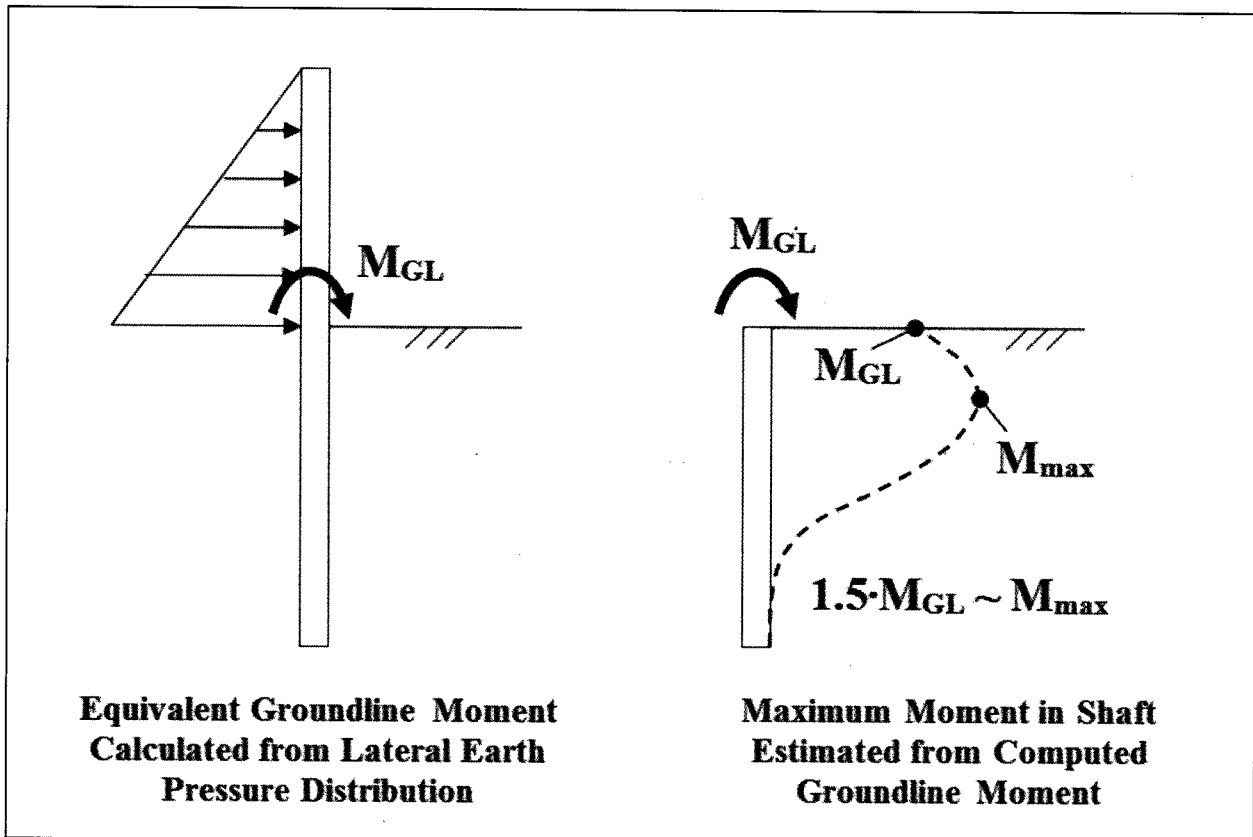
Figure 2.1: Initial estimation of maximum moment using TxDOT design procedure.

4
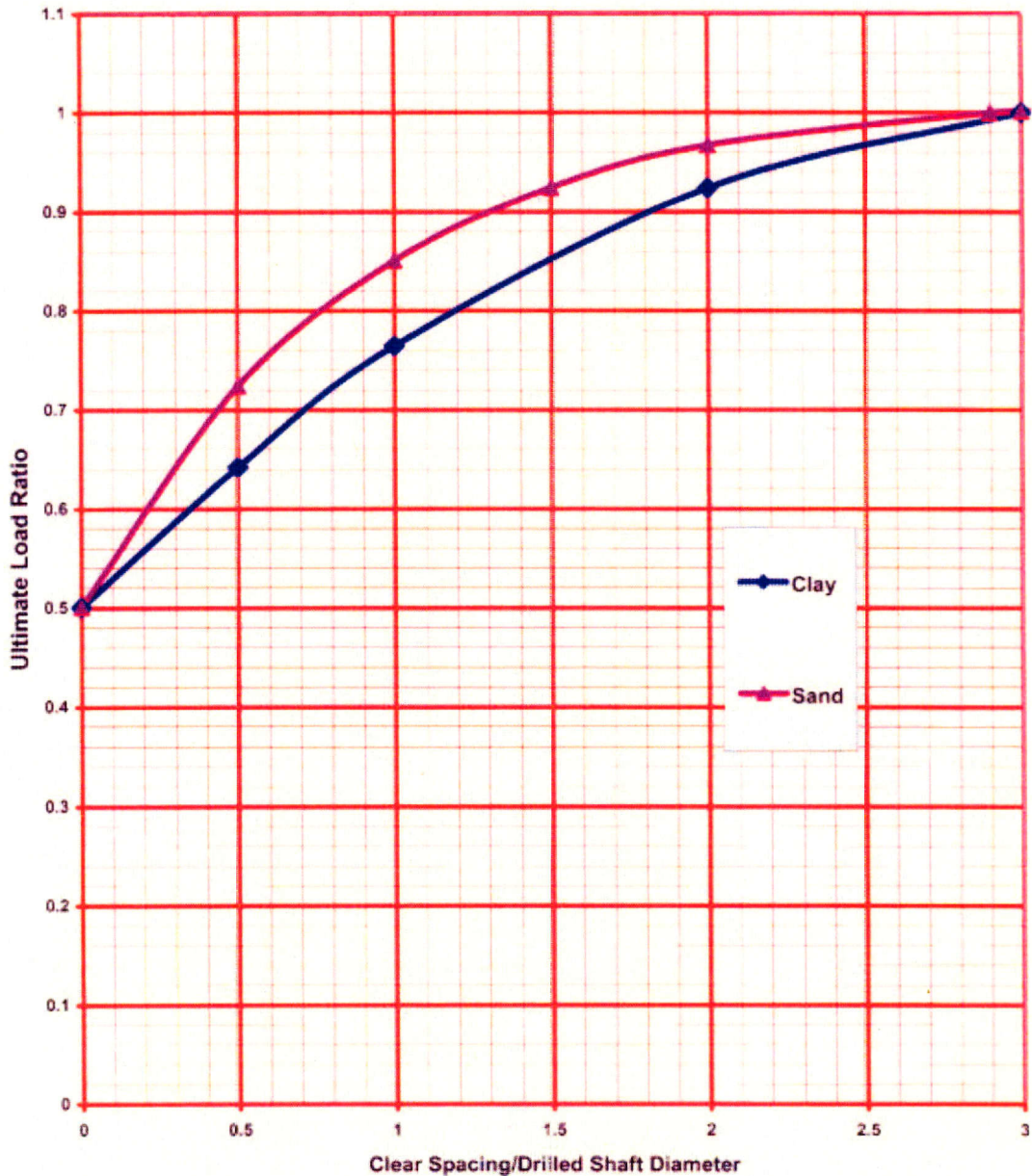
Figure 2.2: Ultimate load ratio vs. clear spacing/drilled shaft diameter (after TxDOT, 2012).

2.2: The Effects of Expansive Clay on Retaining Structures

2.2.1: SWELL PRESSURES, OVERCONSOLIDATION, AND OTHER CONCERNS

There have been concerns raised over the potential effects of expansive soils on retaining structures. The most common of these concerns is the magnitude of horizontal swelling pressures exerted on the wall by the expansive soil. Lytton (2007) summarizes some relevant studies that seek to quantify this effect. Variously, the potential lateral pressures acting on a wall in expansive clay have been estimated to be four times the overburden pressure, 6000 psf at 3 feet of depth in a lab study, 8000 psf at 3feet of depth in another lab study, and 1700 psf at 3 feet of

5

depth in a field study—any of these scenarios are significantly higher than the currently accepted values used for retaining wall design. These studies are described in more detail in Lytton (2007). In general, the expansive soil pressure exerted on a wall is considered to be limited by the passive resistance of the retained soil (Pufahl et al. 1983 and Hong 2008).

In addition to the potential for high lateral pressures, other potential concerns have been identified for retaining walls in expansive clay. Pufahl et al. (1983) describe a hypothetical structure "ratcheting" out with wetting and drying cycles. During dry seasons, the soil could pull back from the wall, incompressible debris could fill the gap, and soil expansion could push the wall and debris further out with each new rewetting cycle. Puppala et al. (2011) describe that cracks near drilled shafts could create zones for moisture infiltration, increasing the depth of the active zone near the shafts.

In Texas, many expansive soil deposits are also heavily overconsolidated. In overconsolidated clay, in-situ horizontal stresses can be very large. When the unloading associated with retaining wall excavation takes place, these large horizontal stresses can impact wall performance. Furthermore, the residual strength of overconsolidated clay can be very low— residual friction angles of 18° or less have been widely reported. The transition from peak-drained strength to residual-drained strength could influence the increase in lateral earth pressures with time (Wang and Reese 1986). The lateral swell pressures from moisture changes in overconsolidated clay have been reported to be higher than those in normally consolidated clay (Ellis 2011).

2.2.2: RECENT FAILURES IN OVERCONSOLIDATED, EXPANSIVE CLAY

Because the potential for expansion and a high degree of overconsolidation coexist in expansive clays in Texas, it is difficult to separate the effects of swelling from the effects of overconsolidation when considering wall failures. Smith et al. (2009) examine the failure of a bridge deck completed using top down construction in the overconsolidated, expansive Eagle Ford shale near Dallas, Texas. In this case, the bridge deck was installed before complete excavation of the underpass and installation of tiebacks. Ultimately, an estimated 4 inches of inward movement caused the failure of the bridge deck. The authors concluded that the major issue was the use of a design at-rest earth pressure coefficient (K_o) value of approximately 0.7; actual values of K_o for the Eagle Ford shale and other overconsolidated clays are often reported to be between 2 and 3. Expansive soil movement was cited as a "likely" contributing factor (Smith et al. 2009).

Another wall failure in the Eagle Ford shale, this time of a Vertically Earth Reinforced Technology (VERT) wall system, is detailed by Adil Haque and Bryant (2011). This paper indicates that the high K_o values and low residual strengths of overconsolidated clay, as well as expansion from moisture changes, should have been considered in design. The paper also states that "the swell pressure due to unloading could also exert a significant pressure on the wall, much greater than the swell pressure on the walls from moisture changes" (Adil Haque and Bryant 2011).

2.3: Field Performance of Existing TxDOT Walls

2.3.1: EXPANSIVE CLAY CONCERNS VERSUS REAL-WORLD MITIGATING FACTORS

Despite the numerous problems potentially associated with the expansive soils in Texas, relatively few failures of drilled shaft retaining walls have been observed. There are several

possible explanations for the general lack of problems associated with drilled shaft retaining walls in expansive clays in Texas.

First, the load factors and deflection requirements used by the TxDOT design procedure will result in drilled shafts that can withstand higher pressures than the nominal values used in design. After calculating the maximum moment in the shaft, a load factor of 1.7 is applied to estimate the design moment. If the differences in active Coulomb earth pressures induced by residual soil strength and/or soil swell are within the range encompassed by this load factor, it is possible that the potential increases in soil pressures are not causing visible distress on walls (for reference, a Coulomb analysis using a residual friction angle of 18° results in an equivalent fluid pressure of approximately 60 psf/ft, about 50 percent higher than the nominal value of 40 psf/ft). While the top-of-shaft deflections might exceed 1 percent of the wall height, the structural integrity of the shafts may be preserved. Furthermore, the final as-built drilled shafts may have greater capacity than the minimum allowed by design due to other factors such as constructability (although the risk for lower-than-design capacities due to poor construction exists as well).

Additionally, pavement and drainage systems behind drilled shaft walls may limit the severity of moisture changes causing shrinking and swelling. In pavements with expansive subgrades, moisture contents tend to increase from their natural moisture content to a "steady state" value after the installation of pavement (Snethen et al. 1975, Wise et al. 1971). While the subgrade is still subject to moisture changes, the magnitude of these changes may be smaller than those of exposed soil. The presence of pavement near the shaft can also prevent the problems associated with water and/or debris entering the gap between the shaft and the soil (Puppala et al. 2011).

Finally, despite the potential to generate very large swell pressures under confinement, swell pressures can be reduced by allowing relatively small wall deformations to take place (Thomas et al. 2009). For projects as large as the typical TxDOT drilled shaft retaining wall, it is possible that expansive soil pressures are being accommodated by small wall deformations that would not be noticed without careful instrumentation.

2.4: Analyses Programs

Two commercially available finite difference programs commonly used in the analysis of drilled shaft retaining walls are LPILE (Isenhower and Wang 2013) and PYWALL (Reese et al. 2013). The standard of practice for TxDOT is to use LPILE as part of the design procedure (Section 2.1.3).

LPILE was developed by Ensoft, Inc. and is commonly used to analyze a laterally loaded drilled shaft using the p-y method. LPILE calculates the deflection, bending moment, shear force, and soil response along the length of the shaft by solving the differential equations of static equilibrium for a beam column using soil-reaction springs represented by p-y curves. LPILE was not developed explicitly to analyze a retaining wall with retained soil on one side of the shafts and with shafts spaced closely enough to interact with one another. In practice, LPILE is adapted to analyzing a retaining wall by (1) applying an earth pressure distribution on one side of the shaft to represent the loading from the retained soil; (2) neglecting the difference in vertical and lateral overburden stress on the retained and excavated sides of the shaft; and (3) adjusting the input parameters for the p-y curves to account for the interaction with adjacent shafts.

PYWALL was also developed by Ensoft to specifically analyze a retaining wall. It uses the same theory as LPILE for a single shaft but implicitly accounts for the loading, the differences in overburden stresses, and the effects of shaft interactions on p-y curves.

2.5: Models for Lateral Earth Pressure Loading

Long-term conditions generally govern retaining wall design in high plasticity clays. Often, for embankments and retaining walls, the development of drained, fully softened strengths is a suitable ultimate condition for design (Wright 2005). A variety of models have been proposed for representing the long-term earth pressures induced by expansive soil. For clays in the Taylor formation, where the Lymon C. Reese research wall is constructed, peak drained friction angles are approximately 37° (Long 1983 and Ellis 2011), and average fully softened friction angles in the upper 15 feet are estimated to be approximately 24° based on liquid limit relationships (e.g., Wright 2007) and laboratory test data discussed in Chapter 7. The resulting earth pressure envelopes using the fully softened strengths of the Taylor clay, assuming both no water behind the wall and hydrostatic conditions behind the wall, are pictured in Figure 2.3, along with TxDOT's typical design earth pressure envelope and a hypothetical model of expansive soil swelling pressures similar to that presented in Hong (2008).
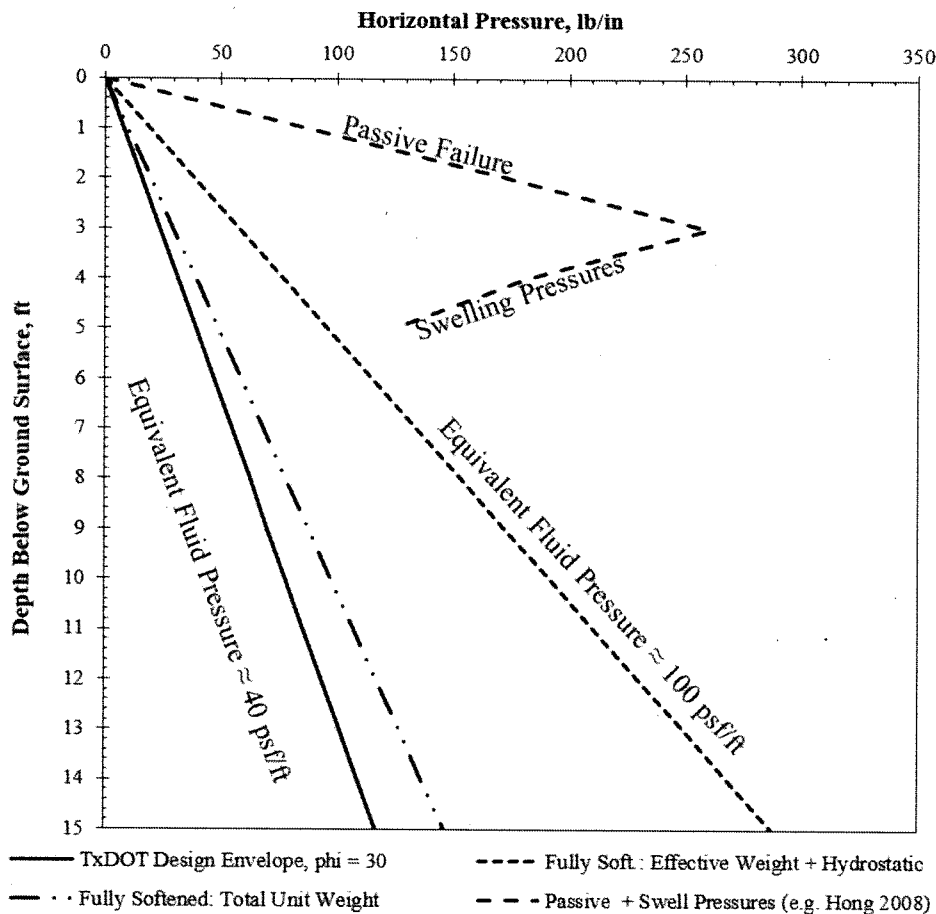
Figure 2.3: Examples of proposed long-term earth pressure envelopes for expansive clay (pressures are acting on a 2.5-foot shaft width).

2.6: P-y Models of Foundation Soil Response

In addition to the uncertainty associated with the behavior of the retained soil, several p-y models have been proposed to model the response of the foundation soil in expansive clay. Some of these curves are briefly explained below; illustrations of the calculated curves at a depth of 16 feet below the original ground surface (1 foot below the design excavation base) for the Lymon C. Reese research wall are provided for comparison in Figure 2.7.

2.6.1: STIFF CLAY WITHOUT FREE WATER

Typically, the TxDOT design procedure for stiff clays uses p-y curves for "stiff clay without free water," developed from tests in Houston, Texas (TxDOT 2009, Reese et al. 2006, Reese and Welch 1972). To account for strength reductions due to the removal of overburden pressures during excavation, a common procedure for excavations in stiff-fissured clay is to reduce strengths by 50 percent in the upper 10 feet and/or translate the profile of undrained strengths from the original ground surface down to the excavation line. Additionally, soil strengths are reduced to account for the effect of close pile spacing as shown in Figure 2.2 (TxDOT 2012; Wang and Reese 1986). For the Lymon C. Reese wall, average undrained strengths used for the development of representative p-y curves shown in Figure 2.7 were approximately 1600 to 2000 psf (before strength reductions). Total soil unit weights are used for these curves.

2.6.2: STIFF CLAY WITH FREE WATER

It is possible that if water stays in the excavation base, the use of curves developed for "stiff clay in the presence of free water" may be appropriate. These curves were developed from load tests in the Taylor formation in Manor, Texas (Reese et al. 1975). Strength reductions to account for the removal of overburden pressures and close pile spacing are applied before calculating the curves as shown in Reese et al. 2006. Curves developed for clays in the presence of free water use effective unit weights.

2.6.3: DRAINED P-Y CURVES FOR COHESIONLESS SOIL

If the long-term conditions of drilled shaft walls in expansive clays are governed by the development of drained conditions, the use of drained p-y curves developed for cohesionless soils may be appropriate. Because the initial stiffness of the clay in response to loading at small strains is governed by undrained behavior, the initial stiffness value kpy for the p-y curves is selected according to the undrained properties of the clay as shown in Figure 2.4. The use of default kpy values for modeling curves at low friction angles associated with expansive clay soils results in unrealistically low values of initial stiffness (Figure 2.5). The selection of unit weight is based on the expected hydrologic conditions on the project site to represent effective stresses. Strength reduction to account for close pile spacing is accounted for by reducing the p-y curve by a reduction factor (Figure 2.6) that is applied to all points along the curve.
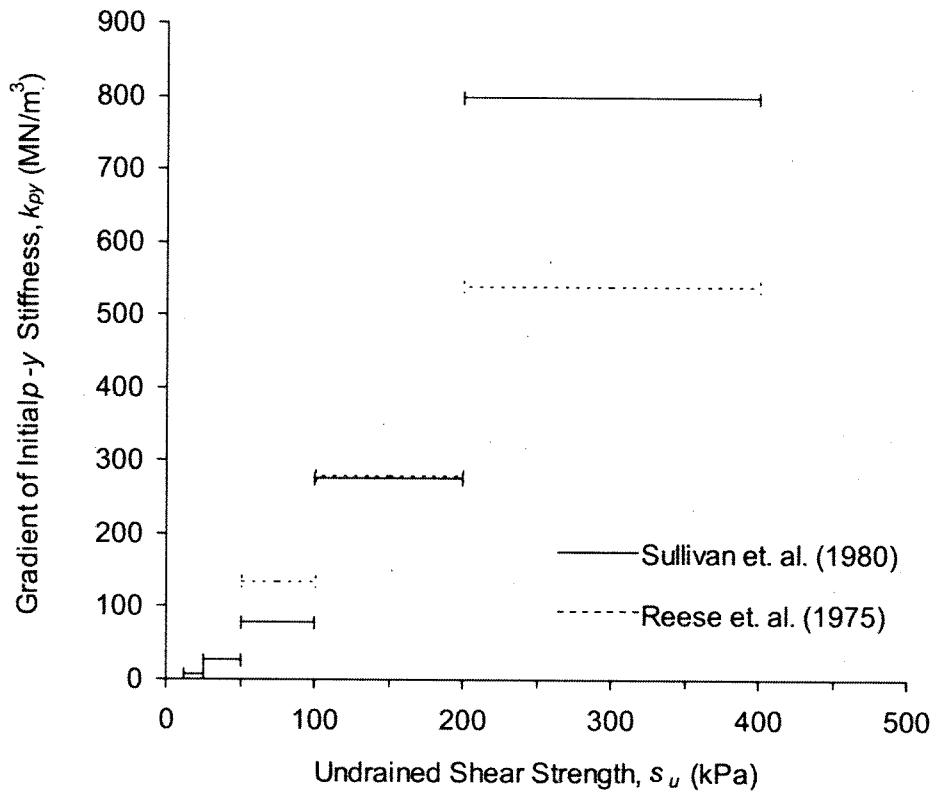
Figure 2.4: Typical k_{py} values for clays (after Dodds and Martin 2007).
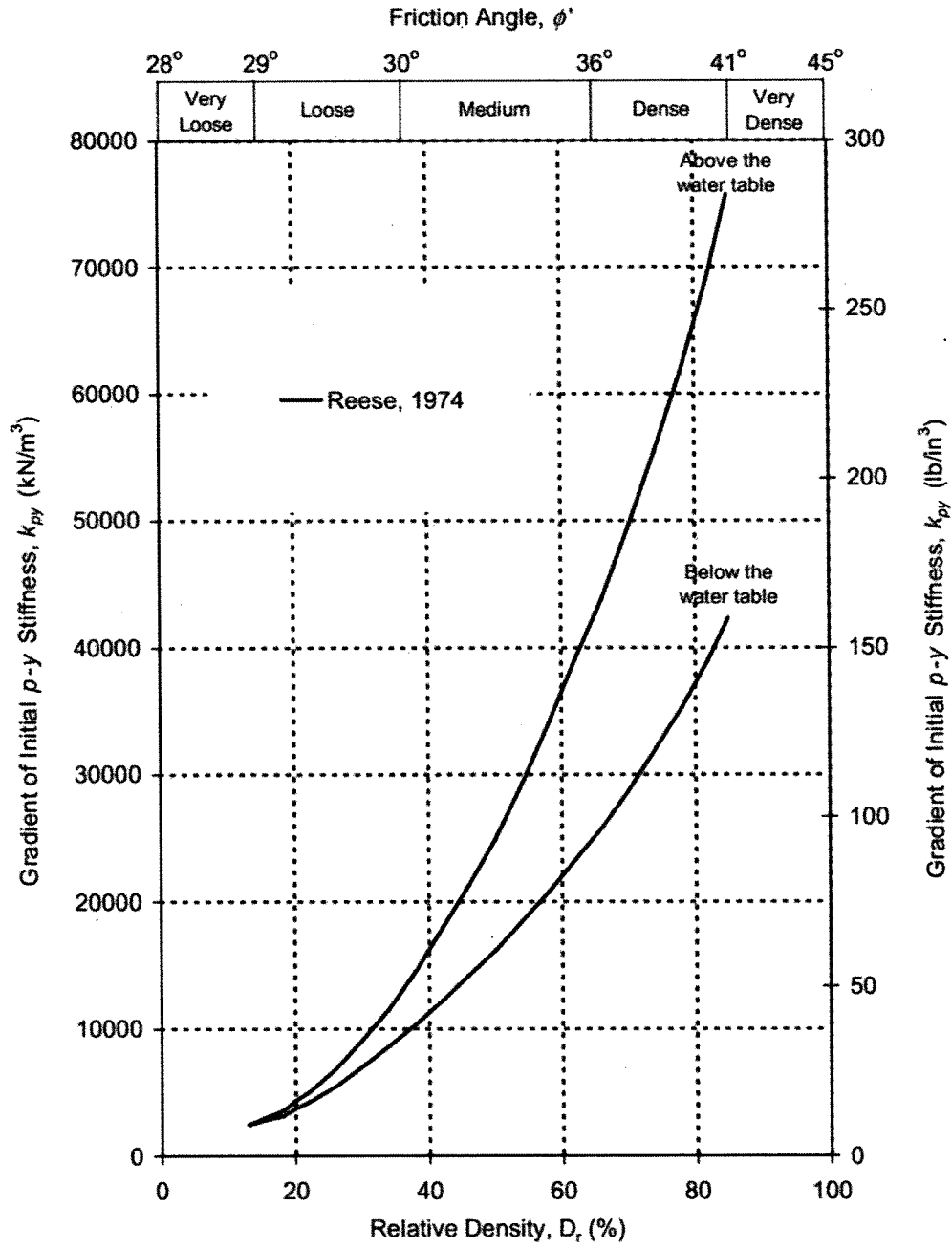
Figure 2.5: Typical k_{py} values for sands (after Dodds and Martin 2007).
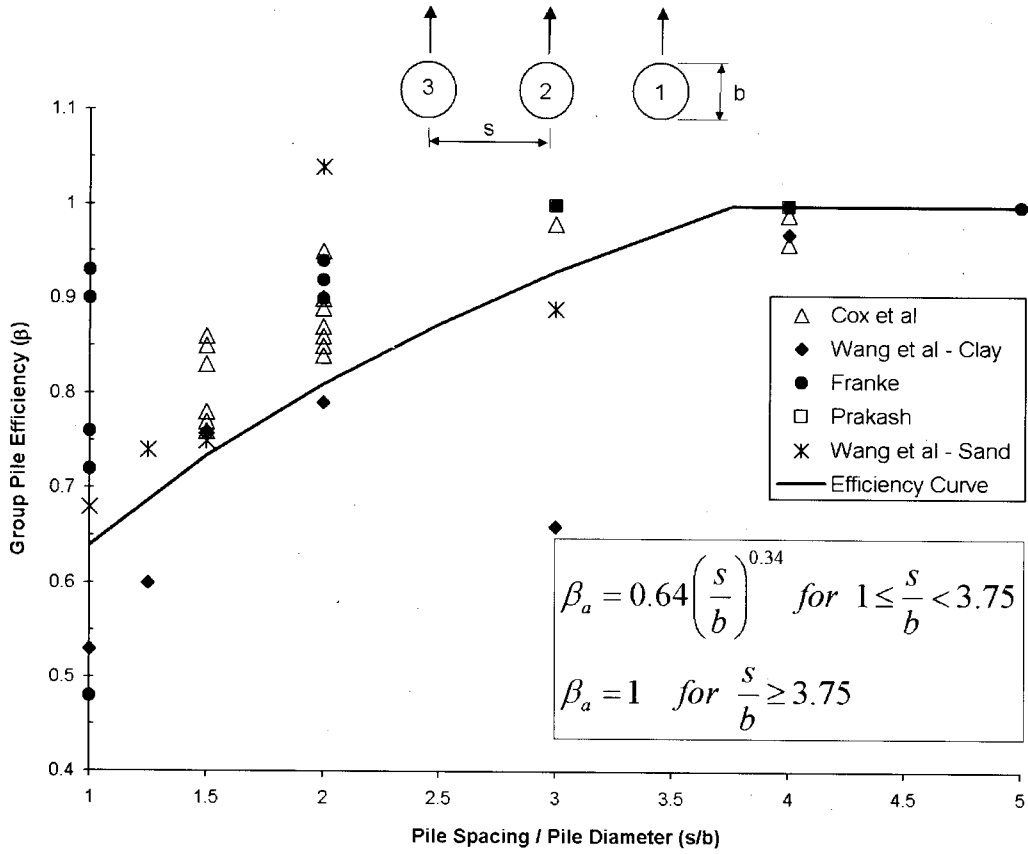
Figure 2.6: Curves giving group reduction factors for piles in a row (Reese et al. 2006).

2.6.4: SUMMARY OF PROPOSED P-Y CURVES FOR COMPARISON

A summary of the proposed p-y curves discussed in the previous sections, calculated for the test wall at a depth of 16 feet below the original ground surface (1 foot below the excavation line) is shown in Figure 2.7 for comparison. For this research study, p-y curves estimated from test wall data will be compared with the family of curves discussed in this section.
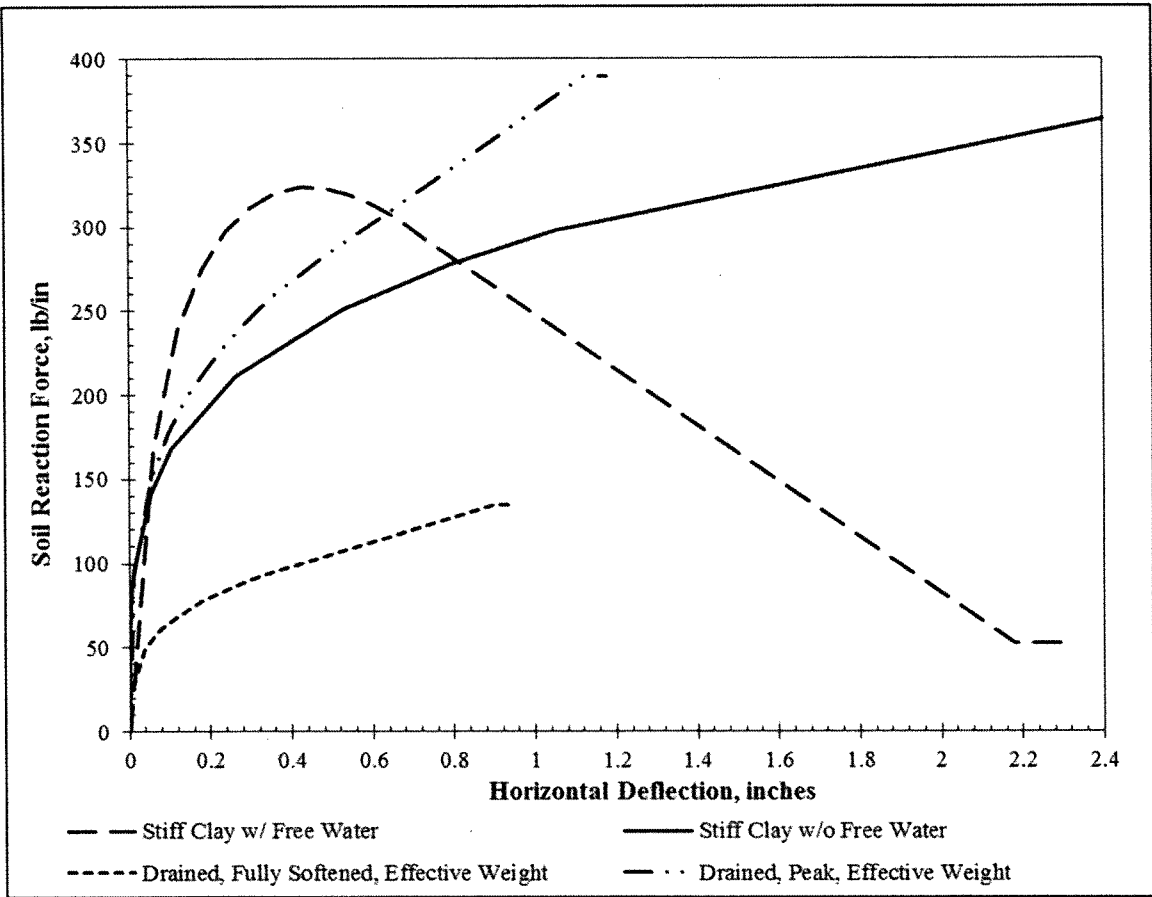
Figure 2.7: Summary of proposed p-y curves, calculated for the test wall at a depth of 16 feet below the original ground surface (1 foot below excavation line).

CHAPTER 3: ASSESSMENT OF EXISTING TXDOT WALLS

3.1: Candidate Walls

Three existing walls were selected for assessment with the cooperation of TxDOT managers. While there may be additional walls throughout Texas that warrant further study, the following three walls from the Houston district were the only candidates that could be identified with the information provided by TxDOT.

1. FM 1960 at Kuykendahl (CSJ # 1685-01-082)

2. US 59 at Hazard Street (CSJ # 0027-13-165)

3. IH 45 at GREENS ROAD (CSJ # 0110-06-102)

3.1.1: FM 1960 at Kuykendahl (CSJ # 1685-01-082)

This retaining wall is located in north Houston, Texas, where Kuykendahl Road passes under FM 1960 (Figure 3.1). The underpass was built to relieve congestion at the intersection. Based on TxDOT's payment records and satellite imagery, excavation was likely completed in late 2008 (Ozuna 2011). The area had been developed prior to construction, and the project represents a change to an existing roadway that was already covered with pavement (Figure 3.2 and Figure 3.3). The wall is a hybrid structure consisting of a cantilever drilled shaft wall over the middle depths and a tieback wall over the deeper depths. As of June 30, 2011, no obvious signs of distress have been observed.
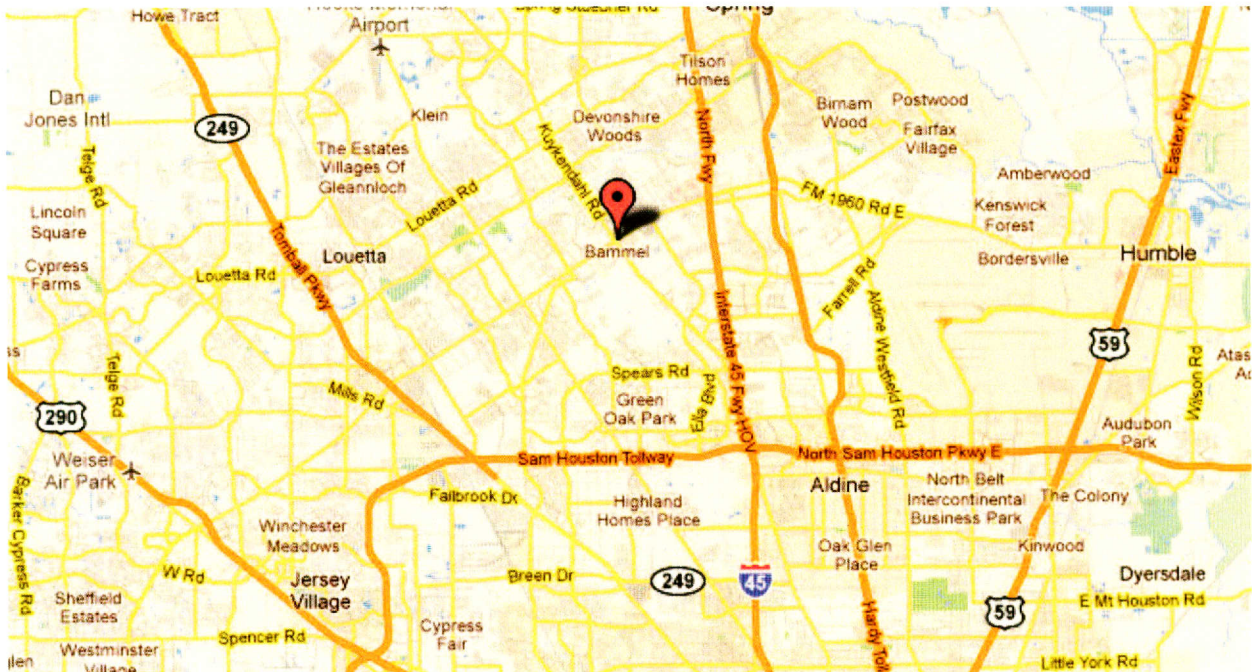
Figure 3.1: View of wall location within greater Houston (Google Inc., 2011).

15
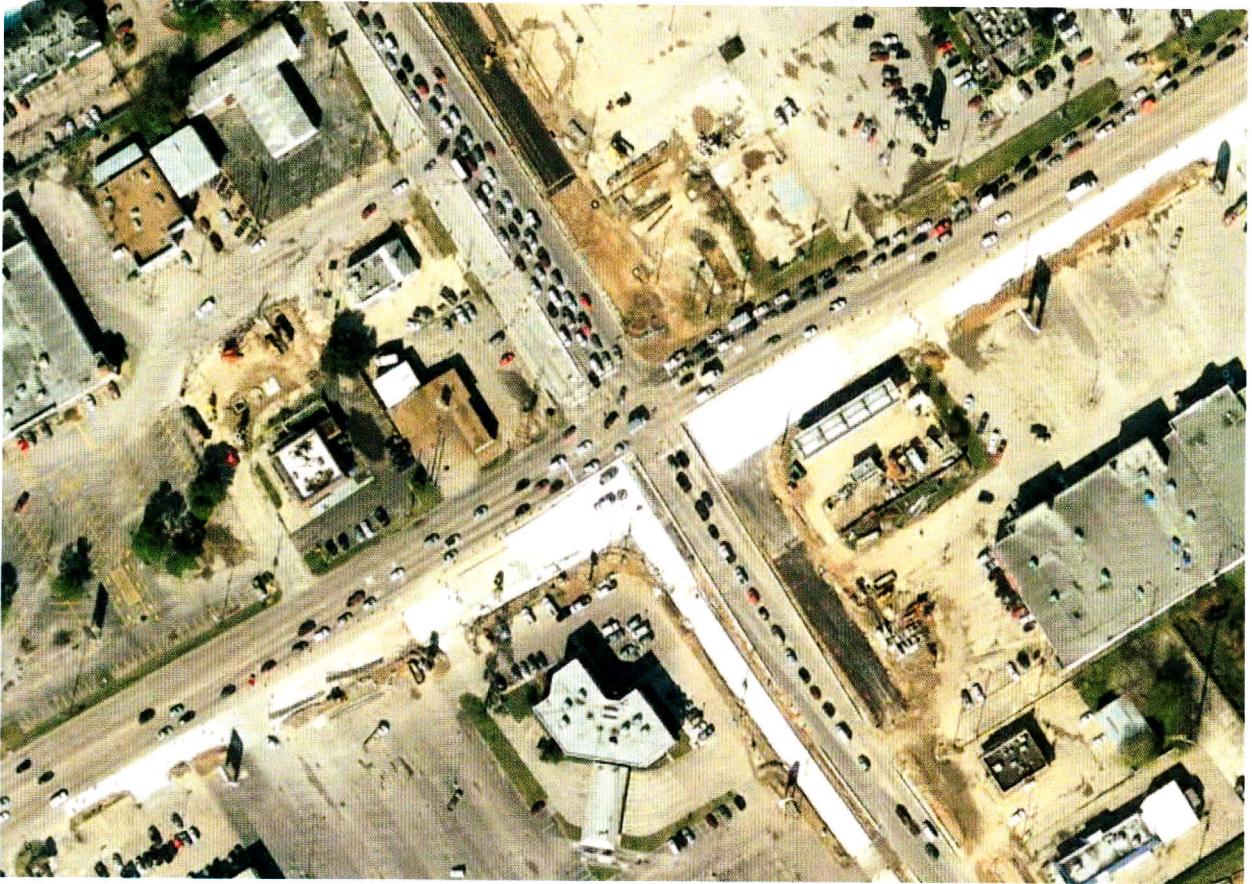
Figure 3.2: Aerial view of project area before excavation (image date: January 2008) (Google Inc., 2011).
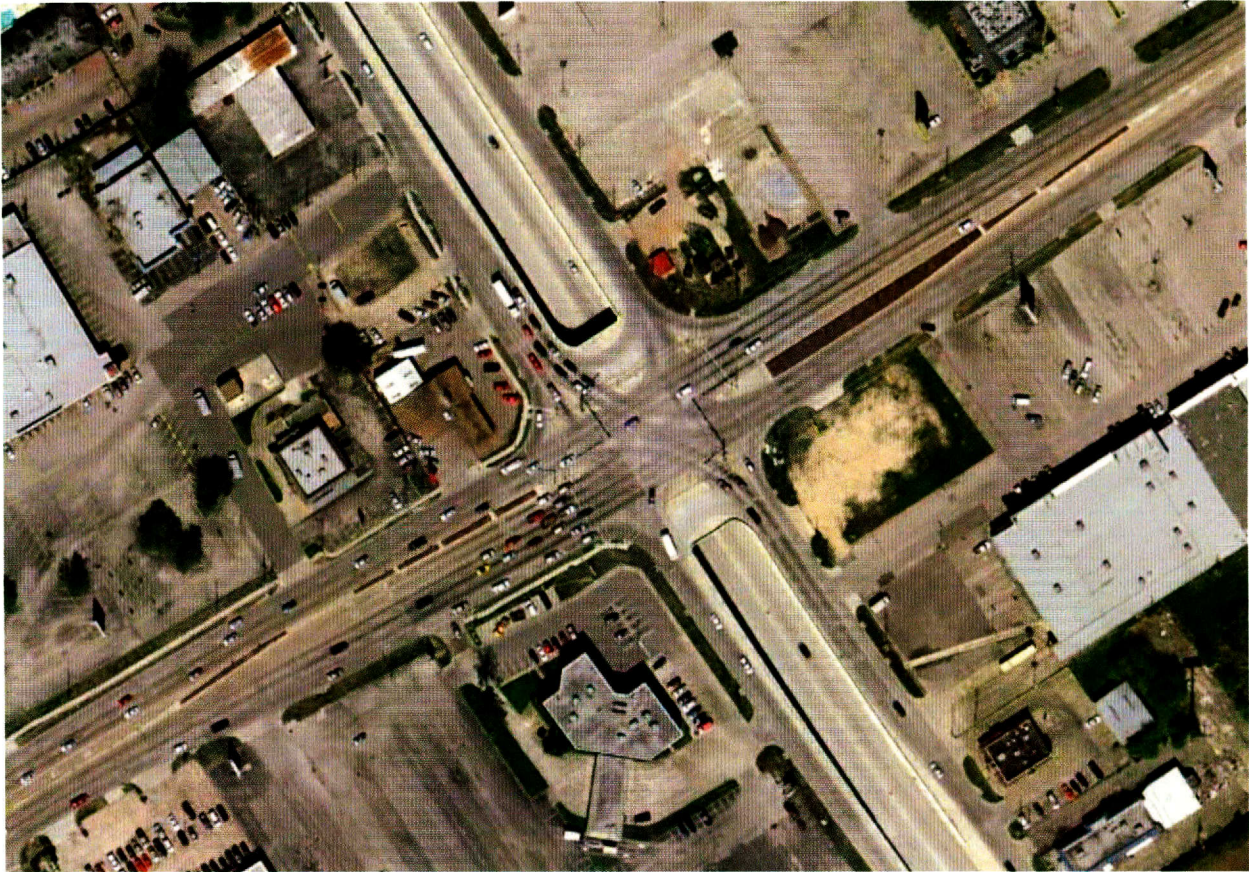
Figure 3.3: Aerial view of project area after completion (image date: March 2011) (Google, Inc., 2011).

3.1.2: US 59 AT HAZARD STREET (CSJ # 0027-13-165)

This retaining wall is located in Houston on US Highway 59 between South Shepherd Street and Mandell Street (Figure 3.4 and Figure 3.5). Based on satellite imagery and available information from TxDOT, excavation was likely completed in mid-2002 (Figure 3.6 and Figure 3.7). The wall consists of several sections of similar cantilever drilled shaft walls, interrupted by bridge abutments at regular intervals. During an assessment performed June 30, 2011, some gaps between the retained soil and the wall were observed, but no signs of wall distress were clearly present.
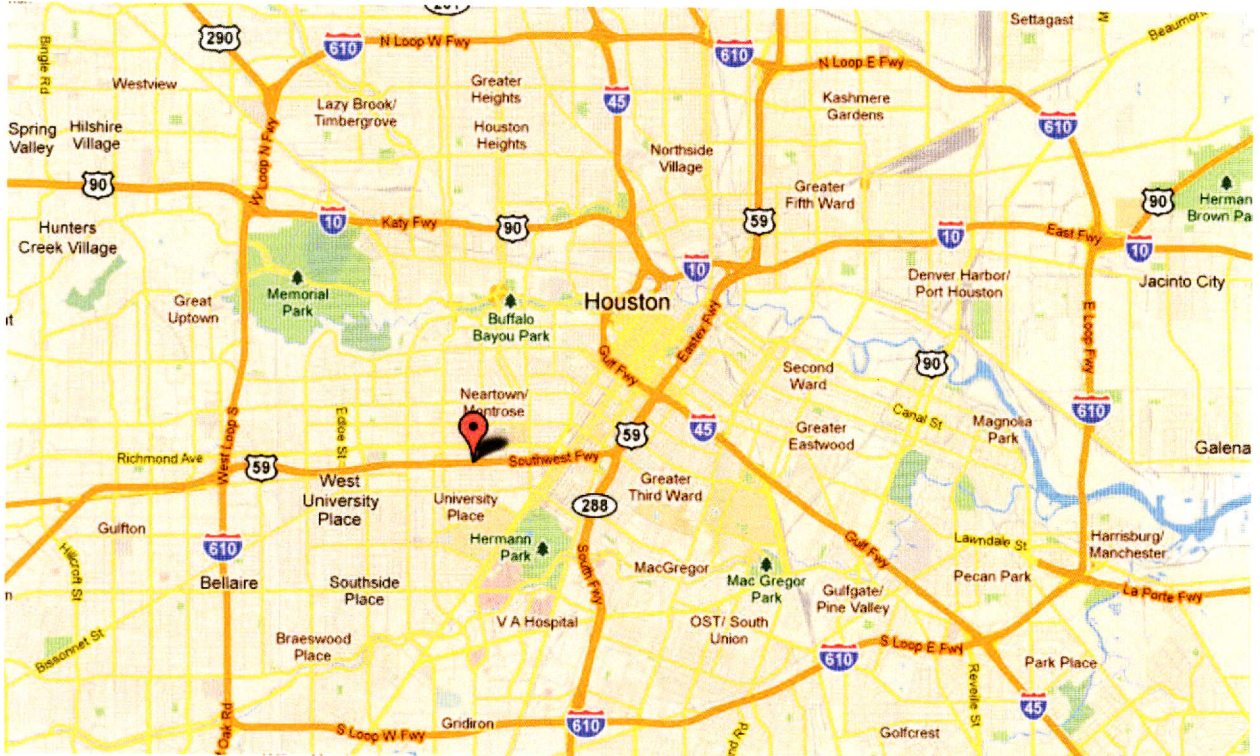
Figure 3.4: View of wall location within Houston (Google Inc., 2011).
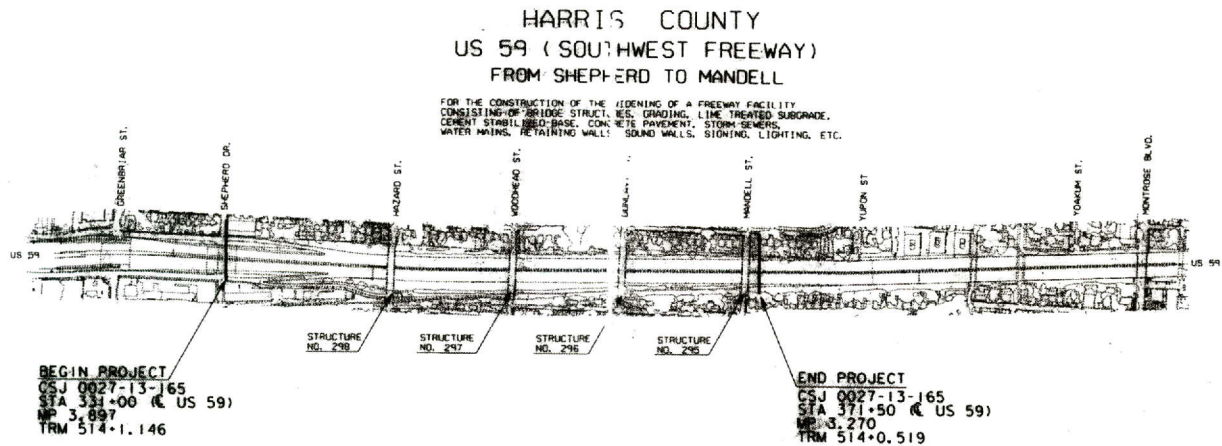
Figure 3.5: View of project area along US 59.

18
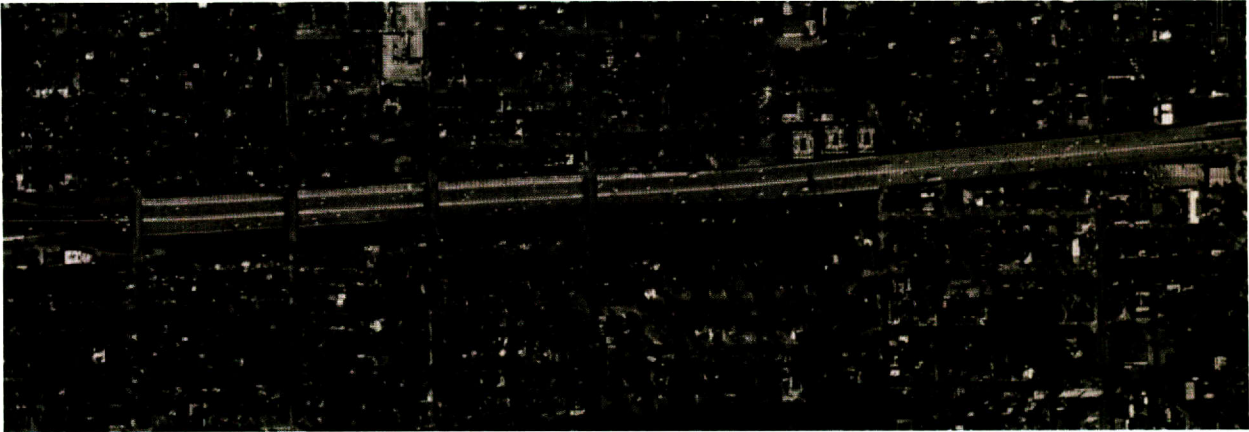
Figure 3.6: Aerial view of the project area before construction (image date: January 1995) (Google Inc., 2011).
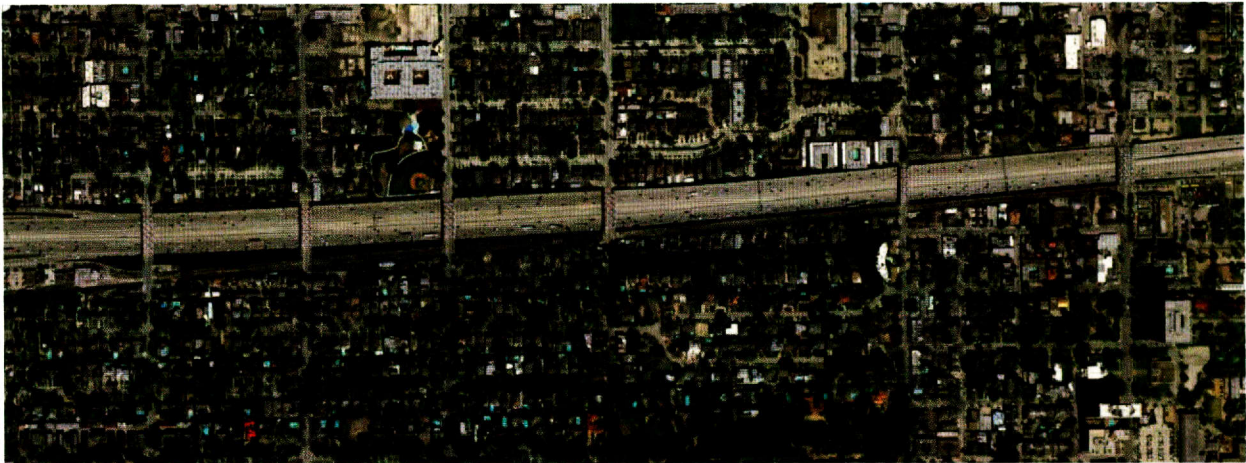
Figure 3.7: Aerial view of the project area after completion (image date: March 2011) (Google Inc., 2011).

3.1.3: IH 45 AT GREENS ROAD (CSJ # 0110-06-102)

The retaining wall is located in north Houston, where Greens Road passes under the Interstate Highway 45 frontage road (Figure 3.8). A highway overpass existed prior to construction. Based on satellite imagery and correspondence with TxDOT, excavation was likely completed in mid-1997. Aerial images of the site before and after wall construction are shown in Figure 3.9 and Figure 3.10. The wall is a hybrid structure consisting of a cantilever drilled shaft wall at shallow depths and a tieback wall at higher design heights. As of June 30, 2011, no obvious signs of distress have been observed.
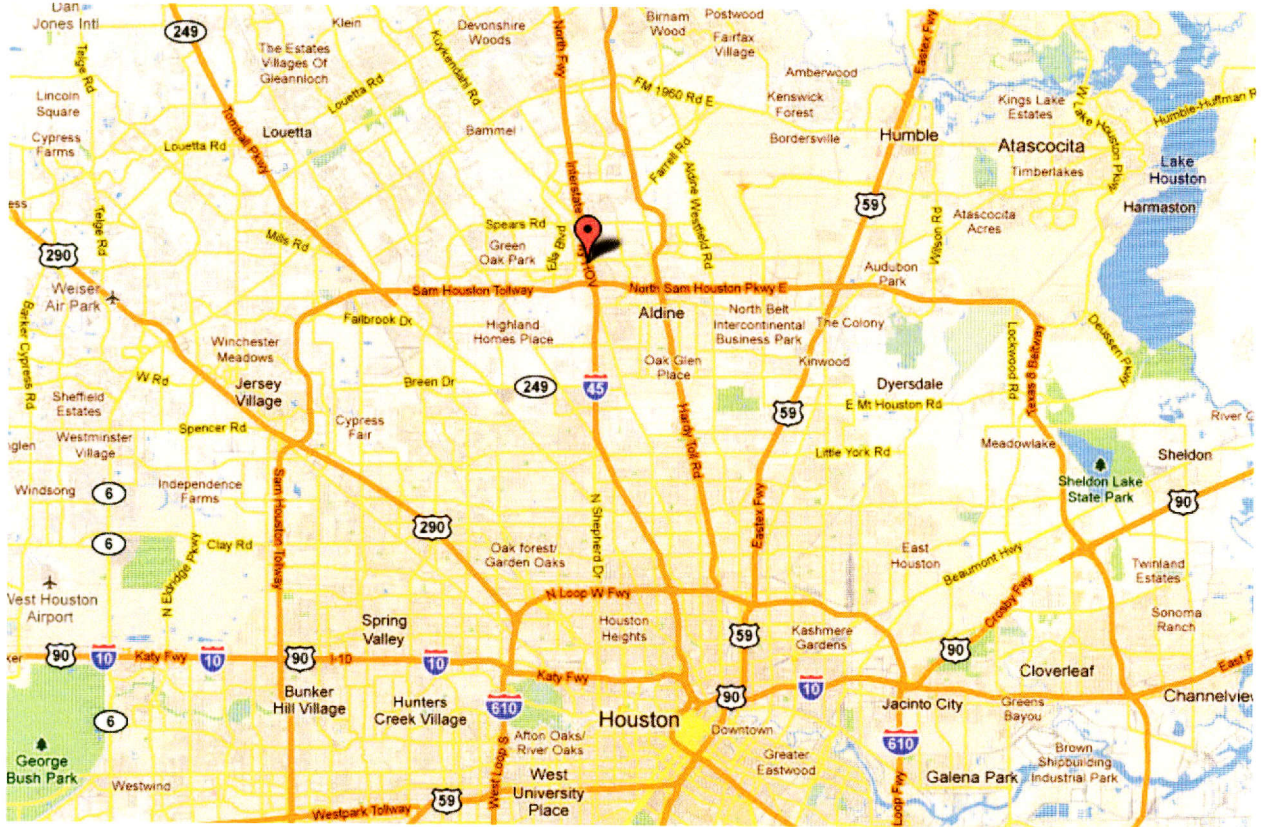
Figure 3.8: View of wall location within greater Houston (Google Inc., 2011).

Figure 3.9: Aerial view of the project area before construction (image date: January 1995)
(Google Inc., 2011).

20
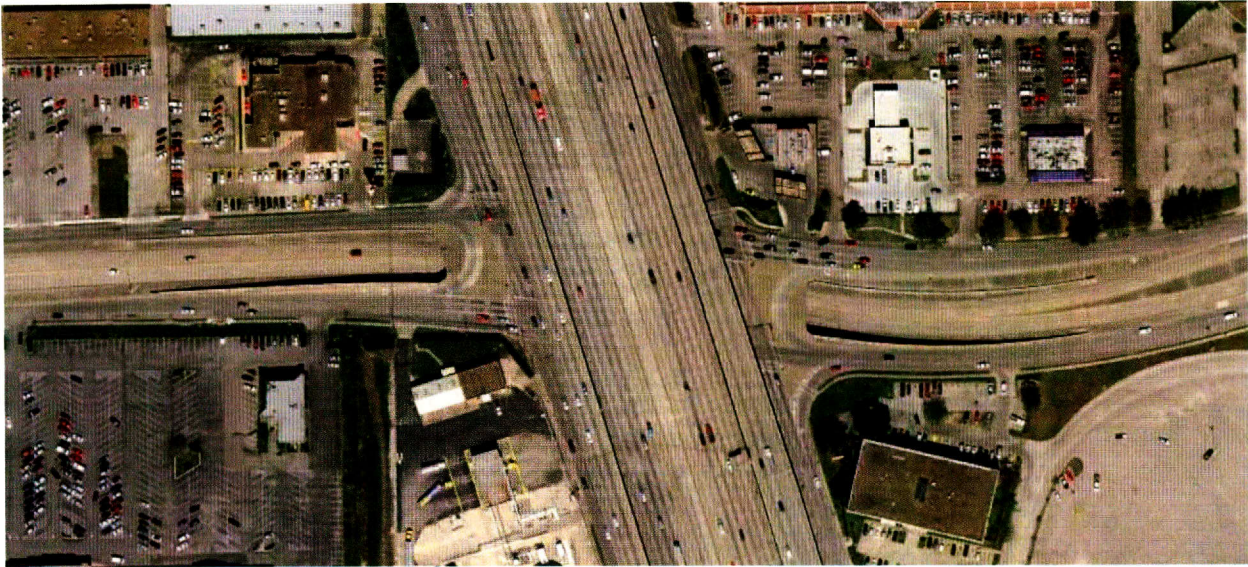
Figure 3.10: Aerial view of the project area after completion (image date: March 2011) (Google Inc., 2011).

3.2: Climate Information

In order to identify the potential for expansive soil movement, climatic cycles between wet and dry seasons need to be examined. Because the three candidate walls are located in Houston, the climate data for all three should be sufficiently similar. Additionally, no construction records were available for the candidate walls. To estimate construction dates, TxDOT suggested that we go back 1 year from the final payment date from TxDOT to the contractor (Ozuna 2011). Because we lack precise information about when the shafts were installed and the excavations completed, conclusions drawn from site-specific climate data should be qualified.

Vipulanandan and Joseph (2011) examined moisture fluctuations in the active zone for the city of Houston from the years 2000 through 2007. While this information is not directly applicable to the candidate walls, it does indicate that Houston experienced a range of climate-related soil moisture fluctuations that could potentially lead to expansive soil movement. During the month of January (lowest average temperature), the average moisture content in the upper 10 feet of soil was approximately 16 percent. During the month of July (highest average temperature), the average moisture content in the upper 10 feet was approximately 18 percent. Year-to-year fluctuations were much greater. The highest fluctuations occurred at depths from 0 to 5 feet. While temperature effects on soil moisture were seen immediately, the effects of rainfall did not appear until "the following months" (Vipulanandan and Joseph 2011). A graph of monthly rainfall and temperature in Houston from 2000–2011 is provided in Figure 3.11. A comparison of yearly precipitation with the historical average yearly precipitation is provided in Figure 3.12.
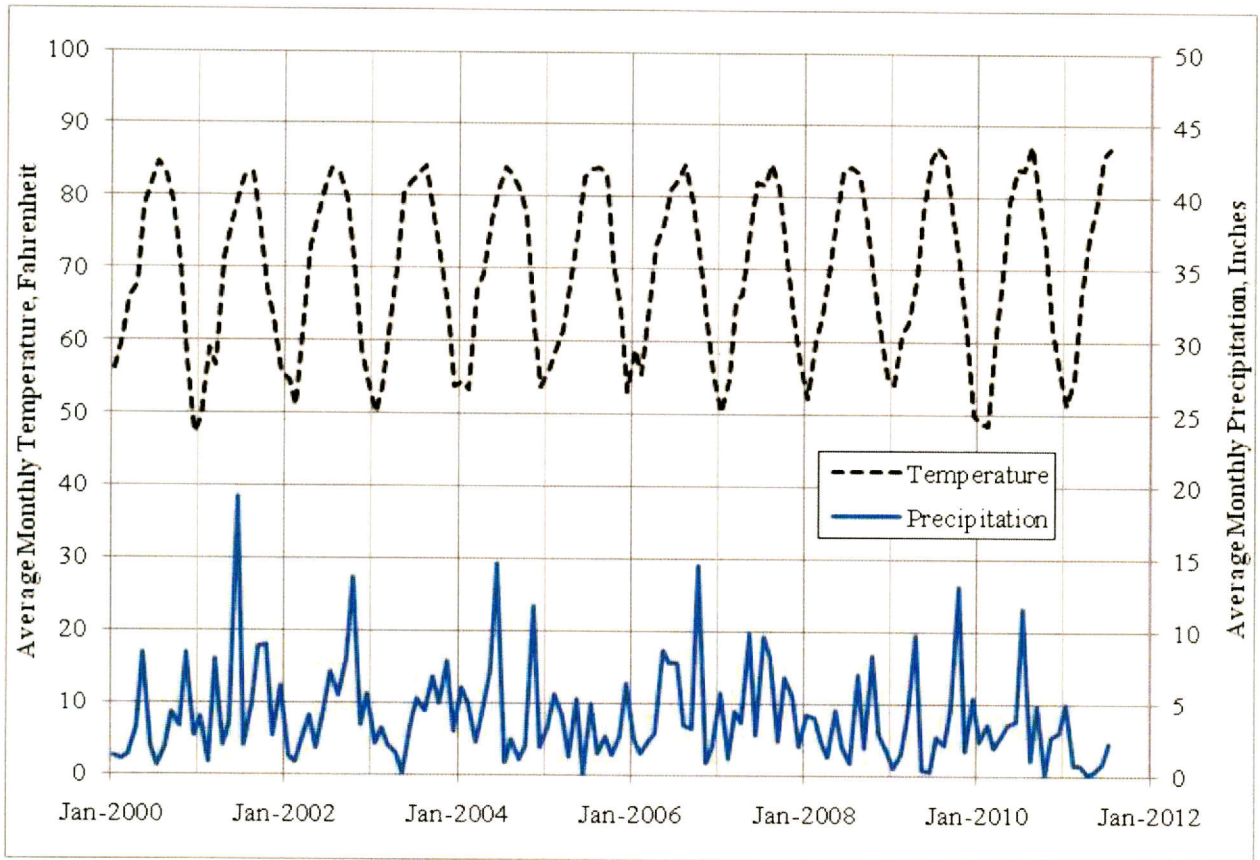
Figure 3.11: Average monthly precipitation and temperature for Houston (2000–2011). Data from Weather Underground (2011).
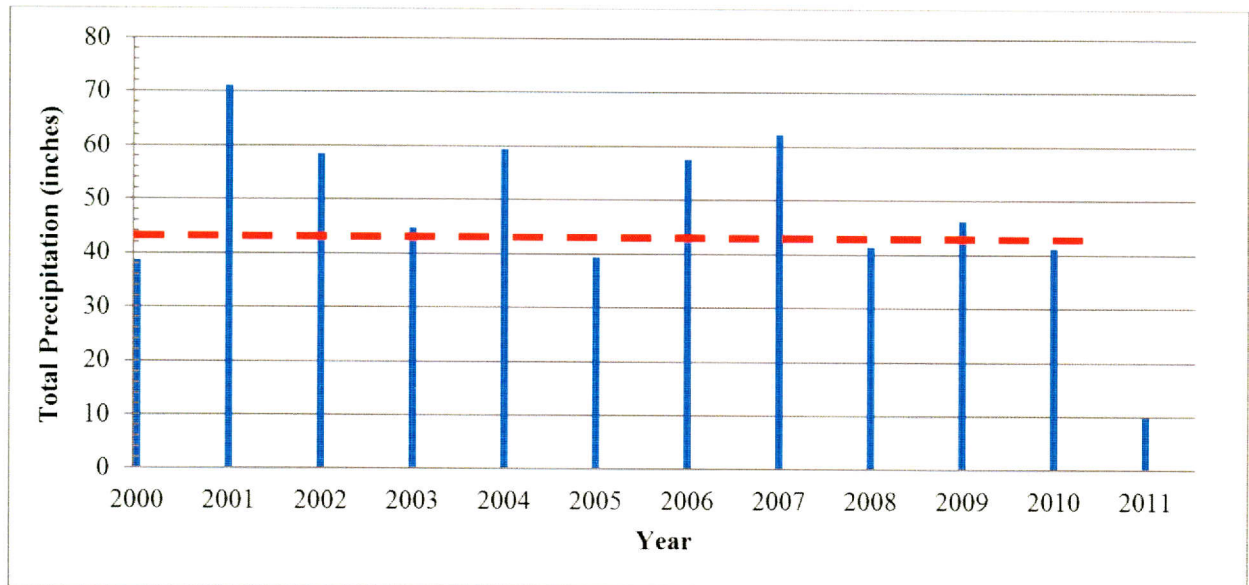
Figure 3.12: Yearly precipitation totals since 2000.
The dashed red line denotes the yearly historic average. The 2011 total is of the end of July. The historic average from January through July is 19.2 inches of precipitation. Data from Weather Underground (2011).

3.3: Design Information

This section presents the geotechnical and design information for the candidate walls. This information is based on design documents provided by TxDOT.

3.3.1: FM 1960 AT KUYKENDAHL

3.3.1.1: Geotechnical Information

Nine geotechnical borings were drilled near the project site between April 26, 2001, and May 7, 2001. Boring logs indicate the soil profile consists of very stiff clay to a depth of approximately 10 feet, which is underlain by approximately 10 feet of dense sand to a depth of about 20 feet. Below 20 feet, there are alternating layers of dense sand and stiff clay that show some variability across the project site (boring locations are not indicated in the available documents).

The very stiff clay in the upper 10 feet is of particular interest because it may be subjected to moisture changes causing shrinking and swelling. The plasticity index of this layer ranged from 11 to 39, but is typically in the mid 20s, indicating marginal swell potential (Department of Army 1983). Liquid limits ranged from 24 to 54 percent. Moisture contents in the upper 20 feet ranged from 11 to 23 percent. A water table location was not reported in any of the boring logs. The average undrained shear strength reported in the boring logs ranges from approximately 2000 to 4000 psf, based on the results of pocket penetrometer and unconsolidated-undrained (UU) testing.

3.3.1.2: Design Information

The retaining wall at FM 1960 and Kuykendahl Road consists of a combination of cantilever drilled shaft walls and tieback walls (Figure 3.13). For this investigation, only the cantilever drilled shaft wall is considered.
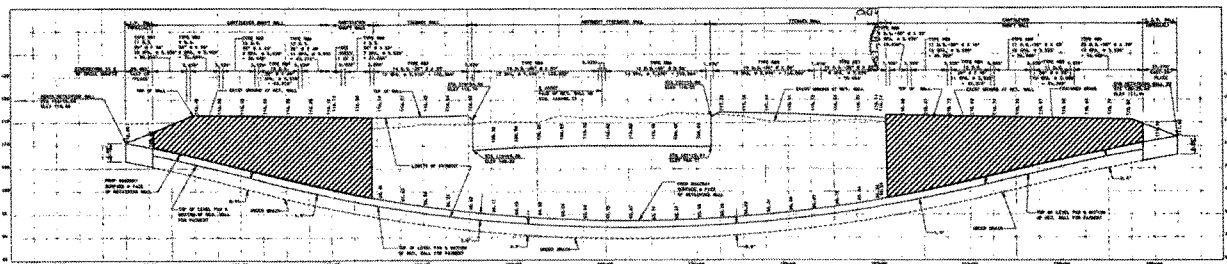
Figure 3.13: Composite sketch of northbound side of underpass. Shaded areas indicate locations of cantilever drilled shaft wall.

The drilled shaft wall consists of 36-inch diameter shafts that are 31 to 52 feet in length. Design heights range from 14 to 23 feet. As shaft length increases, more steel reinforcement is used (Figure 3.14 and Figure 3.15). The center-to-center spacing of the shafts is approximately 47 inches (Figure 3.16). Wall facing consists of 8.5 inches of cast-in-place concrete and 5.5 inch precast panels (Figure 3.17).

NORTH BOUND RETAINING WALL			
TYPE ②	WALL DESIGN HEIGHT "H"	VERTICAL REINF.	LENGTH OF DRILLED SHAFT
TYPE NB1	14	10 #9	36'
TYPE NB2	16	12 #9	39'
TYPE NB3	18	12 #11	43'
TYPE NB4	20	14 #11	46'
TYPE NB5	22	16 #11 ③	49'
TYPE NB6	23	18 #11 ③	52'

SOUTH BOUND RETAINING WALL			
TYPE ②	WALL DESIGN HEIGHT "H"	VERTICAL REINF.	LENGTH OF DRILLED SHAFT
TYPE SB1	12	10 #9	31'
TYPE SB2	14	10 #9	36'
TYPE SB3	16	12 #9	39'
TYPE SB4	18	12 #11	43'
TYPE SB5	20	14 #11	46'
TYPE SB6	23	18 #11 ③	52'

② SEE RETAINING WALL LAYOUT FOR LOCATION AND DRILLED SHAFT SPACING.
③ BUNDLED BARS ~ 2 BARS PER BUNDLE.

Figure 3.14: Design heights, reinforcement type, and shaft length for cantilever drilled shaft wall.
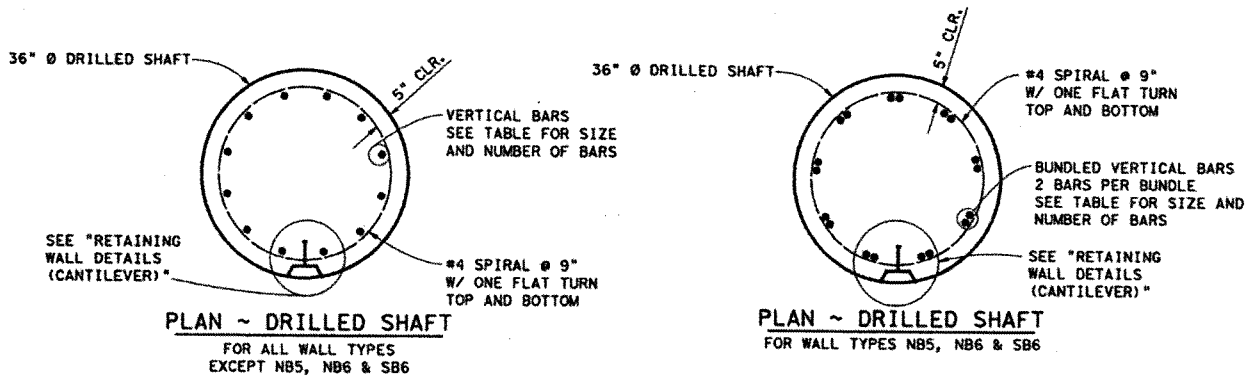
Figure 3.15: Reinforcement types for cantilever drilled shaft wall.
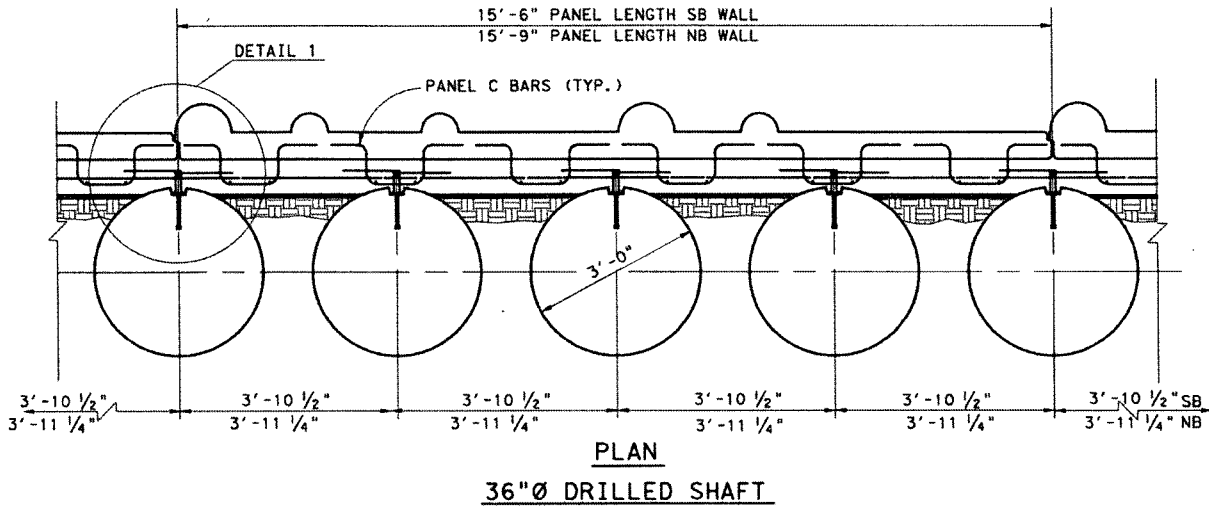
Figure 3.16: Shaft spacing.
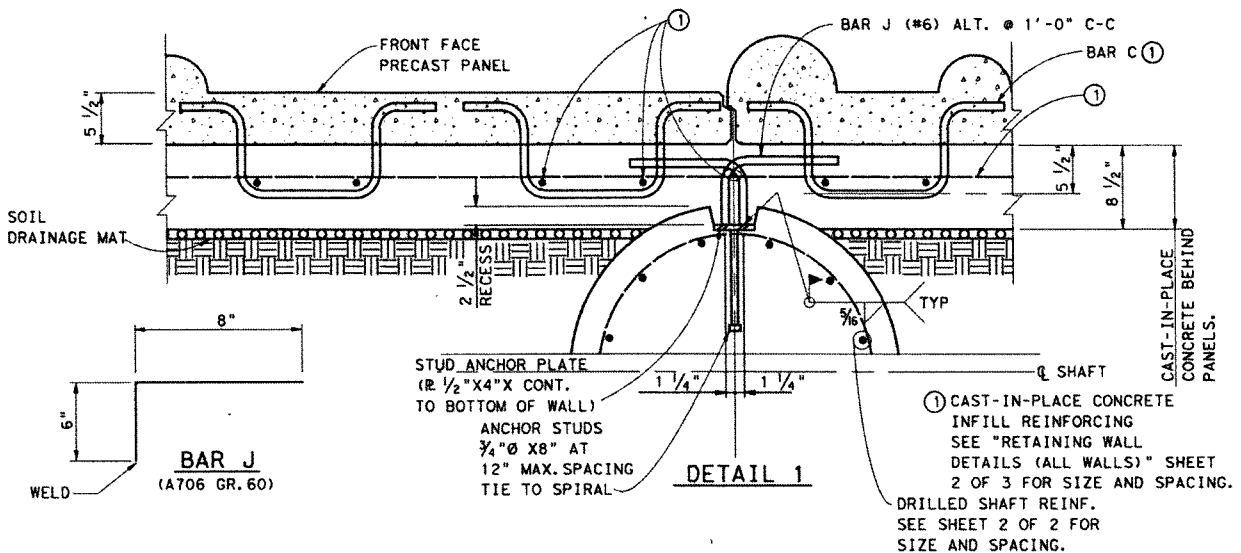
Figure 3.17: Detail of wall facing.

3.3.2: US 59 AT HAZARD STREET

3.3.2.1: Geotechnical Information

Across the project area, several geotechnical borings are present in the available documents. The soil profile consists primarily of stiff clay. At depths of 0 to 30 feet, the average plasticity index is approximately 40, indicating high swell potential (Department of Army 1983). Measured moisture contents in the upper 10 feet were generally between 15 and 30 percent. Based on the results of UU testing, undrained shear strengths ranged from approximately 2000 psf to 4500 psf over the depth of the wall.

3.3.2.2: Design Information

A secant wall consisting of alternating 48-inch and 18-inch shafts is the primary retaining structure for this project. In two locations, 48-inch shafts are used by themselves. At varying distances behind the wall, a sound wall is installed using 36-inch shafts on 5-foot center-to-center spacing (Figure 3.18). In some cases, these 36-inch shafts contribute to the strength of the main retaining structure. Details on internal shaft geometry are provided in Figure 3.19. Facing consists of precast concrete panels. The wall height across the project site is approximately 15 feet (Figure 3.20).
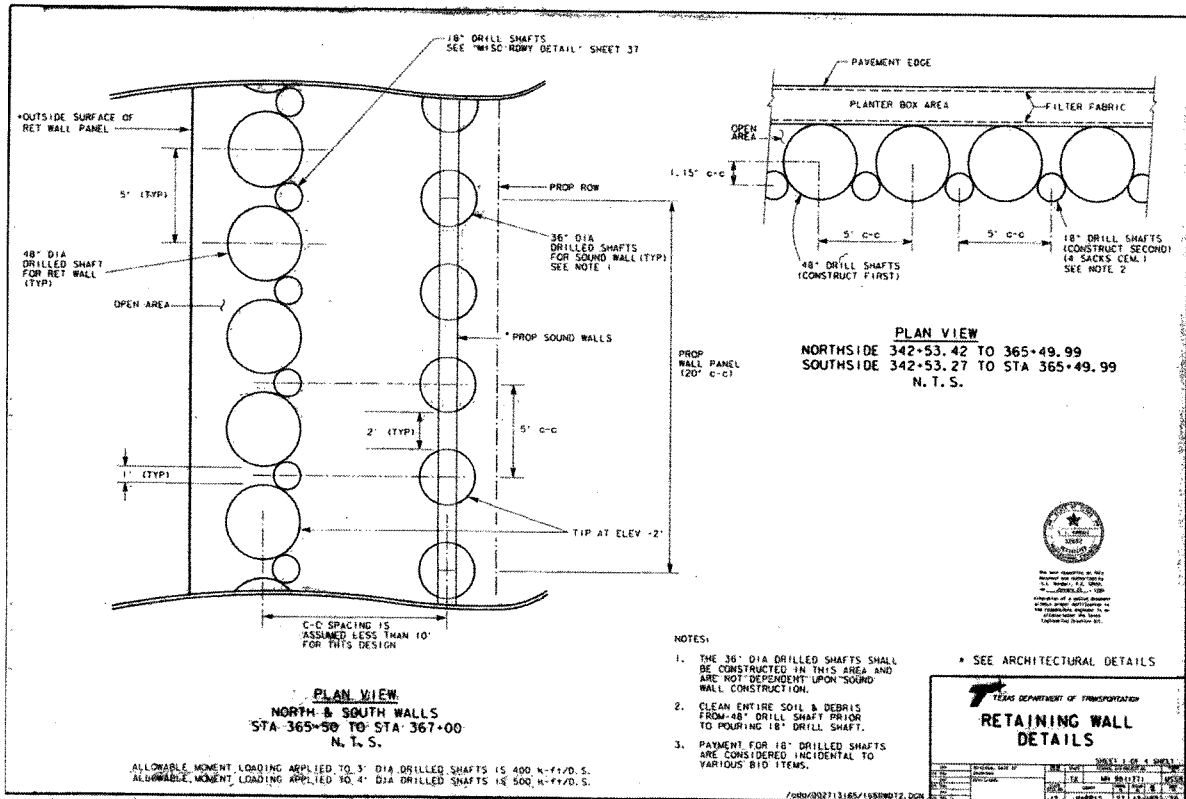
Figure 3.18: Details of drilled shafts for secant wall and sound wall foundation.

TYPICAL DETAILS
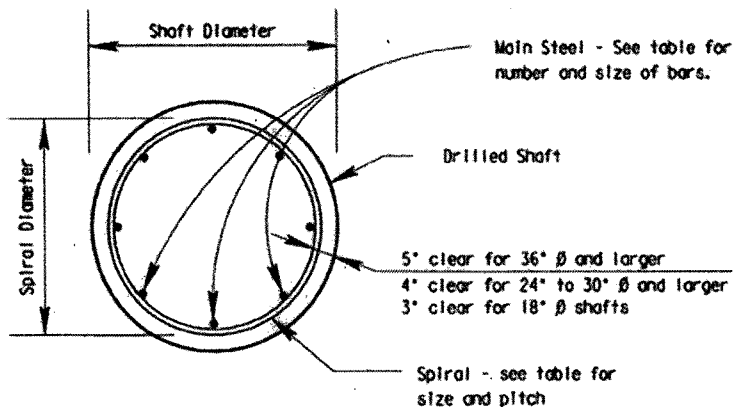
DRILLED SHAFT REINFORCING STEEL (unless noted otherwise)		
Drilled Shaft Diameter (Inches)	Main Steel	Spiral
18	6-#6	#3 at 6"
24	8-#7	#3 at 6"
30	8-#9	#3 at 6"
36	8-#10	#4 at 9"
42	12-#10	#4 at 9"
48	12-#11	#4 at 9"
54	18-#10	#4 at 9"
60	22-#10	#4 at 9"

Figure 3.19: Reinforcement and internal dimensions of drilled shafts.

DRILLED SHAFT RETAINING WALL					
STA 342+53.27 TO 342+95.25 STA 343+38.75 TO 365+50					
WALL HEIGHT H (FT)		EMBEDMENT D (FT)			
48"	18"	48"	18"		
15	15	32.5	5		
STA 342+95.26 TO 343+38.75					
48"		48"			
15		32.5			
STA 365+50.01 TO 367+00					
48"	36"	18"	48"	36"	18"
15	15	15	33.5	33.5	5

DRILLED SHAFT RETAINING WALL DETAIL (N-T-S)
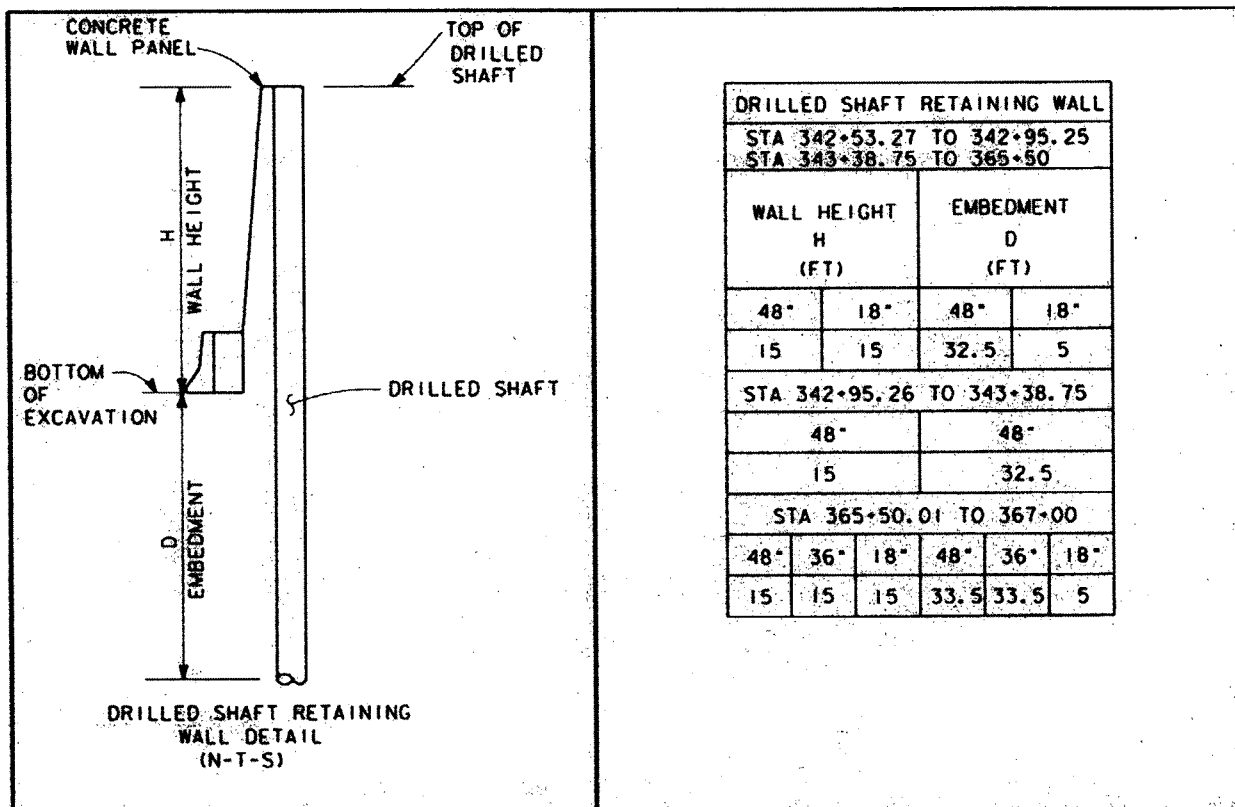
Figure 3.20: Typical cross section showing wall geometry.

27

3.3.3: IH 45 AT GREENS ROAD

3.3.3.1: Geotechnical Information

Two boring logs are available for the project site, drilled on November 2, 1987 and November 4, 1987. The soil profile consists of stiff to very stiff clay. At depths of 0 to 30 feet, the average liquid limit is approximately 40 and the average plasticity index is approximately 23, indicating low swell potential (Department of Army 1983). Measured moisture contents in the upper 30 feet were generally between 20 and 30 percent. The results of several unconfined and UU tests, run at confining pressures up to 5000 psf, indicate shear strengths of between 1500 and 3000 psf over the depth of the wall.

3.3.3.2: Design Information

The retaining wall at Greens Road and IH 45 consists of a combination of cantilever drilled shaft walls and tieback walls (Figure 3.21). For this investigation, only the cantilever drilled shaft wall is considered.
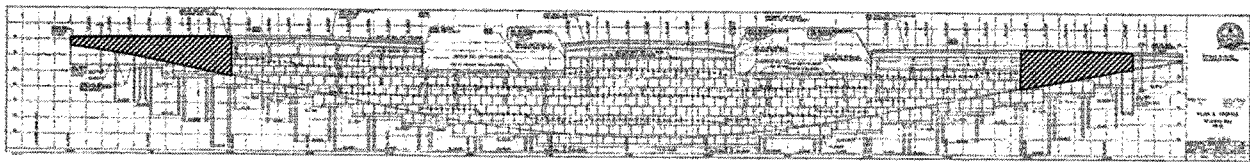
Figure 3.21: Composite sketch of project area. Shaded areas indicate locations of cantilever drilled shaft wall.

The cantilever drilled shaft wall consists of 18- to 36-inch diameter shafts with a spacing of 7 feet on center (Figure 3.22). Design heights range from approximately 3 to 10 feet, and shaft lengths range from approximately 15 to approximately 35 feet (Figure 3.23). Reinforcement details are provided in Figure 3.24. Wall facing consists of either cast-in-place concrete or precast concrete panels (Figure 3.25).
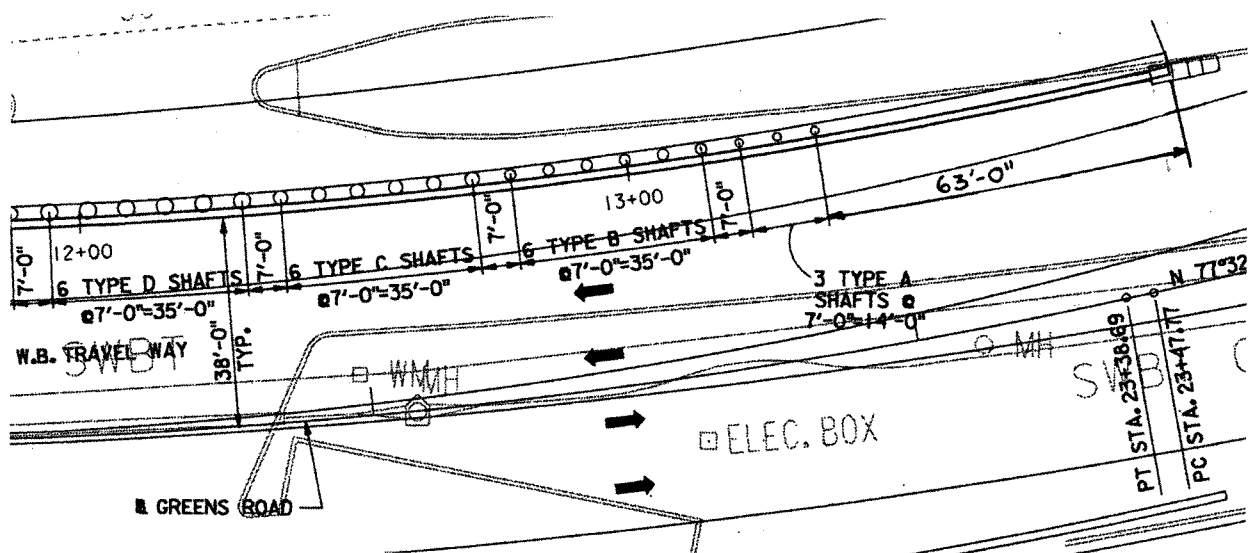
Figure 3.22: Plan view of typical drilled shaft layout.

28
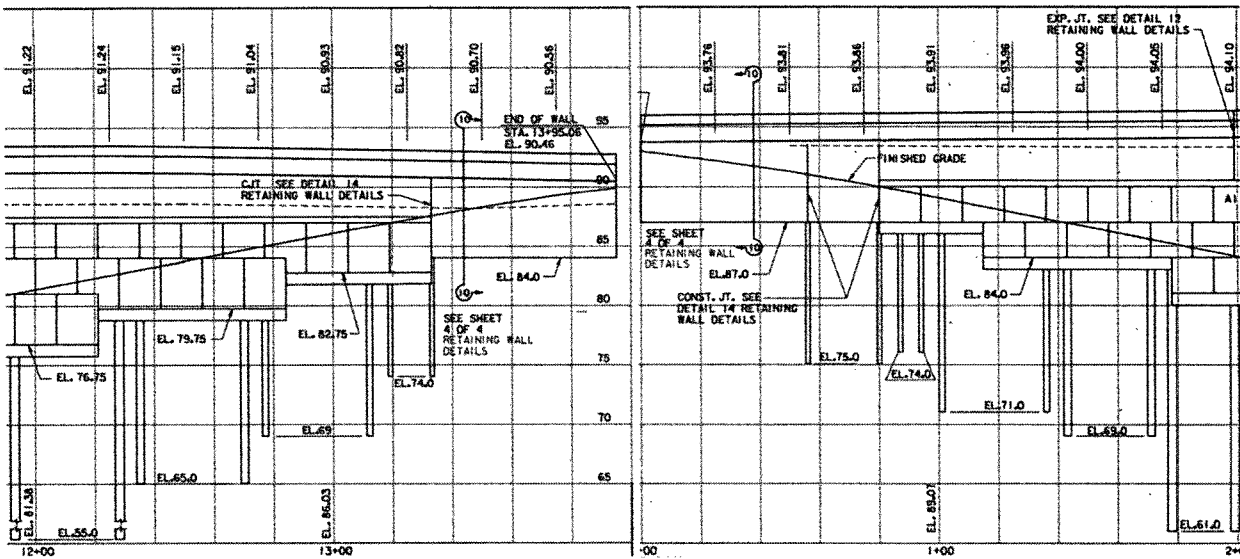
Figure 3.23: Profiles of two typical drilled shaft walls.

DRILLED SHAFT REINFORCEMENT TABLE

TYPE	DIAMETER (INCHES)	REINFORCING STEEL		SPIRAL (SIZE OF PITCH)	REQUIRED SECTION MODULUS (IN.³) *
		BARS A	BARS B		
A	18	4#7	1#6	#3 @ 18" PITCH	-
B	24	4#9	1#6	#3 @ 18" PITCH	-
C	30	6#7	1#6	#3 @ 18" PITCH	-
D	36	6#10	1#6	#3 @ 18" PITCH	-
E	30				30
F	30				40

* PER INDIVIDUAL CHANNEL

Figure 3.24: Drilled shaft reinforcement table.
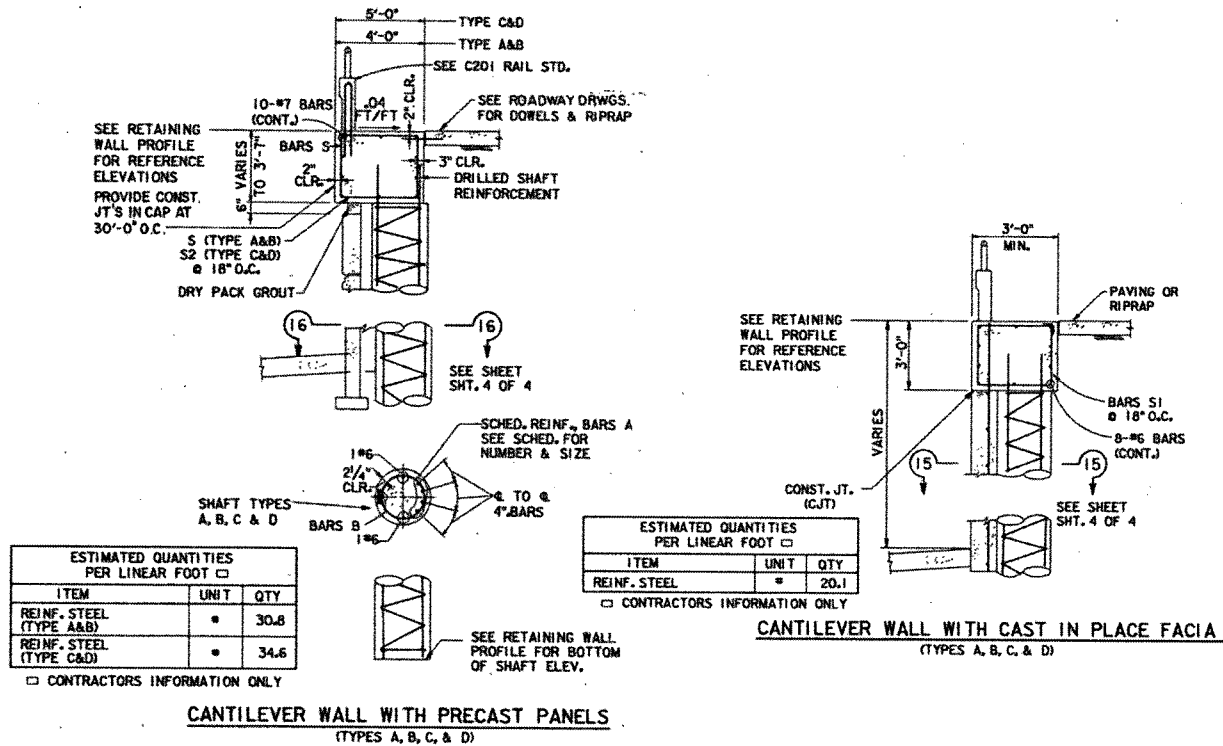
Figure 3.25: Details of precast and cast in place facing.

3.4: Performance Assessment

On June 30, 2011, an assessment was conducted at the wall site. This was limited to what could be safely conducted on foot without disrupting traffic flow. As a result, most insights into wall performance are qualitative.

3.4.1: FM 1960 AT KUYKENDAHL

From a distance, the wall appears to be in excellent condition (Figure 3.26). No obvious signs of distress were observed when walking along the top and base of the wall. A four-foot carpenter's level showed the panels to be vertical (Figure 3.27). This is consistent with the overall condition of the wall.

At all cantilever drilled shaft wall locations, the retained soil is covered with pavement for at least three traffic lanes (Figure 3.28). This could limit the potential for large moisture fluctuations near the wall. There are a few grass medians in the area with widths of approximately 4 feet. The nearest location for larger scale moisture infiltration is at the southeast corner of the intersection, at least 40 feet from the nearest shafts (Figure 3.29). A closer inspection of this unpaved area shows that some potential for water ponding exists, but offers no clear evidence that it has occurred near the wall (Figure 3.30). An inspection of the wall showed no indication of differential movements in the shafts nearest to the unpaved area.

Figure 3.26: View of north and southbound walls from FM 1960 bridge (facing southeast).

Figure 3.27: Wall facing was observed to be vertical and in good condition throughout the project area.

Figure 3.28: Paved area behind the wall. In all locations, pavement extends at least 30 feet behind the wall.

Figure 3.29: View of nearest location for moisture infiltration, at southeast corner of intersection.

Figure 3.30: Unpaved area near southeast corner of intersection.

3.4.2: US 59 at Hazard Street

A large scale view of the project area is presented in Figure 3.31. Because the facing was installed at an angle and is currently covered with dense vegetation, very little information about the shafts can be obtained from road level (Figure 3.32).

Figure 3.31: Large-scale view of project area (facing east). Sound wall is located above the main retaining structure.

Figure 3.32: Dense vegetation and batter angle on concrete facing panels. Sound wall is located above main retaining structure.

An inspection of the area behind the north wall near Hazard Street showed approximately 40 feet of exposed soil between the drilled shaft wall and the sound wall (Figure 3.33). Along the length of the project site, the distance between the drilled shaft wall and the sound wall can range from 0 to approximately 50 feet. At several locations, gaps were observed between the retained soil and the shafts (Figure 3.34). Some of these gaps were up to 8 feet deep and 1 foot back from the wall. The potential for water to drain into these gaps during heavy rainfall seems high.

The soil behind the wall is well vegetated and water flow is directed to large grates leading to an underdrain system. Of the walls we studied, this wall appears to have the largest potential for moisture change. Despite this, every measurement that could be made indicated that the wall is vertical and no major red flags were observed (apart from the gaps between the soil and the wall).

Figure 3.33: Approximately 40 feet of exposed soil behind the wall near Hazard Street (facing west).

Figure 3.34: Several gaps were observed between the shafts and the soil behind the wall.

3.4.3: IH 45 AT GREENS ROAD

From a distance, the wall appears to be in good condition (Figure 3.35). No obvious signs of structural distress were observed when walking along the top and base of the wall, but some superficial facing damage was observed. Most of this damage appears to be age-related and not caused by any structural distress on the wall. Some imperfections in the white concrete facing appear to be caused by seams in the concrete formwork (Figure 3.36). Some cracking and differential settlement is present in the sidewalks near the wall, but no signs of corresponding wall distress were observed at these locations (Figure 3.37). Some concrete cracking was seen at the connection between two facing elements (Figure 3.38).

Figure 3.35: View of current wall conditions, facing west.
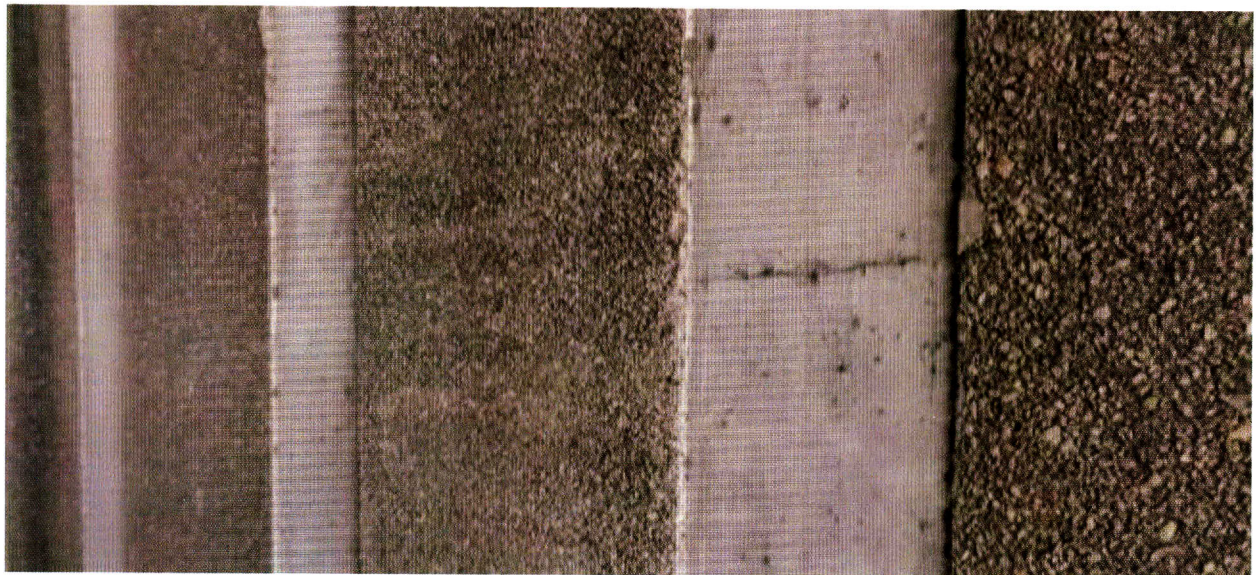
Figure 3.36: Example of imperfection in white concrete facing, possibly caused by a seam in the plywood formwork.

36

Figure 3.37: View of sidewalk damage along the base of the wall.

Figure 3.38: Some cracking was seen at the connection between two facing panels on the southwestern portion of the wall.

At least 30 feet of pavement covers the soil behind the wall in all directions (Figure 3.39). This could limit the potential for large moisture fluctuations near the wall. There are a few grass medians in the area, and runoff is directed into a system of storm drains. The extent of pavement near the wall is shown in Figure 3.40 and Figure 3.41.

Figure 3.39: View of pavement coverage along southwestern side of intersection (facing west).

Figure 3.40: Aerial view of western portion of wall (Google Inc., 2011).

Figure 3.41: Aerial view of eastern portion of wall (Google Inc., 2011).

3.5: LPILE Analyses

An LPILE analysis was performed for each wall in order to predict the effects of different loads applied to the walls. These analyses were done on the portions of the walls that were just cantilever drilled shafts. For clay layers within 5 feet below the excavation line, the undrained shear strength was reduced by 50 percent to account for the reduction in strength from the reduction in vertical stress due to the excavation of soil above. This reduction in strength is consistent with the TxDOT Manual. Loading scenarios considered were equivalent fluid pressures of 40, 60, and 80 psf/ft, each with a surcharge load directly behind the wall equivalent to two feet of 120-pcf soil.

3.5.1: FM 1960 AT KUYKENDAHL

Seven different shaft layouts were used for this analysis. Soil, shaft, and loading properties used in this analysis are presented in Table 3.1 and Table 3.2. Results show that the shaft layout that deflected the most relative to the height of the wall was the wall layout with shaft lengths of 52 feet and a height of 23 feet. At an equivalent fluid pressure of 40 psf/ft with two feet of soil surcharge, the top-of-wall deflection was 1.22 percent of the wall height (3.36 inches). At an equivalent fluid pressure of 80 psf/ft with two feet of surcharge, the wall deflected 2.96 percent (8.17 inches) of the wall height. The shortest shafts analyzed (L=31 ft, H=12 ft), deflected 0.16 percent of the wall height at an equivalent fluid pressure of 40 psf/ft. Results from the LPILE analysis are summarized in Figure 3.42 through Figure 3.48.

Table 3.1: Input Soil Properties for FM 1960 at Kuykendahl

Layers	Soil Model	Top Depth	Bot Depth	γ, pcf	φ', deg	c, psf
1	Stiff Clay	0	10	120	-	3600
2	Sand	10	25	110	35	0
3	Stiff Clay	25	35	120	-	3600
4	Sand	35	75	110	35	0

Table 3.2: Shaft and loading properties used in LPILE analysis for FM 1960 and Kuykendahl

Case	Shaft				Reinforcement						Concrete		Loading	
	Total Length, ft	Wall Height, ft	Diam, in	C-C Spacing (ft)	Size, #	# of bars	# per group	concrete cover, in	σ_y, psi	E, psi	σ_c, psi	Max Agg. Size, in	Load, psf/ft	Surcharge, ft
1	52	23	36	3.916667	11	18	2	5	60000	29000000	4000	0.75	40	2
2	52	23	36	3.916667	11	18	2	5	60000	29000000	4000	0.75	60	2
3	52	23	36	3.916667	11	18	2	5	60000	29000000	4000	0.75	80	2
4	49	22	36	3.916667	11	16	2	5	60000	29000000	4000	0.75	40	2
5	49	22	36	3.916667	11	16	2	5	60000	29000000	4000	0.75	60	2
6	49	22	36	3.916667	11	16	2	5	60000	29000000	4000	0.75	80	2
7	46	20	36	3.916667	11	14	1	5	60000	29000000	4000	0.75	40	2
8	46	20	36	3.916667	11	14	1	5	60000	29000000	4000	0.75	60	2
9	46	20	36	3.916667	11	14	1	5	60000	29000000	4000	0.75	80	2
10	43	18	36	3.916667	11	12	1	5	60000	29000000	4000	0.75	40	2
11	43	18	36	3.916667	11	12	1	5	60000	29000000	4000	0.75	60	2
12	43	18	36	3.916667	11	12	1	5	60000	29000000	4000	0.75	80	2
13	39	16	36	3.916667	9	12	1	5	60000	29000000	4000	0.75	40	2
14	39	16	36	3.916667	9	12	1	5	60000	29000000	4000	0.75	60	2
15	39	16	36	3.916667	9	12	1	5	60000	29000000	4000	0.75	80	2
16	36	14	36	3.916667	9	10	1	5	60000	29000000	4000	0.75	40	2
17	36	14	36	3.916667	9	10	1	5	60000	29000000	4000	0.75	60	2
18	36	14	36	3.916667	9	10	1	5	60000	29000000	4000	0.75	80	2
19	31	12	36	3.916667	9	10	1	5	60000	29000000	4000	0.75	40	2
20	31	12	36	3.916667	9	10	1	5	60000	29000000	4000	0.75	60	2
21	31	12	36	3.916667	9	10	1	5	60000	29000000	4000	0.75	80	2
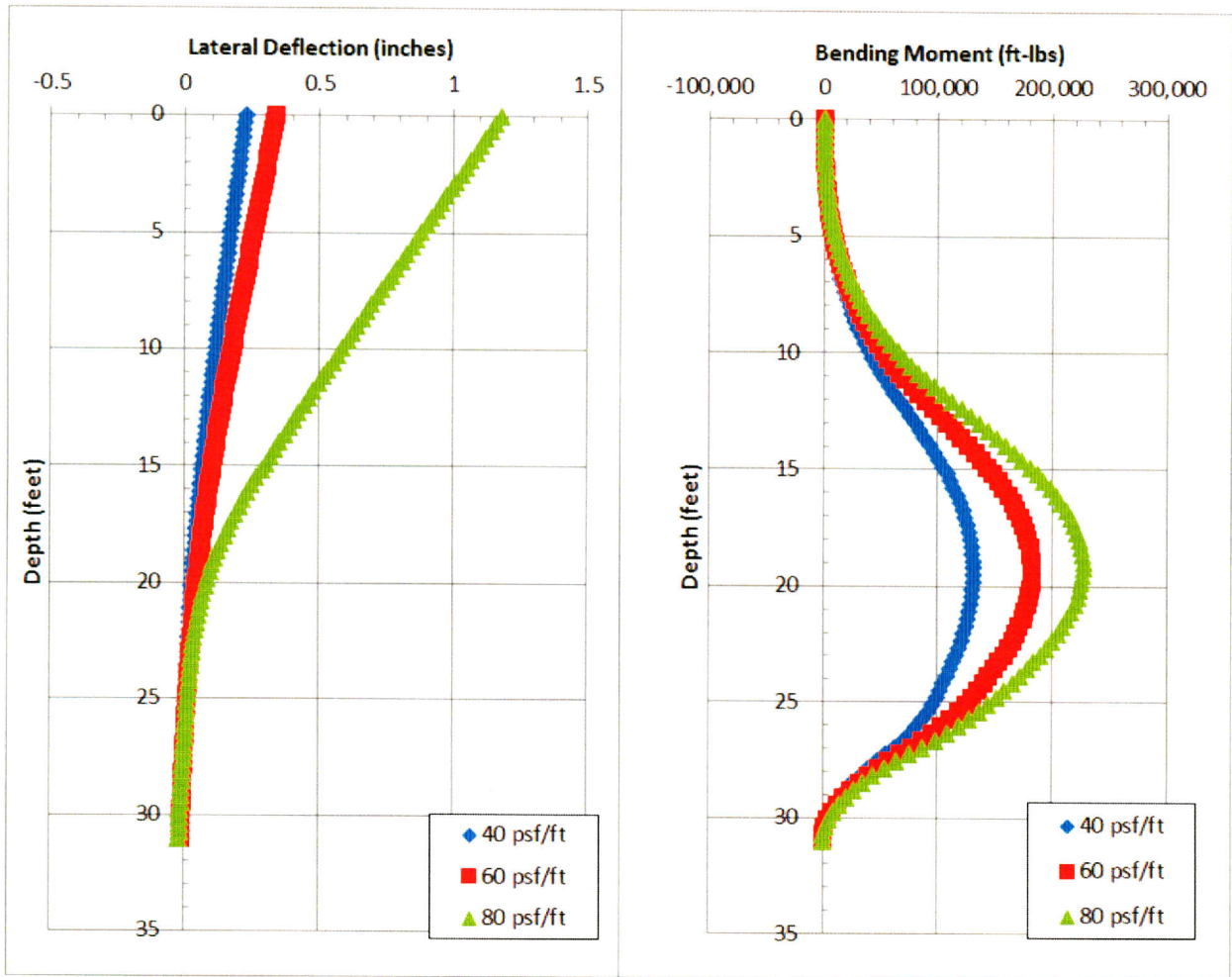
Figure 3.42: Results of LPILE analysis for FM 1960 at Kuykendahl; shaft length = 31 feet; wall height = 12 feet.
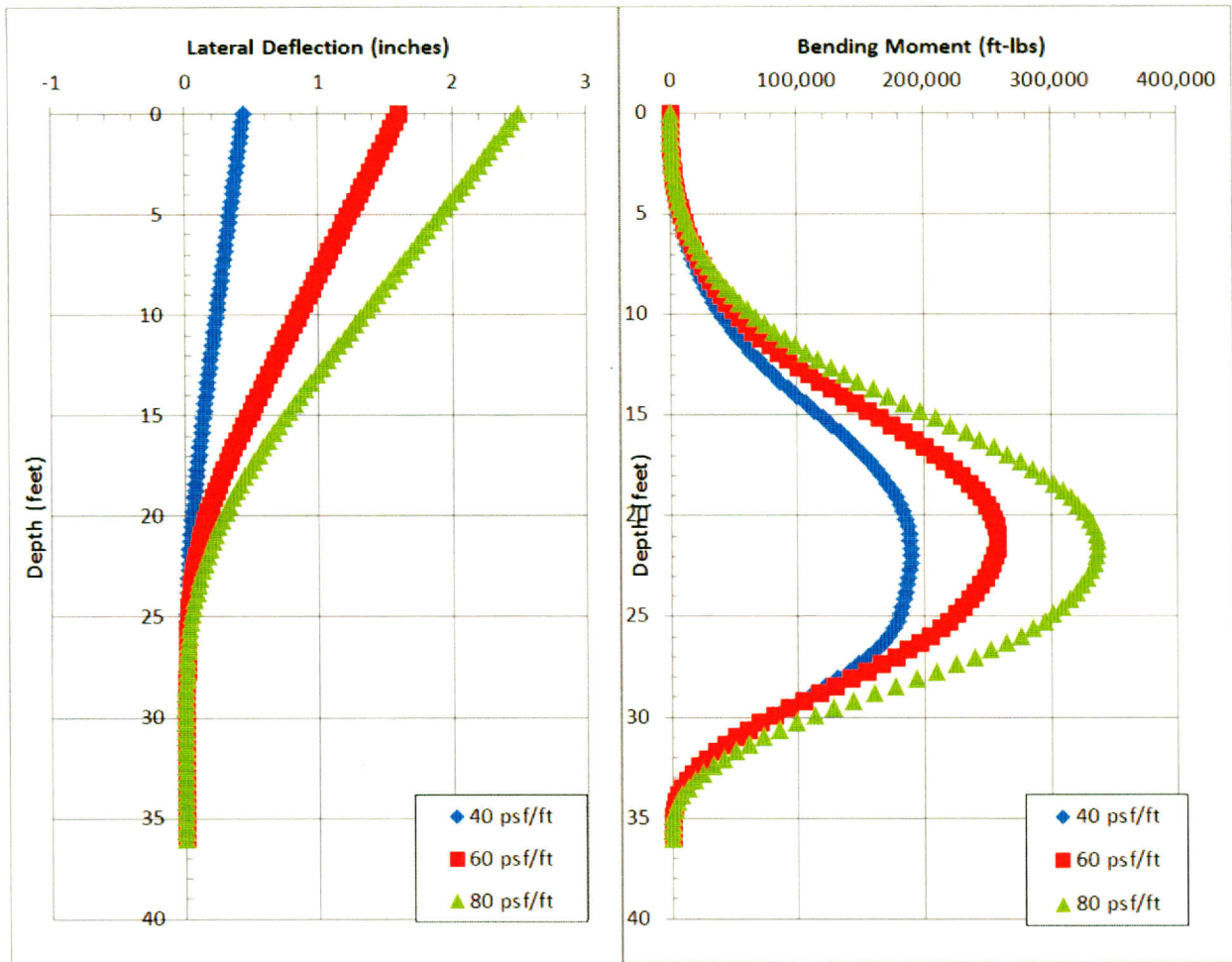
Figure 3.43: Results of LPILE analysis for FM 1960 at Kuykendahl; shaft length = 36 feet; wall height = 14 feet.
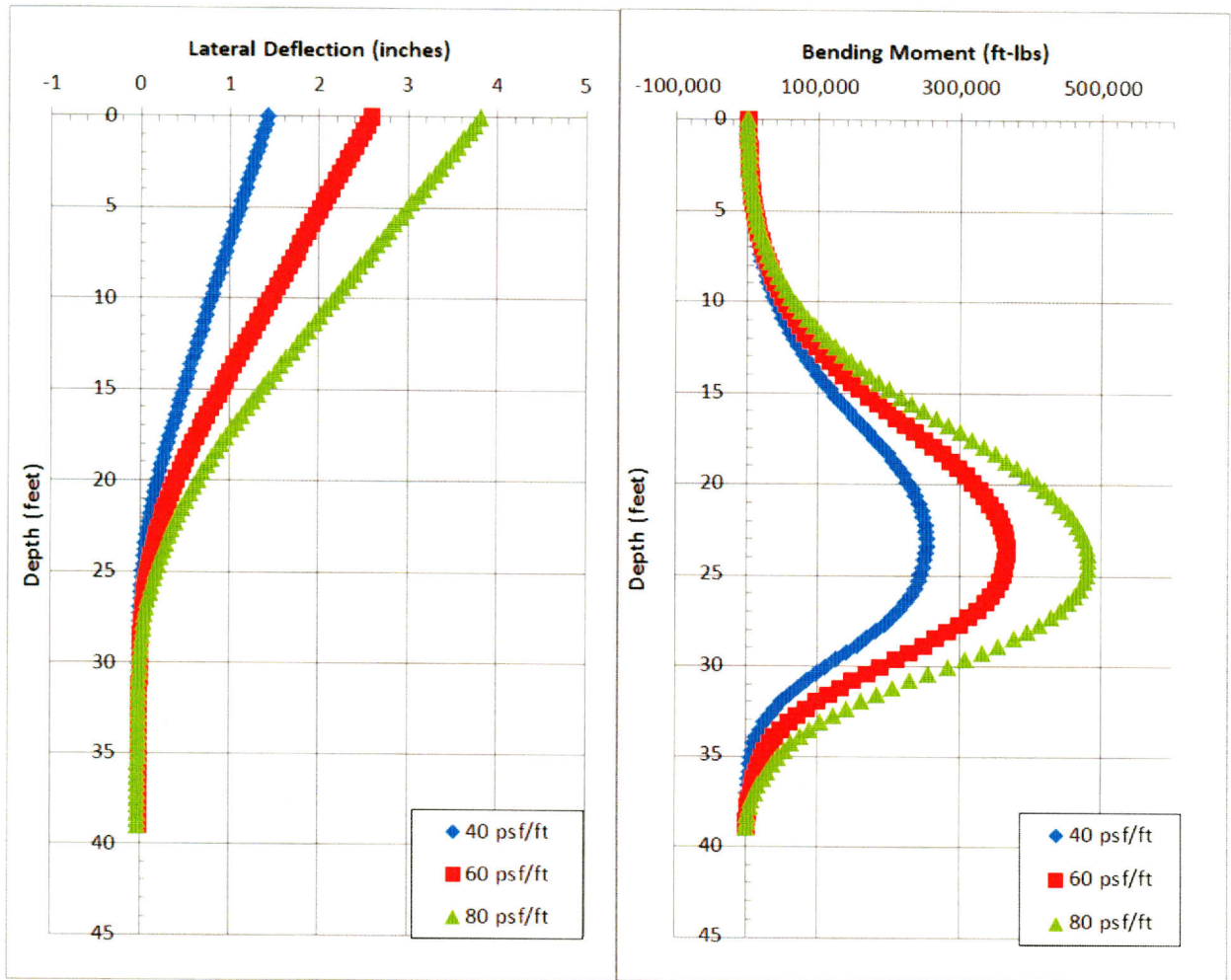
Figure 3.44: Results of LPILE analysis for FM 1960 at Kuykendahl; shaft length = 39 feet; wall height = 16 feet.
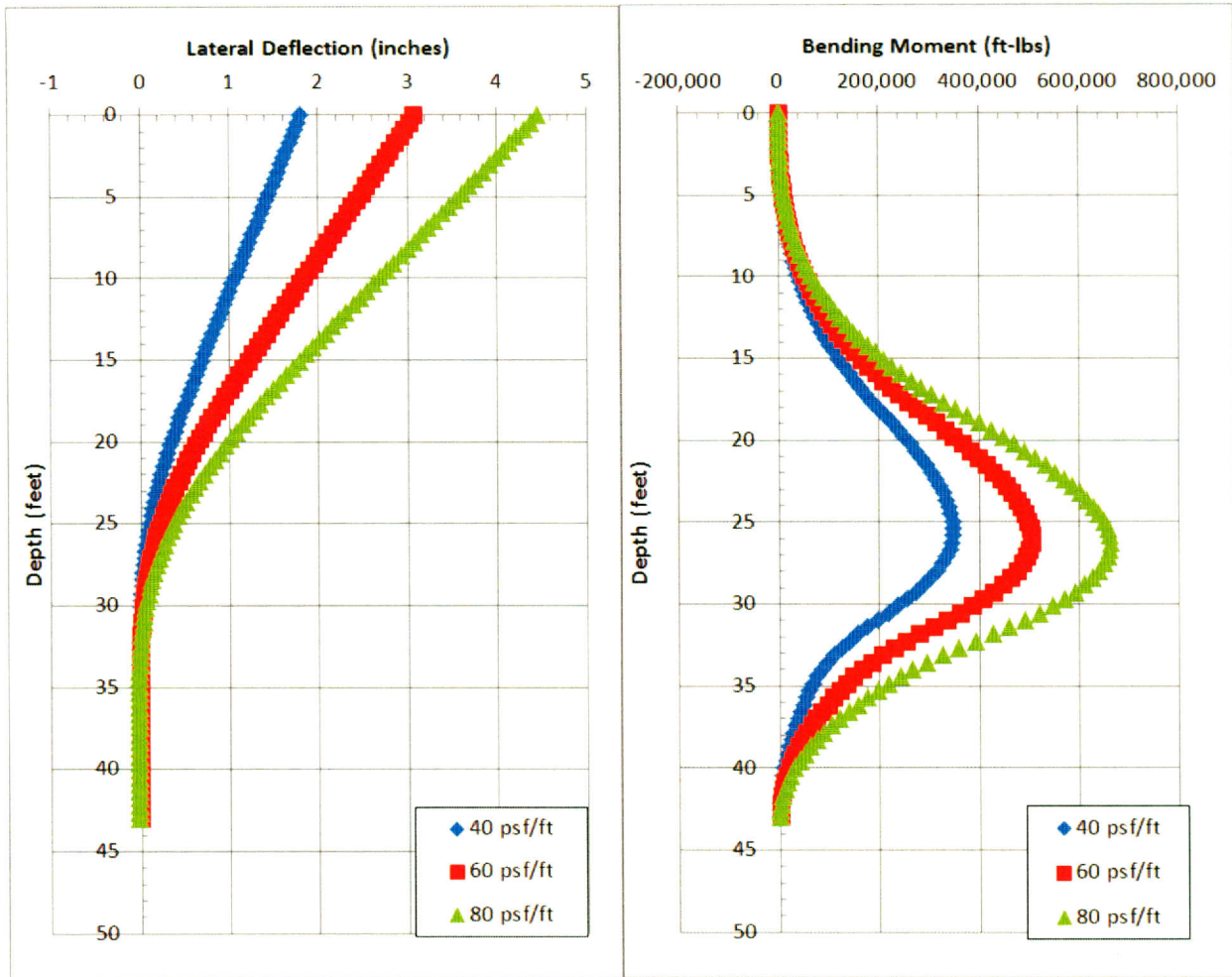
Figure 3.45: Results of LPILE analysis for FM 1960 at Kuykendahl; shaft length = 43 feet; wall height = 18 feet.

45
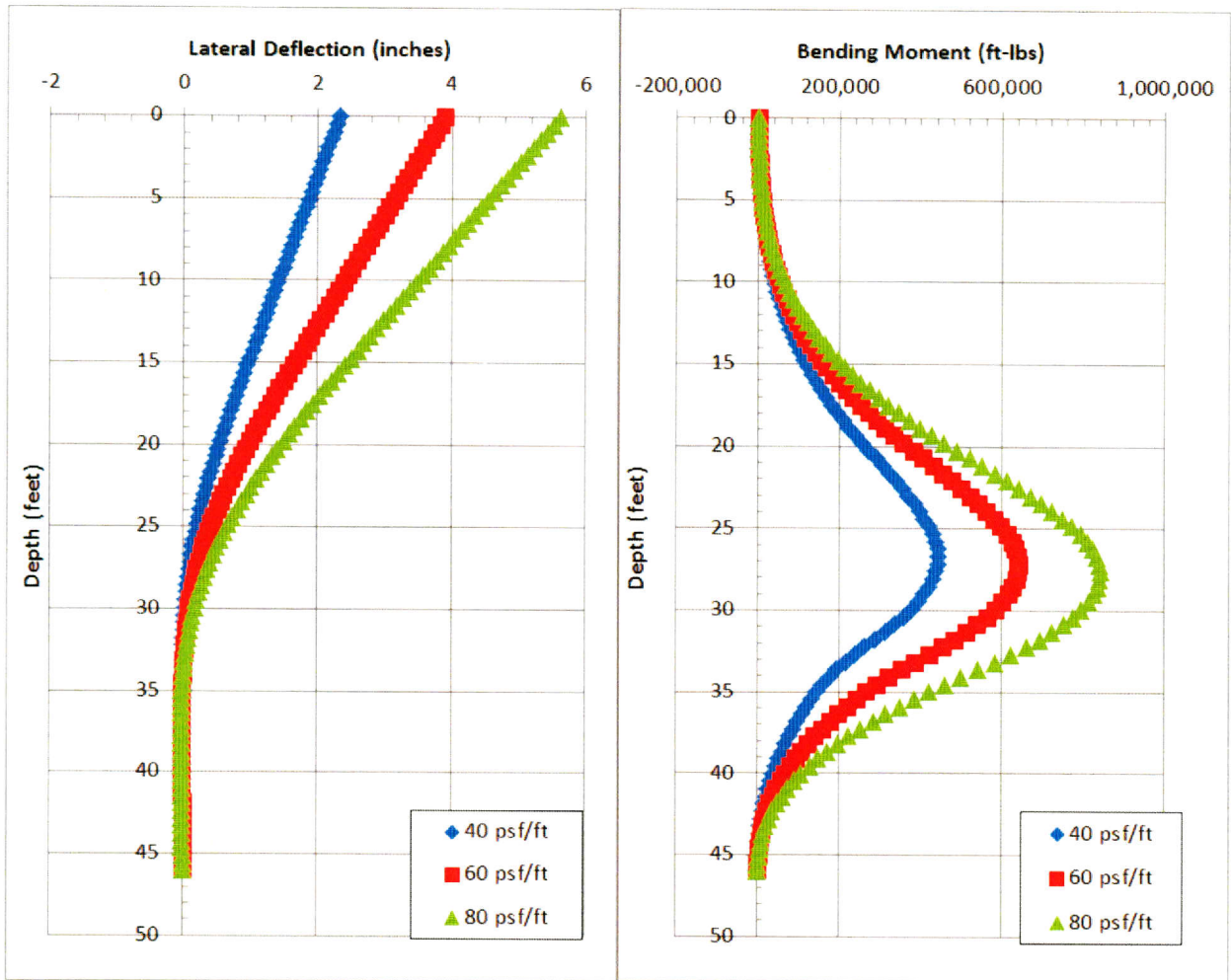
Figure 3.46: Results of LPILE analysis for FM 1960 at Kuykendahl; shaft length = 46 feet; wall height = 20 feet.
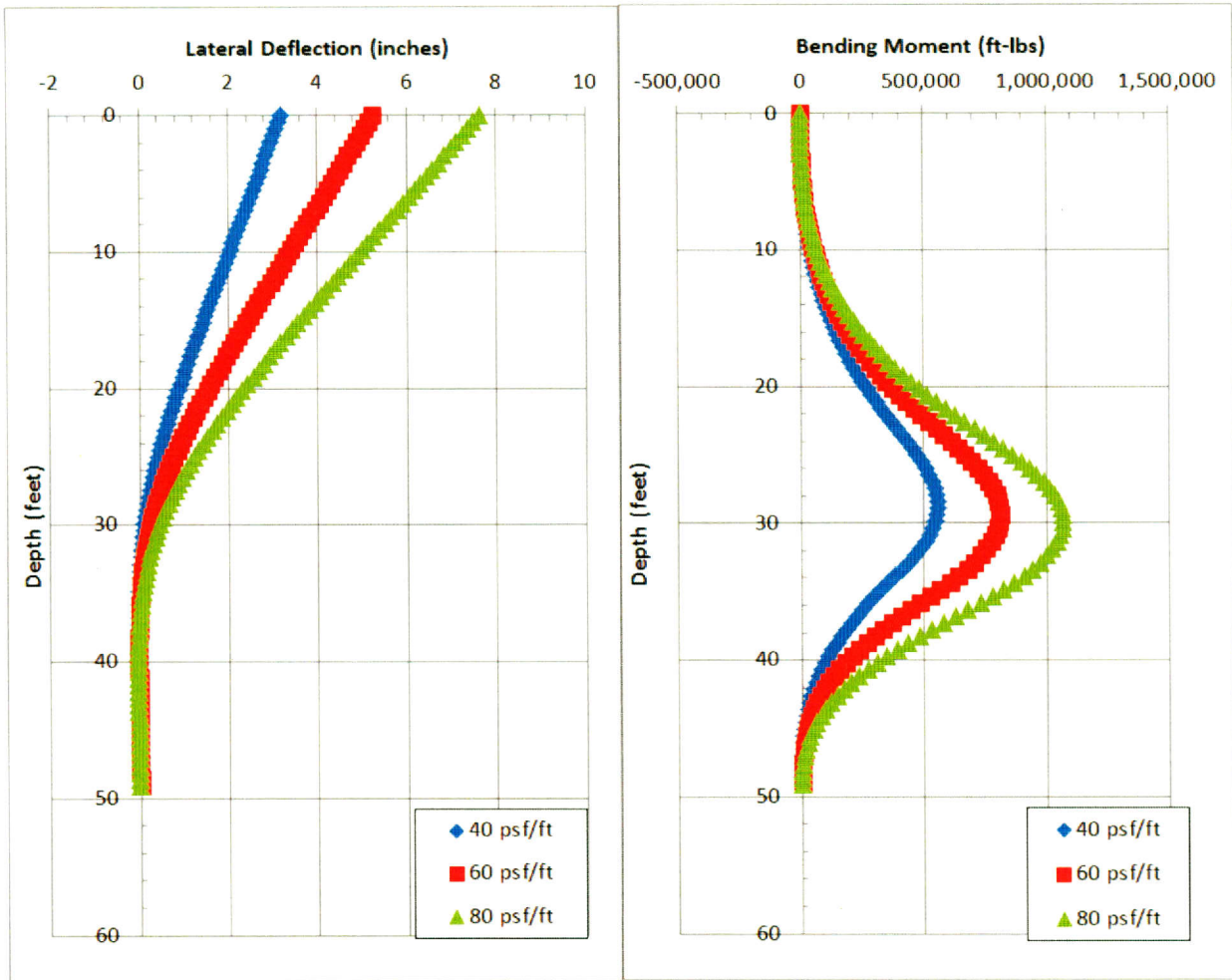
Figure 3.47: Results of LPILE analysis for FM 1960 at Kuykendahl; shaft length = 49 feet; wall height = 22 feet.
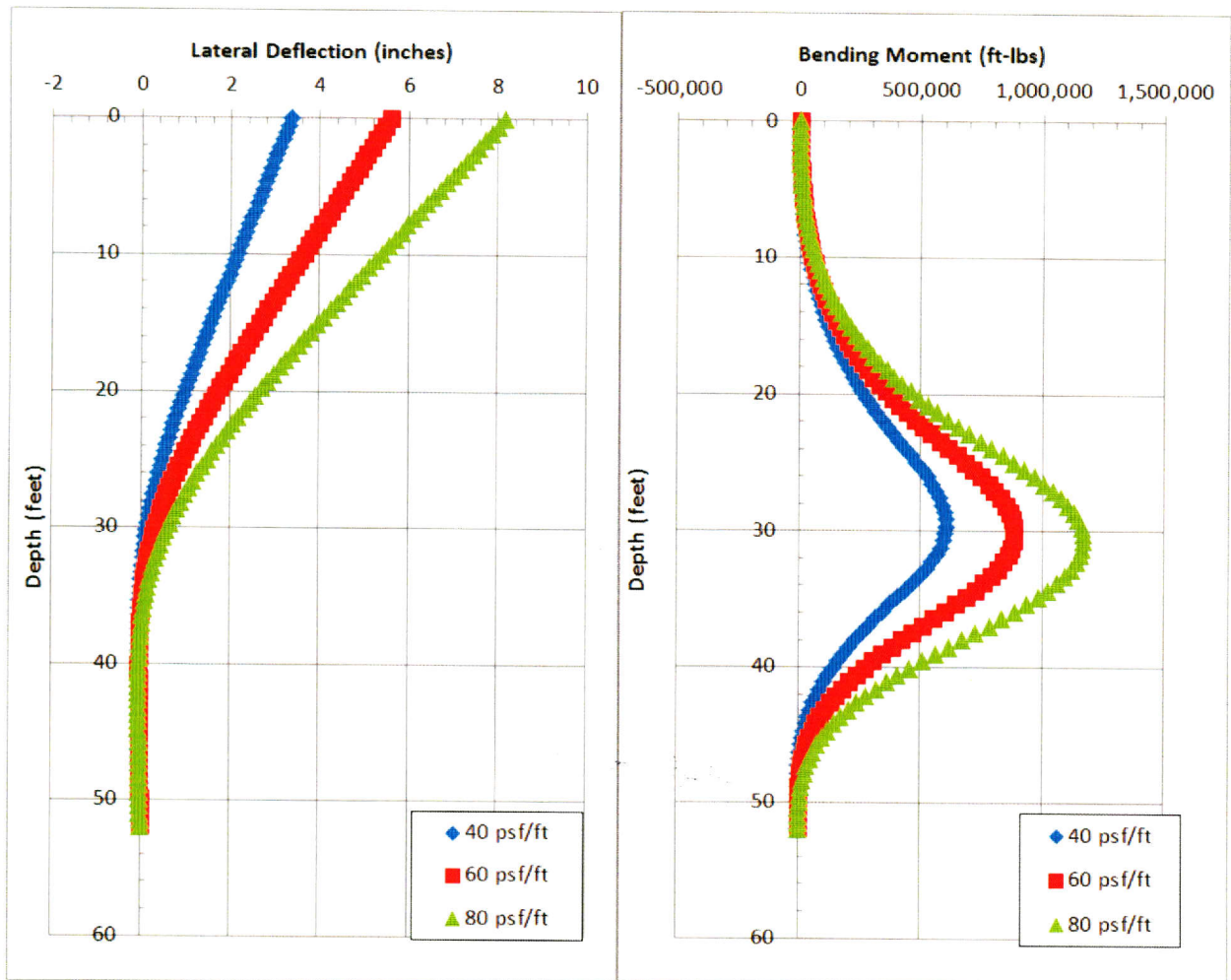
Figure 3.48: Results of LPILE analysis for FM 1960 at Kuykendahl; shaft length = 52 feet; wall height = 23 feet.

3.5.2: US 59 AT HAZARD STREET

Because of the large size of the shafts and potential for moisture changes on the project site, the wall layout was analyzed using one additional loading scenario consisting of an equivalent fluid pressure of 100 psf/ft with two feet of surcharge. Soil, shaft, and loading properties used in this analysis are presented in Table 3.3 and Table 3.4. Results show that the wall will not deflect more than 1 percent of the wall height for any of the loading conditions. Even at an equivalent fluid pressure of 100 psf/ft with two feet of surcharge, the wall deflects just 0.3 percent of the wall height (0.55 inches). Results from the LPILE analysis are summarized in Figure 3.49.

Table 3.3: Soil properties used in LPILE analysis for US 59 and Hazard St.

Layers	Soil Model	Top Depth	Bot Depth	γ, pcf	c, psf
1	Clay	0	7	125	4400
2	Clay	7	11.5	120	2500
3	Clay	11.5	16	130	2150
4	Clay	16	21.5	135	3500
5	Clay	21.5	26	130	2800
6	Clay	26	75	125	2700

Table 3.4: Shaft and loading properties used in LPILE analysis for US 59 and Hazard St.

| Case | Shaft | | | | Reinforcement | | | | | | Concrete | | Loading | |
	Total Length, ft	Wall Height, ft	Diam, in	C-C Spacing (ft)	Size, #	# of bars	# per group	concrete cover, in	σy, psi	E, psi	σc, psi	Max Agg. Size, in	Load, psf/ft	Surcharge, ft
1	47.5	15	48	5	11	12	1	5	60000	29000000	4000	0.75	40	2
2	47.5	15	48	5	11	12	1	5	60000	29000000	4000	0.75	60	2
3	47.5	15	48	5	11	12	1	5	60000	29000000	4000	0.75	80	2
4	47.5	15	48	5	11	12	1	5	60000	29000000	4000	0.75	100	2
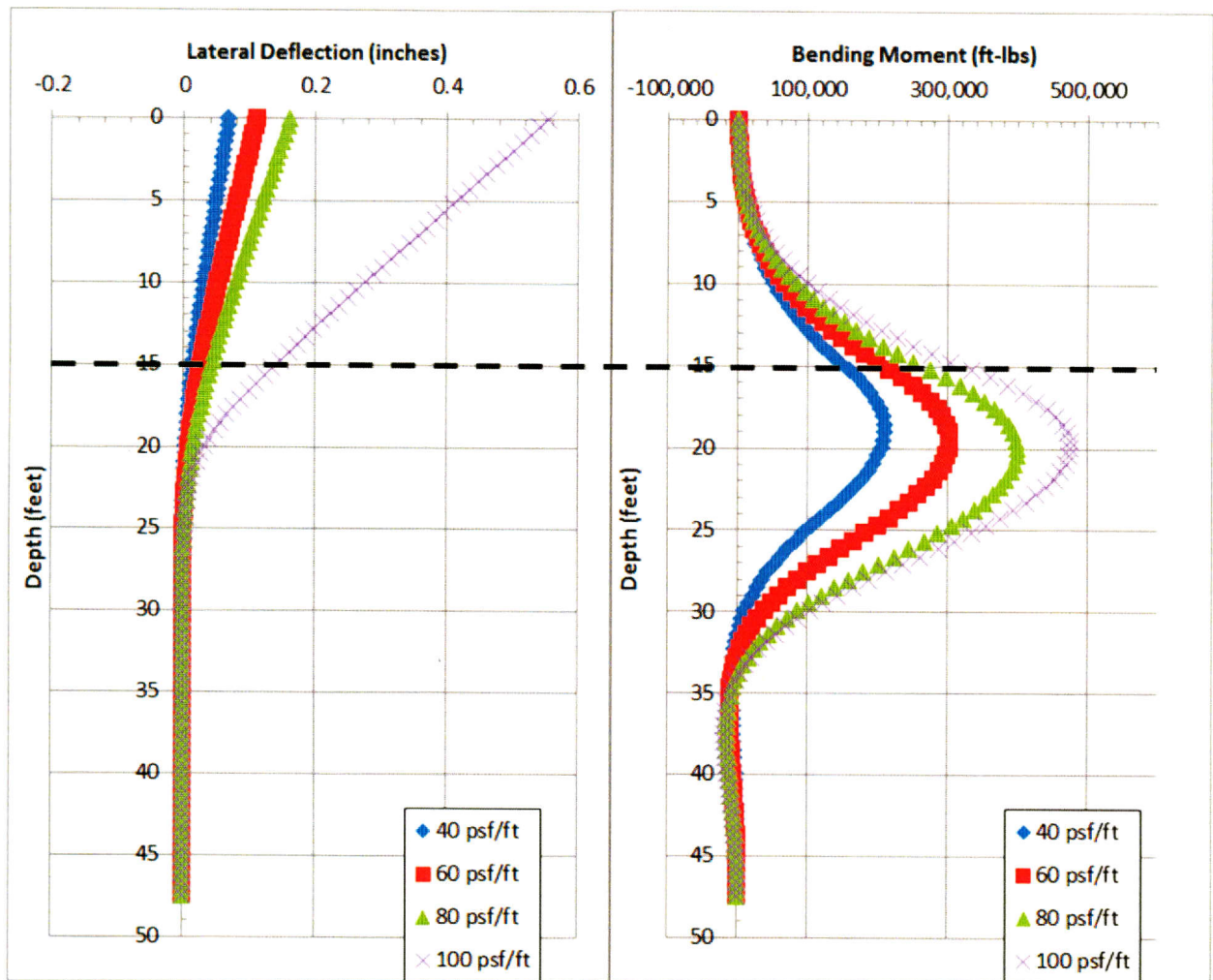
Figure 3.49: Results of LPILE analysis for US 59 and Hazard Street; shaft length = 47.5 feet, wall height = 15 feet. Dashed line indicates excavation depth.

3.5.3: IH 45 AT GREENS ROAD

Four different shaft layouts were used for this analysis. Soil, shaft, and loading properties are presented in Table 3.5 and Table 3.6. Results show that for the 40 psf/ft loading scenario, the top-of-wall deflections are less than 1 percent of the wall height for each of the four different layouts. For wall heights of 5, 7, and 9 feet (total shaft lengths of 18, 19, and 25 feet, respectively), the top-of-wall deflections did not exceed 1 percent of the wall height until the 80 psf/ft loading scenario. For a wall height of 11 feet (total shaft length of 34 feet), the maximum top-of-wall deflection was 0.9 percent of the wall height for the 80 psf/ft loading scenario.

It should be noted that determining the shaft lengths and wall heights were estimated based on the design files provided by TxDOT. This estimation was due to the lack of clear documentation in the design files. The analysis of the wall with a height of 7 feet and a total shaft length of 19 feet shows that embedment depth is not sufficient to reach fixity for all the loading scenarios. It is likely that either the as-built wall height was smaller than reported, or the as-built shaft length was larger than reported, but without supporting documents that clearly indicate the

50

layout of the shafts, this cannot be determined with certainty. Results from the LPILE analysis are summarized in Figure 3.50 through Figure 3.53.

Table 3.5: Soil properties used in LPILE analysis for IH 45 at Greens Rd.

Layers	Soil Model	Top Depth	Bot Depth	Location 1 γ, pcf	Location 1 c, psf	Location 2 γ, pcf	Location 2 c, psf	Aveage γ, pcf	Aveage c, psf
1	Stiff Clay	0	5	125	1510	125	1650	125	1580
2	Stiff Clay	5	8	125	850	125	1850	125	1350
3	Stiff Clay	8	14	125	2000	125	2750	125	2375
4	Clay	14	24	130	1600	125	1080	127.5	1340
5	Clay	24	42	130	2860	125	2860	127.5	2860

Table 3.6: Shaft and loading properties used in LPILE analysis for IH 45 at Greens Rd.

Case	Shaft Total Length, ft	Shaft Wall Height, ft	Shaft Diam, in	Shaft C-C Spacing (ft)	Reinforcement Size, #	Reinforcement # of bars	Reinforcement # per group	Reinforcement concrete cover, in	σ_y, psi	E, psi	Concrete σ_c, psi	Concrete Max Agg. Size, in	Loading Load, psf/ft	Loading Surcharge, ft
1	18	5	18	8	7	7	1	2.25	60000	29000000	4000	0.75	40	2
2	18	5	18	8	7	7	1	2.25	60000	29000000	4000	0.75	60	2
3	18	5	18	8	7	7	1	2.25	60000	29000000	4000	0.75	80	2
4	19	7	24	7	9	7	1	2.25	60000	29000000	4000	0.75	40	2
5	19	7	24	7	9	7	1	2.25	60000	29000000	4000	0.75	60	2
6	19	7	24	7	9	7	1	2.25	60000	29000000	4000	0.75	80	2
7	25	9	30	7	7	9	1	2.25	60000	29000000	4000	0.75	40	2
8	25	9	30	7	7	9	1	2.25	60000	29000000	4000	0.75	60	2
9	25	9	30	7	7	9	1	2.25	60000	29000000	4000	0.75	80	2
10	34	11	36	7	10	9	1	2.25	60000	29000000	4000	0.75	40	2
11	34	11	36	7	10	9	1	2.25	60000	29000000	4000	0.75	60	2
12	34	11	36	7	10	9	1	2.25	60000	29000000	4000	0.75	80	2

51
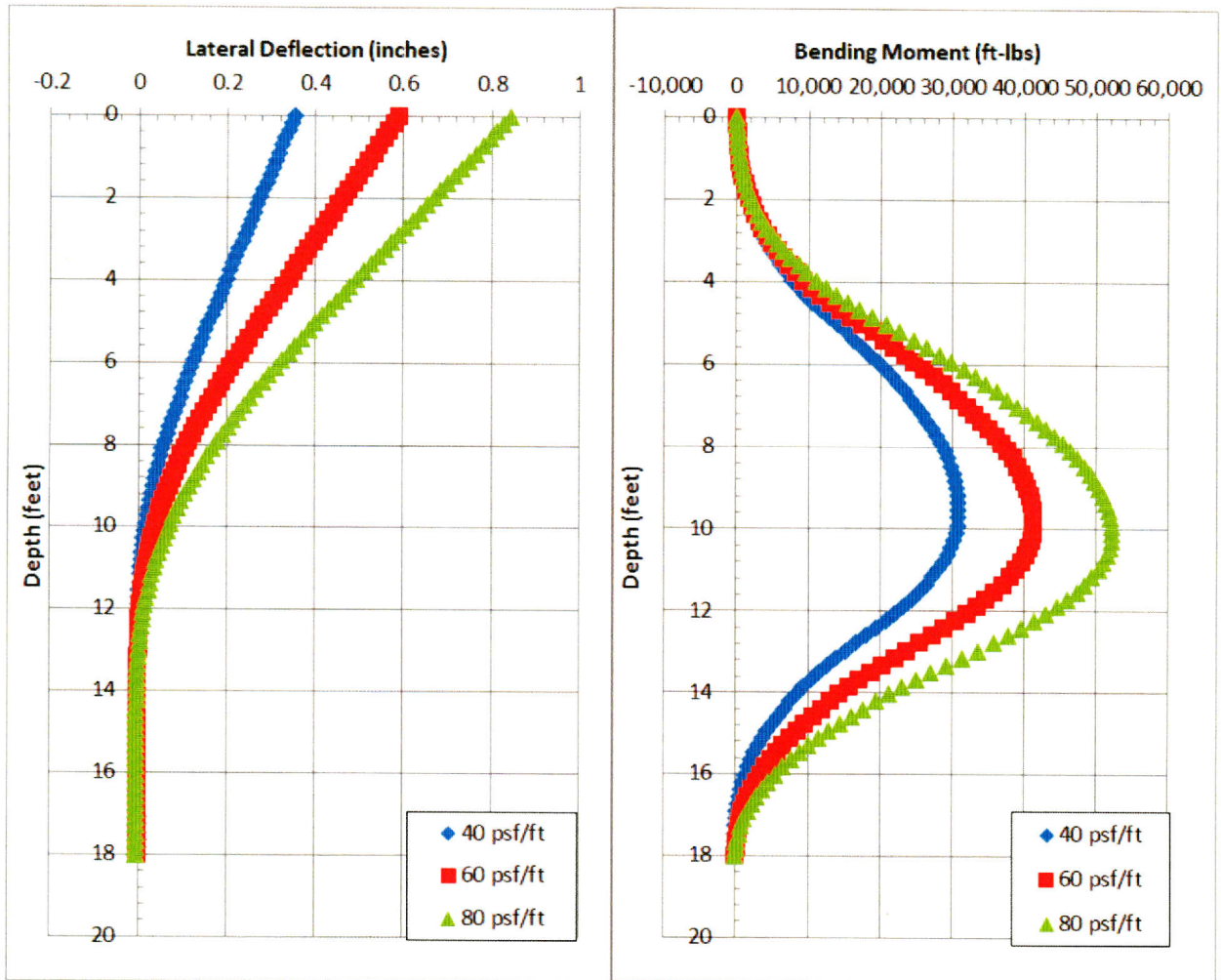
Figure 3.50: Results of LPILE analysis for Greens Rd at IH 45; shaft length = 18 feet, wall height = 5 feet.
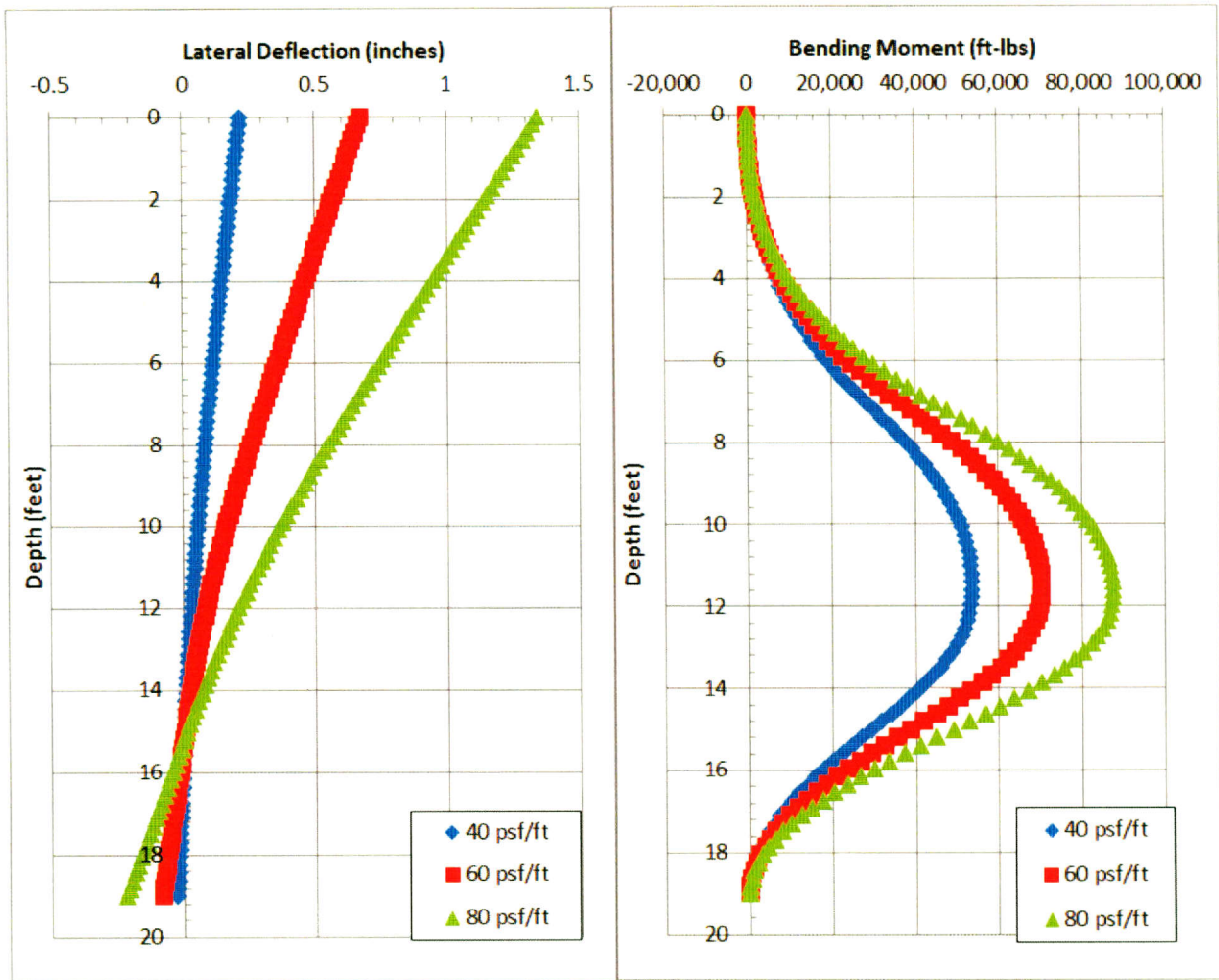
Figure 3.51: Results of LPILE analysis for Greens Rd at IH 45; shaft length = 19 feet, wall height = 7 feet.
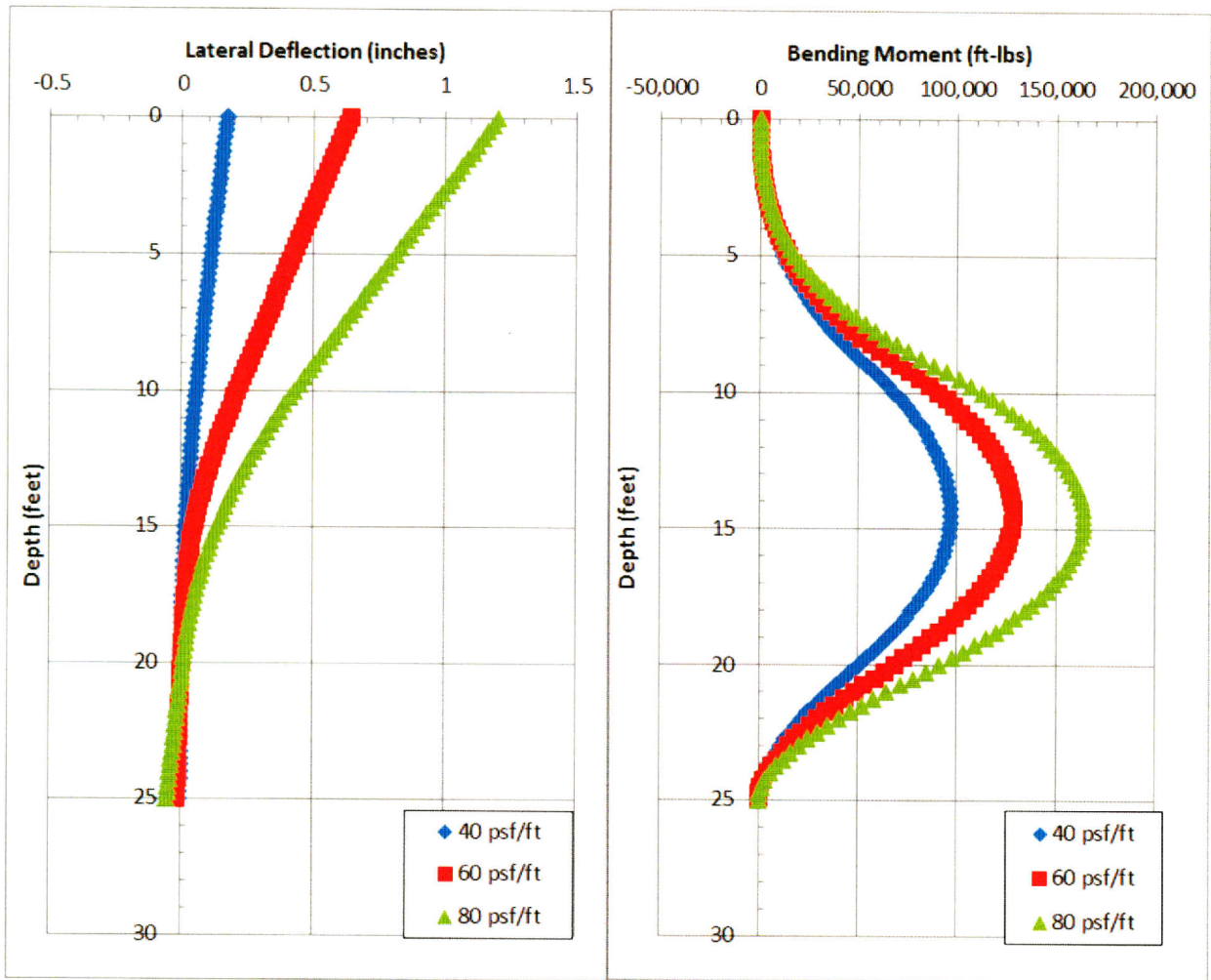
Figure 3.52: Results of LPILE analysis for Greens Rd at IH 45; shaft length = 25 feet, wall height = 9 feet.
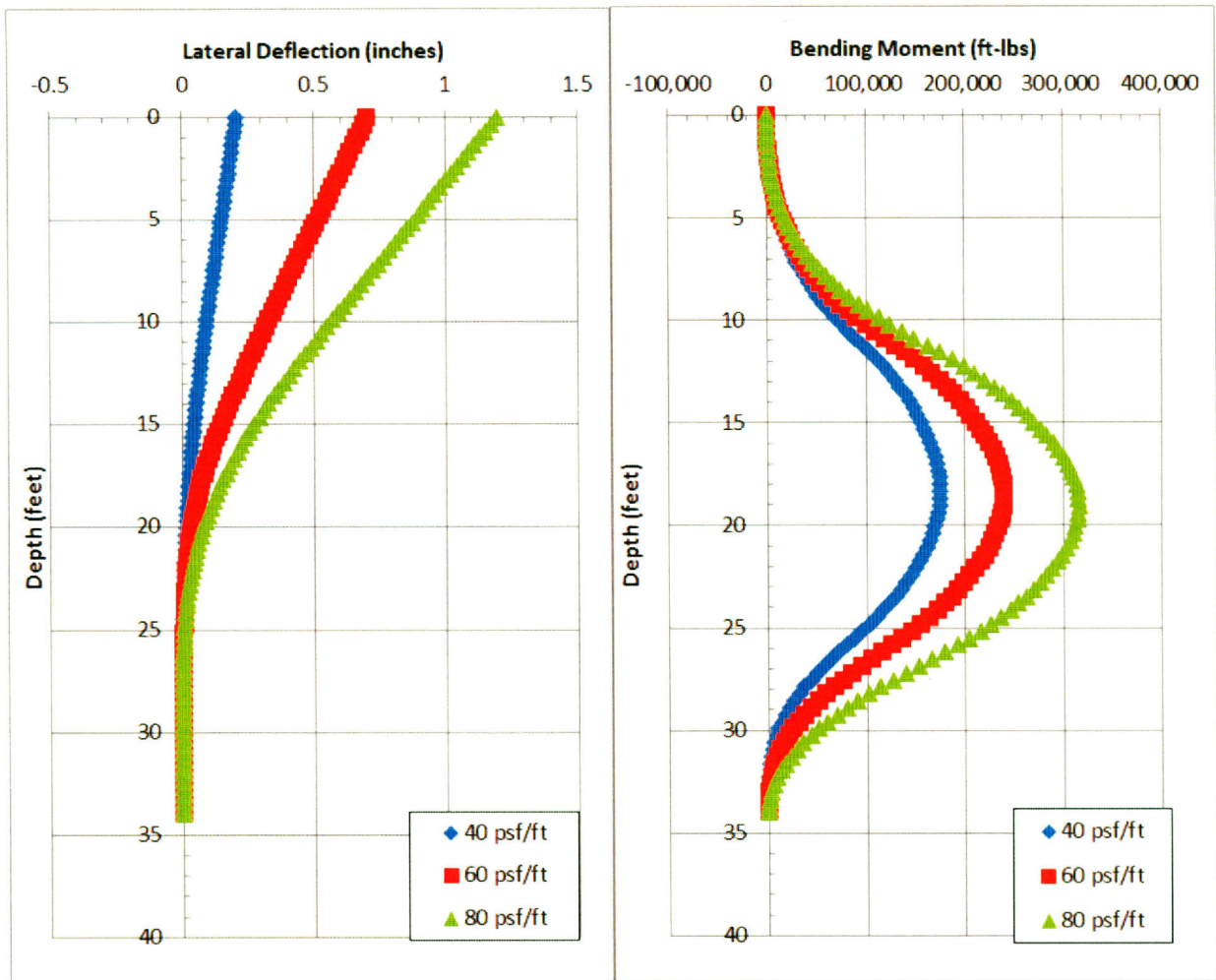
Figure 3.53: Results of LPILE analysis for Greens Rd at IH 45; shaft length = 25 feet, wall height = 11 feet.

3.6: Conclusions

The walls we have assessed in this study are generally representative of typical drilled shaft walls in Texas. The three walls have been in service for 14, 9, and 2 years, respectively, and have cantilevered heights ranging from 5 to 23 feet. A field inspection of each wall revealed no obvious signs of significant distress. Based on LPILE analyses of these walls, earth pressures greater than a linear increase of 80 psf/ft would likely be required to produce significant distress that could be readily observed.

CHAPTER 4: DESIGN AND CONSTRUCTION OF INSTRUMENTED TEST WALL

4.1: Location of Test Wall

To allow for complete control of project scheduling and access to the test site, a full-scale test wall was constructed specifically for this project. The Lymon C. Reese research wall is located in Manor, Texas, on the property of R&L Transfer & Storage Co., Inc. (Figure 4.1). The site plan in Figure 4.2 shows the location of the test wall.
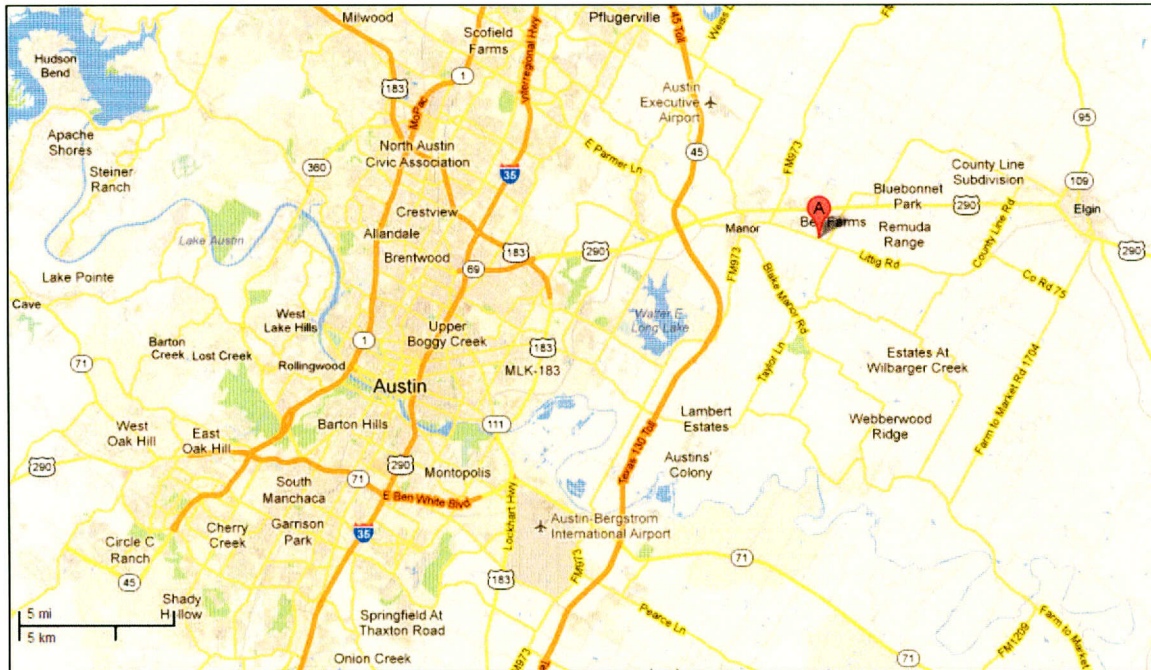
Figure 4.1: Location of full-scale test wall (Google, Inc.).
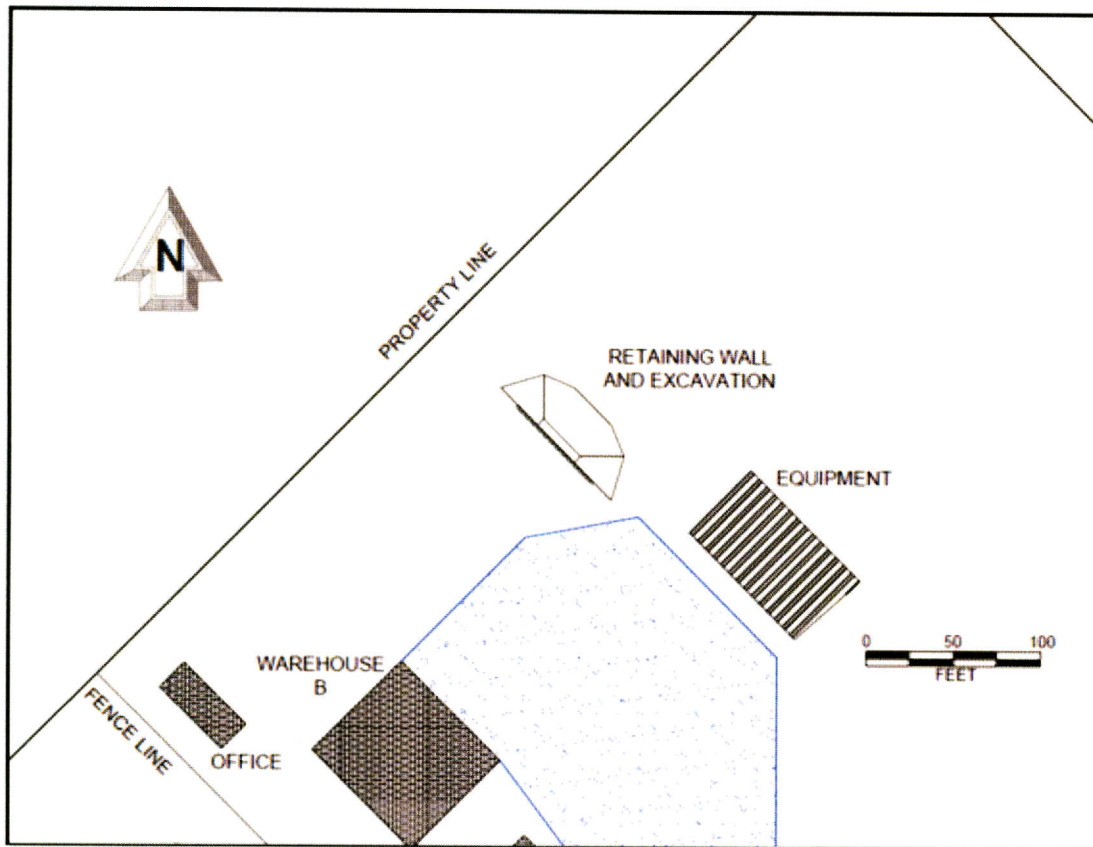
Figure 4.2: Detailed site plan with location of test wall.

4.2: Subsurface Conditions

4.2.1: OVERVIEW

The test wall is underlain by approximately 50 feet of the Taylor Formation, a highly plastic, stiff, fissured clay. A sample of the Taylor Formation from the project site is pictured in Figure 4.3.

Figure 4.3: Unweathered Taylor Clay from the project site in Manor.

4.2.2: PRELIMINARY GEOTECHNICAL INVESTIGATION (JANUARY 2010)

Three 50-foot deep soil borings were drilled in January 2010, a relatively wet season. Both Texas Cone Penetrometer (TCP) testing and Standard Penetration Testing were performed to provide information consistent with the standard of practice in Texas. An inclinometer was installed in one boring and a piezometer in another. The details for this investigation are provided in Ellis (2011), which is included in Appendix K.

The subsurface to a depth of 50 feet is a stiff-to-hard, highly plastic clay. The upper 6 feet of clay is weathered and dark brown, while underlying unweathered clay is yellow (Figure 4.3). The water table is approximately 8 feet below the ground surface based on the piezometer (note that it took several months for the piezometer to reach equilibrium with the formation after it was installed).

TCP blow counts are shown in Figure 4.4 and Atterberg limits and natural moisture contents are shown in Figure 4.5. The liquid limit in the weathered zone ranges from about 50 to 70 percent, while it is generally greater than 100 percent in the unweathered zone. The plastic limit ranges from about 20 to 30 percent. Natural water contents at the time of investigation ranged from 20 to 40 percent (Figure 4.5). The total unit weight in the upper 15 feet averaged about 125 pcf.
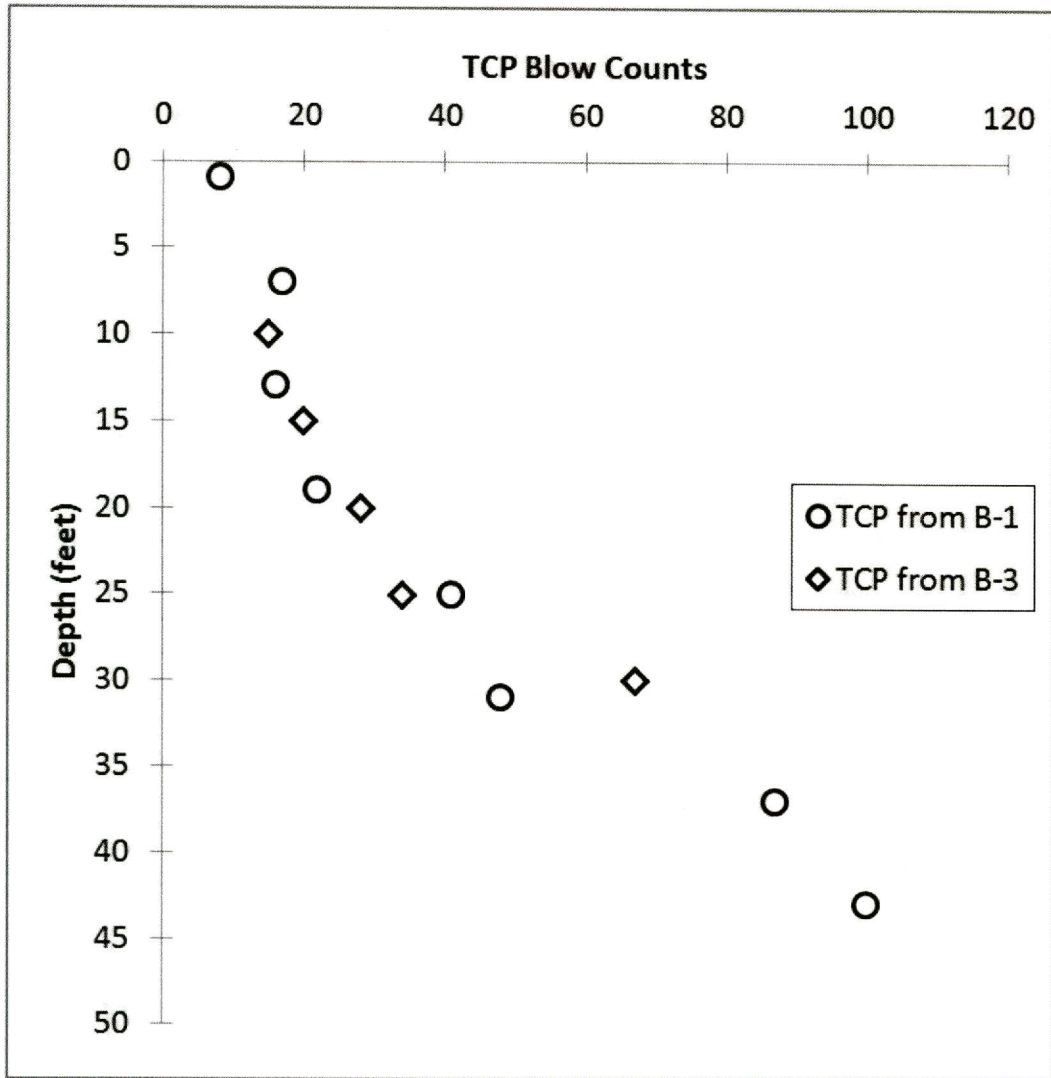
Figure 4.4: TCP blow counts versus depth.
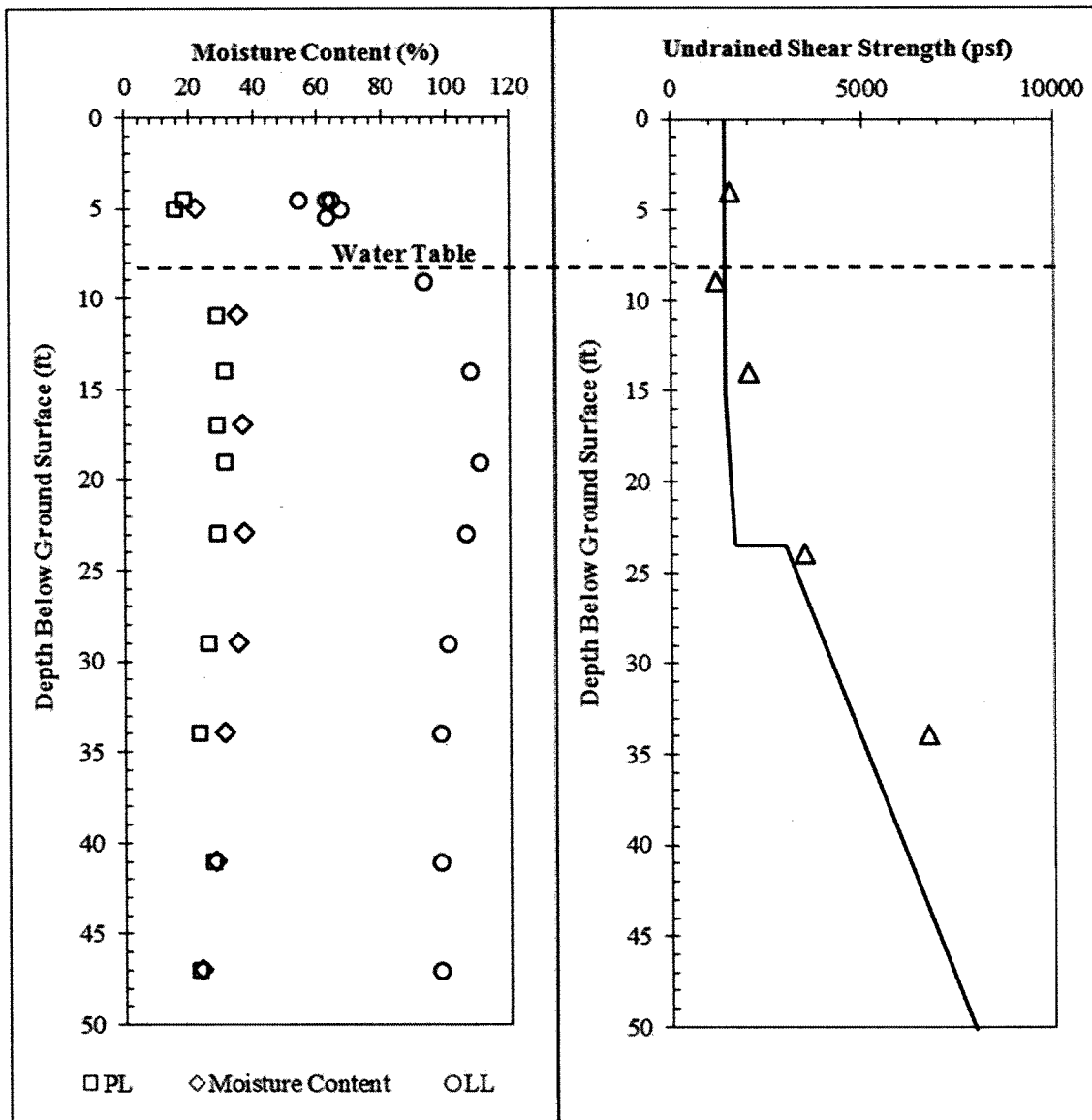
Figure 4.5: Results of Atterberg Limit and UU testing from January 2010 (3 months before shaft construction; 7 months before excavation).

Samples of the formation for laboratory testing were obtained using seamless pushed tubes, the standard of practice in this region. Laboratory testing included conventional one-dimensional consolidation tests, cyclic shrink-swell tests on horizontally oriented specimens, UU triaxial compression tests, and direct shear tests. Details for these tests and their results are provided in Ellis (2011), which is included in Appendix K.

Information for the undrained shear strength measured at the time of the preliminary investigation is summarized in Figure 4.5. These tests were conducted on 2.8-inch diameter specimens that were trimmed on the ends but not the circumference, which is the standard of practice in this region. Trimming the circumference in these stiff fissured clays is very difficult and tends to cause more damage to the specimen than the original sampling.

Information for the drained shear strength is summarized in Figure 4.6 and Figure 4.7. Long (1983) conducted triaxial compression tests with pore water pressure measurements to measure the effective stress failure envelope for the Taylor Formation (Figure 4.6). These samples were obtained from a location several miles from the project site. Ellis (2011) conducted direct shear tests on samples from the preliminary site investigation at the project site. One set of tests was intended to measure the peak, drained shear strength of intact (undisturbed) clay. A second set of tests was conducted with repeated shearing in an attempt to measure the large-displacement shear, drained shear strength. These direct shear tests were conducted using the slowest constant shear rate possible with our direct shear equipment, about 0.0001 inches per minute, which required 4 days per test. However, even at this slow rate it is unlikely that the tests were fully drained based on the consolidation data. Therefore, the data points from Ellis (2011) in Figure 4.7 may overestimate both the peak and the large-displacement strengths.

Additional direct tests were conducted using samples from the project site to measure the fully softened, drained shear strength. The fully softened, drained shear strength is the strength recommended for the design of slopes and retaining walls in highly plastic clays by many practitioners (e.g., Skempton 1970; Stark and Eid 1997; Duncan et al. 2011 and Gregory and Bumpas 2013), including several TxDOT research reports (Wright 2005 and Wright et al. 2007). The fully softened, drained shear strength is measured in the laboratory by conducting direct shear tests on reconstituted, normally consolidated specimens. Since these specimens are prepared to be close to their critical state, shear-induced pore water pressures are relatively small and the test results are relatively insensitive to the shear rate. For this project, the fully softened shear strength for the clay was measured on samples from the unweathered and weathered zones (Figure 4.7). These measurements compare very favorably to empirical correlations based on liquid limit that were developed by Wright et al. (2007) (Figure 4.7).

Based on these data, the peak, drained shear strength is approximately represented by a friction angle of 37° and the fully softened, drained shear strength is approximately represented by a friction angle of 24° (Figure 4.7).
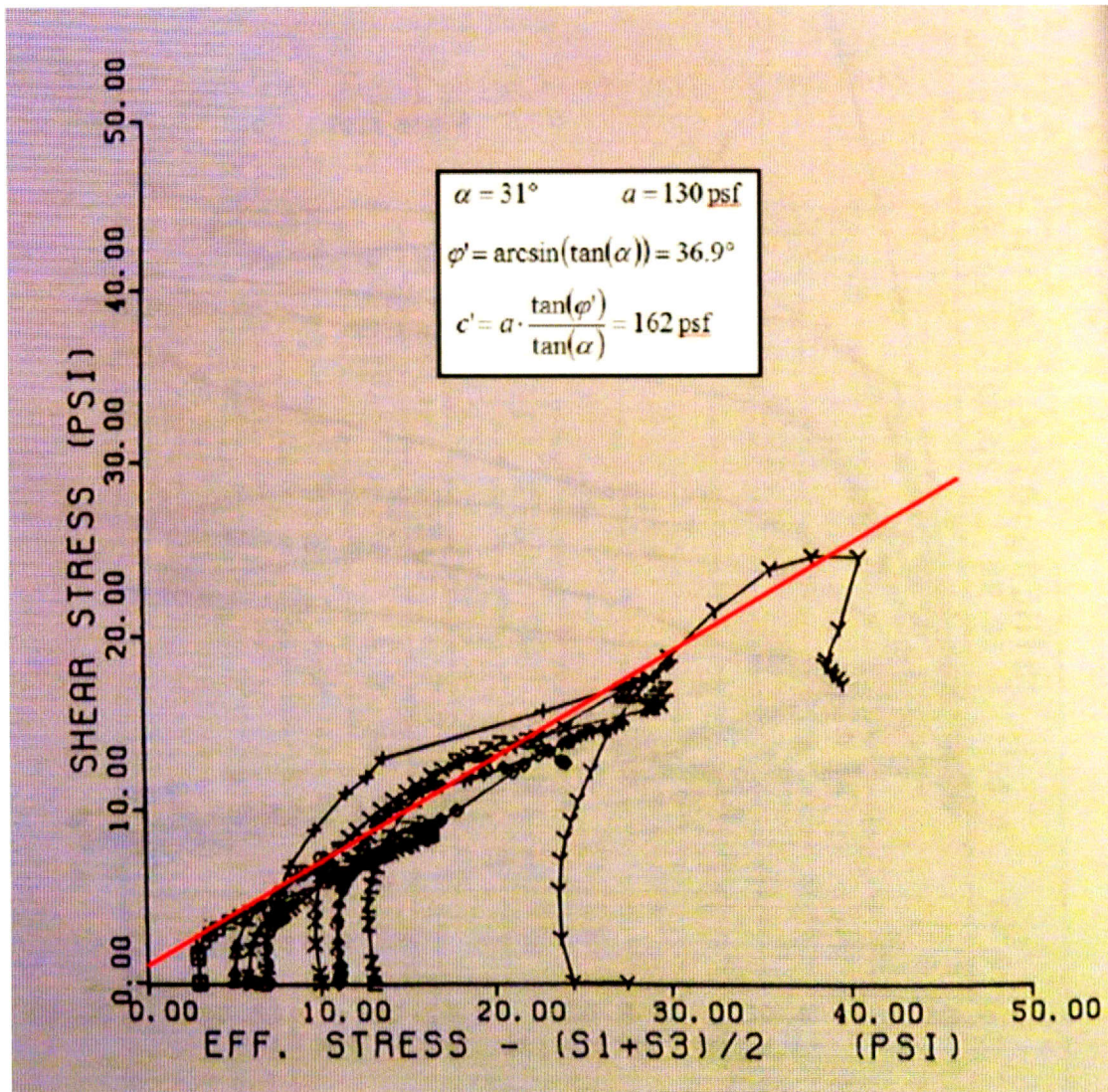
Figure 4.6: Results of triaxial testing to measure drained shear strength (figure from Ellis 2011 based on test results by Long 1983).
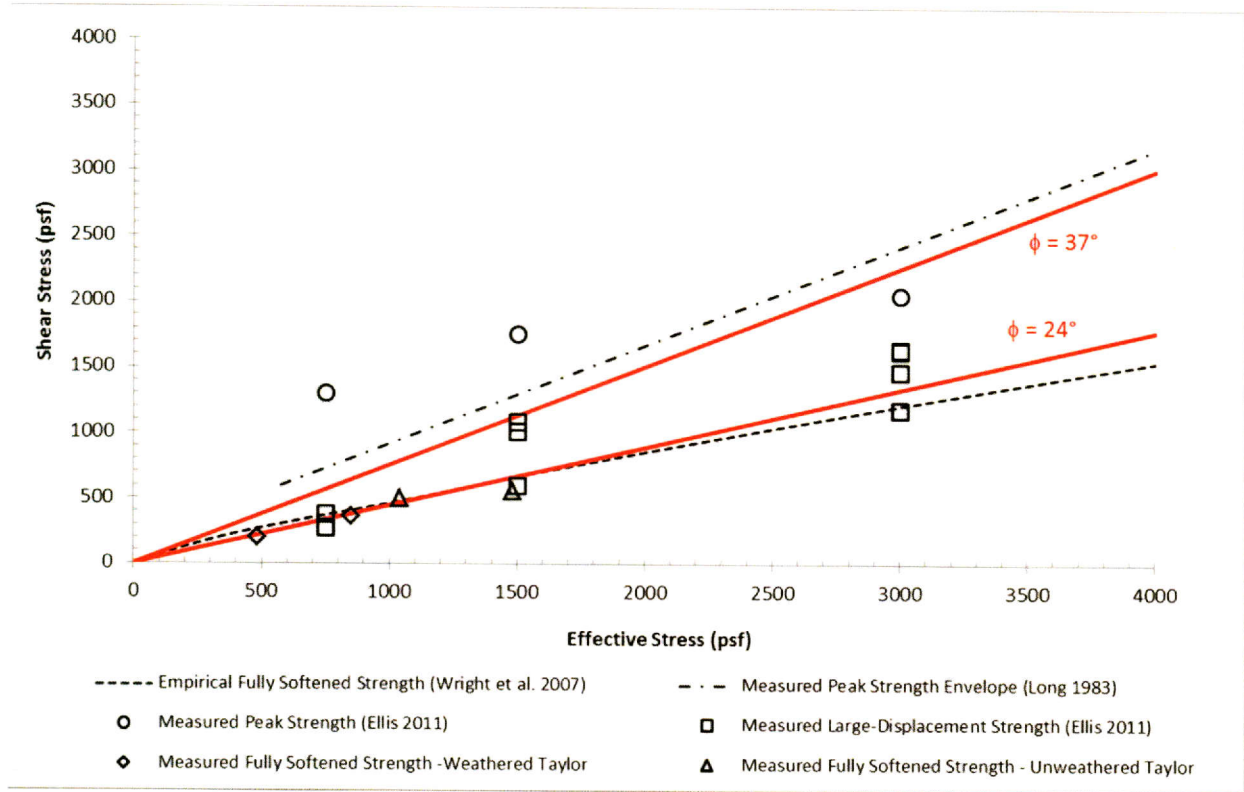
Figure 4.7: Results of direct shear testing to measure drained shear strength for Taylor Clay compared with empirical correlations and previous triaxial testing.

4.3: Design of Test Wall

The design for the test wall was developed using a procedure similar to the existing TxDOT design procedure for cantilever drilled shaft walls (TxDOT 2009). The goal was to create a structure that would be structurally sound and consistent with typical TxDOT walls, but would produce enough deformations to infer the earth pressures acting on the wall. A summary of design assumptions and shaft geometry for the test wall provided in Table 4.1 shows the baseline design assumptions for the initial analyses. Figure 4.8 shows the deflection and moment profiles for the baseline design. The top-of-wall deflection is approximately 0.8 inches. Sensitivity checks were included for the earth pressures from the retained soil and the undrained shear strength in the foundation soil. Details for the design analyses are presented in Appendix A.

The final wall design is pictured in Figure 4.9 and Figure 4.10. The test wall consists of 25 drilled shafts embedded to depths from 18 to 35 feet below ground surface (Figure 4.9). The shafts have a diameter of 24 inches and a center-to-center spacing of 30 inches. The reinforcing bar cage consists of 12 #7 bars. The cantilevered height is 15 feet, the penetration depth is 20 feet, and the shafts end 4 feet above ground surface. The shaft stickup allows the project team to run a lateral load test if desired; it also allows the site owner to use the wall as a loading dock upon completion of the project.

64

Table 4.1: Baseline assumptions and design parameters for test wall

Parameter	Value
Total Unit Weight of Soil, γ_t	130 pcf
Equivalent Fluid Pressure Loading, γ_{EF}	40 psf/ft[*]
Coefficient of Active Earth Pressure, k_a	0.31 (from γ_{EF} / γ_t)
Undrained Shear Strength, S_U	3,000 psf[**]
Foundation Soil p-y Curves	Stiff Clay Without Free Water
Cracking Moment, M_{Cr}	680 k-in.
Yielding Moment, M_y	3,200 k-in.
Uncracked Bending Stiffness, EI_{uc}	67×10^6 k-in^2
Cracked Bending Stiffness, EI_{cr}	18×10^6 k-in^2
c-c Spacing Between Shafts, B	30 in.
Shaft Diameter	24 in.
Height of Retained Soil, H	180 in.
Reinforcement	12 #7 bars (1.6% of gross area)

[*]Sensitivity checked with equivalent fluid pressure of 80 psf/ft.
[**]Sensitivity checked with undrained shear strength of 1,500 psf
.
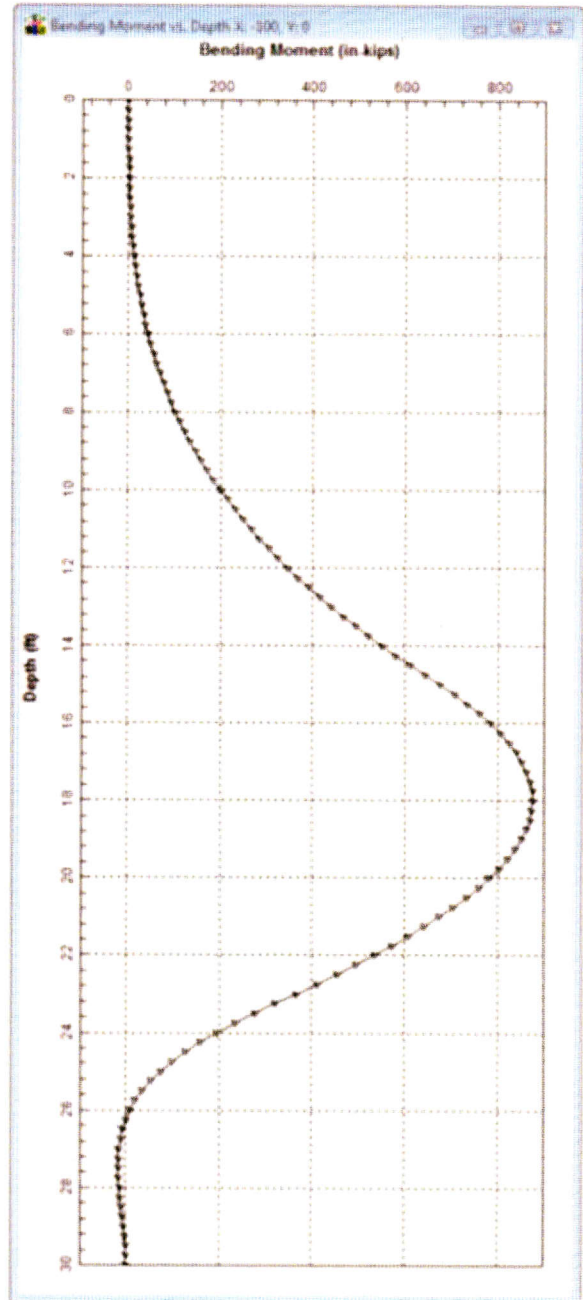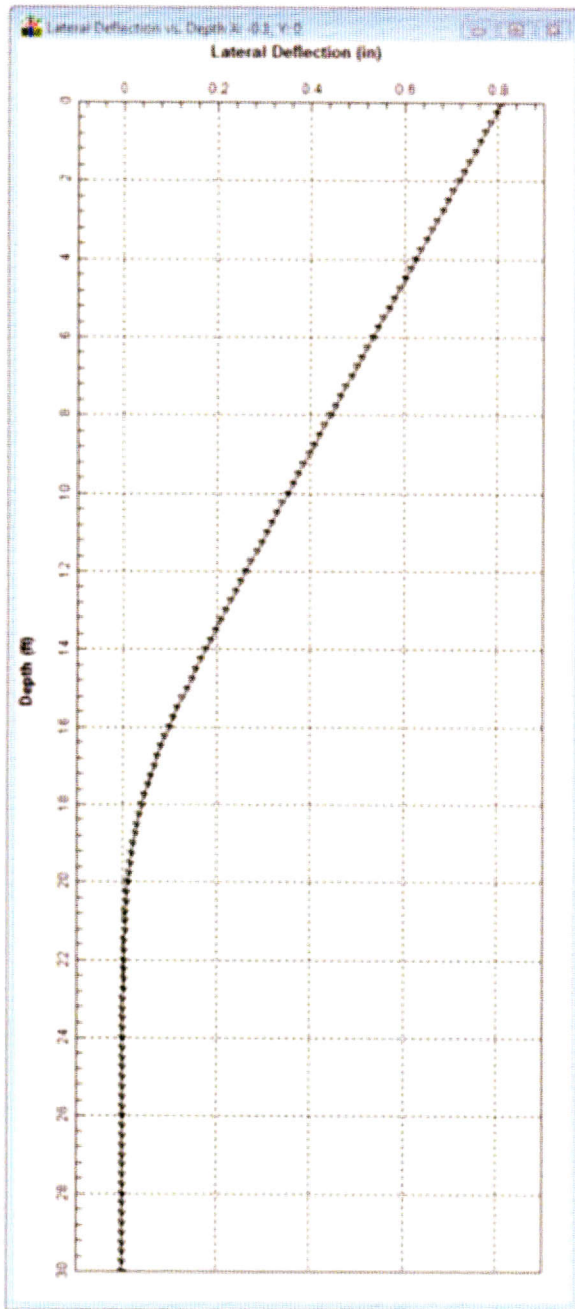
Figure 4.8: LPILE deflection and moment profile outputs for baseline design.
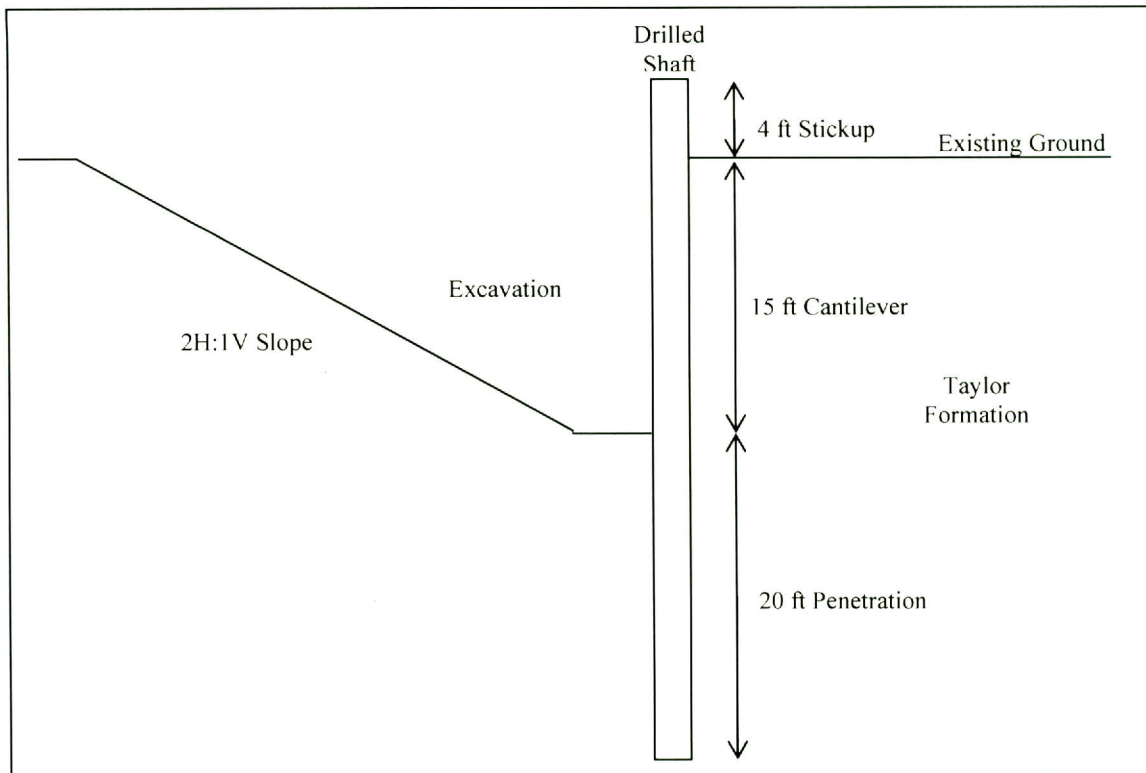
Figure 4.9: Cross section of wall and excavation at center shaft, facing east (not to scale).
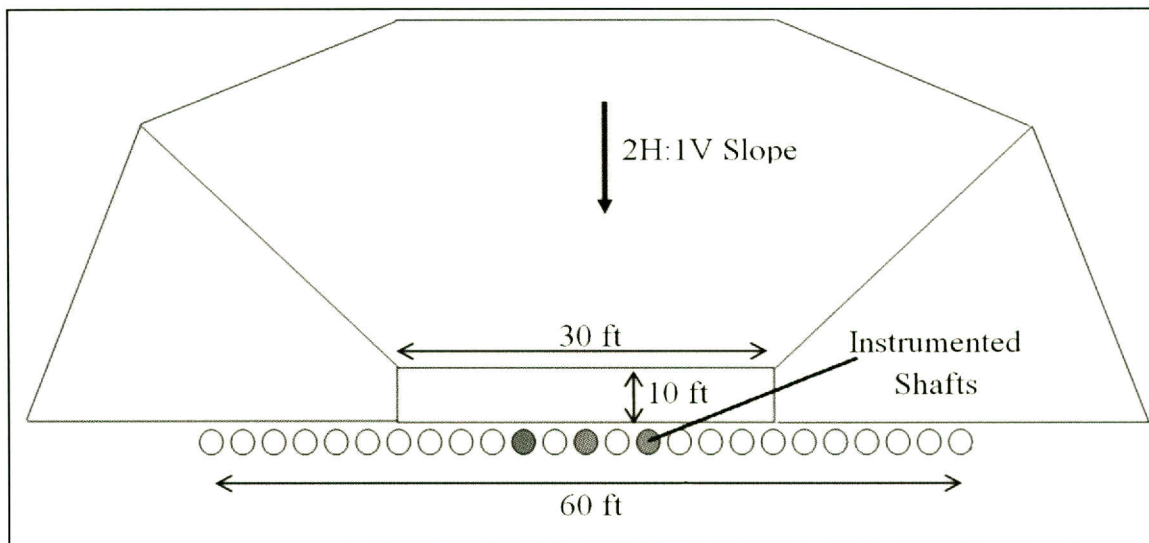
Figure 4.10: Plan view of wall and excavation.

4.4: Design of Instrumentation Program

The primary objectives of the instrumentation program are to accurately monitor deformations in the test wall, and to estimate the lateral earth pressures applied to the shaft over a period of 3 years. Three shafts in the test wall are instrumented (shaded in Figure 4.10). In each of these shafts, there are 30 fiber optic strain gauges and one inclinometer casing. Additionally,

one inclinometer casing was installed 5.5 feet behind the wall, and thermocouples were installed in the center shaft at depths of 3, 15, and 29 feet below ground surface for temperature monitoring. In the soil surrounding the wall, 20 time domain reflectometry (TDR) moisture sensors were installed after excavation. Figure 4.11 shows an instrumented cage as it is lowered into the ground, and Figure 4.12 shows the distribution of sensors within each instrumented shaft.
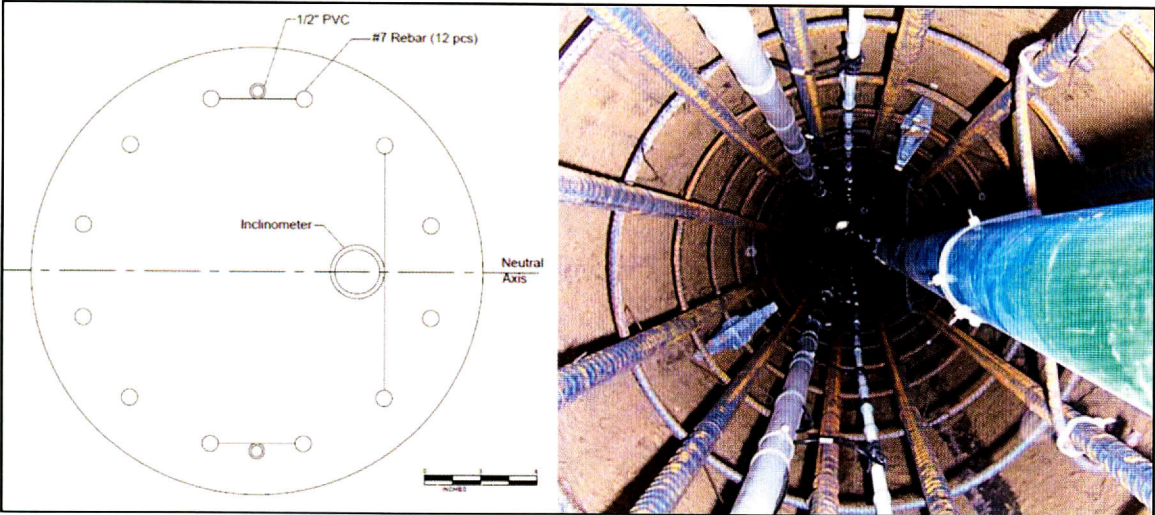
Figure 4.11: Plan view of instrumented rebar cage before concrete placement.
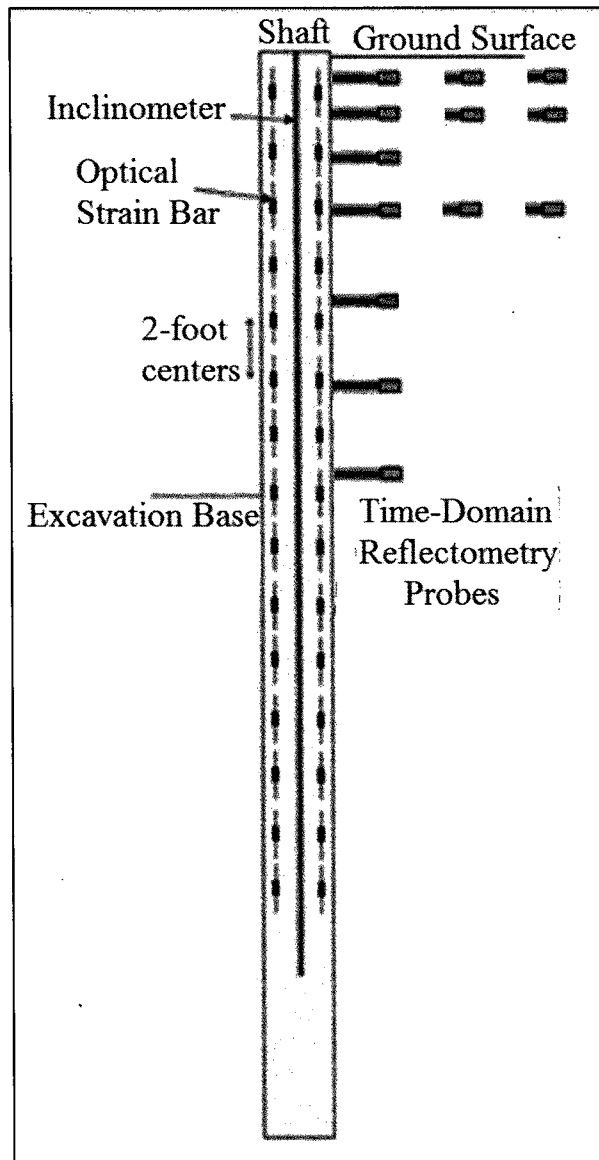
Figure 4.12: Distribution of sensors within an instrumented shaft.

4.4.1: STRAIN GAUGES

Because of their reputation for stability with time and relative insensitivity to moisture and temperature changes, optical strain gauges (Fabry-Perot type) were selected for strain monitoring. Optical gauges provide higher resolution than conventional electrical resistance or vibrating wire gauges, and are less susceptible to zero-drift over time. Additionally, because their strain measurements are generated using a light source, optical strain gauges are less affected by moisture and temperature changes than conventional gauges. The optical strain gauges were purchased from OPSENS in Canada, and the sister bars were fabricated by Lymon C. Reese and Associates of Austin, Texas. Prior to installation, each sister bar was calibrated to ensure linearity in the readings within the operating strain range of 1,000 microstrains and to establish a response curve. There are a total of 90 optical strain gauges installed in the test wall; in each instrumented shaft, there are 15 gauges on either side of the neutral axis (Figure 4.12).

Large temperature fluctuations occurred at the project site, and thermal expansion of the shafts produced significant strains. Additionally, the potential for errors in measurements due to rapid changes in temperature of the optical light source and datalogger was a design consideration. To minimize these errors, temperature resistant dataloggers were designed and installed in enclosures that limit rapid temperature change (Figure 4.13).

4.4.2: INCLINOMETERS

The rotation profile along the length of the drilled shaft was measured directly with an inclinometer, and integrated to yield a profile of deflected shape. Three inclinometer casings were attached to the reinforcing bar cage and cast into the shaft during construction. Readings were taken every 2 feet over the length of the shaft using a readout unit manufactured by Slope Indicator.

4.4.3: ADDITIONAL INSTRUMENTATION

To provide redundancy in top-of-wall deflections measured by the inclinometers, a linear potentiometer was installed on the project site prior to excavation and anchored to the wall near the ground surface. It was attached to shaft #16, adjacent to the west instrumented shaft (shaft #15). The linear potentiometer provides continuous data on top-of-wall deflection and redundancy with the inclinometer data. To provide information on the moisture conditions in the retained soil, a total of 20 TDR moisture probes were installed in behind the wall. Because of the high spatial variability of rainfall across the region, an electronic tipping bucket rain gauge was installed at the test wall to augment measurements from nearby weather stations. The linear potentiometer, TDR moisture probes, and rain gauge were monitored continuously. Figure 4.13 shows some of the instrumentation installed on the project site.

Figure 4.13: Instrumentation on the project site.
Clockwise from top left: temperature resistant datalogger and enclosure for continuous strain readings; signal conditioner for individual strain readings; linear potentiometer; TDR probe installed through facing.

4.5: Construction Activities on Project Site

4.5.1: CONSTRUCTION OF FULL-SCALE INSTRUMENTED TEST WALL

The drilled shafts and instrumentation were installed in early April 2010 by McKinney Drilling Company (Figure 4.14). In order to prevent excessive bending of the rebar cage and damage to the instrumentation, the instrumented cages were lifted with two cranes (Figure 4.15). To prevent sensor damage during concrete placement, cables were protected within slotted PVC pipes and concrete was directed down the center of the rebar cage with shovels. Initial sensor survivability was excellent, with 88 of 90 strain gauges and all inclinometer casings functional after rebar cage placement and concrete installation. A summary of wall construction activities and concrete strength data is provided in Table 4.2.

Figure 4.14: Construction of test wall, April 2010.

Figure 4.15: Lifting an instrumented cage with two cranes.

Table 4.2: Summary of wall construction activities and measured concrete strengths

Date	Notes (* = Instrumented Shaft)	7-Day Concrete Strength (psi)	28-Day Concrete Strength (psi)
March 30, 2010	Mobilize Equipment, Assembled Instrument Cages, Constructed Shafts 1 and 4	6055	7955
March 31, 2010	Constructed Shafts 7, 10, 13*, 22, and 25	4970	7000
April 1, 2010	Constructed Shafts 2, 5, 8, 11*, 15*, and 17	4480	6065
April 2, 2010	Constructed Shafts 3, 6, 9, 16, 19, and 23	4410	5875
Apr. 3 - 4, 2010	Weekend	N/A	N/A
April 5, 2010	Constructed Shafts 18, 21, and 24	4000	5950
April 6, 2010	Constructed Shafts 12, 16, and 14	4400	6800
April 7, 2010	Demobilize Equipment	N/A	N/A

4.5.2: INSTALLATION OF SHOTCRETE FACING

To prevent soil erosion from between the shafts and provide consistency with design practice, shotcrete facing material was installed on October 1, 2010 (Figure 4.16).
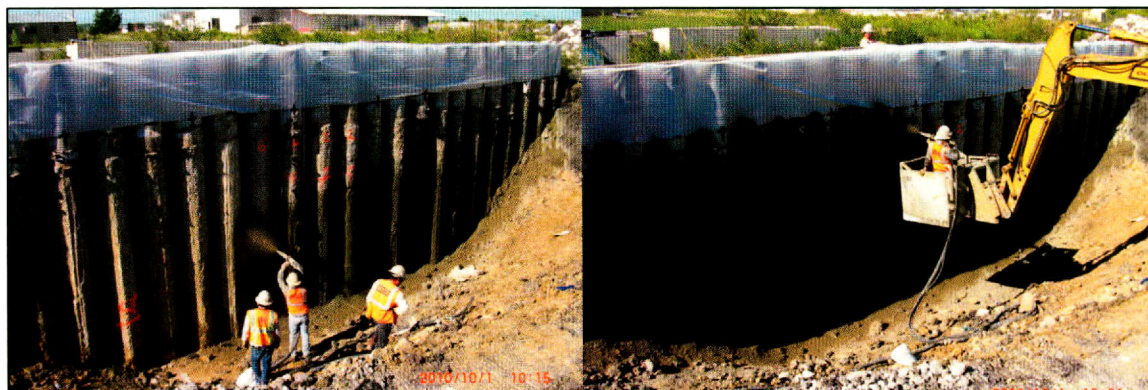
Figure 4.16: Installation of shotcrete facing on October 1, 2010.

4.5.3: INSTALLATION OF TIME-DOMAIN REFLECTOMETRY PROBES

Prior to the application of shotcrete facing, time-domain reflectometry probes were installed. A total of 10 probes were installed through the wall facing on September 30–October 1, 2010 (as shown in Figure 4.17), and 10 were installed through the ground surface on October 14 (as shown in Figure 4.18). The approximate locations of all installed TDR probes are shown in Figure 4.19. Additional discussion of TDR probe installation, calibration, and data analysis can be found in Dellinger (2011).
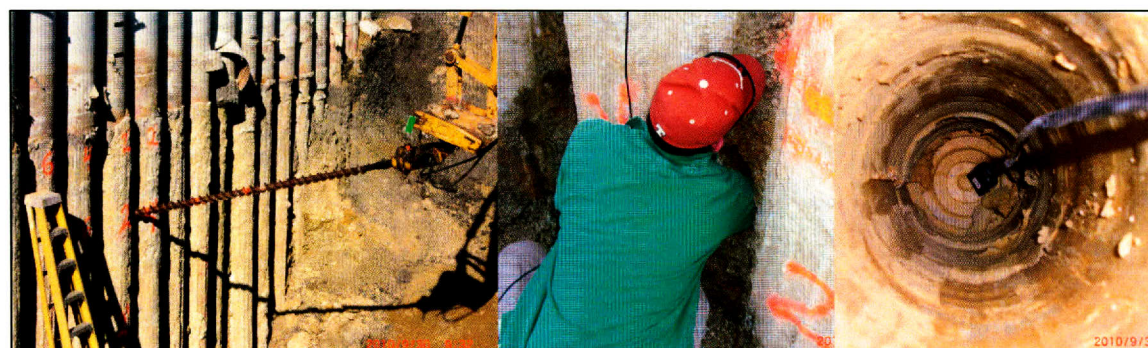
Figure 4.17: Installation of TDR moisture probes behind wall facing.
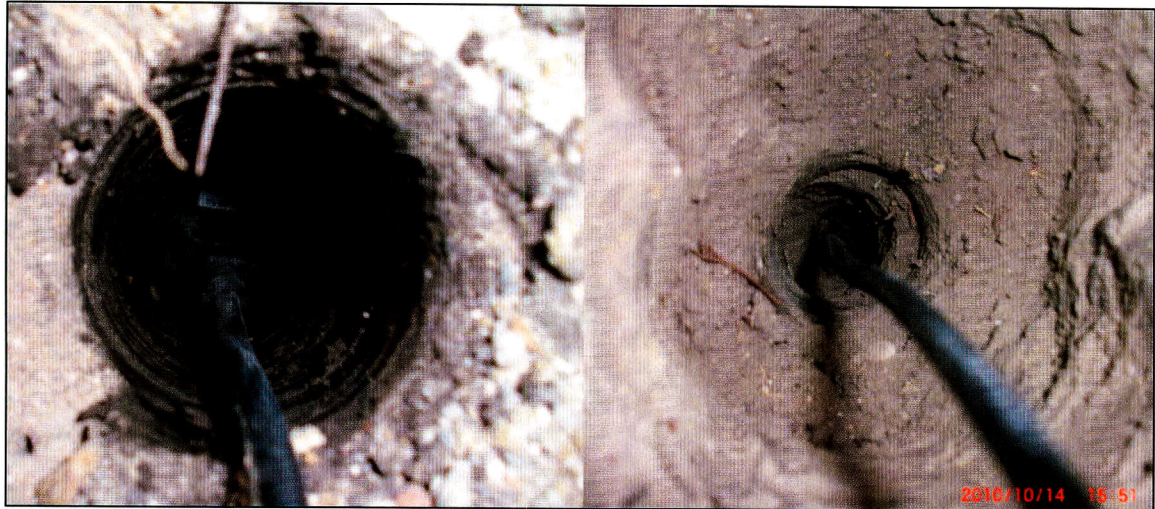
Figure 4.18: Installation of TDR moisture probes through ground surface.
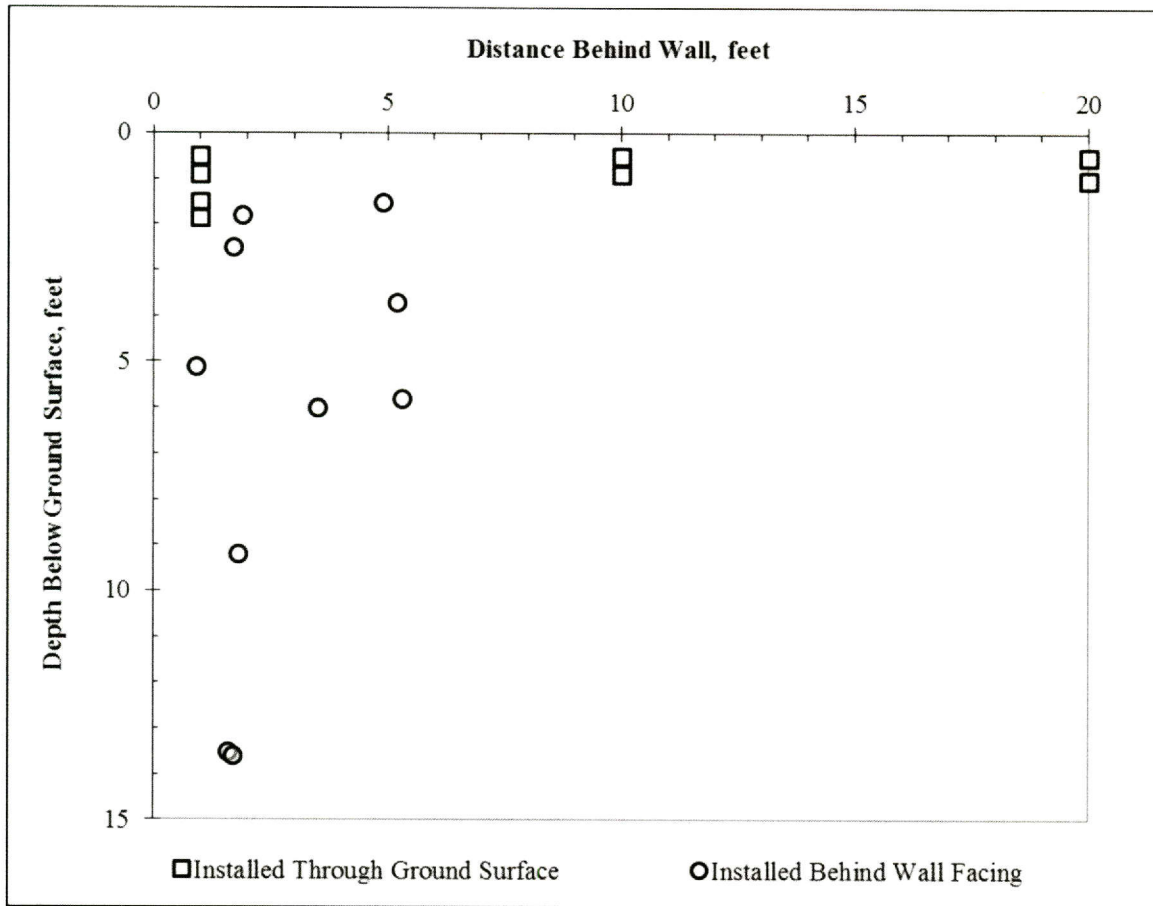
Figure 4.19: Approximate locations of TDR moisture probes.

4.5.4: EXCAVATION SLOPE REPAIR AND EROSION CONTROL

On August 17, 2011, the slopes were reshaped to reduce erosion and prevent surface water from draining into the excavation (Figure 4.20). On October 8, 2011, erosion control material was installed (Figure 4.21).

Figure 4.20: Excavation slopes are reshaped on August 17, 2011.

Figure 4.21: Erosion control material is installed on October 18, 2011.

4.5.5: PIEZOMETER INSTALLATION

Five piezometers were installed on site; Table 4.3 and Figure 4.22 provide the locations. On January 12, 2010, a piezometer screened 5 to 15 feet was installed in a boring from the site investigation by Fugro, Inc. (Figures 4.23–4.25). This piezometer was used to monitor the local water level conditions. On February 23, 2012, four more piezometers were installed in boring holes for a site investigation by Fugro, Inc. (Figure 4.26). These piezometers were used to monitor the water levels in the inundation test area. The piezometers were surrounded with a permeable sand and gravel interface between the piezometer and the walls of the borehole. Readings were taken using a buzzing water level indicator and a tape measure.

Table 4.3: Location, installation date, and screen location for the piezometers

Piezometer	Installation date	Diameter	Screen location	Location	
				Distance perpendicular from the wall	Distance from wall center-line
B-3	12-Jan-10	2 inches	5 to 15 feet	16 feet	54 feet east
A	23-Feb-12	2 inches	5 to 15 feet	9 feet	9 feet west
B	23-Feb-12	1 inch	3.4 to 4.6 feet	15.1 feet	5.5 feet west
C	23-Feb-12	2 inches	5 to 15 feet	15.5 feet	3 feet east
D	23-Feb-12	1 inch	3.6 to 4.8 feet	7.3 feet	7.5 feet east
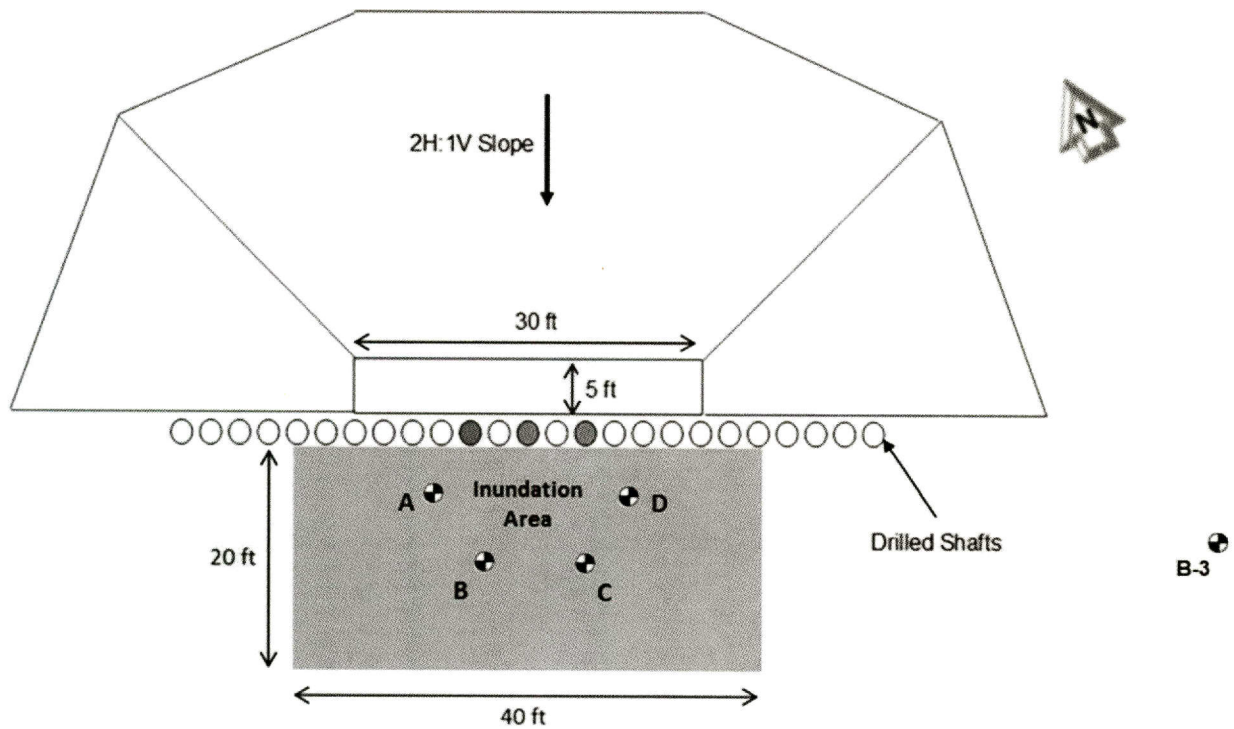
Figure 4.22: Plan view of piezometer locations.
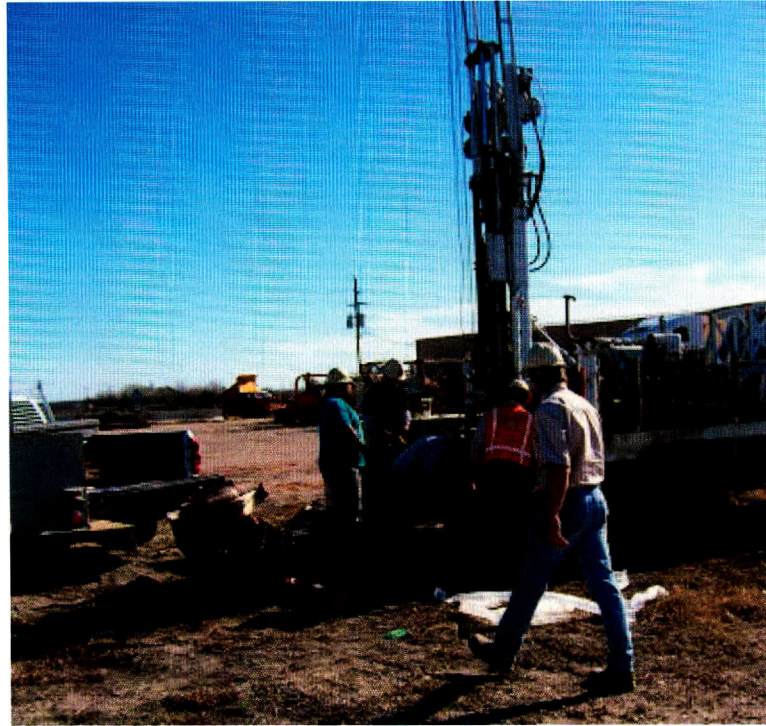
Figure 4.23: The piezometer installed in borehole B-3 being lowered into position.

Figure 4.24: The piezometer installed and covered in borehole B-3.

Figure 4.25: Piezometer being installed in borehole A.
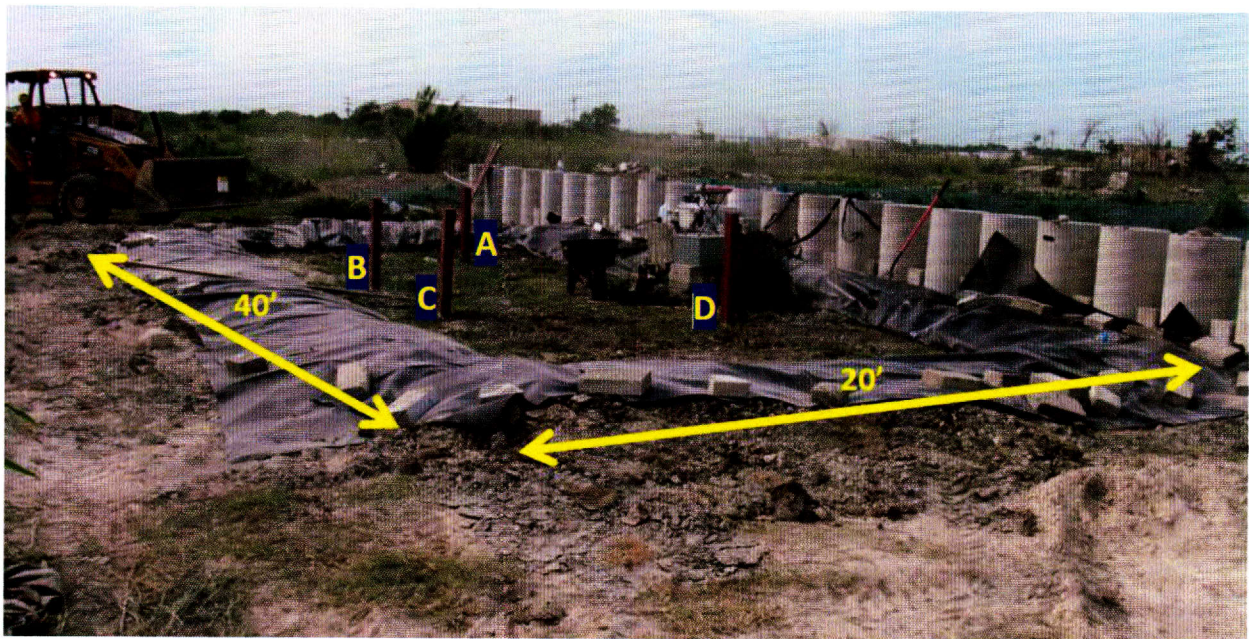
Figure 4.26: The four standpipe piezometers installed behind the wall in the inundation berm.

4.5.6: INUNDATION BERM CONSTRUCTION

The inundation berm encloses an area approximately 40 feet wide and 20 feet behind the test wall (Figure 4.27). A cross section of the berm design is shown in Figure 4.28. The berm is keyed into the native soil with a 2-foot deep trench and is lined with a geomembrane to minimize the lateral loss of water (Figure 4.29).

The inundation berm was constructed by Ranger Excavating on April 26, 2012. A backhoe was used to excavate the trench (Figure 4.30). After excavation of the trench, the geomembrane was installed (Figure 4.31). The soil was replaced and compacted, along with

78

stockpiled soil from the project site, using the backhoe bucket (Figure 4.32). After the installation of the geomembrane and compacted soil (Figure 4.33), the seams were joined together with duct tape (Figure 4.33). The completed inundation berm is shown in Figure 4.34. Initial filling of the berm occurred on May 2, 2012 (Figure 4.35). While some leakage of the seams occurred, the leakage rate was slow enough that the water level could be maintained with water from the on-site supply (Figure 4.36–Figure 4.37).
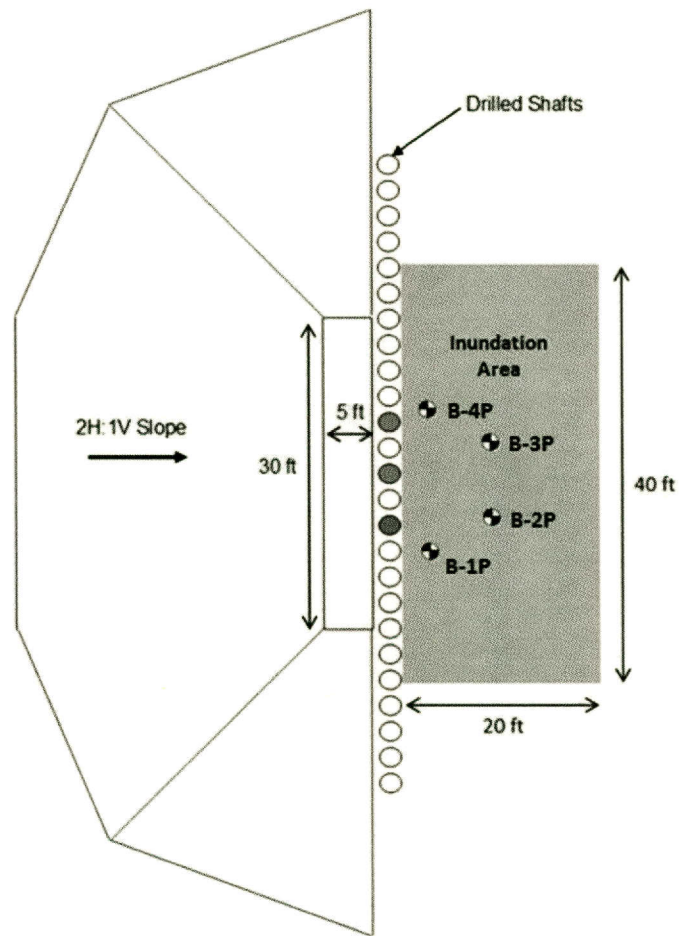
Figure 4.27: Plan view of inundation zone.
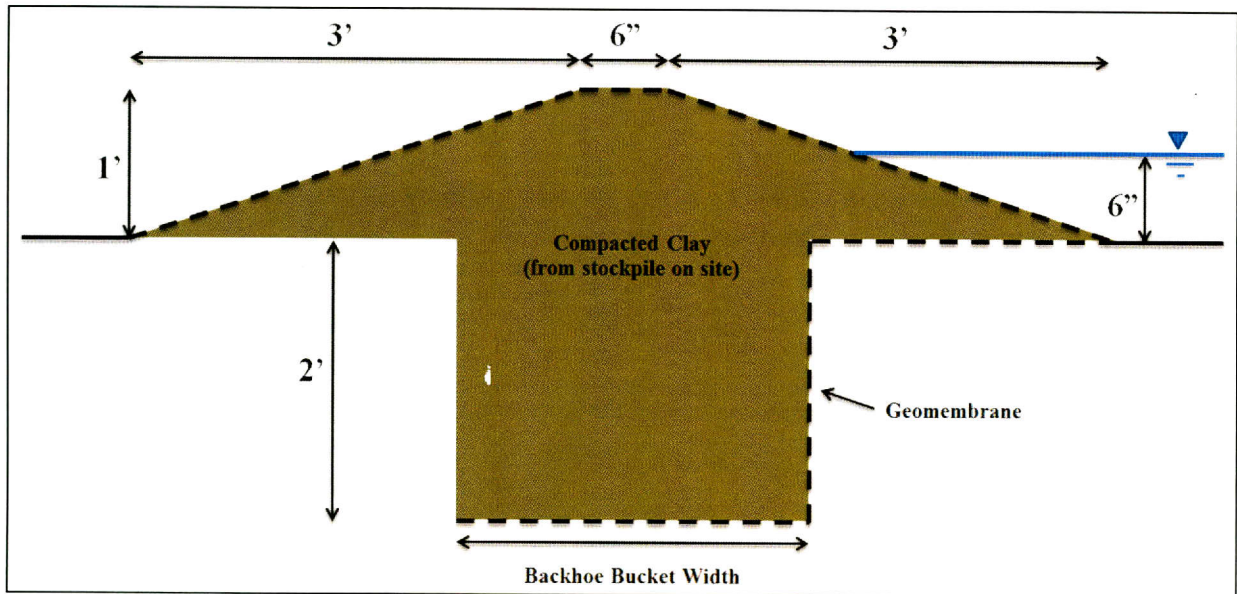
Figure 4.28: Cross section of inundation berm design.

Figure 4.29: Excavation of trench for inundation berm.

Figure 4.30: Installation of geomembrane in trench.

Figure 4.31: Compacting soil with backhoe bucket.

Figure 4.32: Compacting soil with backhoe bucket.

Figure 4.33: Detail of geomembrane seam.
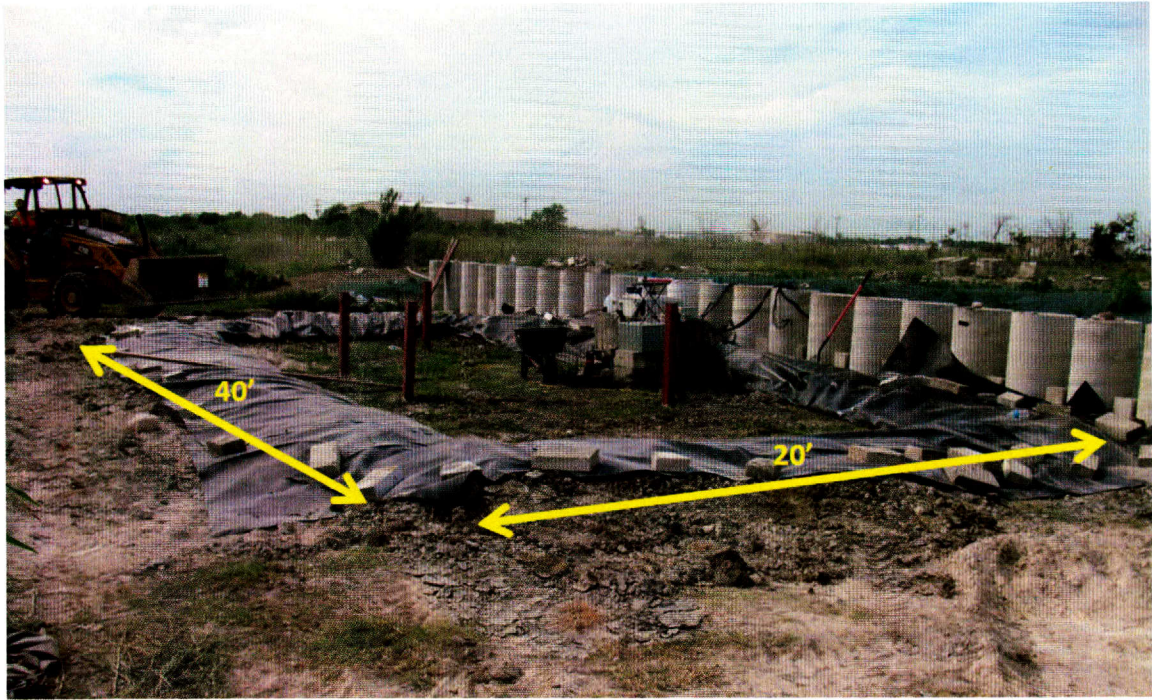
Figure 4.34: Completed inundation berm.

Figure 4.35: Filling the inundation zone.

Figure 4.36: Leakage from southeast corner of inundation zone.

Figure 4.37: Leakage from west side of inundation zone.

84

4.6: Monitoring Plan

Since installation of instrumentation, the activity of the test wall has been closely monitored. An automated datalogger records strain readings from the center shaft at 6-minute intervals. The linear potentiometer, rain gauge, thermocouples, and TDR moisture probes are measured by another datalogger at 15-minute intervals. Inclinometer profiles, piezometer water levels, and strain readings from the east and west shafts are recorded, on average, once per week. The frequency of these measurements has changed according to the amount of activity at the wall site, ranging from several readings per day to once per month. Additionally, meteorological data from nearby weather stations and observational information from the test wall supplement our instrumentation data.

4.7: Data Reduction and Analysis

Because assessing the magnitude and distribution of earth pressures acting on the test wall is a primary goal of this research, methods of using strain gauge and inclinometer data from the test wall to estimate earth pressures must be developed. A summary of the mathematical relationship between deflection, slope, bending moment, shear, and earth pressures for a typical pile is shown in Figure 4.38. The methods described in the following section are applicable to data from the Manor test wall only, and should not be used for other projects or data sets without careful validation.
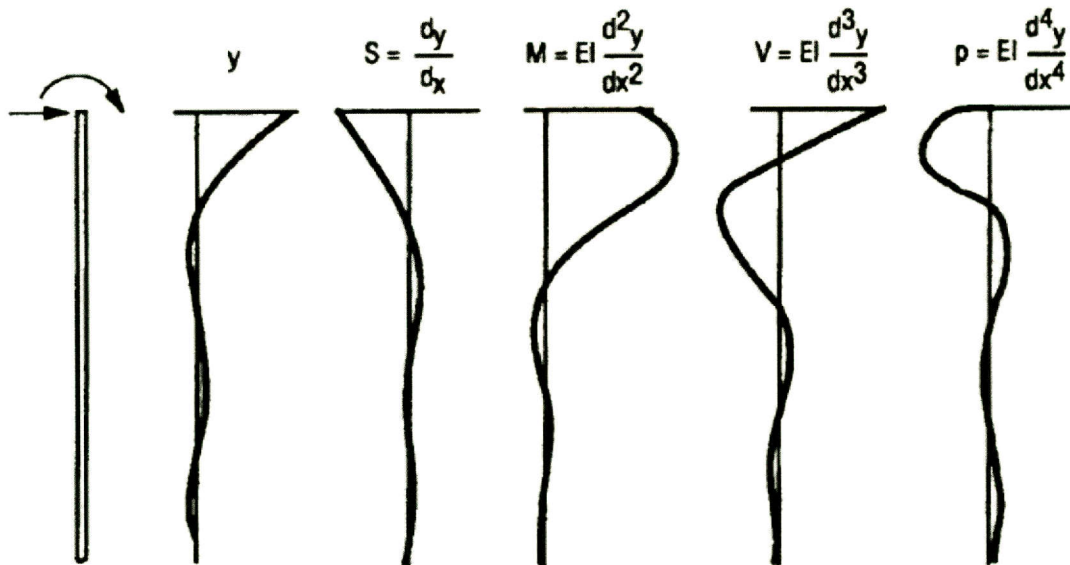
Figure 4.38: Mathematical relationship between deflection (y), slope (S), bending moment (M), shear force (V), and soil reaction force (p) for a laterally loaded pile (after Reese and Van Impe, 2001).

4.7.1: STRAIN GAUGE DATA REDUCTION

The strain gauges placed on either side of the shaft's neutral axis measure axial strains in the tensile and compressive direction (ε_t and ε_c, respectively). The difference in tensile and compressive strains on either side of the neutral axis is divided by the horizontal distance

85

between the gauges to obtain a value of bending curvature at a given depth. The calculated value of bending curvature is converted to a value of bending moment according to the moment-curvature relationship defined by the structural properties of the shaft. Following this procedure at each depth where strain gauges are installed yields a profile of bending moment in the shaft versus depth, which can be differentiated once to obtain a profile of shear force versus depth, or differentiated twice to obtain a profile of soil resistance versus depth. This process is summarized in Figure 4.39. A more detailed explanation of strain gauge data reduction for the Lymon C. Reese research wall can be found in Koutrouvelis (2012).
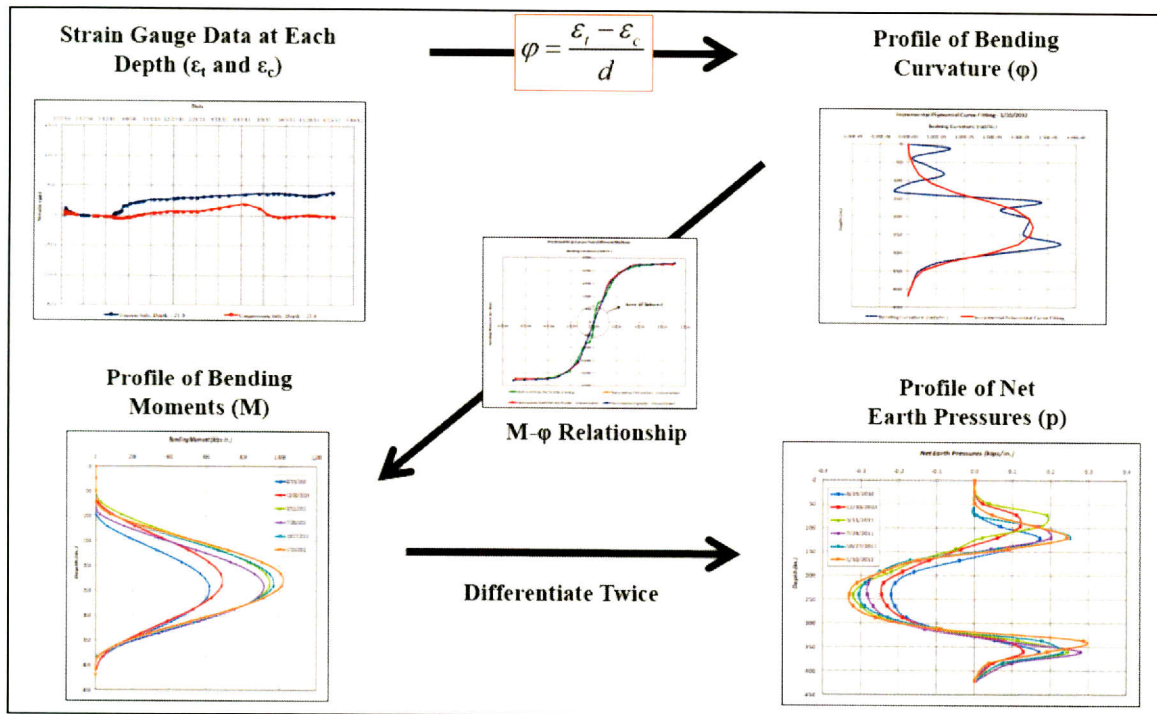
Figure 4.39: Strain gauge data reduction (after Koutrouvelis 2012).

For this research study, strain gauge nomenclature indicates which instrumented shaft the gauge is installed in (east, center, or west), the depth of the strain gauge below original ground surface (1–29 feet), and which side of the neutral axis the gauge is installed on (Tension or Compression; tensile strains are positive). Using this nomenclature, gauge E.17.T is located in the east instrumented shaft, 17 feet below ground surface, on the tensile side of the neutral axis.

4.7.2: INCLINOMETER DATA REDUCTION

4.7.2.1: Rotation Profiles Recorded in the Field

While inclinometer data is most commonly presented as a displacement profile, the instrument itself records rotation data; these data are then integrated to calculate displacement. By extracting the raw rotation data from the instrument, a profile of bending curvature can be obtained with just one derivative. Sample rotation data from the three instrumented shafts on May 28, 2013, when the wall was near its maximum deflection, is presented in Figure 4.40. It is

important to note that the last data point is at a depth of 32 feet for the center and west shafts, and 30 feet for the east shaft (shaft base is at 35 feet).

The inclinometer probe measures the shaft rotation in two directions: the A-axis (in the direction of the wheels) and the B-axis (in the direction perpendicular to the wheels). This allows for the lateral deflection to be determined in any direction. For the purposes of this analysis, all deflections are assumed to be perpendicular to the wall, and the cumulative deflection is calculated by combining the rotation profiles from the A-axis and B-axis using the distance formula:

$$y_{total} = \sqrt{y_A{}^2 + y_B{}^2}$$

This method of estimating deflections can slightly overestimate deflections in the case of very noisy data set, since it interprets any small amount of instrument error to be a positive deflection perpendicular to the wall. However, the method is reliable, slightly conservative, and is much more straightforward to apply to the data set than more advanced correction methods.
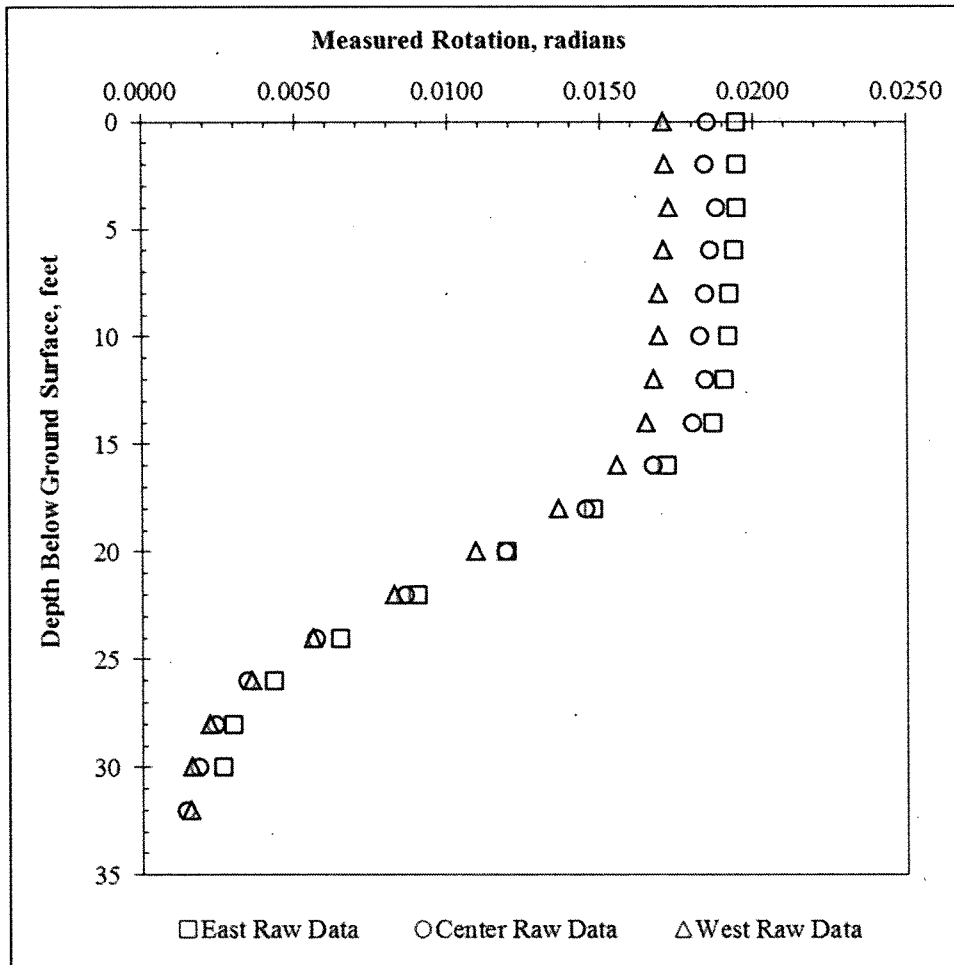
Figure 4.40: Sample rotation data from May 28, 2013. Reference survey is July 27, 2010, immediately before excavation.

4.7.2.2: Combining and Smoothing Rotation Profiles

While there are small differences in the behavior of the instrumented shafts, combining the three slope profiles into an average slope profile results in values that are similar to those obtained from the center instrumented shaft, and provides a much smoother curve for differentiation. To account for the presence of base rotation, the final rotation measurement is extended vertically down from the last measurement to the shaft base. In a typical analysis, the shaft base is assumed to be a fixed point—zero deflection, zero rotation. However, based on the instrumentation data from the test wall, it is clear that some base rotation occurred (rotation measurements near the shaft base were consistently above zero throughout the life of the test wall; unrealistic loads would need to be present to return the shaft base rotation to zero in the remaining few feet). Mathematically, extending the final slope measurement to the shaft base indicates that the shaft base has rotated, but is not experiencing a bending moment.

A smoothing algorithm was applied to the data from each shaft before averaging the three profiles. The final averaged profile was smoothed again, although after averaging, the effects of smoothing are minimal. The smoothing algorithms are summarized in Tukey (1977), and are adapted for use in Excel by Quantdec (2004). To smooth each shaft's rotation profile, a "3RH" smooth with re-roughing is applied to the original data set. The process is summarized below; more detailed explanations of the individual smoothing processes are explained in the subsequent paragraphs, Figure 4.41 to Figure 4.44, and in Tukey (1977).

1. Apply a repeated medians-of-three smooth (3R) to each rotation profile.

    a. Each point in the data set is replaced by the median of the original point and the two adjacent data points:

    $$\theta_{i,3\,smoothed} = median(\theta_{i-1}, \theta_i, \theta_{i+1})$$

    b. Repeat the process until there are no further changes in the data:

    $$\theta_{i,3R\,smoothed} = \theta_{i,3\,smoothed} = median(\theta_{i-1}, \theta_i, \theta_{i+1})$$

2. Hann the 3R smoothed data to create a 3RH smooth (end values are not Hanned):

    $$\theta_{i,hann\,smoothed} = 0.25\theta_{i-1} + 0.50\theta_i + 0.25\theta_{i+1}$$

3. "Re-rough" the smooth.

    a. Calculate a profile of residuals:

    $$\theta_{i,residual} = \theta_{i,original} - \theta_{i,smoothed}$$

    b. Smooth the profile of residuals using a 3RH smooth as described above.

    c. Add the profile of smoothed residuals to the original smoothed data set:

    $$\theta_{i,smoothed,re-roughed} = \theta_{i,smoothed} + \theta_{i,residual}$$

End values are smoothed after the application of the 3R smooth (before Hanning) by calculating the median of the previous two points on the smoothed curve and a point extrapolated one unit beyond the end of the smoothed curve (e.g., $(\theta_{32'})$ is the median of $(\theta_{28'})$, $(\theta_{30'})$, and $(3 \cdot \theta_{28'} - 2 \cdot \theta_{30'})$, after Quantdec (2004)). In the author's opinion, while the method developed by Quantdec (2004) is simple and easy to apply to a large data set, it is less accurate than the original method described by Tukey (1977), which also incorporates the original raw data into the final end value (Figure 4.41). For this research study, however, because the most important conclusions are drawn from the middle portions of the data set, the method of end value

smoothing does not greatly affect the final results and the simple method developed by Quantdec (2004) is adequate.

To "re-rough" the smooth, a profile of residuals is calculated as the difference between the original raw data and the smoothed data. A 3RH smooth is then applied to the profile of residuals, and the smoothed residuals are added to the original smoothed data set. An illustration of the 3RH smooth with re-roughing is provided in Figure 4.42 for depths of 0 to 14 feet in the center shaft, with the entire profile shown in Figure 4.43. Re-roughing ensures that the smoothed data points remain reasonably close to the original values. This smoothing method kept the maximum bending moments and top-of-wall deflections consistent with the original raw data values, but provided a curve more suitable for piecewise differentiation. Other combinations of smoothing methods (e.g., medians-of-three smoothing only, 3RH smoothing without re-roughing, etc.) provide similar results when applied to the measured rotation data, but change the final data points slightly more than the re-roughed 3RH smooth that was selected for subsequent analysis. A comparison of the original raw data from the three instrumented shafts with the final smoothed slope profile for differentiation is provided in Figure 4.44.

End-value smoothing: parts and result

THE ACTUAL

THE LAZY ONE

STRAIGHT BEYOND

ALL THREE
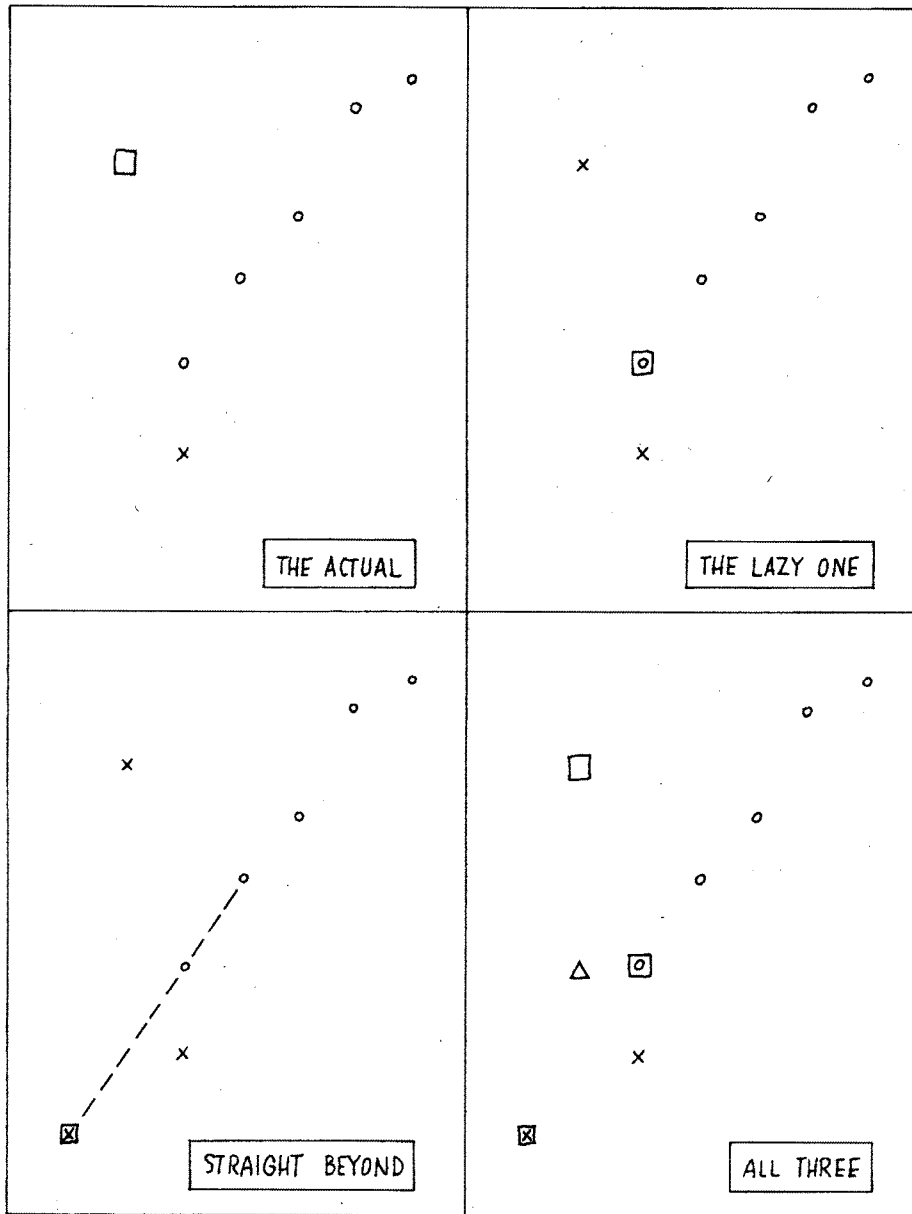
x = end input values   □ = the actual   △ = the smooth end value
o = medians of 3   ◙ = the lazy one   = the median of ⊠, ◙,
                     ⊠ = straight beyond   and □

Figure 4.41: Tukey's method of end value smoothing (after Tukey 1977).
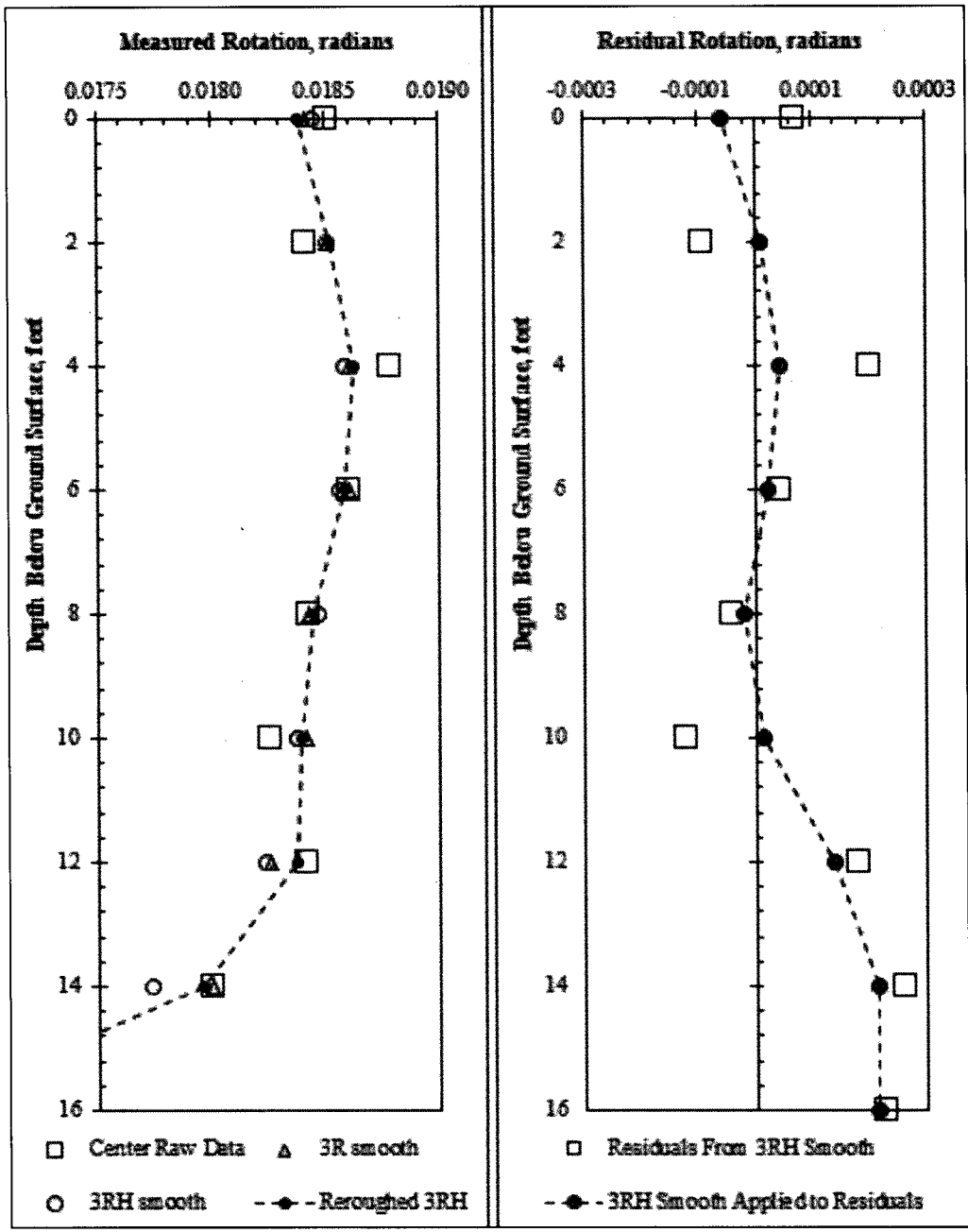
Figure 4.42: Illustration of the 3RH smooth with re-roughing applied to the center shaft rotation data between 0 and 14 feet.
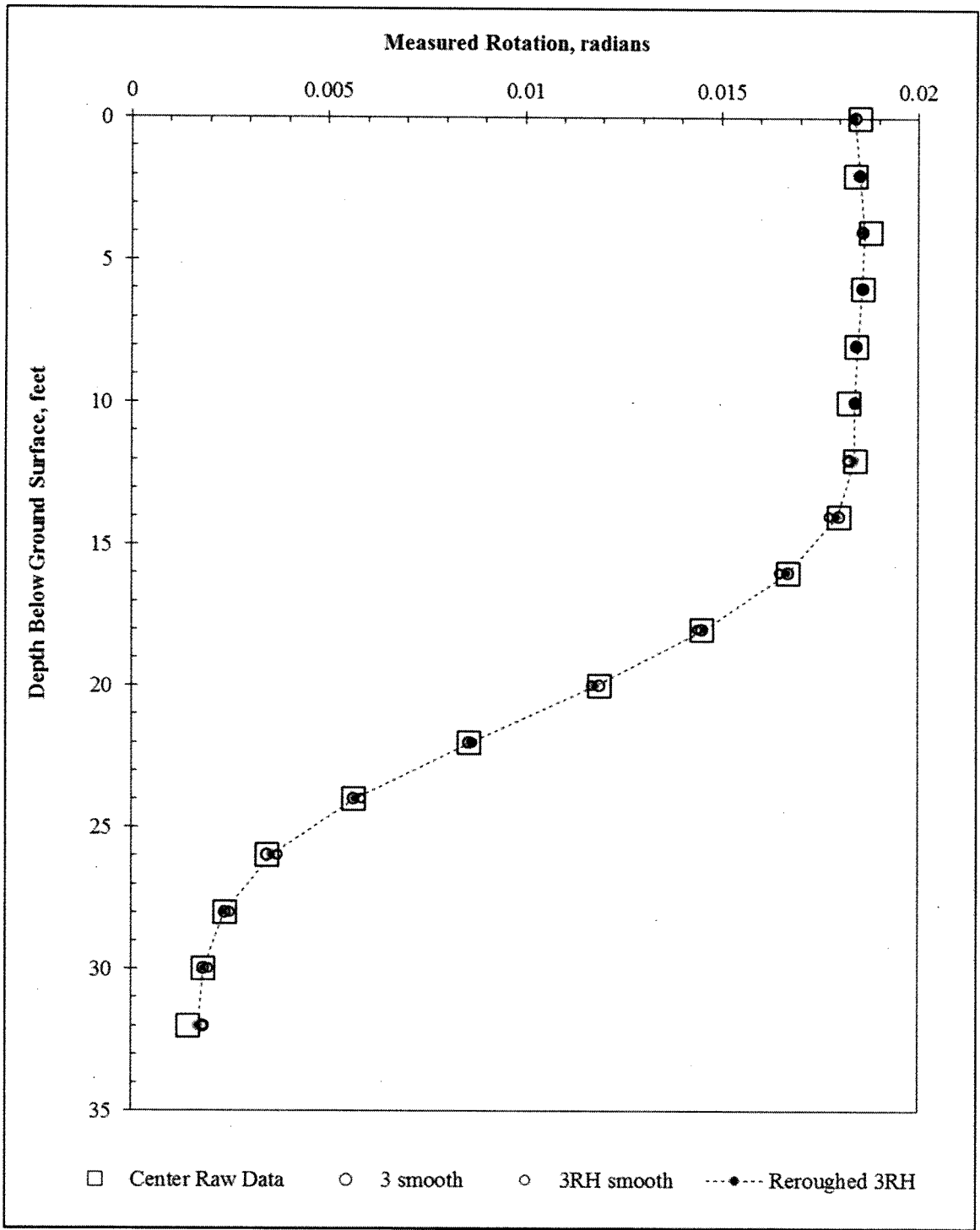
Figure 4.43: Comparison of original and smoothed rotation data from the center shaft on 5/28/2013.
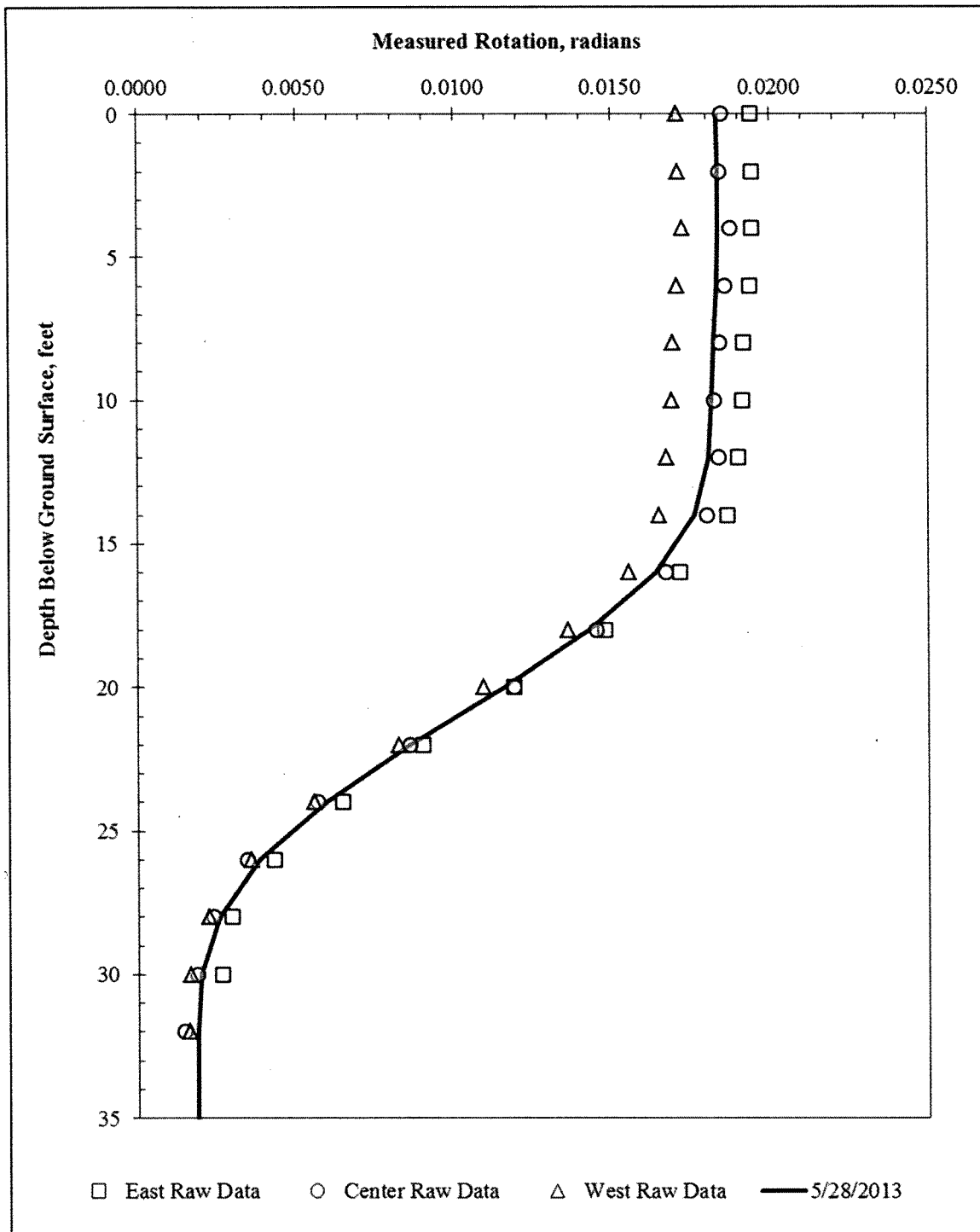
Figure 4.44: Comparison of raw rotation data from the three instrumented shafts with the final smoothed rotation profile for differentiation.

4.7.2.3: Obtaining Bending Moment Profiles from Rotation Data

Ooi and Ramsey (2003) detail a variety of methods for obtaining bending moments and curvatures from inclinometer data. Of the methods surveyed, the most favorable was found to be

93

fitting a third-order polynomial to a moving window of five points along the deflection profile, then analytically taking the second derivative of this curve to obtain a profile of bending curvature. For inclinometer data recorded at the test wall, a third-order polynomial was fit to a moving window of five points along the smoothed rotation profile, and the first derivative was taken numerically at the center point (using a central difference approximation at depths +/- 0.5 feet from the center point). This process is illustrated in Figure 4.45 at a depth of 14 feet.
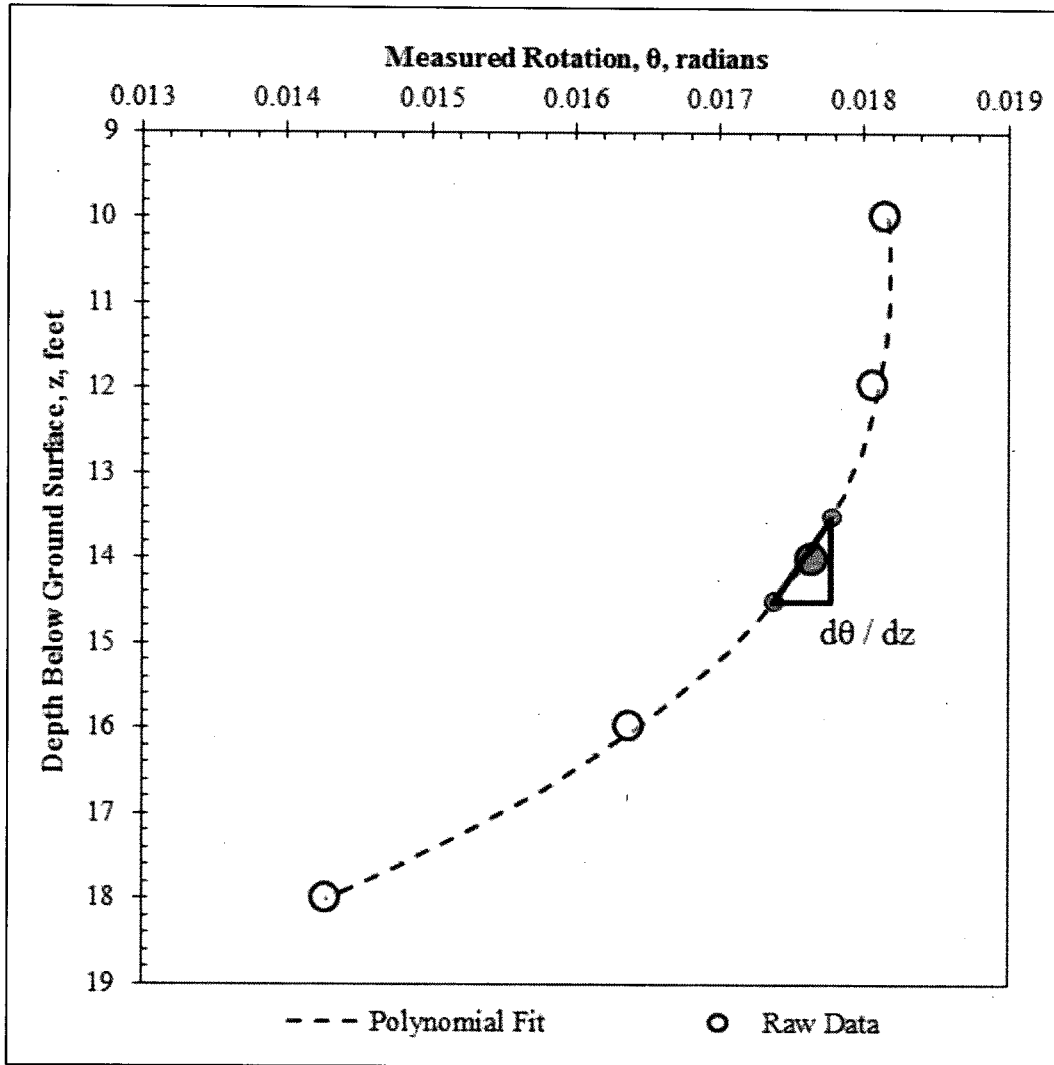
Figure 4.45: Illustration of piecewise third-order polynomial fitting to a moving window of five points at a depth of 14 feet.

First derivative at 14 feet is estimated numerically using a central difference approximation between polynomial values at 13.5 and 14.5 feet.

Repeating the piecewise polynomial fitting process for each depth yields a profile of bending curvature. The profile of bending curvature is smoothed using a 3RH smooth with reroughing. To provide consistency with standard of practice methods, the values of bending curvature are converted into bending moments using the M-Φ relationship generated by the computer program LPILE (Figure 4.46). Figure 4.47 shows the resulting bending moment

94

profile, calculated by converting values of bending curvature to the corresponding values of bending moment as shown in Figure 4.46. Using cracked section properties in the M-Φ relationship generates a smoother profile of bending moment versus depth (there is no "hitch" near the cracking moment), but analysis of the test wall data for this project indicates that the earth pressures estimated at locations with small bending curvatures are unrealistically small when using cracked section properties. This may be a function of the heterogeneous nature of the concrete itself, which inherently produces variations in local stress-strain behavior at different locations within the shaft. If structural stresses are concentrated in the stiff (i.e., uncracked) sections of the shaft, and deformations are primarily located in the more flexible (i.e., cracked) sections, some difficulty in data interpretation can be encountered in the range of small strains. Despite this difficulty, because bending moments in the range of interest are larger than the cracking moment, the interpretation of maximum bending moment in the shaft is relatively unaffected by the choice of cracked or uncracked properties. The influence of concrete cracking on data interpretation is discussed in more detail in subsequent chapters.
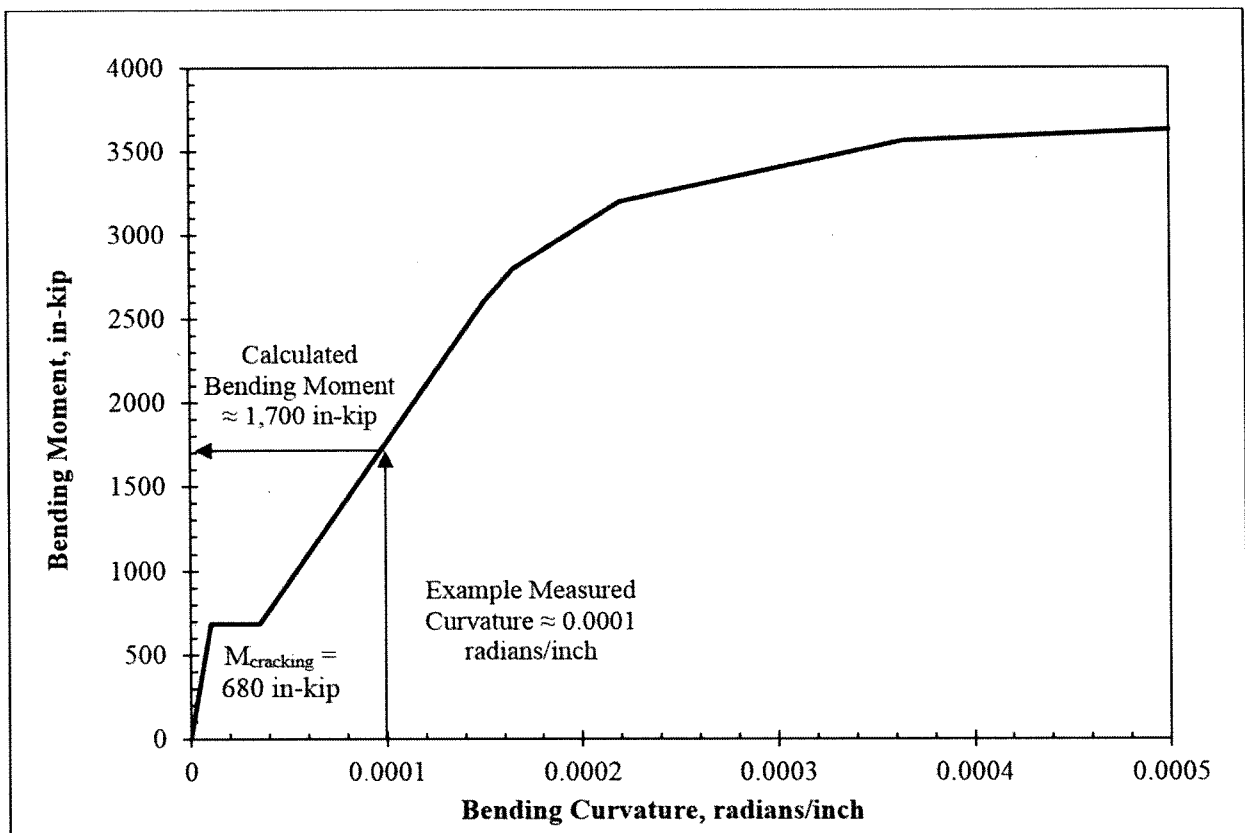
Figure 4.46: Relationship between bending curvature and bending moment (M-Φ relationship) used for LPILE and field instrumentation data analysis.
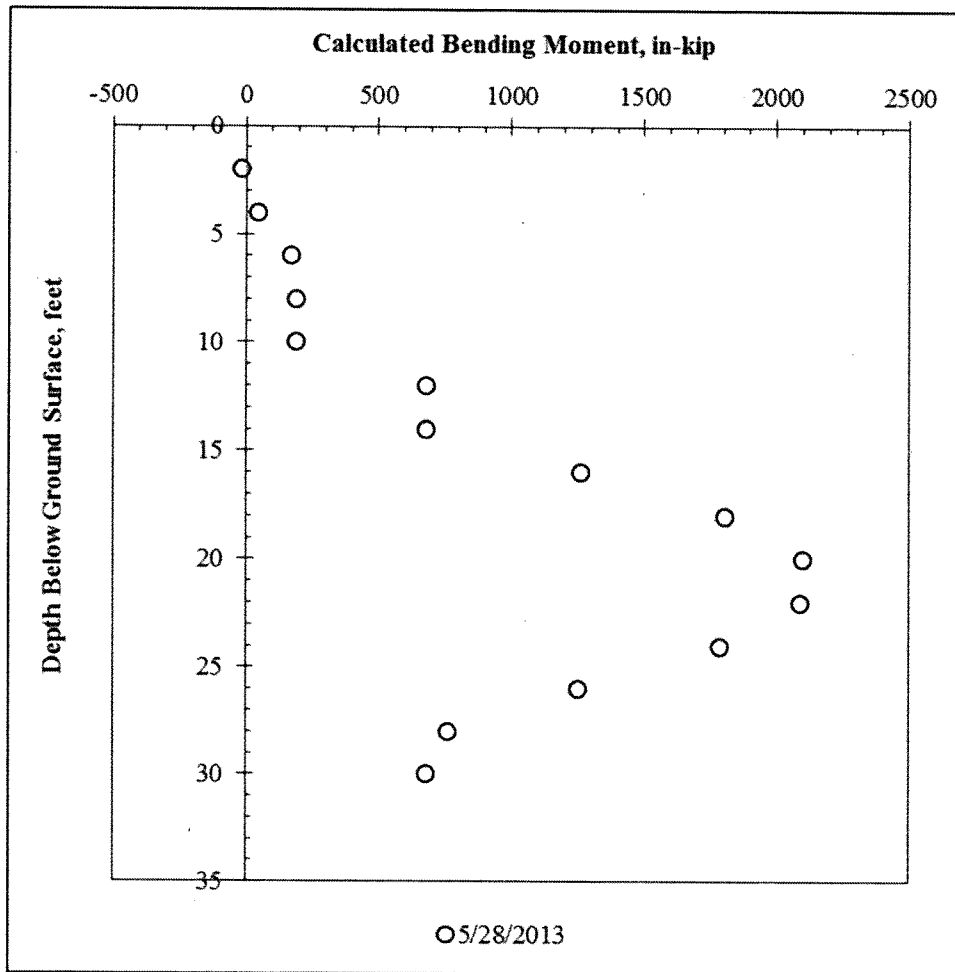
Figure 4.47: Bending moment profile generated from piecewise polynomial fitting of smoothed rotation profile and M-Φ relationship from LPILE.

4.7.2.4: Obtaining Net Earth Pressures from Moment Profiles

To generate profiles of shear forces in the shaft, the same procedure used to differentiate the smoothed rotation profile is applied to the bending moment profile. Because the bending moment profile was generated from a smoothed profile of bending curvature, and to preserve the nonlinear moment-curvature behavior displayed in Figure 4.46, no smoothing is applied to the bending moment profile. To differentiate the profile of bending moment, piecewise third-order polynomials are fit to a window of five points along the depth of the shaft. The resulting shear force profile is smoothed using a 3RH smooth with re-roughing, then differentiated using piecewise polynomials to obtain a profile of soil resistance, which is smoothed again with a re-roughed 3RH smooth. The resulting soil resistance values for the 5/28/13 profile are shown in Figure 4.48, along with comparison values calculated using only the averaged rotation profile with piecewise polynomial differentiation (no smoothing used). In Figure 4.48, the large values of soil resistance in the non-smoothed data above the excavation line are the result of small errors in the original raw rotation data. Small jumps in the original data set become larger with each successive differentiation; after three differentiations, small errors can become large, unrealistic spikes. The judicious use of data smoothing during differentiation can minimize the effects of random errors on the final result.

96
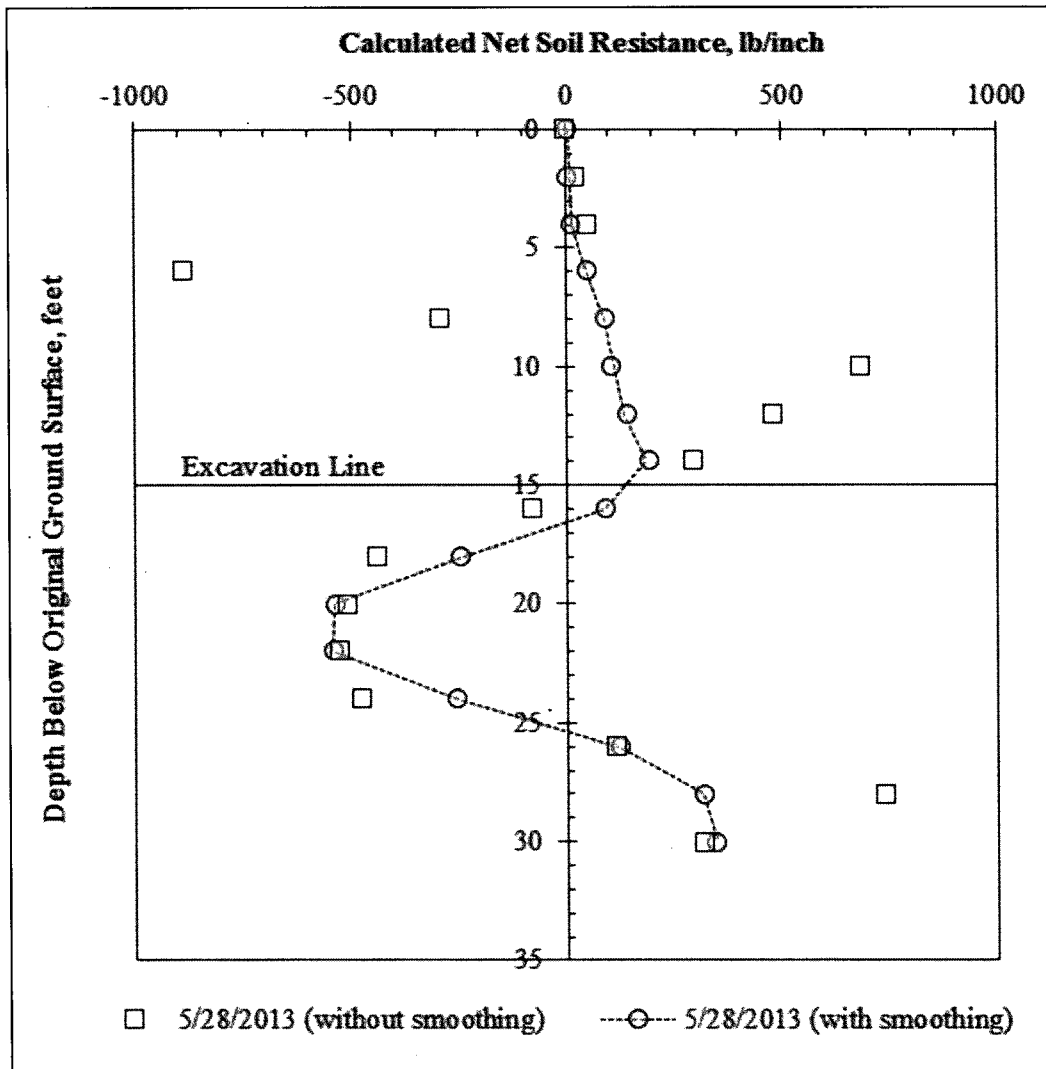
Figure 4.48: Soil resistance profiles generated using piecewise polynomial differentiation of averaged rotation profiles (with and without data smoothing applied during the differentiation process).

On inspection, the differentiation process produces reasonable results when the data smoothing algorithm is used throughout the differentiation process. The profile of net soil resistance reaches zero value close to the excavation depth of 15 feet, and reaches zero again near the shaft's center of rotation at approximately 27 feet. While the soil pressures between 30 and 35 feet must be inferred due to the lack of inclinometer data at those depths, the earth pressures above 30 feet are consistent with those obtained from LPILE results.

4.7.2.5: Generating p-y Curves from Inclinometer Data

With the procedure described above, values of soil resistance (p) and horizontal deflection (y) are obtained for each depth. With readings for a variety of dates, corresponding to a variety of deflections, p and y can be plotted against each other at each depth to create a family of p-y curves.

97

4.7.2.5.1: Discussion of "Net" Soil Resistance

In the following sections, it should be noted that the driving earth pressures acting toward the excavation are defined as (w), and the earth pressures resisting this motion are defined as (p). The profile of net soil resistance generated using the differentiation process is actually a profile of (w – p). Above the excavation line, p is zero and (w – p) = w. At large depths below the excavation line, w is generally assumed to be negligible relative to p, and (w – p) = p. However, near the excavation line, both w and p are acting on the shaft, and their effects can be difficult to separate from one another. For the purposes of this analysis, w is assumed to reach zero at the excavation line.

4.7.2.5.2: Correcting Soil Resistance for Excavation Location

Because the soil resistance values near the excavation line are influenced by points above the excavation line, and the influence of driving earth pressures extending slightly beyond the shaft base, the soil resistance at the excavation line obtained from point-by-point differentiation is often a negative value. Because this is not physically possible with a positive deflection, polynomial curve fitting is applied to ensure net soil resistance values are not negative at the excavation line. To provide consistency with design practice, which often assumes a value of zero soil resistance at the excavation line, a third-order polynomial fit using least-squares regression was used to represent the profile of soil resistance versus depth. This maintains the general magnitude and shape of the soil resistance profile, but allows every profile to reach zero at the excavation line (Figure 4.49).
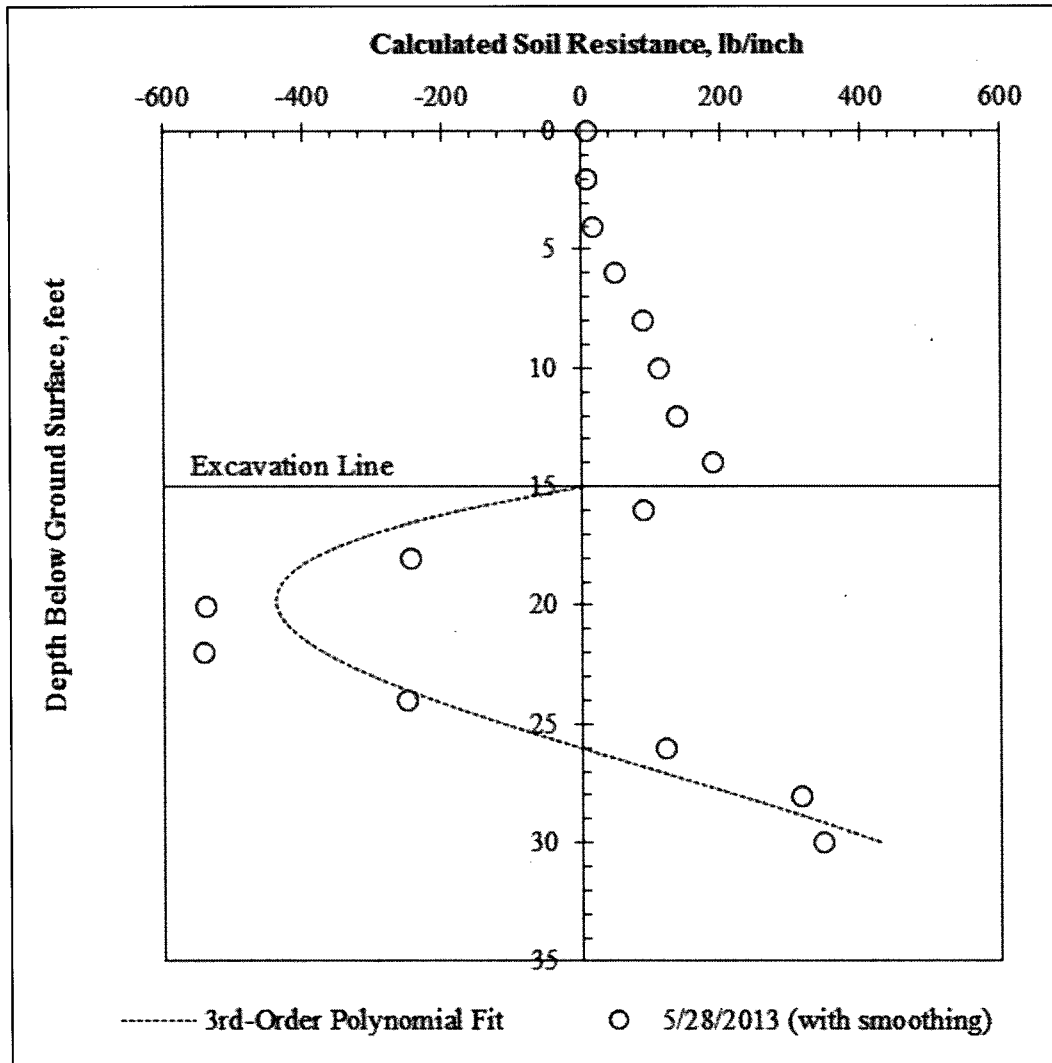
Figure 4.49: Using a third-order polynomial to adjust values of net soil resistance for p-y curves.

4.7.2.5.3: Correcting Horizontal Deflections

In limit equilibrium and numerical models such as LPILE, the shaft rotates about a center of rotation (at approximately 26 feet in Figure 4.1). Above the center of rotation, deflections are positive, and below, the deflections are negative. In a standard deflected shape generated from inclinometer data, however, the shaft base is assumed to be fixed, and all deflections appear to be positive. This can provide misleading results for p-y curves; if the raw inclinometer deflections are used, at the center of rotation, the shaft appears to have moved without any corresponding increase in earth pressure. Similarly, without corrections to deflection data, at the shaft base, nonzero soil forces appear to be present without any shaft deflections. To prevent unrealistic results such as these in data interpretation, and to allow for pile conditions closer to force equilibrium, the inclinometer data is adjusted to allow the shaft to rotate about the center of rotation (defined for the purposes of this analysis as the depth at which the soil resistance below the excavation is equal to zero) as shown in Figure 4.50.

99
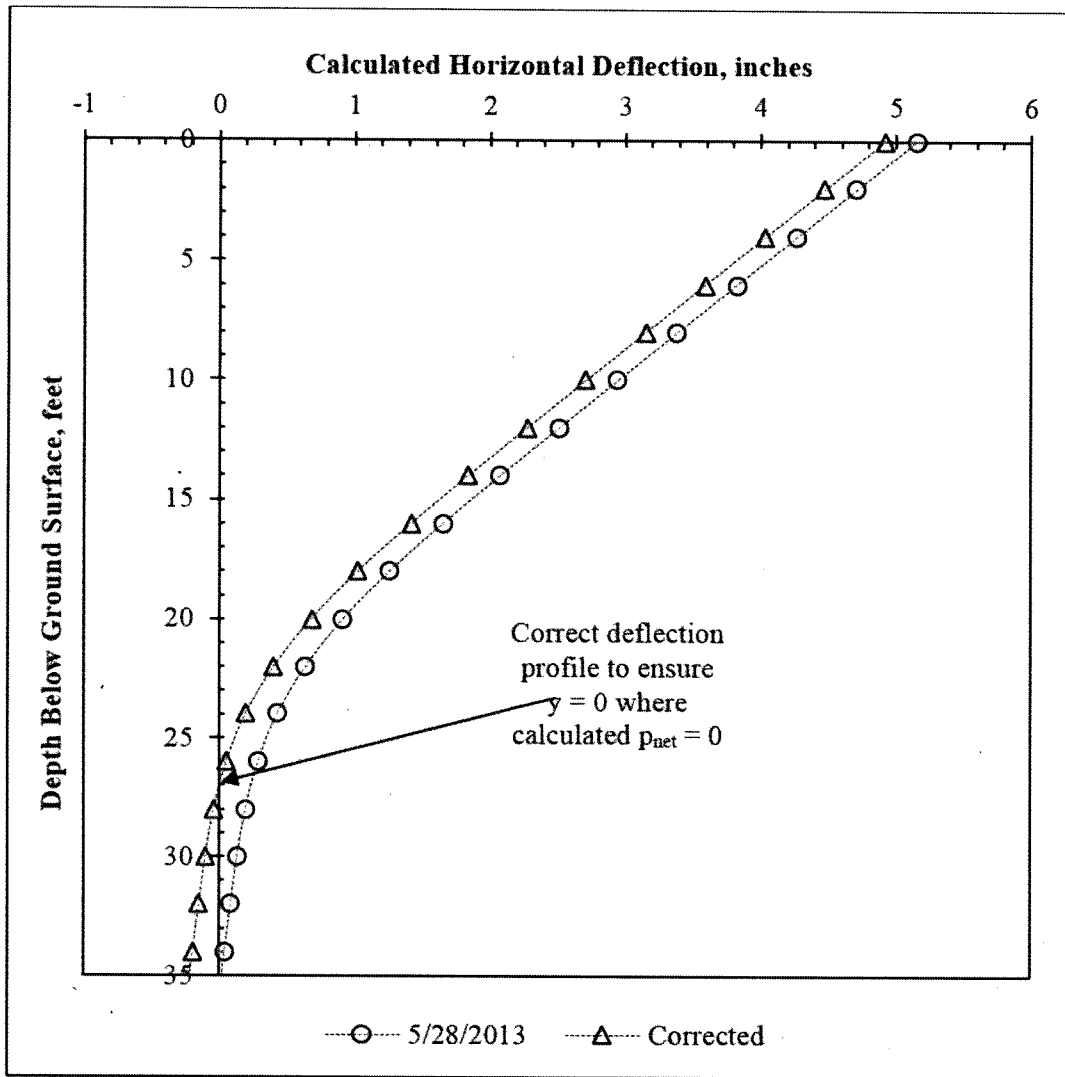
Figure 4.50: Correction of deflected shape about center of rotation for p-y curves

4.7.2.5.4: Example p-y Curves from Inclinometer Data

By plotting corrected values of soil resistance (p) against corrected values of deflection (y), p-y curves comparable to those used for analysis in programs such as LPILE can be generated. An example family of curves for depths between 16 and 24 feet below the original ground surface, zeroed on October 8, 2010, and consisting of all measurements through May 28, 2013, is shown in Figure 4.51.
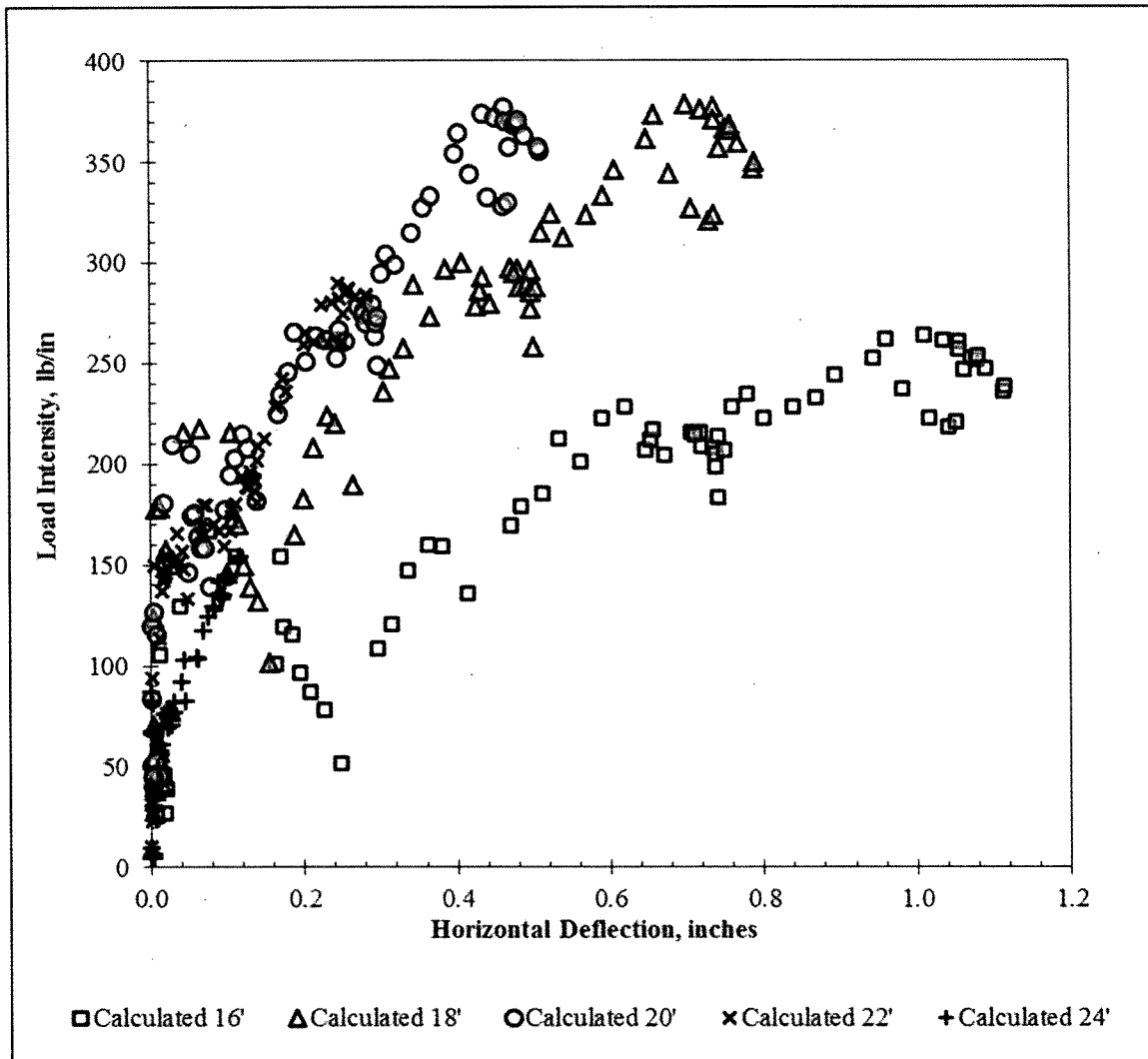
Figure 4.51: Example p-y curves generated from inclinometer data at the test wall. Reference survey is October 8, 2010.

4.8: Summary and Conclusions

The Lymon C. Reese research wall is constructed through expansive clay in Manor. The wall was designed according to standard of practice methods, and is instrumented with inclinometers, strain gauges, and TDR moisture probes. Highlights of the data gathering include the following:

- The drilled shafts and instrumentation were installed during early April 2010. The design goal was to provide a wall that was structurally sound and consistent with design practice, but would produce enough deformations to infer the earth pressures acting on the wall.

- Strain gauges record values of axial strain on either side of the shaft's neutral axis. By dividing the difference in axial strain at a given depth by the horizontal distance between gauges, axial strains can be converted to values of bending curvature.

101

Values of bending curvature can be converted to values of bending moment using standard nonlinear moment-curvature relationships for reinforced concrete.

- Inclinometers record values of rotation along the length of the shaft. The rotation profile can be integrated to calculate a profile of lateral deflections, or differentiated to calculate a profile of bending curvature.

A method of developing p-y curves from inclinometer data is presented. Rotation profiles from the three instrumented shafts are combined and differentiated using a combination of piecewise polynomial differentiation and numerical smoothing techniques. To achieve force equilibrium conditions consistent with existing design practice, corrections are applied to the calculated values of soil resistance to ensure soil resistance reaches zero at the excavation line, and to ensure the shaft deflection is zero where the net soil resistance reaches zero at depth. The resulting values of net soil resistance (p_{net}) are compared with calculated horizontal deflections (y) to develop a model of nonlinear soil response at each depth below the excavation line.

CHAPTER 5: TEST WALL PERFORMANCE AND DATA ANALYSIS

5.1: Behavior before Excavation (April 2010–August 2010)

5.1.1: OVERVIEW

Between installation of the drilled shafts and instrumentation in early April 2010, and test wall excavation in August 2010, strain measurements shed light on the processes that take place within the concrete of a drilled shaft retaining wall prior to excavation. In order to fully understand these measurements, excavation was delayed until early August 2010. This section explains the deformations observed in the wall prior to excavation.

5.1.2: CLIMATIC INFORMATION

Monthly rainfall totals for Austin, Texas between January 2009 and July 2010 are presented in Figure 5.1. For approximately 8 months prior to shaft construction in early April 2010, the test wall site experienced average to above average rainfall. Rainfall totals were significant enough that surface water was frequently present at the test wall site beginning in November 2009, softening the surface soils and delaying initial site investigation until January 2010. After shaft construction, the wall site experienced 2 months of below average rainfall in April and May, followed by 2 months of above average rainfall in June and July.
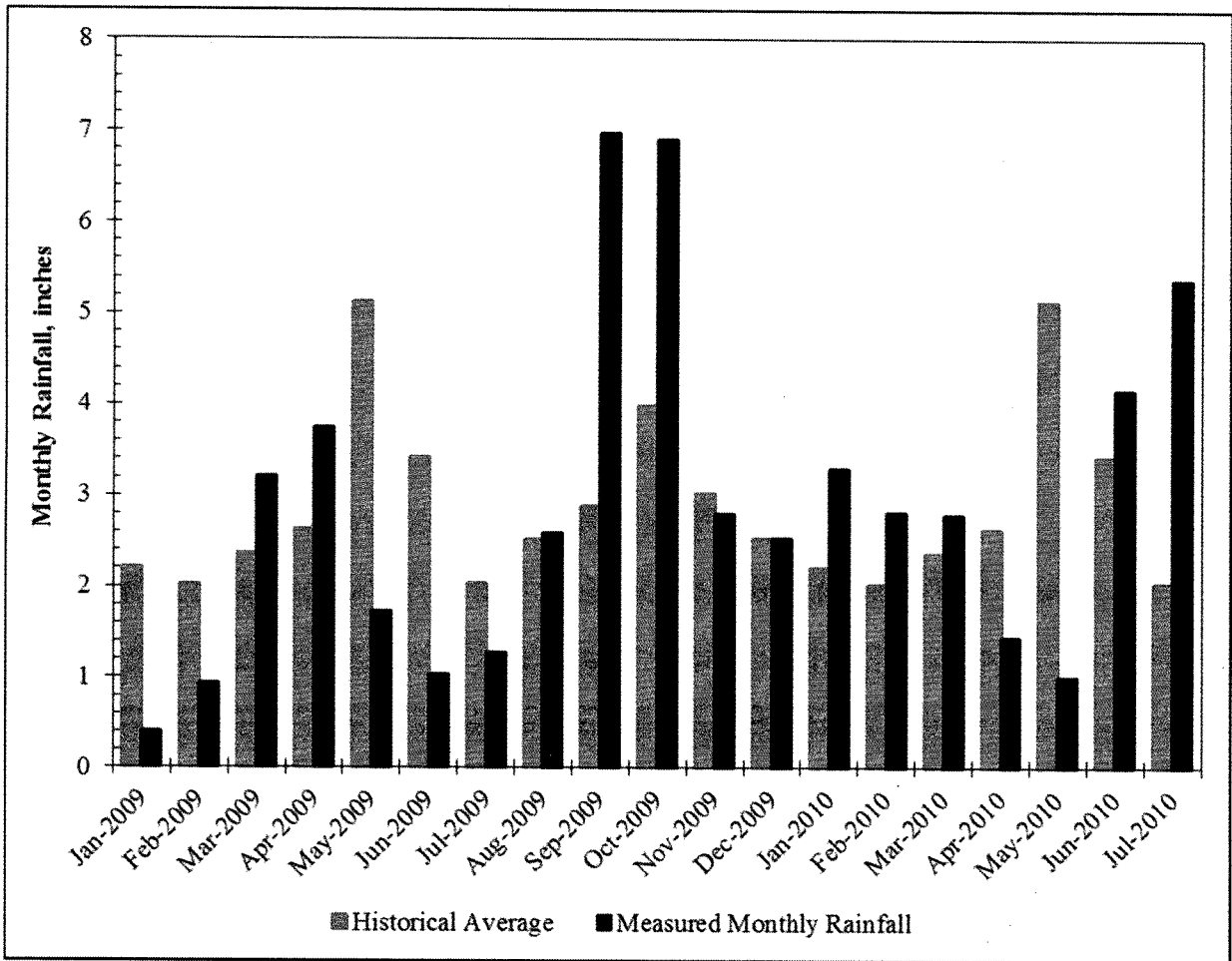
Figure 5.1: Monthly rainfall totals for Austin, Texas (Jan. 2009–Jul. 2010; data from www.wunderground.com). Drilled shafts were installed in early April 2010.

5.1.3: DATA INTERPRETATION

5.1.3.1: Concrete Curing

After successful installation of the strain gauges and field enclosure, strain measurements were taken at least once per day for several weeks. Initial strain measurements behaved similarly as other published data from concrete curing (e.g., Fellenius et al. 2009). As the concrete heated after placement, tensile strains tended to rise sharply and then decrease gradually as the concrete cooled (Figure 5.2). Heating from adjacent shafts also caused less pronounced spikes in tension (Figure 5.2). Because the gauges were zeroed in the lab to a value of zero force and no drift has been observed, nonzero initial strains are assumed to represent forces picked up during installation and concrete placement prior to the first reading.
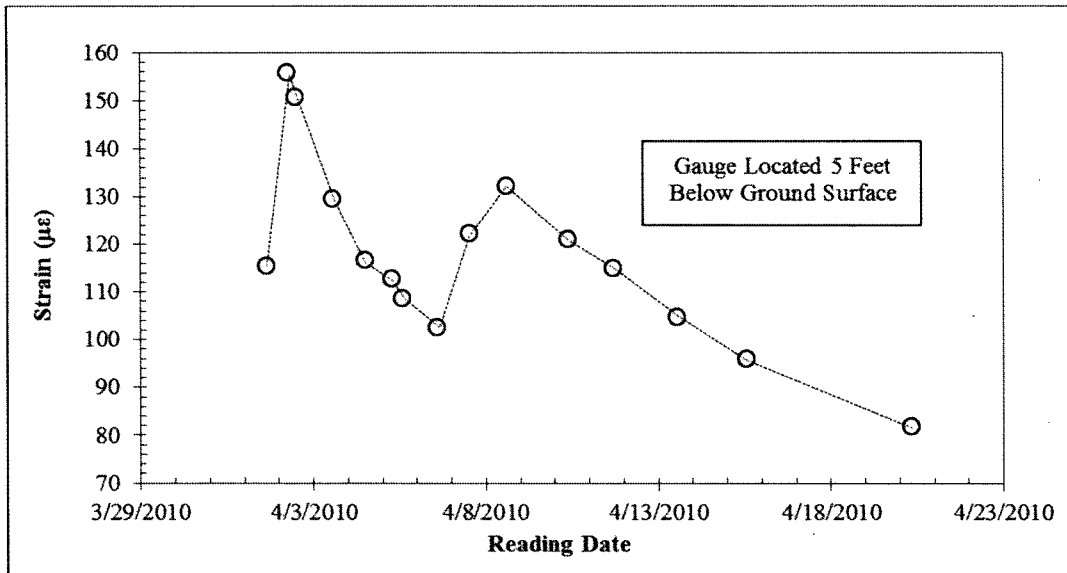
Figure 5.2: Three weeks of strain measurements during concrete curing. Concrete placed on April 1; concrete in adjacent shafts placed on April 6. Positive strain indicates tension.

5.1.3.2: Shrinkage Cracking in Concrete

Beginning approximately 1 week after concrete placement, and continuing over the next several weeks, about 20 percent of the strain gauges exhibited large and sudden jumps into tension. These jumps occurred between 1 and 4 weeks after concrete placement, were most frequent in the second and third weeks, and have no clear relationship with depth. Figure 5.3 shows measurements recorded for one gauge as an example.

These jumps are likely the result of small tension cracks forming in the concrete due to shrinkage. For example, at 7 days, the concrete compressive strength was approximately 4 kips/in^2, giving an average tensile strength of about 0.4 kips/in^2. Distributed throughout the shaft, this represents a tensile load of about 180 kips. If this tensile load is released as a crack extends across the shaft, the load will be redistributed to the 12 #7 bars. A tensile force of 180 kips corresponds to a strain of about 900 microstrains in the bars, which is consistent with the magnitude of tensile strains associated with these jumps (Figure 5.3).

105
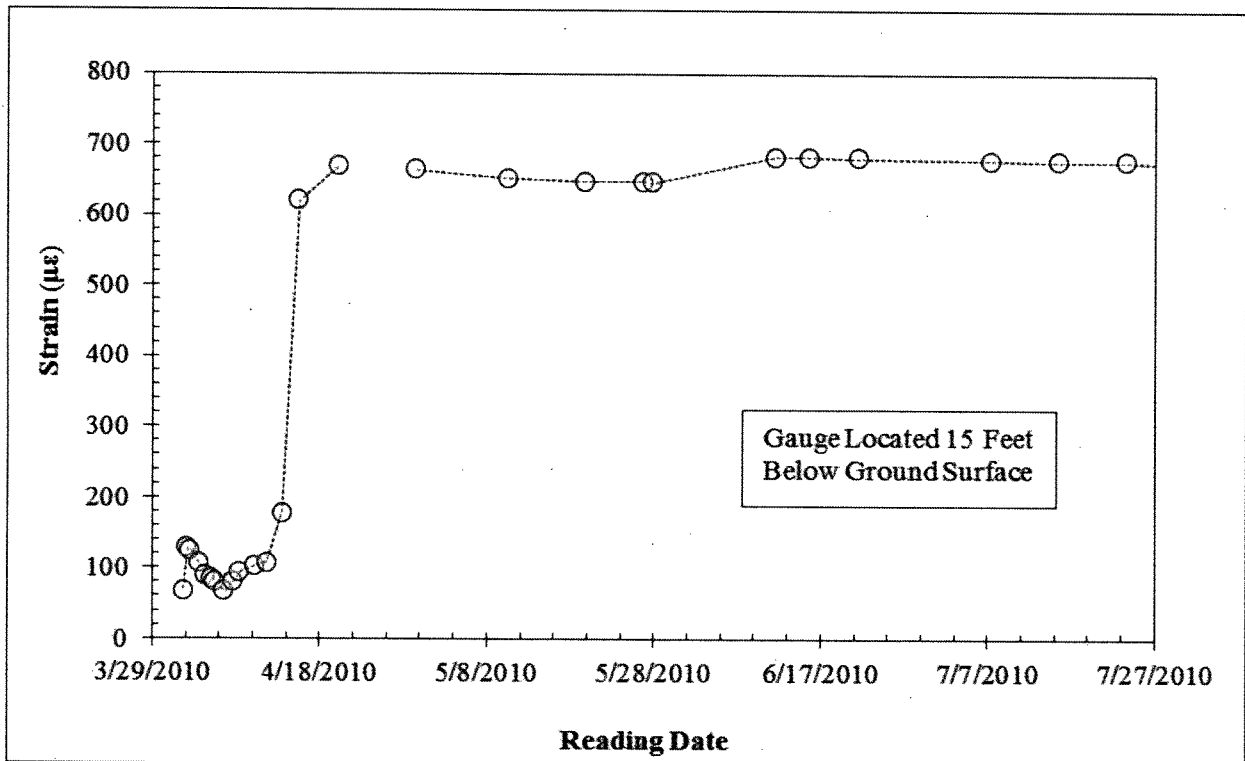
Figure 5.3: Illustration of tension crack formation in concrete near gauge.

Another issue with concrete cracking is the risk of breaking the strain gauge. If a tension crack forms very close to the exposed optical fiber, the fiber can be damaged and the gauge can be lost (Fuhr et al., 1993). Soon after cracking in the concrete began, two gauges jumped to over 3,000 microstrains, which was outside their range of measurement and likely indicated damage to the gauge. Over the course of the project, gauges that suddenly register measurements in this range have usually malfunctioned shortly thereafter.

5.1.3.3: Expansive Soil Movement

After the influence of concrete curing and tension cracks diminished, approximately 10 percent of gauges showed steady increases in tension over the remaining 3 months between concrete placement and excavation. The increases in tension occurred most commonly in gauges located between 0 and 10 feet below the ground surface. Figure 5.4 shows a gauge located 7 feet below ground surface exhibiting this behavior. A gauge at 23 feet showed similar strain behavior early on, but did not exhibit the same increase in tension with time. Qualitatively, the increase in tension begins at a similar time as the transition from below average rainfall in April and May to above average rainfall in June and July. A pre-excavation strain value of approximately 700 microstrains also suggests that a tension crack may also be present near the gauge. The shaft may be experiencing changes in side shear stresses due to moisture content changes in high plasticity clay (e.g., Kim and O'Neill, 1998), along with the effects of tension cracking in the concrete. This behavior is most pronounced in gauges located between 5 and 9 feet below ground surface, above the water table where the natural moisture content fluctuates in response to weather patterns.

106
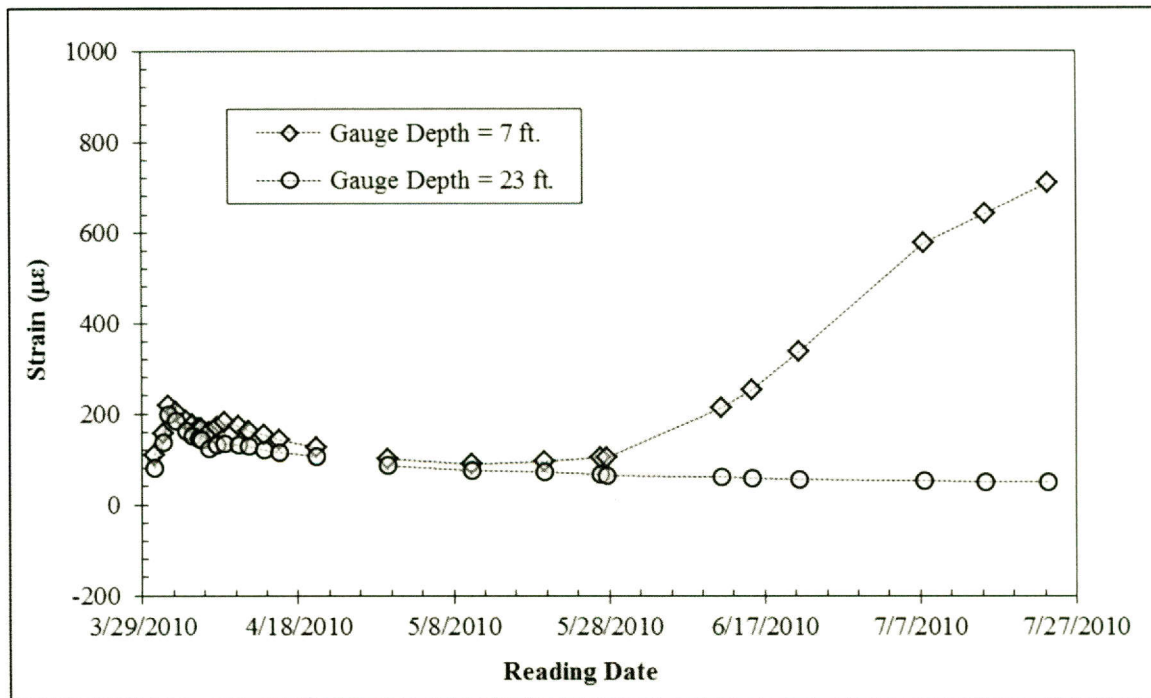
*Figure 5.4: Strains occurring between concrete curing and excavation.
The gauge at a depth of 7 feet may be experiencing changes in side shear due to moisture
fluctuations in the active zone (e.g., Kim & O'Neill, 1998).*

5.2: Behavior during Excavation (August 2010–September 2010)

5.2.1: OVERVIEW AND SUMMARY OF EXCAVATION PROGRESS

Excavation of the test wall began on July 29, 2010, and took place over a period of approximately 4 weeks. The full cantilever height of 14 to 15 feet was reached on August 13, 2010, and the preliminary slopes were completed on August 19, 2010. The slopes were improved on September 30, 2010, and facing was installed on October 8, 2010. Photos of the excavation progress are provided in Figure 5.5–Figure 5.6.

Figure 5.5: Photos of initial excavation progress (7/29/2010–8/5/2010).

Figure 5.6: Photos of later excavation progress (8/23/2010 - 10/1/2010).

5.2.2: CLIMATIC INFORMATION

Prior to the start of excavation, the project site had experienced a relatively dry spring, followed by a summer with above average rainfall. During excavation, the hot, dry weather of August was followed by above average rainfall during the month of September (Figure 5.7), punctuated by approximately 1.9 inches of rain on September 7 (Figure 5.8). Average daily

temperatures decreased from about 85° Fahrenheit at the start of excavation to about 65° at the installation of facing, a decrease of approximately 20° (Figure 5.9).
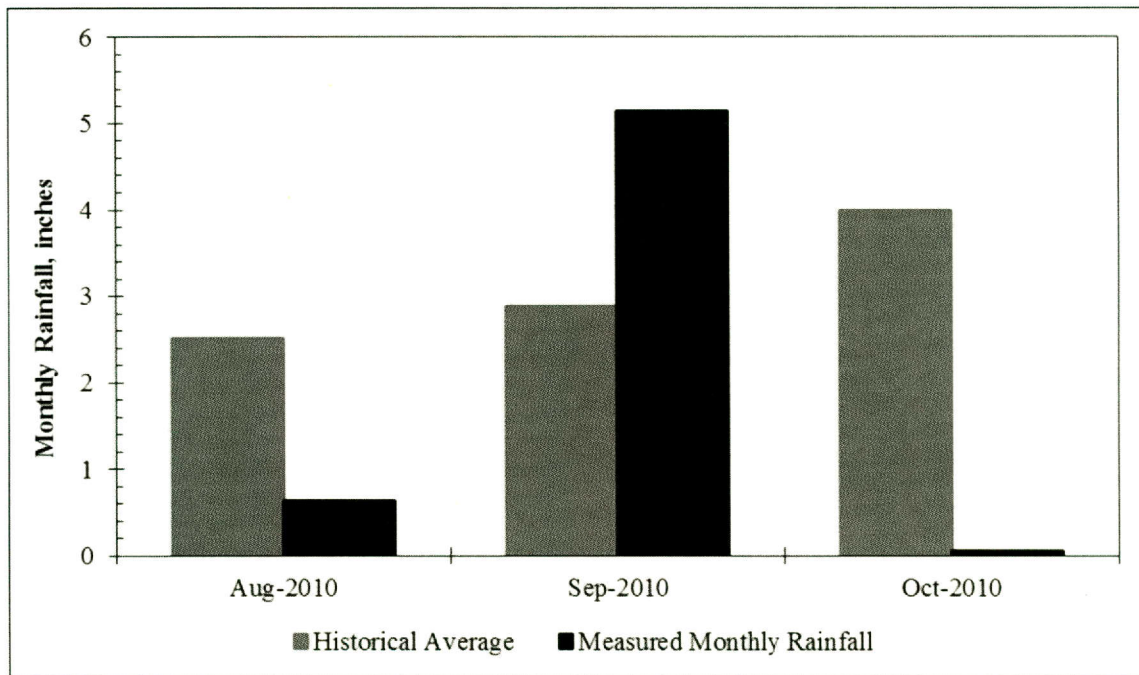
Figure 5.7: Monthly rainfall totals for Austin, Texas (Jul. 2010–Oct. 2010; data from www.wunderground.com).
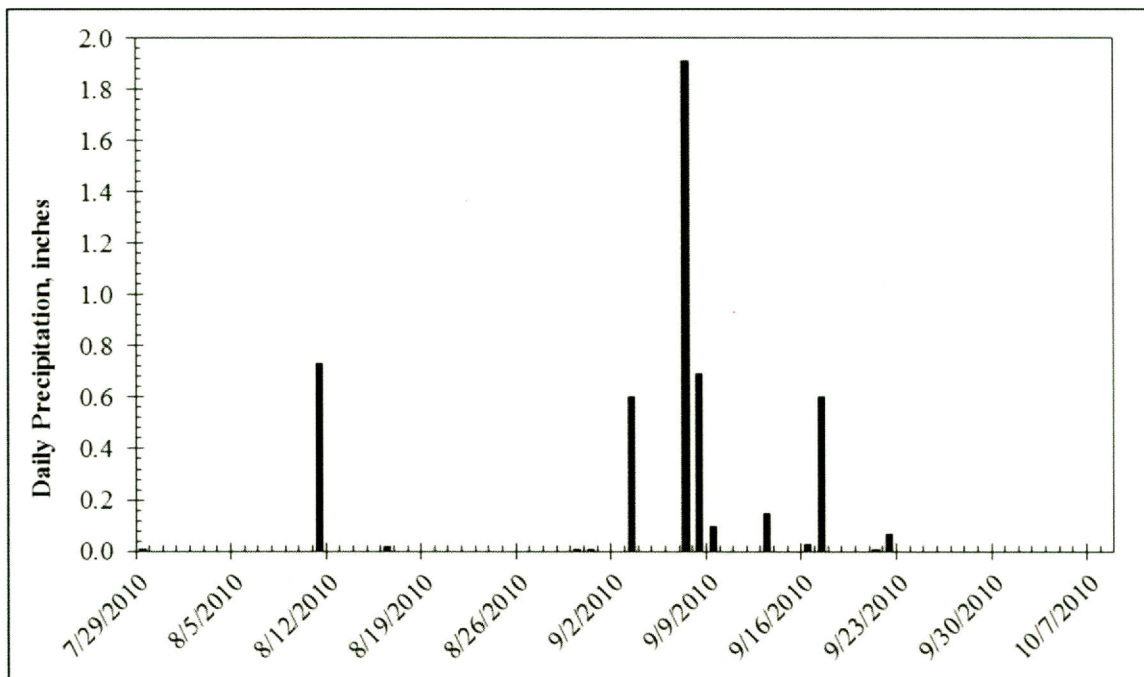
Figure 5.8: Daily precipitation for Manor, Texas (Jul. 2010–Oct. 2010; data from www.wunderground.com).
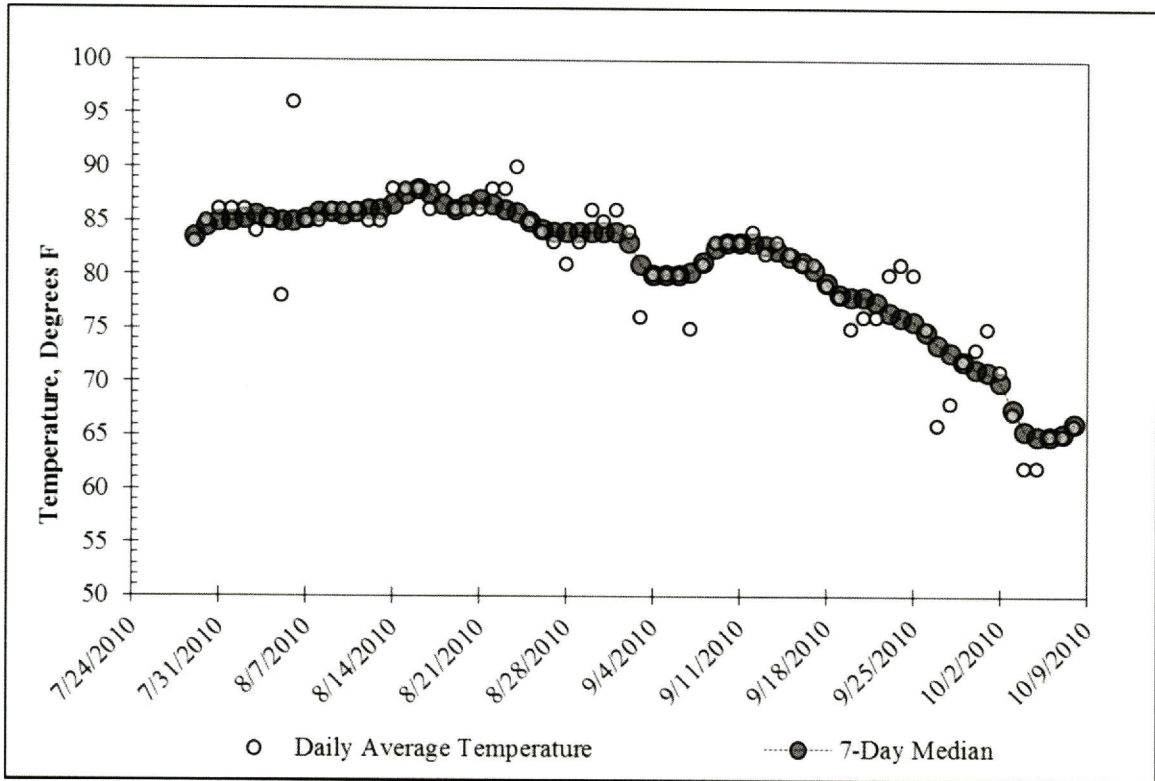
Figure 5.9: Daily temperature data for Manor, Texas (Jul. 2010–Oct. 2010; data from www.wunderground.com).

5.2.3: SUMMARY OF FIELD INSTRUMENTATION DATA

5.2.3.1: Inclinometer Data

Beginning on July 27, 2010, inclinometer data from the east instrumented shaft was recorded at regular intervals throughout the excavation process. Lateral deflections at ground surface and a depth of 14 feet, along with a summary of key excavation events, are shown in Figure 5.10. Deflected shapes at various points during excavation are provided in Figure 5.11, and cumulative deflections in the soil 5.5 feet behind the centerline of the wall are provided in Figure 5.12.
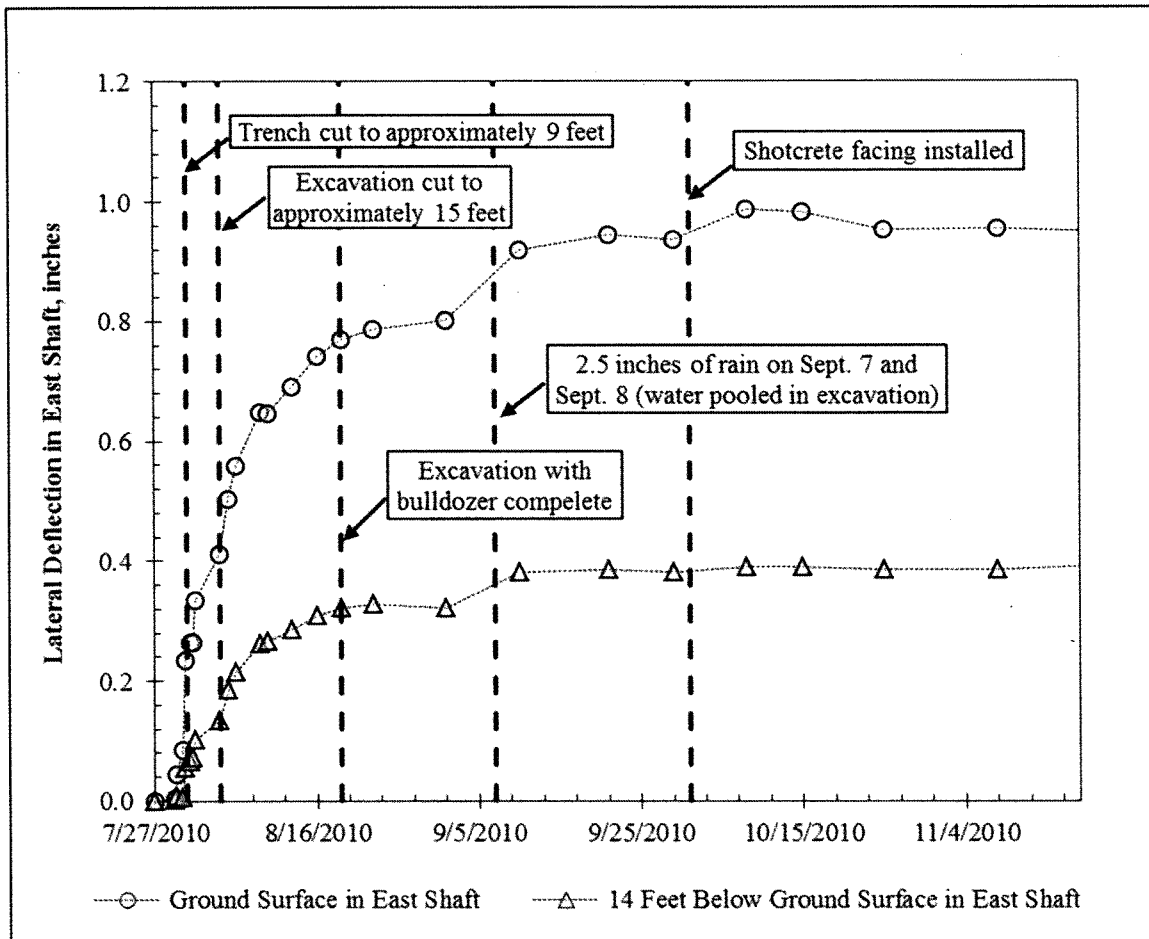
Figure 5.10: Progression of lateral deflections and key events during excavation.
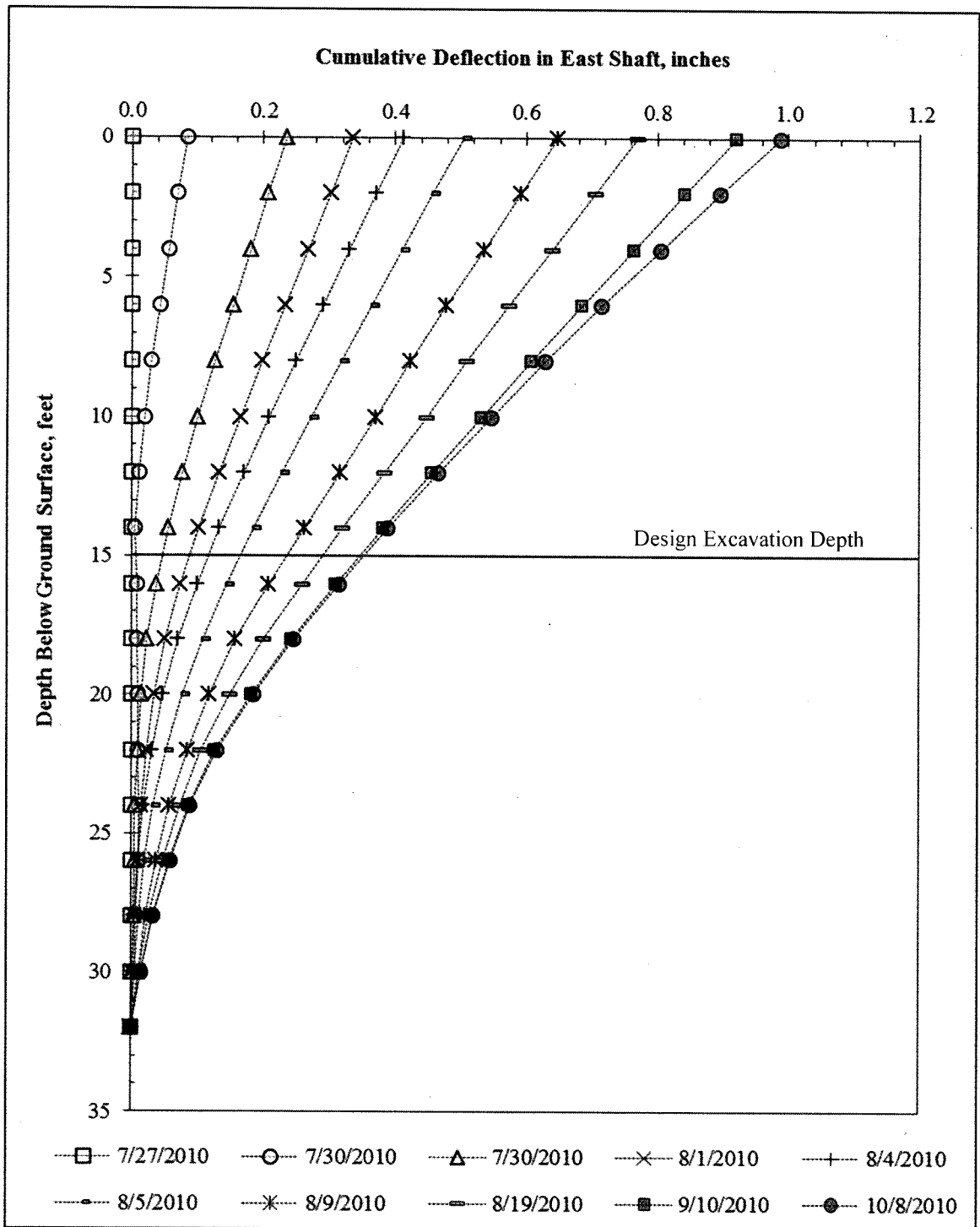
Figure 5.11: Deflected shape of east instrumented shaft at various dates during excavation.
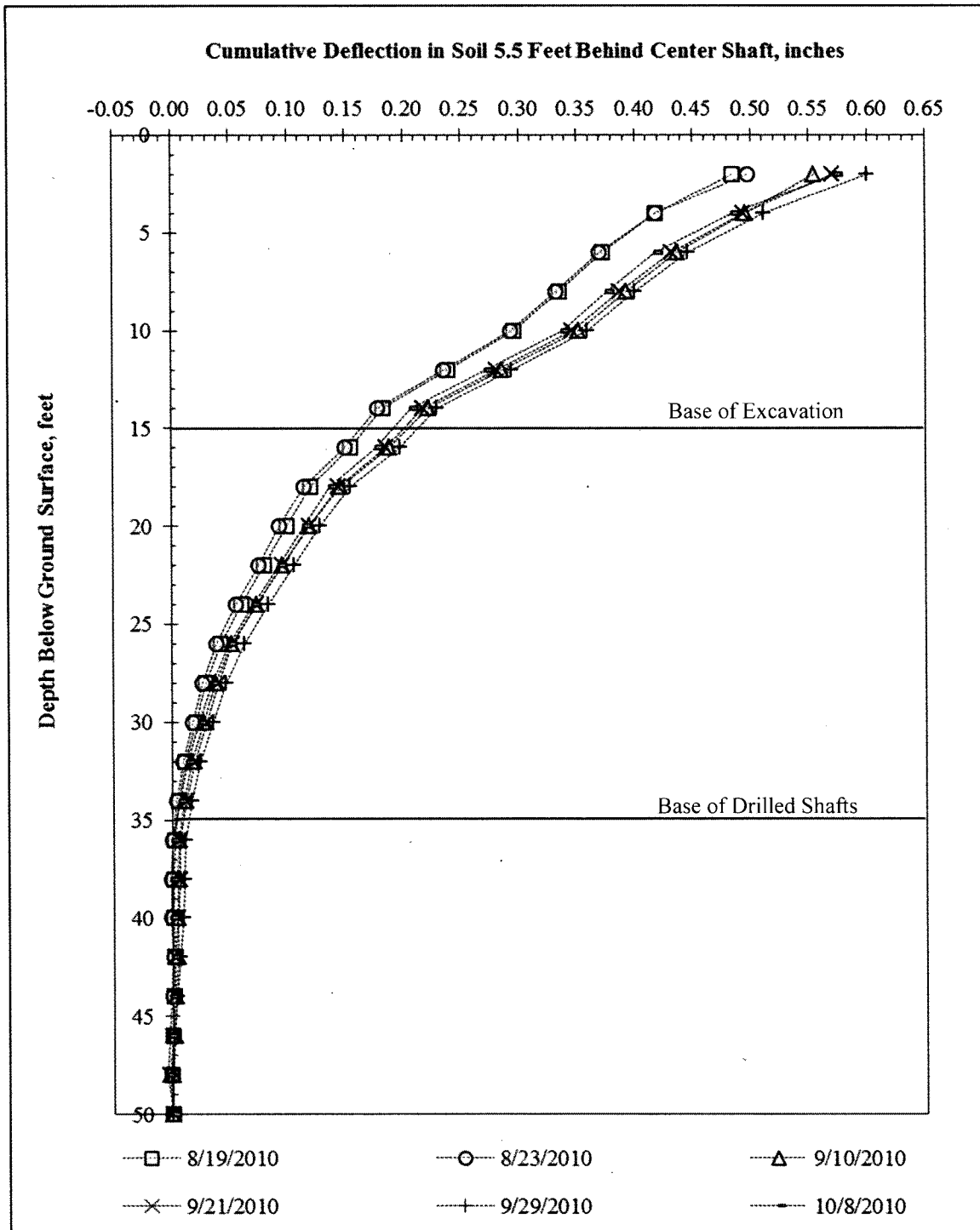
Figure 5.12: Cumulative deflections recorded in inclinometer installed through the soil 5.5 feet behind the center instrumented shaft.

5.2.3.2: Linear Potentiometer Data

A linear potentiometer was installed prior to excavation. It was attached to shaft #16, adjacent to the west instrumented shaft (shaft #15). It provides continuous data on top-of-wall

113

deflection and redundancy with the inclinometer data. Linear potentiometer data recorded during the first month of excavation, along with top-of-wall deflections for the three instrumented shafts, is provided in Figure 5.13.
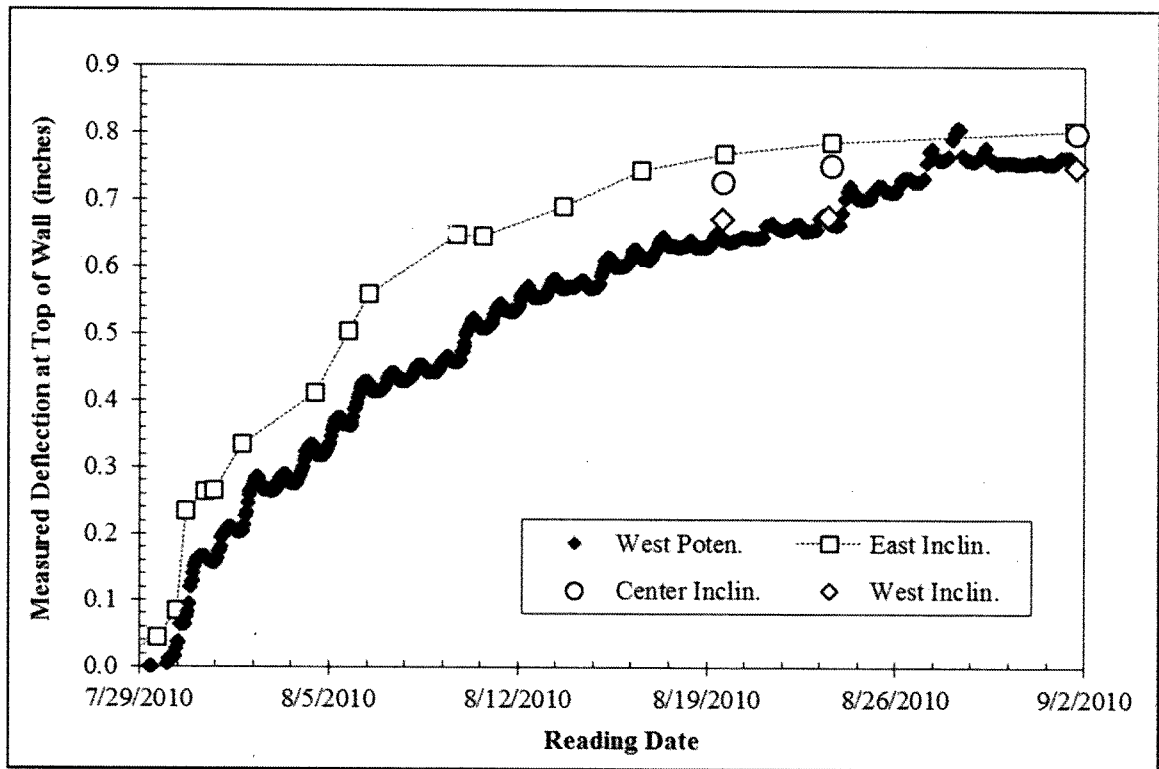
Figure 5.13: Deflection measured at top of wall during excavation.
Excavation began on July 29 and continued through August 27.

5.2.4: DATA INTERPRETATION

During excavation, the wall responded almost immediately to the relief of stress. The deflection at the top of the wall, measured directly with a linear potentiometer and in three inclinometers, is shown on Figure 5.13. The top-of-wall deflections developed more quickly on the east versus the west side because a larger volume of soil was initially removed from the east side (Figure 5.14). The final excavation dimensions at the centerline of the wall were, on average, reasonably close to the design values (Figure 5.15). The final deflections immediately after the excavation was completed were similar between the three shafts (Figure 5.13).

Between depths of 20 and 30 feet below the original ground surface (5 to 15 feet below the cantilever), the shafts developed a bending moment. Figure 5.16 shows axial strains from a pair of strain gauges on either side of the shaft's neutral axis at the approximate location of the maximum bending moment. The strains are nearly equal and opposite, and their development is qualitatively similar to the increase in deflection with time at the top of the wall (Figure 5.13). Additionally, bending strains interpreted from strain gauge data are consistent with those interpreted from inclinometer data (Figure 5.17).

114
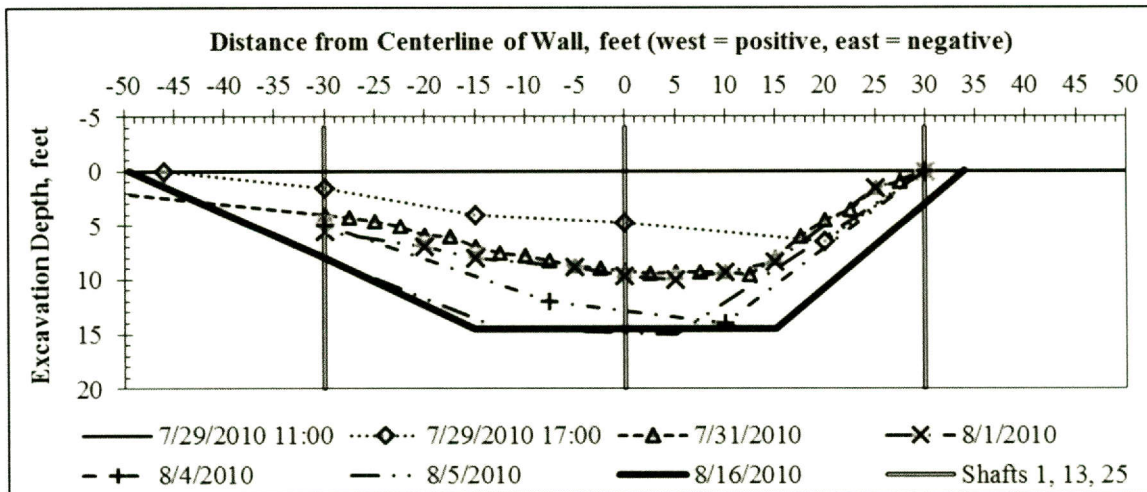
Figure 5.14: Progression of excavation depth along wall face.
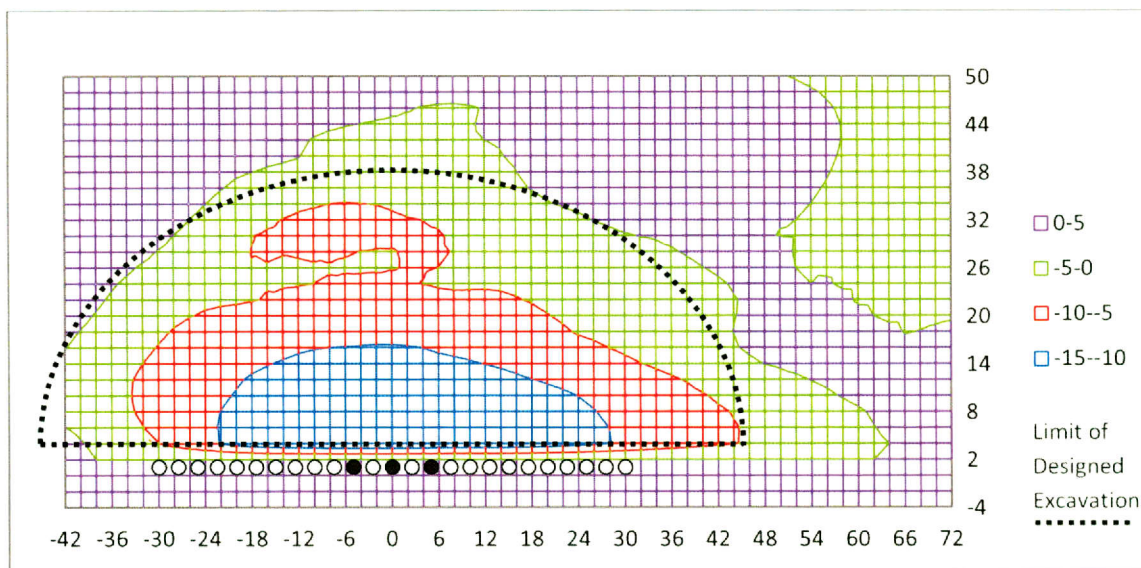
Figure 5.15: Contour plot of final surveyed excavation dimensions (all units in feet).

115
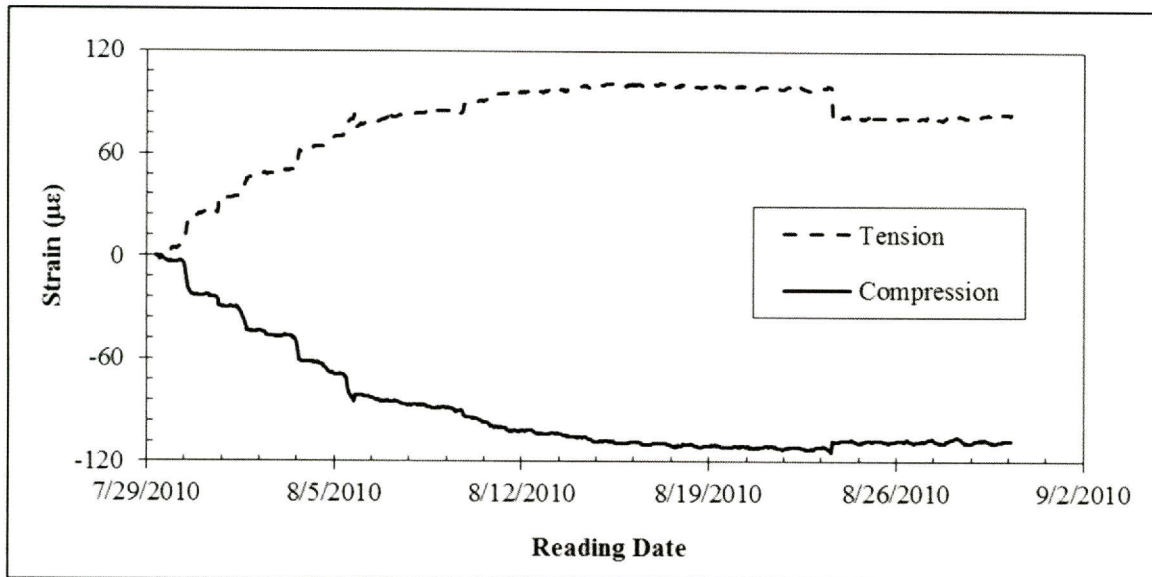
Figure 5.16: Development of bending strains in a pair of strain gauges located 23 feet below ground surface in the center shaft.
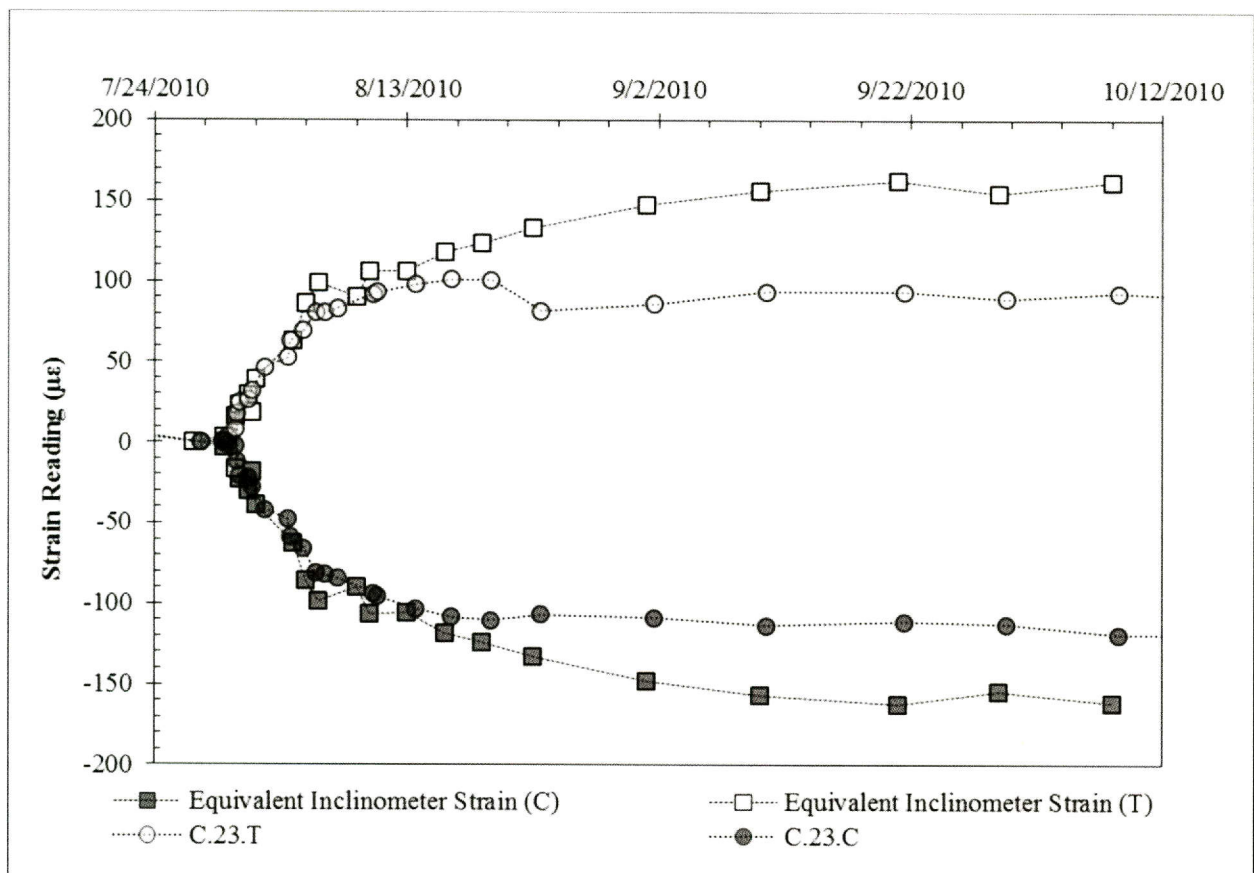
Figure 5.17: Comparison of bending strains interpreted from inclinometer and strain gauge data at a depth of 23 feet.

116

5.3: Behavior during Natural Moisture Cycles

5.3.1: OVERVIEW

After the completion of excavation in September 2010, shotcrete facing material was installed on October 1, 2010. Between October 2010 and April 2012, the wall experienced a range of climatic conditions, which were reflected in the observed wall movements. Because the application of facing represents a practical "zero" value for field measurements, subsequent test wall measurements are referenced to the October 8, 2010, survey (the most recent survey after facing installation).

5.3.2: CLIMATIC INFORMATION

After facing installation was completed in October 2010, the test wall experienced approximately 3 months of below-average rainfall, followed by a series of storms in January 2011. During the spring and summer of 2011, the test wall experienced an extended period of below average rainfall, widely reported to be the most severe drought ever recorded in Austin. During the fall and winter of 2011 and early 2012, rainfall totals were above average, and the project site was frequently flooded by heavy rains. By the time controlled inundation testing had begun in early May 2012, the project site had seen several weeks with high temperatures and minimal rainfall. Rainfall patterns are summarized in Figure 5.18; daily temperature data is presented in Figure 5.19.

Figure 5.18: Monthly Rainfall Totals for Austin, Texas (Oct. 2010–Apr. 2012; data from www.wunderground.com).

117
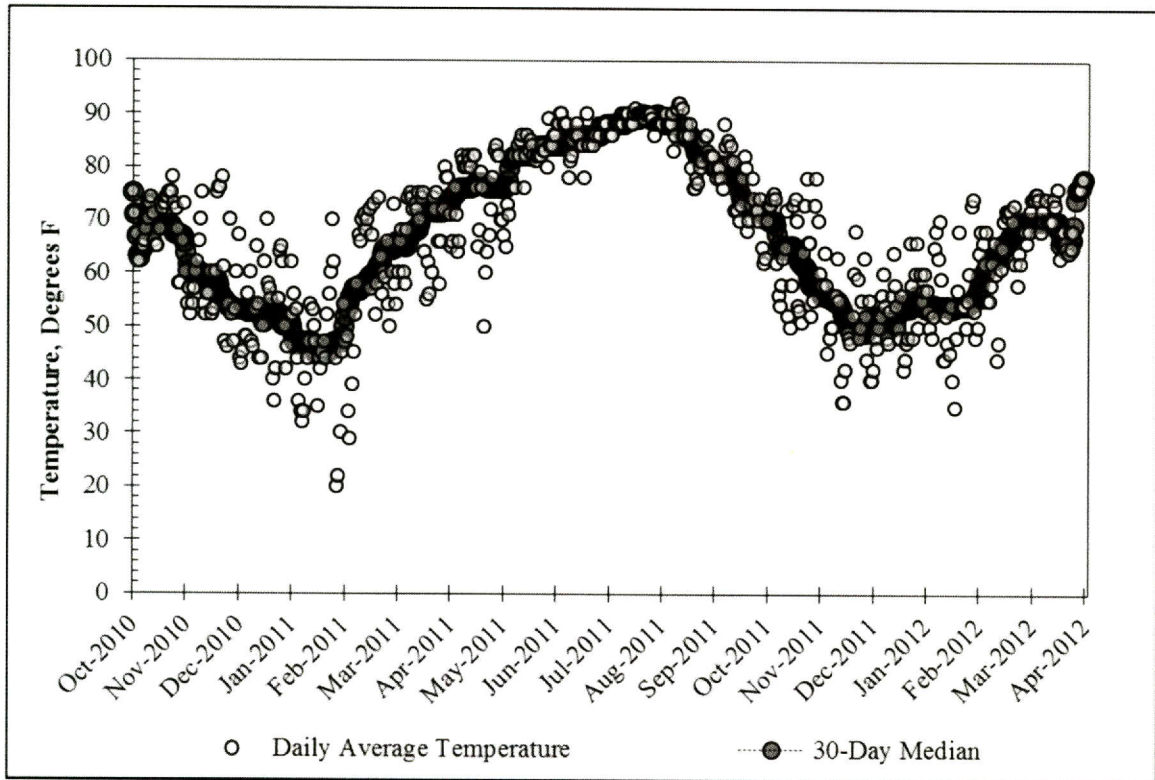
Figure 5.19: Daily Temperature Data for Manor, Texas (Oct. 2010–Apr. 2012; data from www.wunderground.com).

5.3.3: DATA INTERPRETATION

At the time of facing installation, the total top-of-wall deflection was approximately 0.97 inches relative to the beginning of excavation. In practice, the application of facing often represents the de facto "zero" date for a wall in service, because any deformations that have occurred during excavation will be visually obscured by the facing material. Without any internal instrumentation, subsequent wall assessments will rely largely on observed deformations and distress in the facing. For this reason, test wall deformations in response to natural soil moisture fluctuations are referenced to our facing installation date of October 8, 2010. The influence of natural moisture cycles on the measured top-of-wall deflection is illustrated in Figure 5.20. In general, top-of-wall deflections tend to increase with increased rainfall, and stabilize or decrease during periods of drought (rainfall data is presented in Figure 5.18).

118
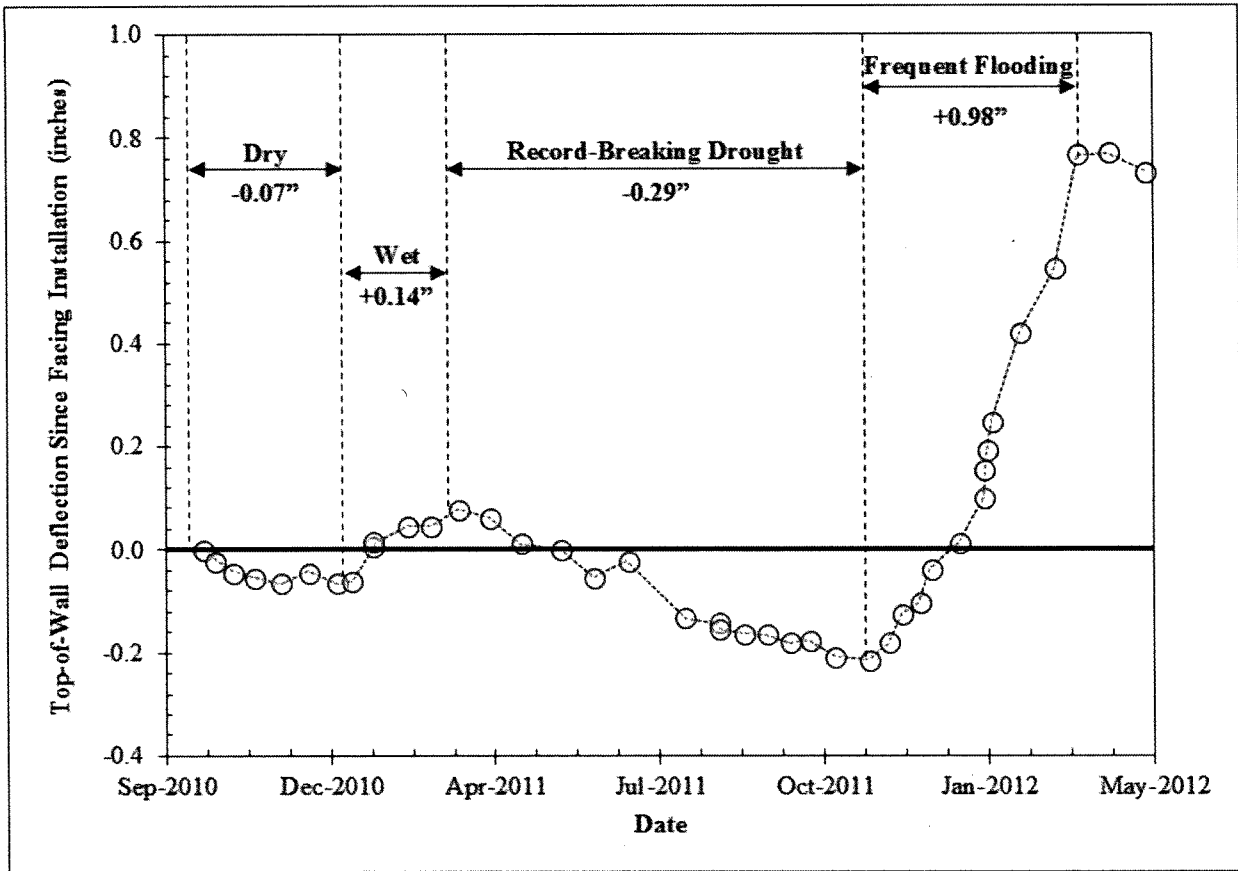
Figure 5.20: Variation of top-of-wall deflection with natural moisture cycles. Deflections are referenced to installation of facing on October 8, 2010.

Between March 2011 and November 2011, a record-breaking drought caused the soil on the project to dry and shrink significantly. In response, the top-of-wall deflections decreased by approximately 0.29 inches over 8 months. As an indication of drying-related soil shrinkage on the project site, noticeable differential settlement between the inclinometer casing (installed to a depth of 50 feet) and its surrounding concrete pad (connected to the ground surface independently of the casing) was observed. While this is far from a perfect measurement, it does indicate significant shrinkage of the retained soil occurred (Figure 5.21). The top-of-wall deflections reach a minimum during this phase.

119
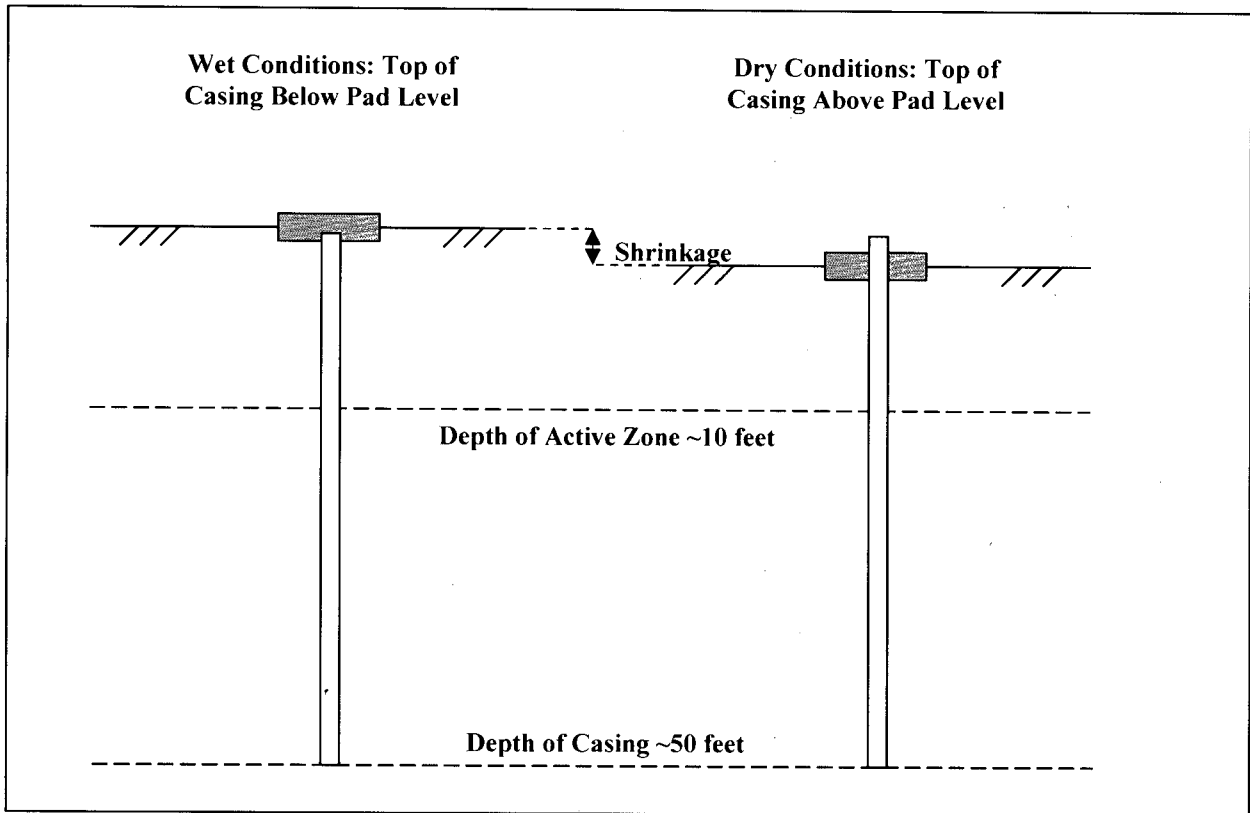
Figure 5.21: The use of a deep inclinometer casing and concrete pad as a qualitative indicator of soil shrinkage near the test wall (not to scale).

During each of the phases of wall motion illustrated in Figure 5.20, the deflected shape of the shaft varied in ways that cannot be easily modeled using a typical p-y analysis. In Figure 5.22, the deflected shape of the shaft at the conclusion of each phase of motion is plotted. When these are compared with the deflected shape predicted by the original design p-y analysis using a commonly assumed earth pressure of 40 psf/ft and stiff clay curves for the foundation soil, the qualitative differences in the predicted and measured values are similar to the differences observed during excavation. Throughout both wetting and drying cycles, the observed foundation soil response is softer than the response predicted by the stiff clay curves. More complex loading mechanisms, the influence of shaft base rotation, weakening of the soil in the base of the excavation, and various other factors may all influence these discrepancies.

120
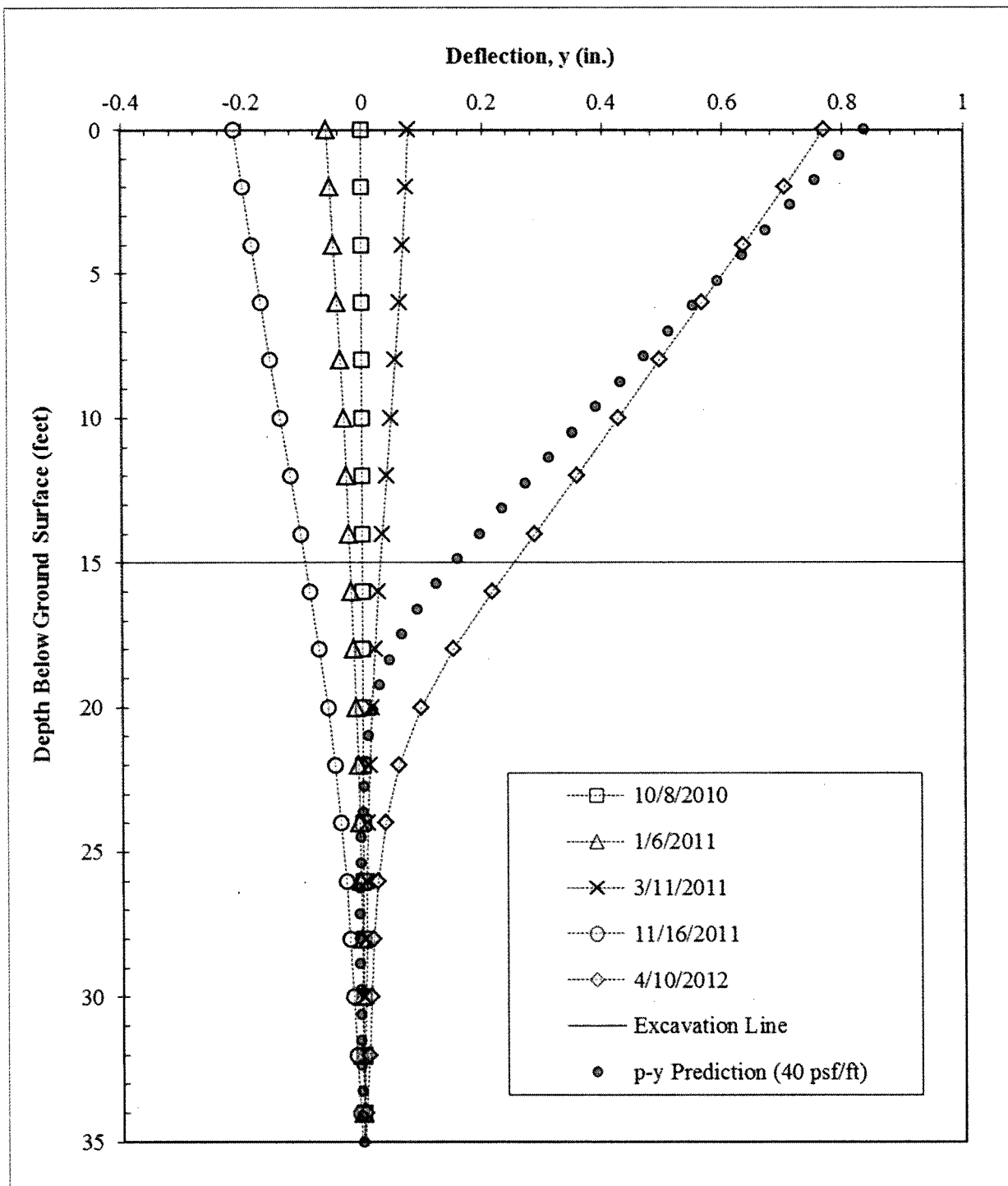
Figure 5.22: Deflected shapes of test wall at key dates, referenced to the installation of facing on October 8, 2010, compared with the initial p-y design analysis.

5.4: Behavior during Controlled Inundation Testing

5.4.1: OVERVIEW

During the extremely dry summer of 2011, the research plan was modified to include cycles of artificial inundation of the retained soil. Based on climatic history and the available long-term weather forecasting, it was deemed unlikely that the soil on the project site would ever sustain the high moisture contents necessary to investigate the effects of soil expansion on wall behavior. By increasing soil moisture content behind the wall to an upper-bound condition, the influence of soil wetting and expansion on the earth pressures can be more readily estimated. Beginning in May 2012, the retained soil was provided unlimited access to water for 2 months, followed by a 7-month drying cycle. In February 2013, the retained soil was inundated until the top-of-wall deflections reached equilibrium, a period of approximately 4 additional months.

5.4.2: SUMMARY OF KEY EVENTS

5.4.2.1: Site Investigation and Installation of Inundation Berm and Piezometers

On February 23, 2012, a site investigation was conducted and four stand pipe piezometers were installed as shown in Figure 5.23. On April 26, 2012, the inundation berm was constructed as shown in Figure 5.24–Figure 5.25.
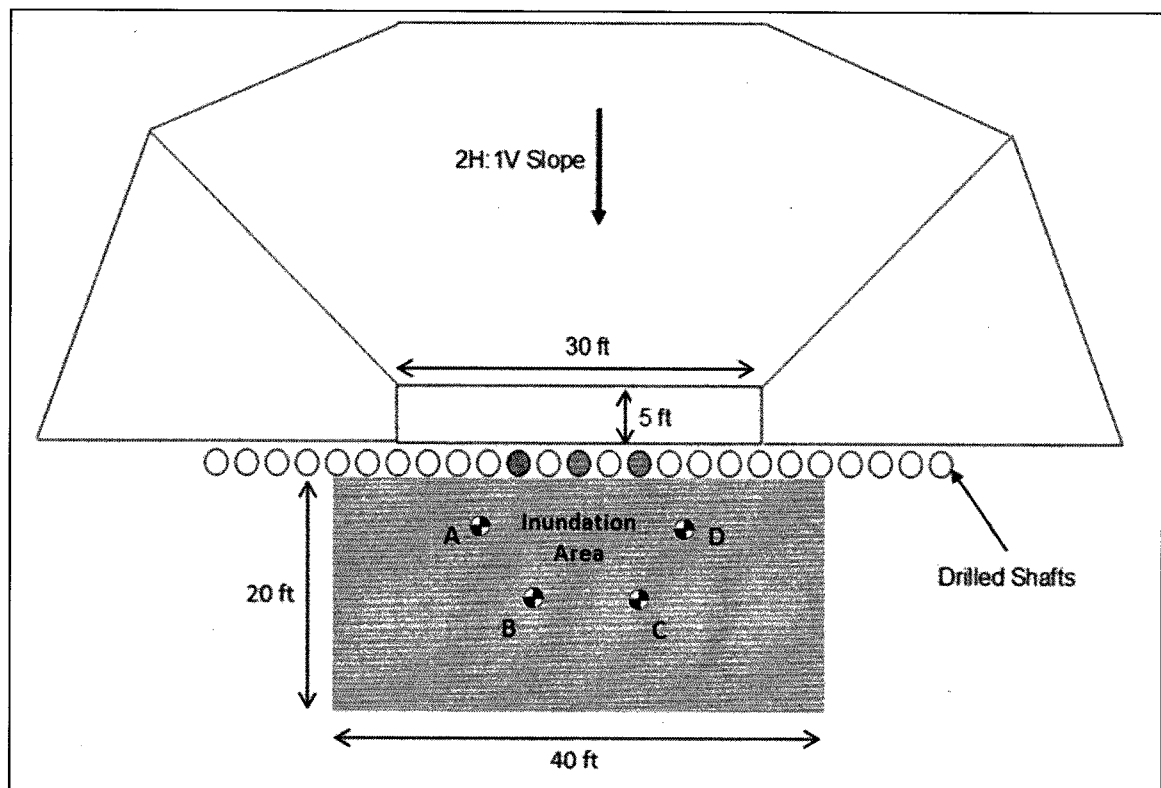
Figure 5.23: Location of inundation zone and stand pipe piezometers.
Piezometers A and C are screened from 5 to 15 feet; piezometer B is screened between 3.4 and 4.6 feet; piezometer D is screened between 3.6 and 4.8 feet.
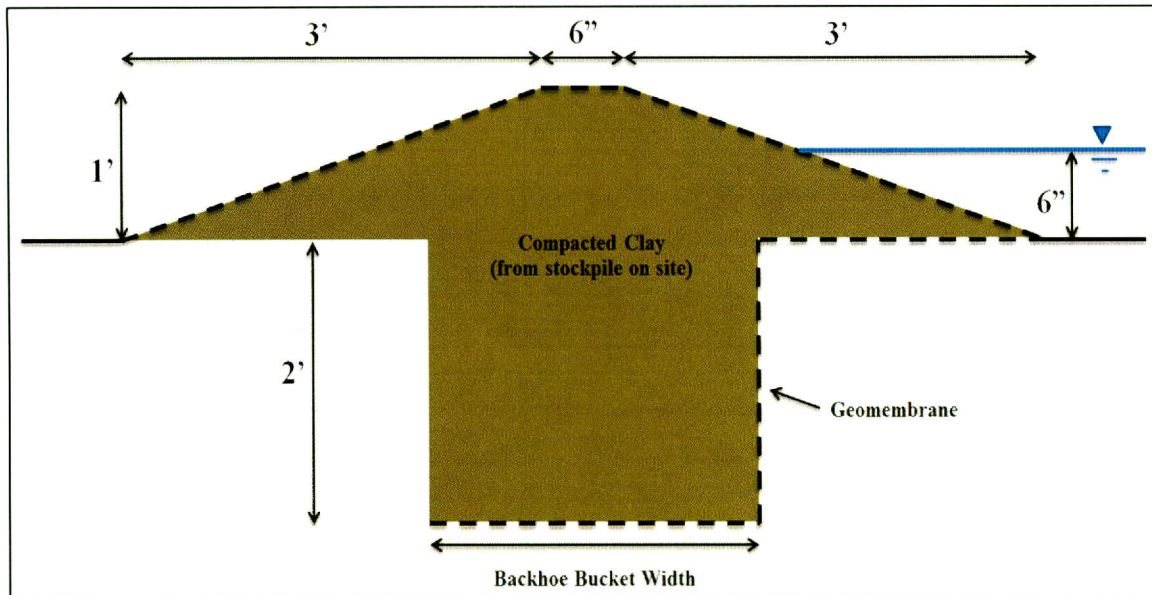
Figure 5.24: Schematic of inundation berm.
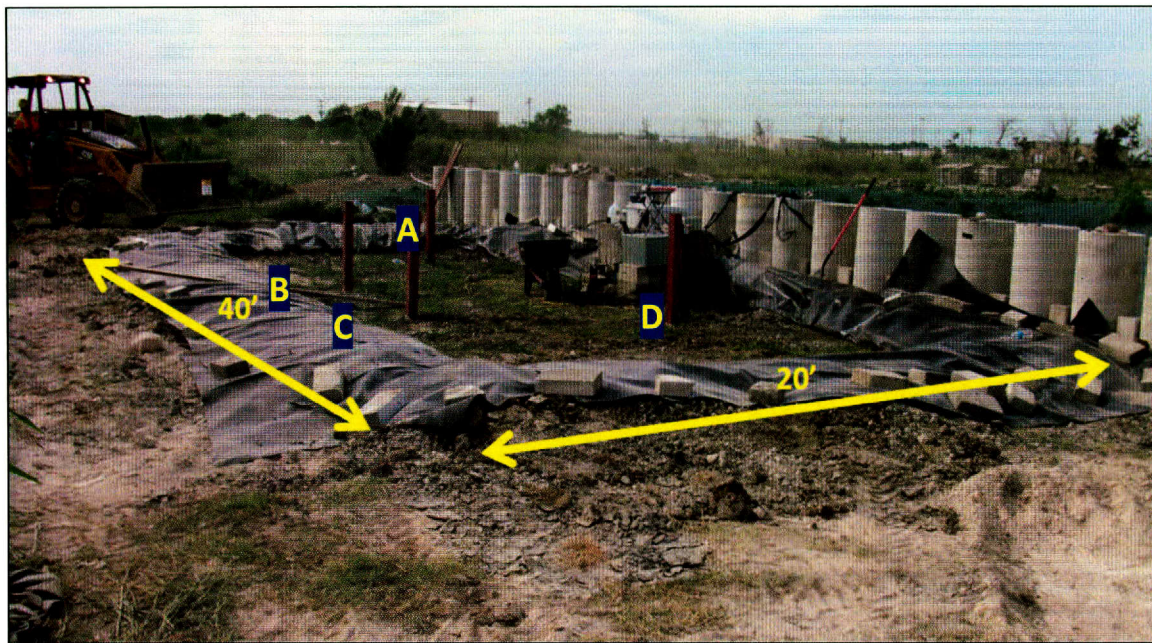
Figure 5.25: Inundation berm and stand pipe piezometers (April 26, 2012).

5.4.2.2: Summary of Inundation Cycles

5.4.2.2.1: First Inundation Cycle (May 2012–July 2012)

Beginning on May 3, 2012, the inundation zone was filled. Wall deflections increased steadily for approximately 2 months until July 2, 2012, when the water supply to the pond was stopped and the wall was allowed to return to its natural state.

5.4.2.2.2: First Drying Cycle (July 2012–February 2013)

From July 2012 to February 2013, the wall was not provided access to moisture beyond naturally occurring rainfall on the project site. Over this time period, deflections fluctuated slightly, but did not increase or decrease to a degree consistent with a significant change in loading conditions.

5.4.2.2.3: Second Inundation Cycle (February 2013–June 2013)

Beginning on February 5, 2013, the inundation zone was filled a second time. After approximately 4 months of inundation, the wall deflections and piezometer water levels stabilized. In response to a large storm event, a major flood occurred in which the water level in the excavation reached the ground surface prior to the inclinometer and strain gauge data surveys recorded on May 6, 2013 (Figure 5.26). During this flood event, significant erosion of the excavation slopes occurred; due to additional soil transported to the excavation base, the excavation depth had decreased to approximately 13.5 feet below ground surface.

Figure 5.26: Flooding in response to a large storm before the May 6, 2013, data surveys. Water level in the excavation reached ground surface.

5.4.2.2.4: Second Drying Cycle (June 2013–July 2013)

On June 3, 2013, a second drying cycle began. Water moved out of the soil quickly, and shrinkage cracks appeared in the surface soil (Figure 5.27). As water moved out of the soil, top-of-wall deflections began to decrease fairly quickly. At the time of this writing, the wall deflections had been monitored during drying for a period of approximately 2 months. At the conclusion of data recording in July 2013, top-of-wall deflections and stand pipe piezometer levels had nearly stabilized, but had not completely reached equilibrium. Based on previous observations, it is likely that when water levels return to their natural values of approximately 8 feet below ground surface, the top-of-wall deflections will stabilize.

Figure 5.27: Inundation zone on June 17, 2013, 2 weeks into second drying cycle. Stand pipe piezometer casing is 4" across.

5.4.3: CLIMATIC INFORMATION

Monthly rainfall totals for Austin during controlled inundation testing are presented in Figure 5.28. Daily temperature measurements for Manor, Texas, are presented in Figure 5.29. While rainfall data during periods of wall inundation is useful to get a sense of the soil conditions outside the influence of the inundation zone, rainfall data during the drying cycle from July 2012 to February 2013 is of most interest. For the first 3 months of the drying cycle during July through September 2012, rainfall totals were above average, followed by 4 months of below average rainfall between October and December 2012. During January 2013, rainfall totals began to increase before the beginning of the second inundation cycle in February 2013.
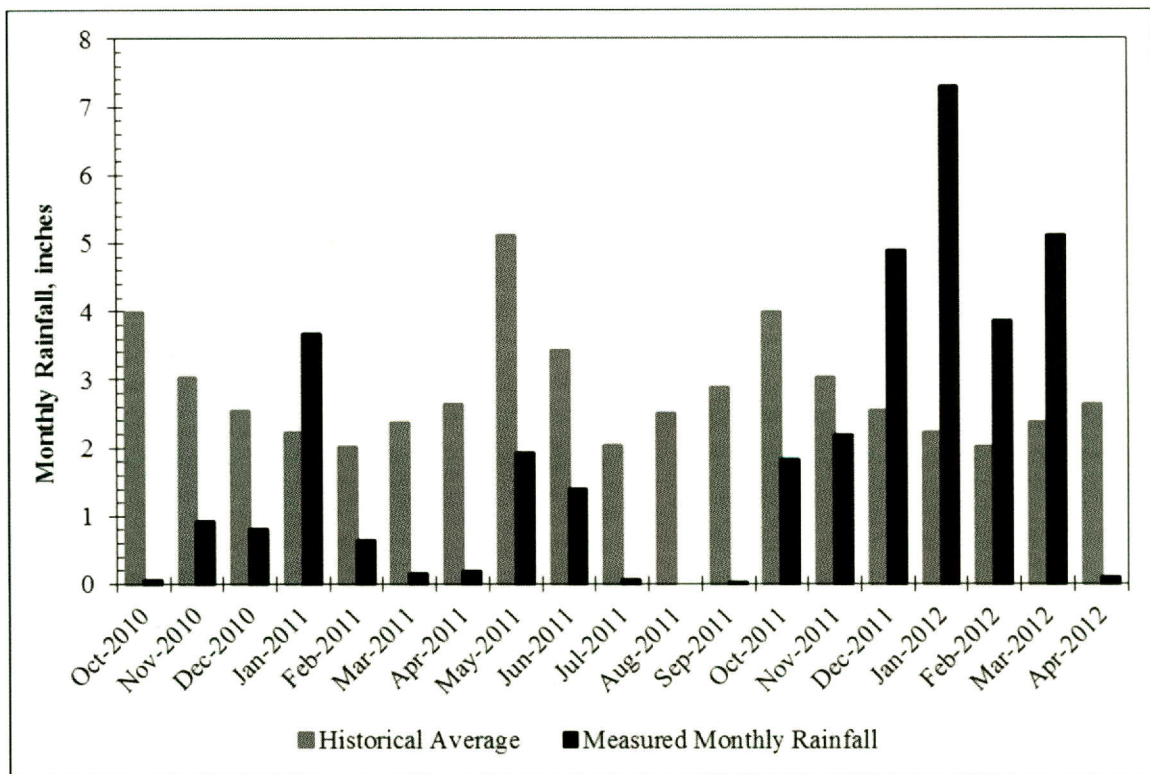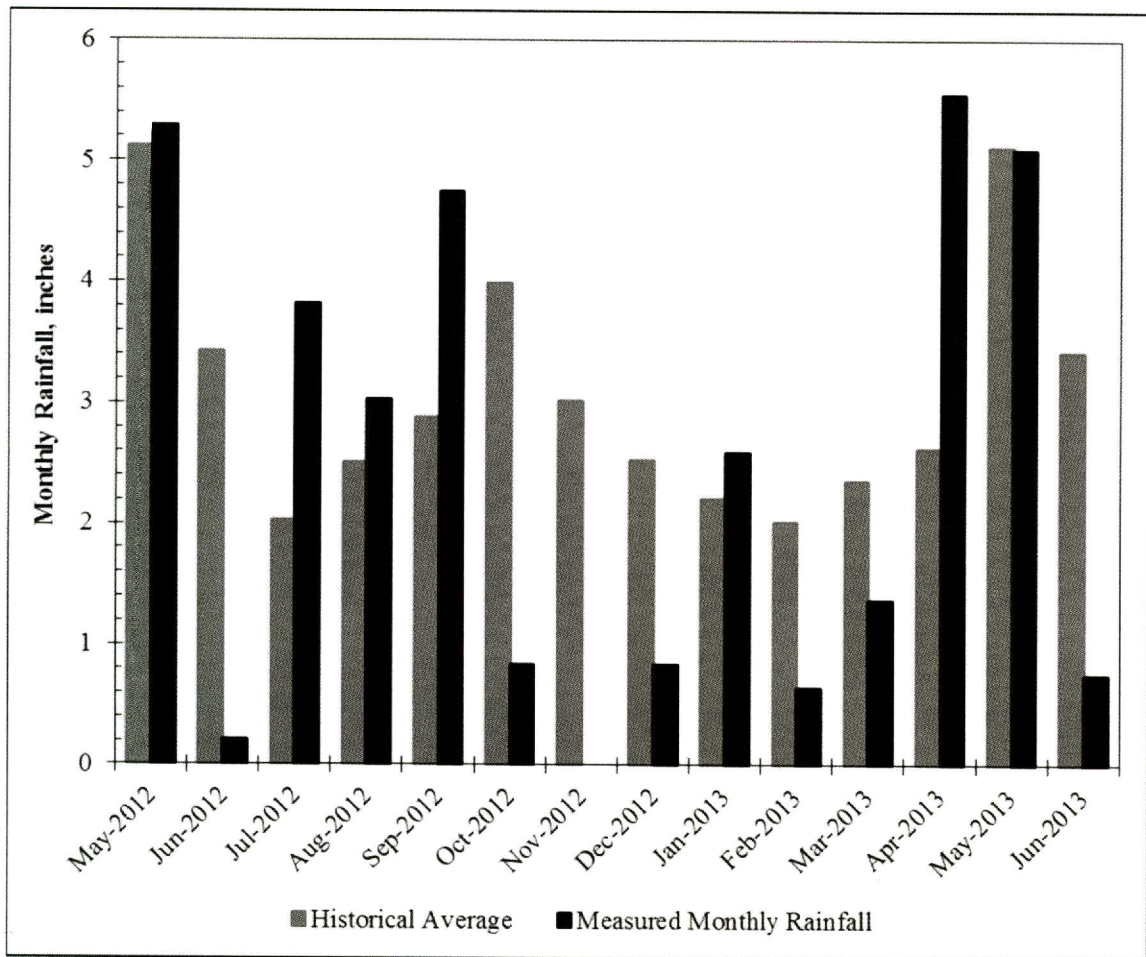
Figure 5.28: Monthly rainfall totals for Austin, Texas (May 2012–Jun. 2013; data from www.wunderground.com).
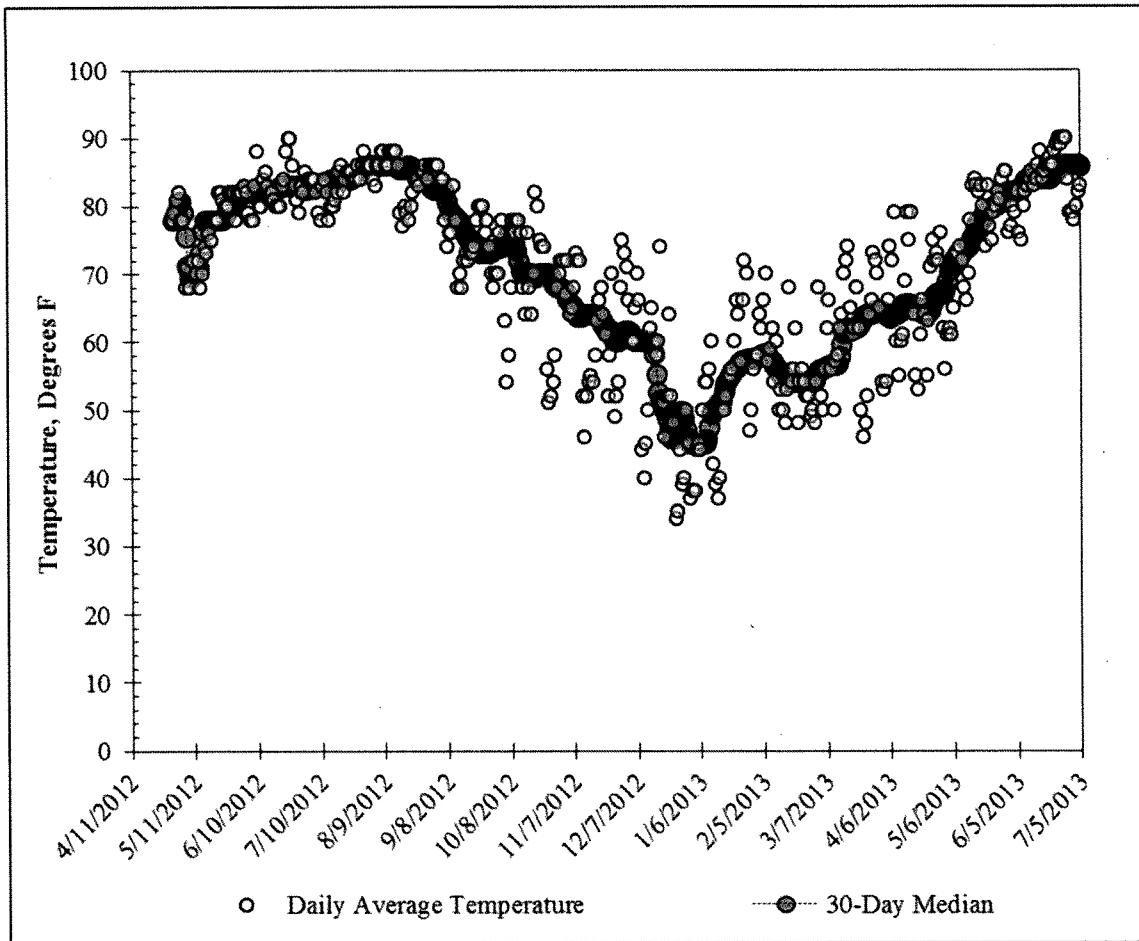
Figure 5.29: Daily average temperature data for Manor, Texas (May 2012–Jul. 2013; data from www.wunderground.com).

5.4.4: SUMMARY OF FIELD INSTRUMENTATION DATA

5.4.4.1: Inclinometer Data

Inclinometer data is referenced to the installation of facing in October 2010. Average deflected shapes are presented in Figure 5.30, and top-of-wall deflections are presented in Figure 5.31.
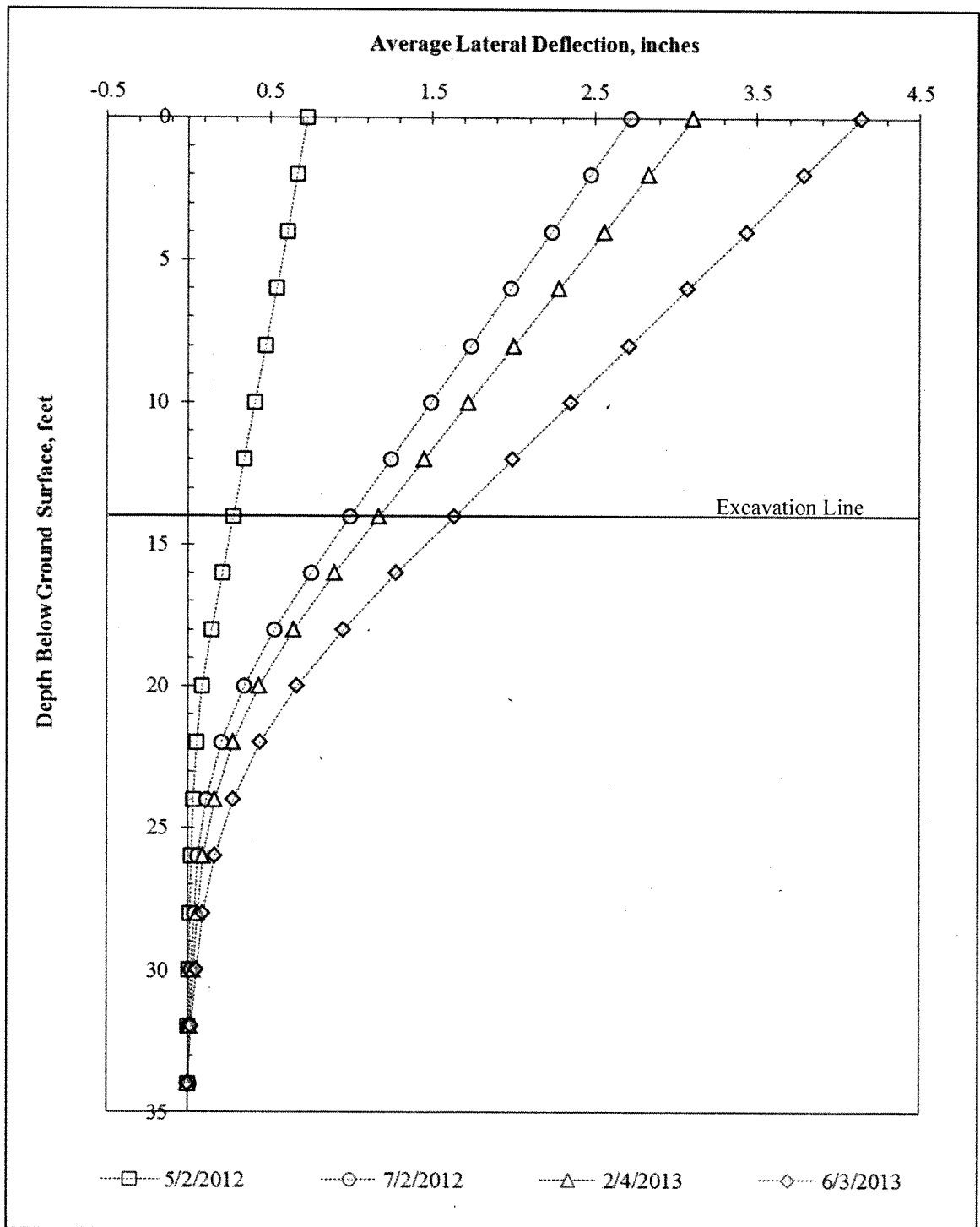
Figure 5.30: Average deflected shapes at key dates during inundation testing. Data is referenced to installation of facing in October, 2010.
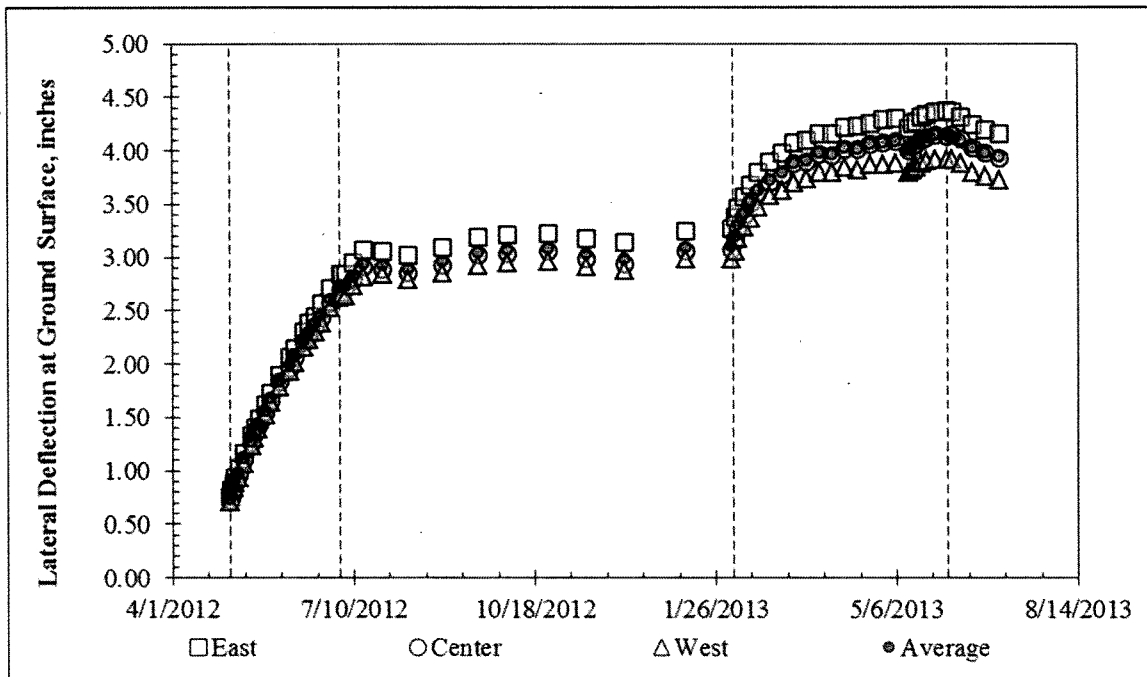
Figure 5.31: Top-of-wall deflections during inundation testing (key dates indicated by vertical dashed lines). Reference survey is facing installation in October 2010.

5.4.5: SOIL MOISTURE CONTENT DATA

A summary of measured soil moisture contents during controlled inundation testing is provided in Figure 5.32. Data from samples obtained using a hand auger, as well as data from geotechnical investigations conducted by Fugro Consultants, Inc., is provided. While a wide range of moisture contents were measured throughout the testing, in general, measured moisture contents ranged from approximately 15 to 35 percent in the zone above the natural groundwater table. At the conclusion of the second inundation cycle, moisture contents had increased to approximately 30 percent over the entire depth of the active zone (above the natural groundwater table at 8 feet below ground surface). While the final values of moisture content were similar at the conclusion of the first and second inundation cycles between 0 and 4 feet below ground surface, the second inundation cycle resulted in additional wetting of the soil between 4 and 8 feet below ground surface. Below the groundwater table at a depth of 8 feet, the soil transitions from dark brown Taylor clay to tan Taylor clay, and the natural moisture contents increase to between approximately 34 and 40 percent.

129
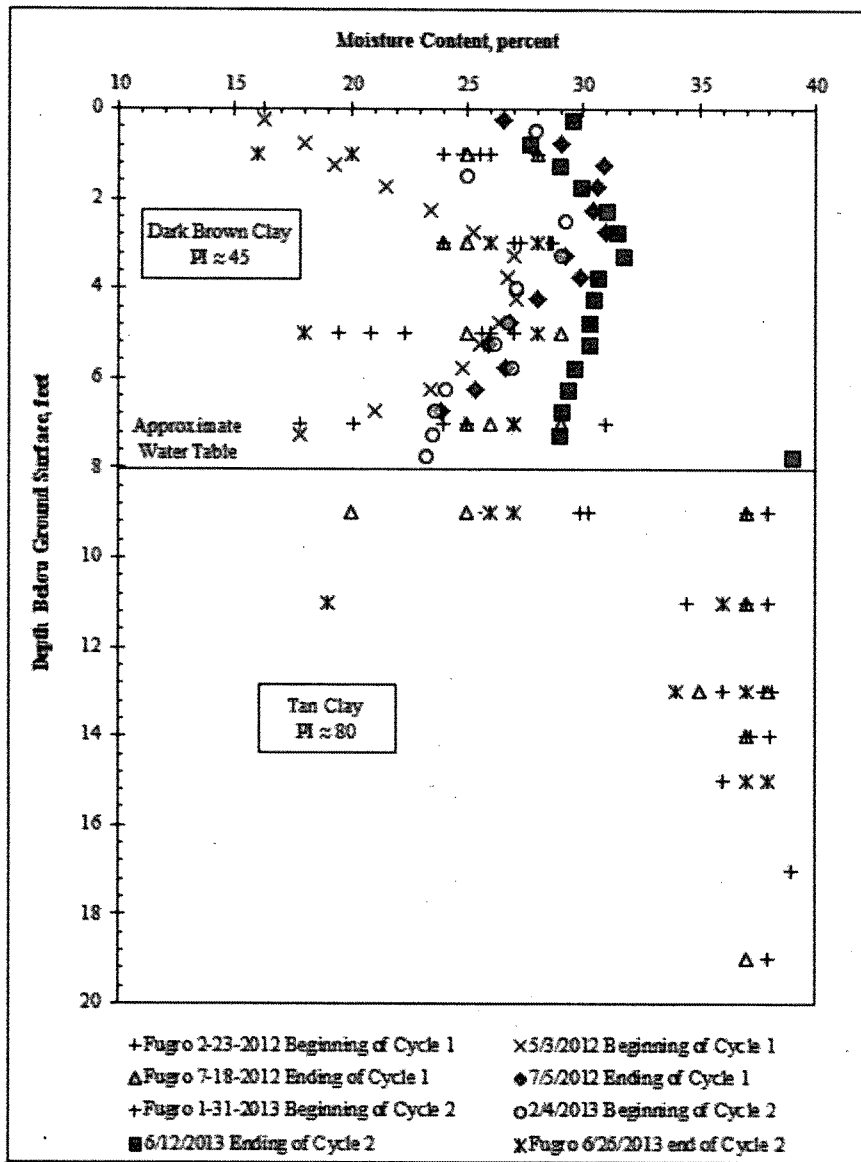
Figure 5.32: Summary of measured soil moisture contents during controlled inundation testing.

5.4.6: STAND PIPE PIEZOMETER DATA

Data from the stand pipe piezometers were recorded at regular intervals for the duration of inundation testing. Piezometer B-3 was installed and developed in 2010; consequently, water levels can be plotted for all inundation cycles (Figure 5.33). Piezometers A, B, C, and D were not properly developed after installation and did not show reliable data until the second inundation cycle. Data from the second cycle is presented in Figure 5.34 (piezometers with shallow screen intervals) and Figure 5.35 (piezometers with deeper screen intervals).

The water level in Piezometer B-3 was relatively unaffected by the presence of water in the inundation zone. The increased values in May, 2012 were associated with flooding on the project site that infiltrated the piezometer casing, and most likely do not represent the actual groundwater conditions. At the conclusion of inundation testing in July 2013, the water level had stabilized at approximately 8.5 to 9 feet below ground surface.

130

The water levels in the piezometers with shallow screen intervals stabilized at approximately 0.5 and 1.3 feet below ground surface during the second inundation cycle, before increasing during a large flood in May 2013 by approximately 0.3 feet. After the flood, water levels returned to values slightly higher than their original equilibrium values. The discrepancy in equilibrium water heights may be due to the development of steady-state seepage conditions, in which a cone of depression near the wall face leads to lowered water levels in stand pipe piezometers close to the wall (Figure 5.34). In piezometers with deeper screen intervals, water levels showed a similar trend, with equilibrium water levels increasing slightly after flooding in May 2013. Water levels were similarly lowered in the piezometer closer to the wall face. At the conclusion of inundation testing, despite the small cone of depression near the wall facing drains, conditions close to hydrostatic pressures had likely developed in much of the retained soil. After the water supply was stopped in June 2013, water levels in all piezometers immediately began to decrease toward their pre-inundation values.
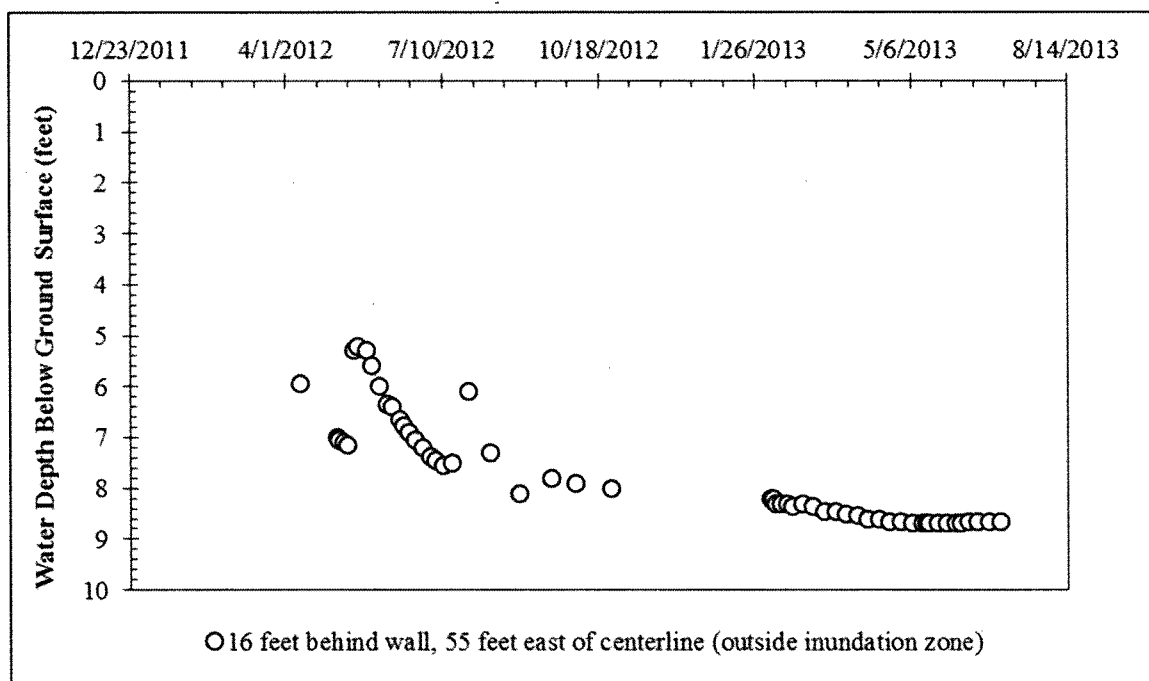
Figure 5.33: Water level in Piezometer B-3 (outside inundation zone) during inundation testing.
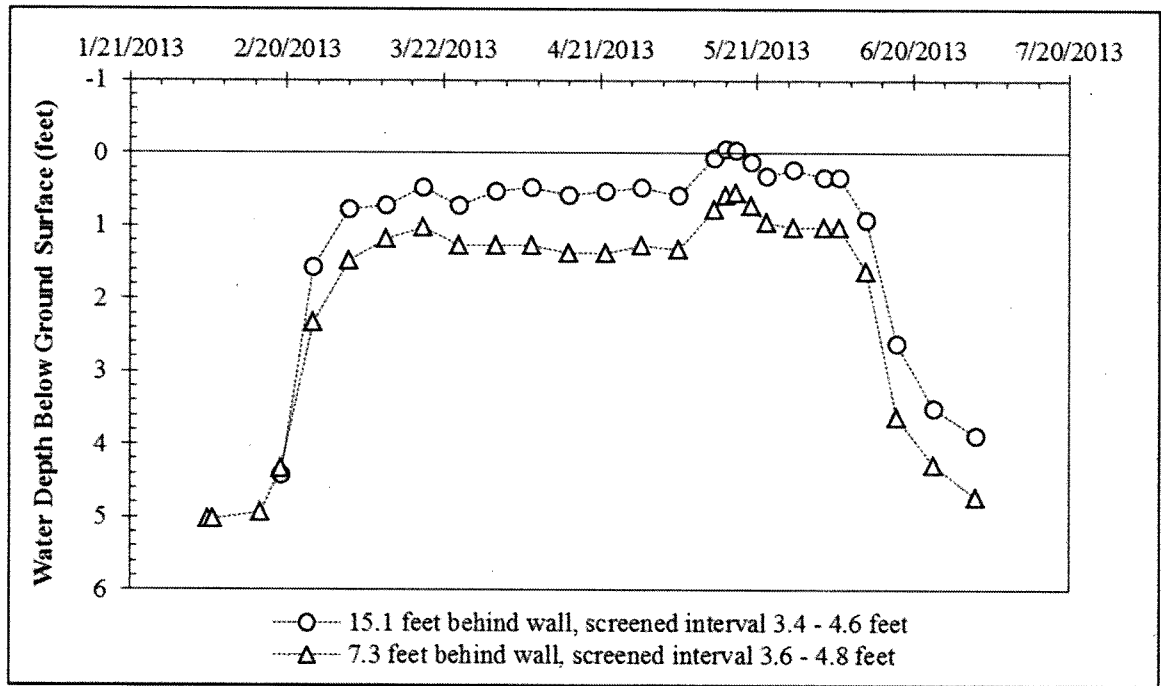
Figure 5.34: Data from shallow-screened stand pipe piezometers during second inundation cycle.
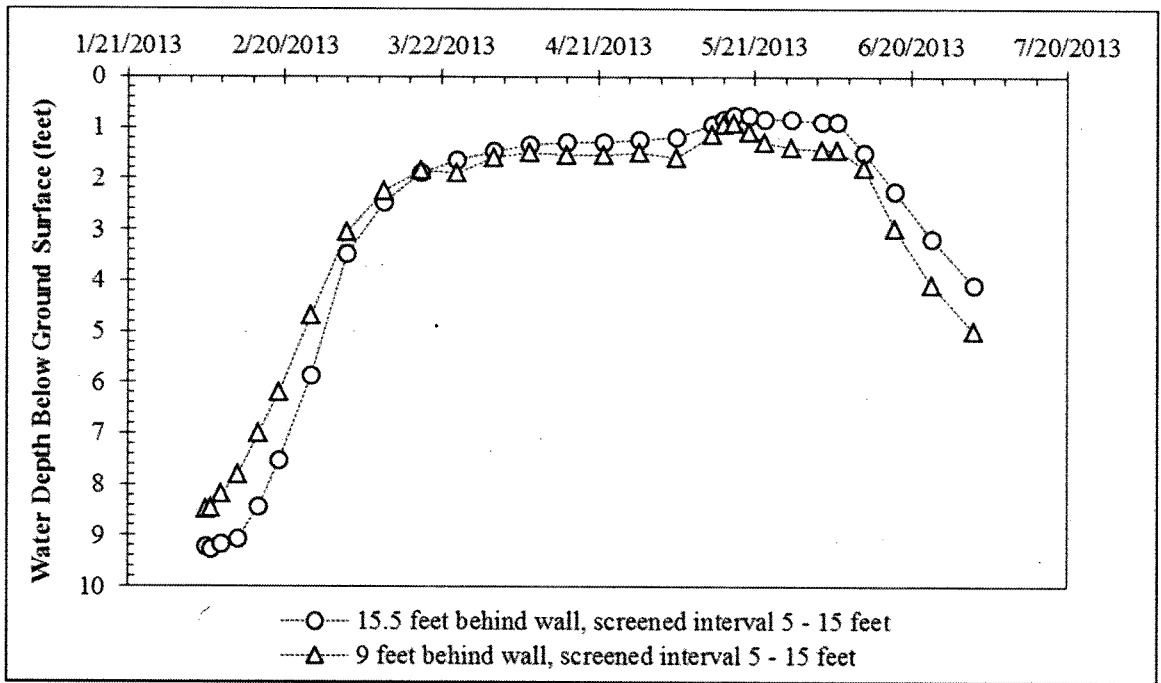
Figure 5.35: Data from deeper-screened stand pipe piezometers during second inundation cycle.

5.4.7: DATA INTERPRETATION

5.4.7.1: Immediate Response to Water

The inundation test began on May 3, 2012, and the wall and soil responded nearly immediately to the presence of water (Figure 5.36). Within minutes, the TDR probes installed throughout the retained soil registered the presence of free water (Figure 5.37), and within hours, water had begun to infiltrate through the wall drainage system into the excavation (Figure 5.38). This immediate response is consistent with the response observed at the test wall during large rainfall events, and suggests that the fissures present in the expansive clay provide preferential pathways for moisture flow.

Figure 5.36: The inundation zone is filled on May 3, 2012.

133
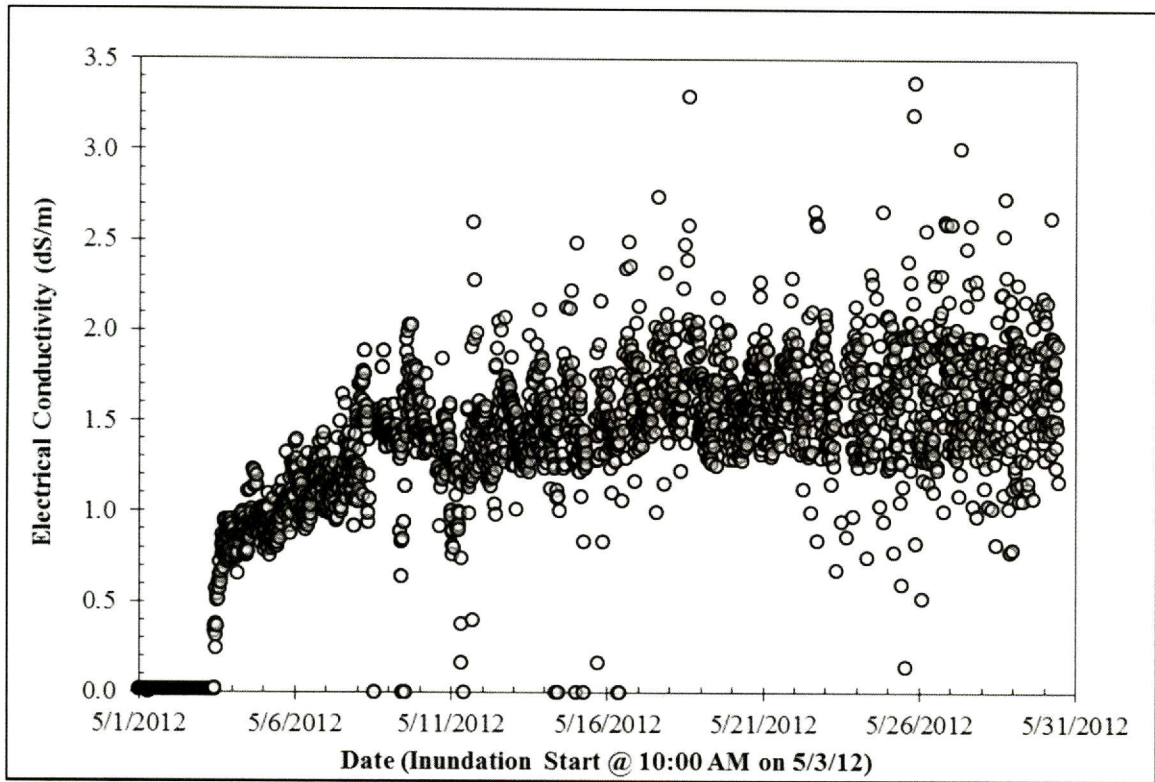
Figure 5.37: Electrical conductivity data from one TDR probe shows a response within minutes of beginning the inundation test. Probe is located 1.5 feet below ground surface.

Figure 5.38: Water infiltration into the excavation was first observed 90 minutes from the start of inundation.

The top-of-wall deflection began to increase almost immediately in response to inundation, and continued at a slightly decreasing rate for the duration of the test (Figure 5.31). Based on the daily rate of deflection, it was inferred that the inundation test would likely need to continue for several additional months before an equilibrium condition was reached. Because of this, and in order to allow the soil time to dry out before the next scheduled inundation cycle in

January 2013, the first inundation cycle was stopped on July 2, 2012. After the water supply to the inundation area was cut off, the wall deflection stabilized within 1 day, again suggesting that fissures in the soil mass provide fairly direct access to moisture. Over the 2-month inundation cycle, the top-of-wall deflections had increased by approximately 2 inches. Had the test not been stopped, it is likely that deflections would have increased beyond this point. After 2 months of inundation, in the soil above the groundwater table, moisture contents had increased by approximately 5 to 10 percentage points in the active zone above the natural groundwater table (Figure 5.32).

5.5: Summary and Conclusions

5.5.1: BEHAVIOR BEFORE EXCAVATION

An examination of test wall behavior between shaft construction and excavation has shed light on the processes that occur in drilled shaft retaining walls prior to excavation. Key findings include the following:

- Prior to shaft construction, the test site experienced approximately 8 months of above average rainfall. Between shaft construction and excavation, the wall experienced 2 months of below average rainfall, followed by 2 months of above average rainfall.

- Axial strains developed in the shafts prior to construction due to a combination of concrete curing and expansive soil movement. In many cases, the development of axial strains suggests that tension cracks developed throughout the shaft.

- Residual stresses and strains are present in the shafts prior to excavation. The distribution of residual stresses and strains is highly variable within each shaft.

5.5.2: BEHAVIOR DURING EXCAVATION

The behavior of the Lymon C. Reese wall suggests that standard of practice design methods may not accurately account for what occurs during excavation. Based on the results of the instrumentation and data analysis program, several conclusions can be drawn:

- The standard design procedure for stiff clay predicts top-of-wall deflections fairly well for the test wall. However, it does not accurately predict the deflected shape at depth, and significantly overestimates the bending stresses in the shaft.

- A significant amount of the measured test wall deflection was due to a combination of global movement of the soil-shaft system and shaft base rotation, neither of which directly stress the wall. These motions are not accounted for in the design analysis, and because they are visually obscured by the application of facing material, they may not be noticed without careful monitoring. While estimates of global movements for the test wall are provided, additional data from other drilled shaft walls in expansive soils are required to formulate reliable recommendations for design.

- Deformations prior to the application of facing accounted for approximately 50 percent of the test wall's allowable top-of-wall deflections. Because deflection requirements often govern design in practice, an understanding of the soil and shaft

deformations during excavation may be important in some cases to ensure adequate wall performance.

5.5.3: BEHAVIOR DURING NATURAL MOISTURE CYCLES

Data recorded at the Lymon C. Reese research wall during natural moisture cycles has provided some insight into the behavior of drilled shaft retaining walls during cycles of wetting and drying. Conclusions include the following:

- During cycles of drying, wall deflections decreased. This is primarily due to volumetric shrinkage of the soil, which leads to an equivalent reduction in earth pressures. After 8 months of extreme drought, deflections at the test wall decreased by approximately 0.3 inches, and the earth pressure reduction corresponds to a decrease in equivalent fluid pressure of approximately 20 psf/ft.

- During cycles of wetting, wall deflections increased. This is primarily due to a combination of soil swelling and the dissipation of negative pore pressures. The presence of water contributes to both increased earth pressures (softening of the retained soil) and decreased resistance (softening of the foundation soil). There is little evidence at the test wall to suggest that high lateral earth pressures due to soil expansion are imposed.

5.5.4: BEHAVIOR DURING CONTROLLED INUNDATION TESTING

The data recorded at the Lymon C. Reese research wall during cycles of controlled inundation testing has provided insights into the behavior of drilled shaft walls in expansive clay. Following are some of these insights:

- Fissures in the clay provide preferential pathways for drainage and moisture flow. Drainage through these fissures occurs very quickly, within minutes, when surface water is present. This is supported by first-hand observations and data from TDR moisture probes and stand pipe piezometers.

- In the 6 total months of controlled inundation, and 8 total months of drying cycles, top-of-wall deflections stabilized at 5.2 inches since shaft installation, and 4.2 inches since the installation of facing. Maximum bending moments in the shaft since installation were approximately 2,100 in-kip, approximately two-thirds of the yield moment.

- Wall deflections stabilized at the same time the water levels in stand pipe piezometers stabilized. As water levels decreased after the conclusion of inundation, top-of-wall deflections decreased accordingly. This result suggests the presence of water behind the wall contributes to the development of deflections.

- Even with continued access to water, there is limited evidence to suggest that large earth pressures due to soil expansion are sustained at the test wall. No evidence of earth pressures exceeding the pressure envelope defined by drained, fully softened strengths with additional hydrostatic pressures was observed.

CHAPTER 6: TEST WALL ANALYSIS

Detailed numerical analyses have been conducted for two conditions the wall experienced: the immediate response of the wall due to the excavation and the long-term response of the wall when it reached equilibrium under full inundation.

6.1: Excavation Loading

6.1.1: OBSERVED BEHAVIOR

The measured response of the wall at the end of excavation is shown in Figure 6.1, Figure 6.2 and Figure 6.3. For comparison, the calculated deflected shape from the baseline design analysis is also shown. While the design calculations are not intended to represent this condition, they are shown in Figure 6.1 to Figure 6.3 to illustrate the important features of how the wall responded during excavation. First, the wall deflected about 0.9 inches at the top during excavation, which is similar to the deflection predicted in design under long-term loading (Figure 6.1) after the excavation is wished into place. Second, the wall tilted as a rigid body rather than bent during excavation (Figure 6.1 and Figure 6.2). This behavior indicates that the wall was moving with the soil rather than retaining the soil (Figure 6.3), which is not surprising since the clay is stable on a vertical face as high as 15 feet in the short term after excavation without any support from a wall.
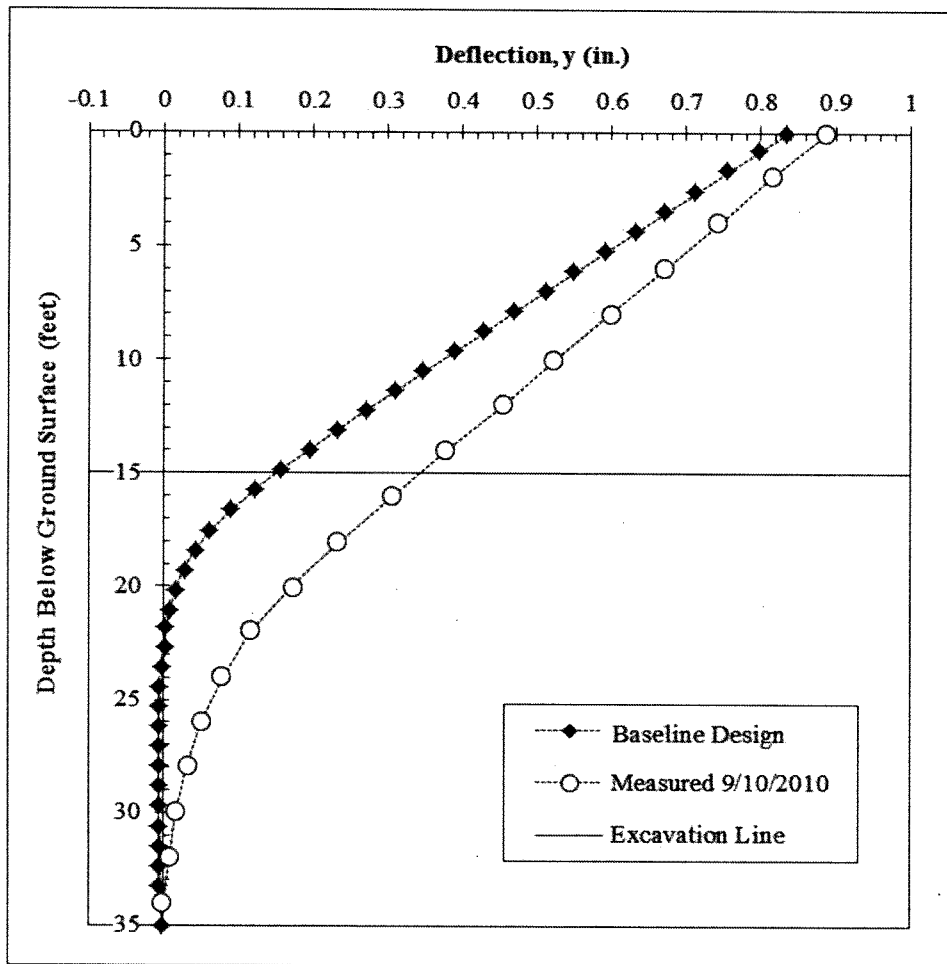
Figure 6.1: Measured deflected shape of wall at end of excavation.
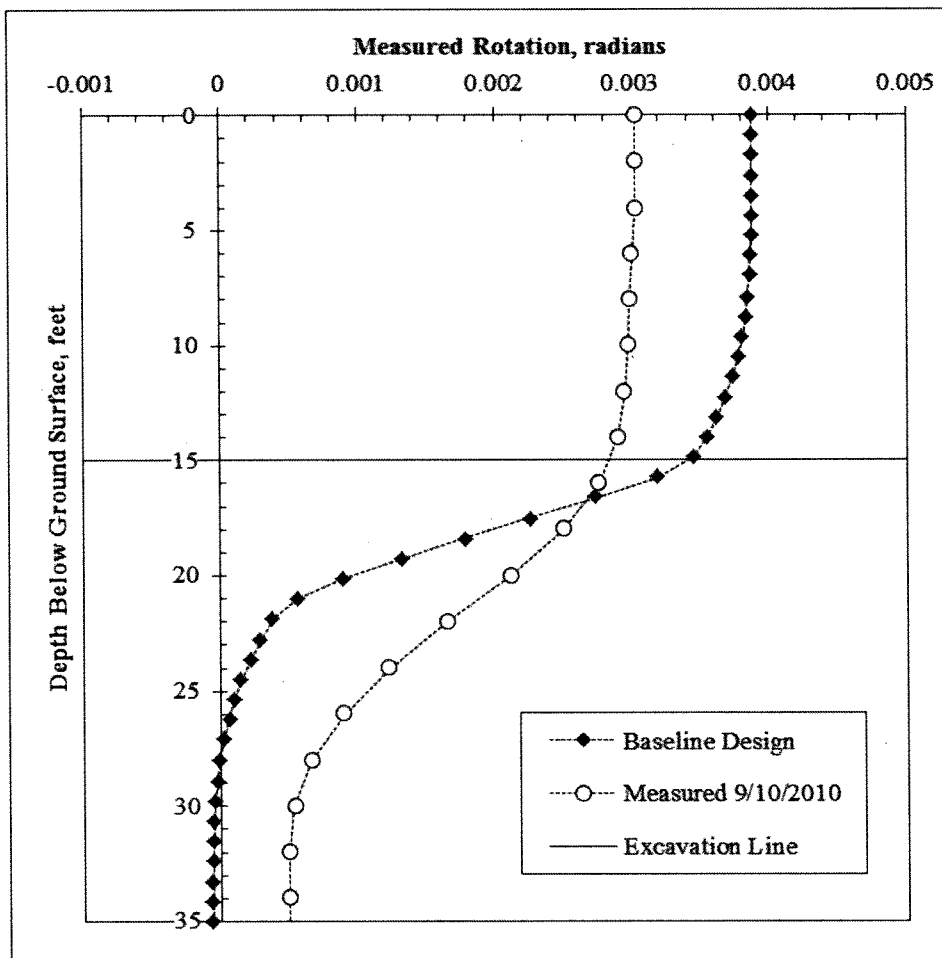
Figure 6.2: Comparison of shaft rotation profile predicted by standard design procedure with rotation profile measured during excavation.

Figure 6.3: Comparison of bending moments predicted by standard design procedure with moments measured during excavation.

6.1.2: FINITE ELEMENT METHOD ANALYSIS

A simplified finite element method (FEM) analysis was conducted to better understand the response of the wall during excavation. The commercially available ABAQUS® software was used for this analysis. This FEM model had the following attributes:

- plane strain (two-dimensional) conditions;

- isotropic, linear elastic soil characterized by a Young's modulus, E, that varies with depth and by a Poisson's ratio assumed equal to 0.45 for undrained conditions;

- anisotropic initial state of stress before excavation;

- linear elastic wall with a constant bending stiffness; and

- rough interface between the wall and soil.

Three stages were used in this modeling. First, the initial state of stress due to the weight of the soil and the input ratio of horizontal to vertical stress (K_0) was imposed. Second, the wall

140

is wished into place. Third, the excavation is simulated by reducing to near zero the unit weight and stiffness of the soil elements within the excavation cross section.

The input for the modeling was based on available information from the preliminary site investigation. The soil unit weight was assumed to be 125 pcf. The Young's modulus values versus depth were estimated based on a design profile of undrained shear strength (s_u) versus depth (Figure 6.4) and a ratio of E/s_u. An E/s_u value of 1000 was first assumed based on laboratory UU triaxial tests and based on in situ Spectral Analysis of Surface Wave (SASW) testing conducted at the project site just prior to the excavation (Figure 6.5 and Figure 6.6).
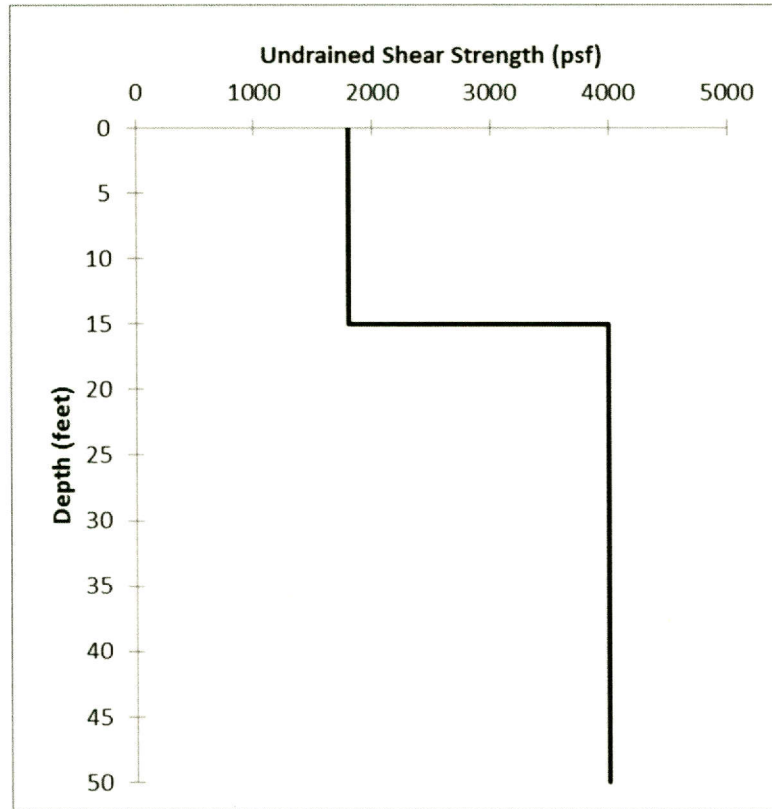
Figure 6.4: Assumed profile of undrained shear strength versus depth for FEM analysis of excavation.

Figure 6.5: SASW testing at the test wall prior to excavation, June 2010.
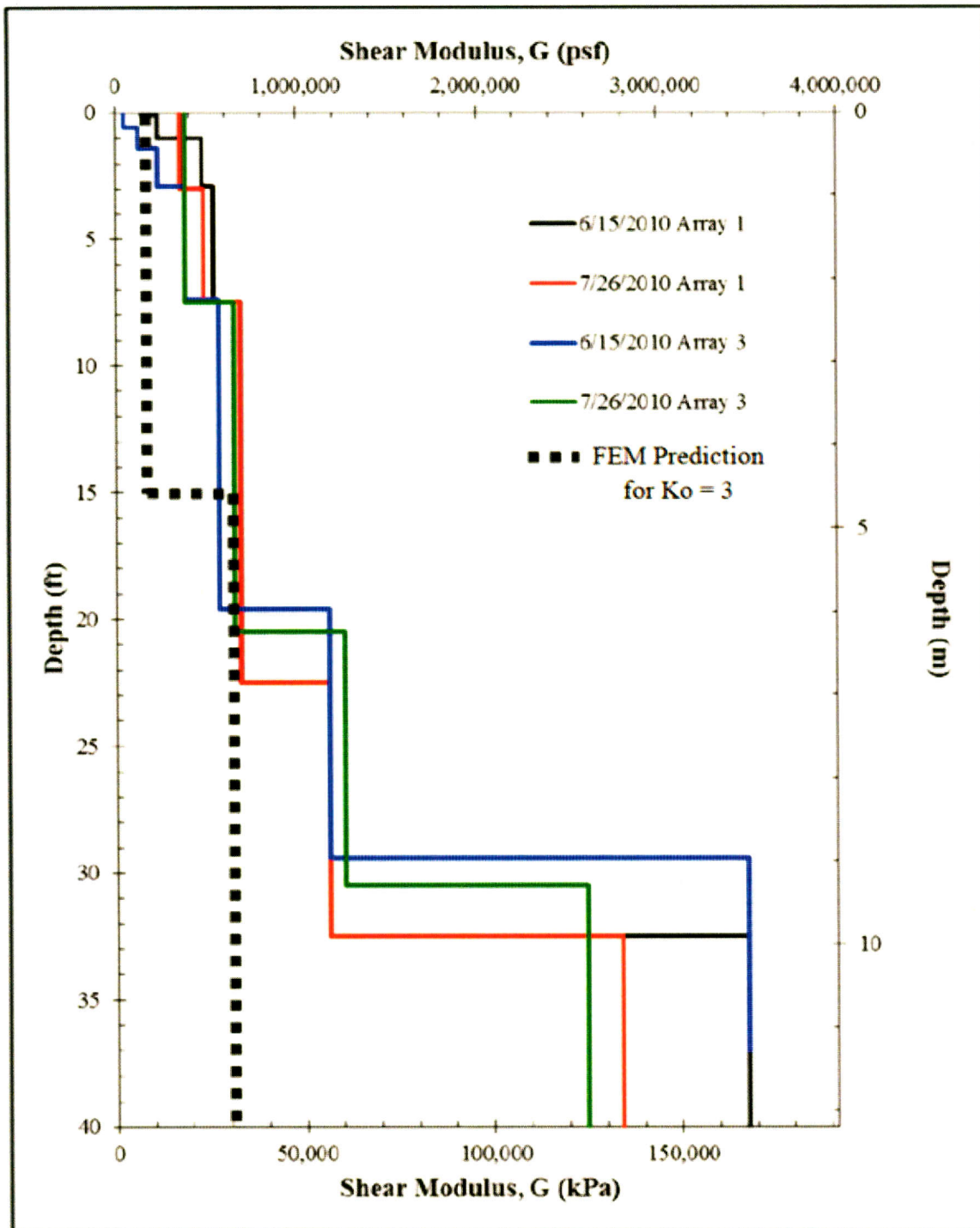
Figure 6.6: Interpreted shear modulus profiles from SASW testing (Ellis 2011).

Results from the FEM analysis are shown in Figure 6.7, Figure 6.8, and Figure 6.9. The first analysis assumed an isotropic initial state of stress ($K_0 = 1$) and a ratio of $E/s_u = 1000$ at all depths. This analysis produces a deflected shape for the wall that is similar to the measurements (i.e., the wall rotating rather than bending); however, the absolute displacements are smaller than the measured displacements (Figure 6.7). In order to obtain a more realistic representation, the

143

possibility of large in situ lateral stresses caused by overconsolidation was considered. Values for K_0 of 2 to 3 have been measured in these highly plastic, overconsolidated clays in Central Texas (e.g., Smith et al. 2009). These larger in situ lateral stresses increase the absolute displacement (Figure 6.7), but the total calculated displacement is still less than one-half the measured displacement. The possibility of the soil mass stiffness being less during unloading than loading (as it was measured in both the laboratory UU tests and in the SASW tests) was also considered. Based on trial and error, a profile of stiffness with E/s_u equal to 180 above the excavation depth, where the unloading is most significant, and E/s_u equal to 400 below the excavation depth produces a calculated displacement profile that is very similar to the measured one (Figure 6.7). This stiffness reduction in unloading is consistent with observations in other stiff fissured clays, such as the London Clay (e.g., Cripps and Taylor, 1981).

The global displacements of the soil (Figure 6.8) and the shear strains in the soil (Figure 6.9) show how the soil is essentially carrying the wall with it in response to the stress relief from the excavation. The displacements in the soil extend well below the depth of the wall (Figure 6.8). To illustrate this behavior further, a sensitivity study was conducted by lengthening the drilled shafts in the FEM analysis. These calculated results predict that even if the shafts had been 50 feet long, embedded below the excavation more than twice the depth of the excavation, the deflected shape would have been similar to the 35-foot long shafts and the deflection at the top of the wall would have been only about 0.1 inches smaller (Figure 6.10).
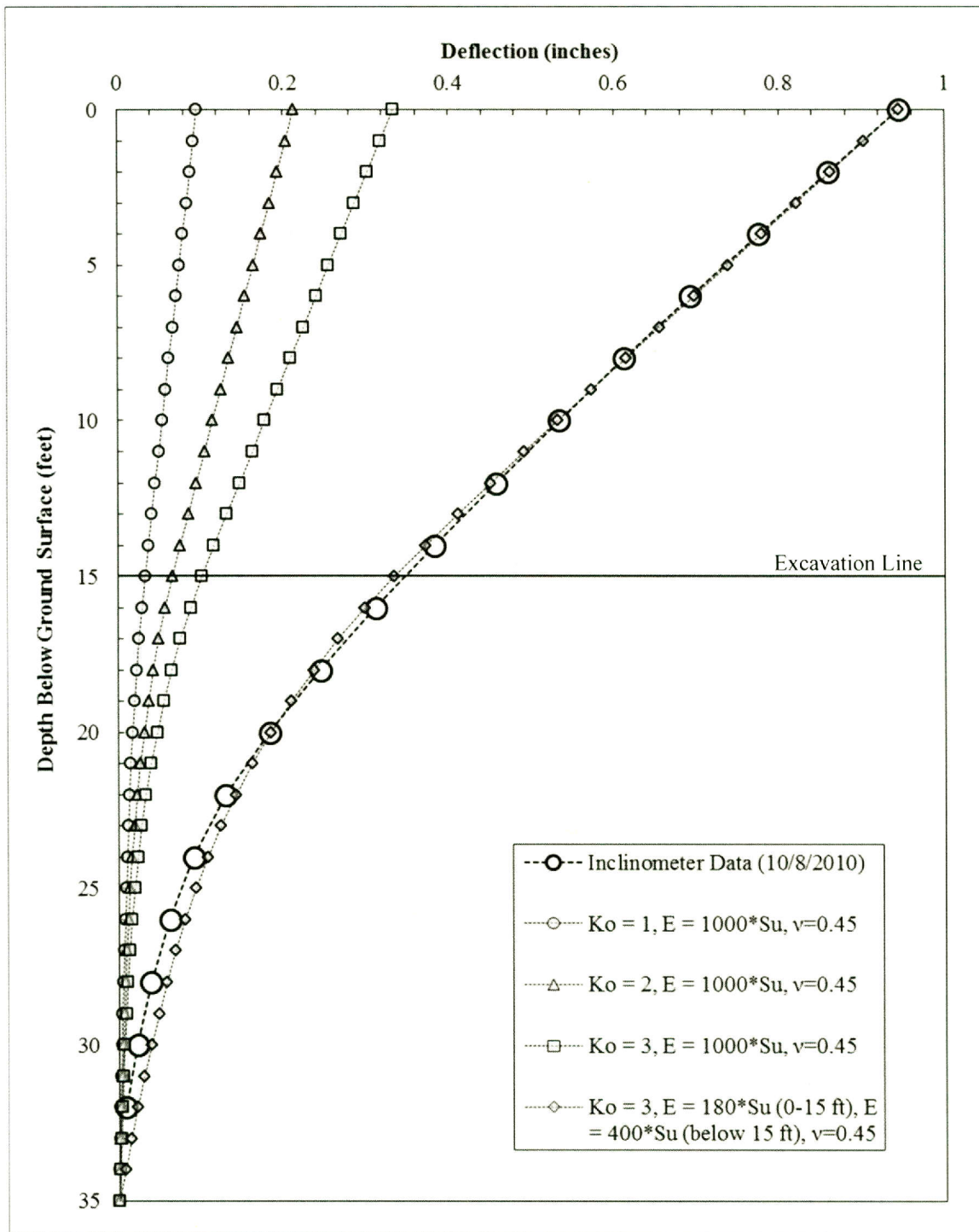
Figure 6.7: Comparison of linear elastic FEM predictions with measured field data.
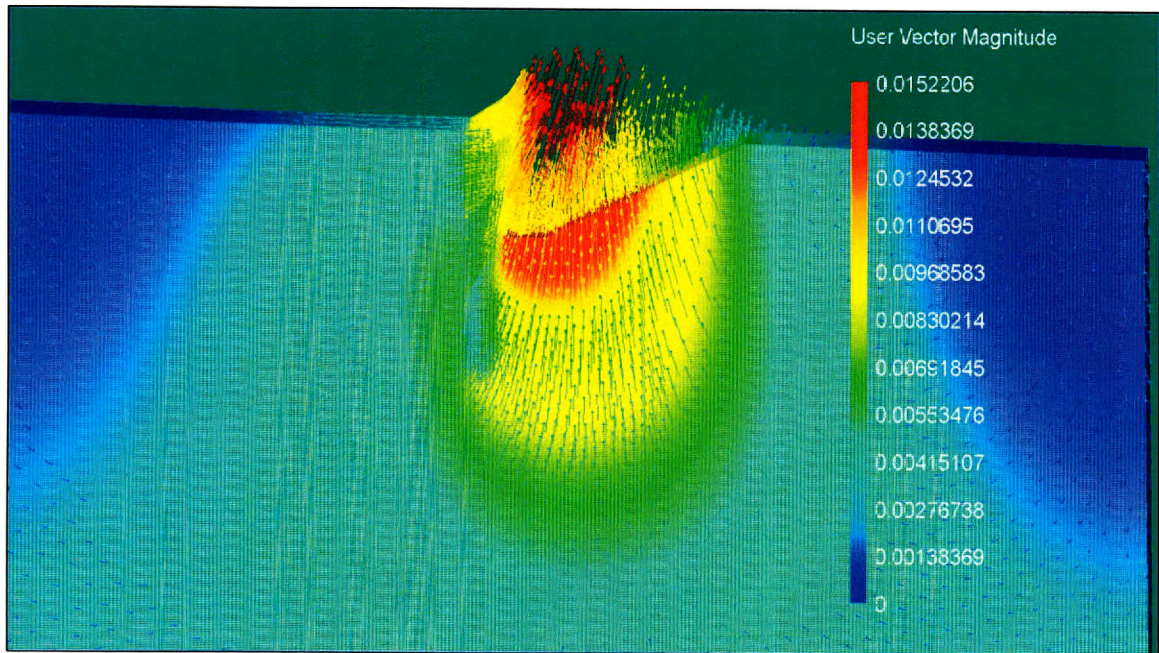
Figure 6.8: Global displacement of soil in response to excavation in linear elastic FEM ($K_0 = 3$, $E/s_u = 180$ for depths from 0 to 15 feet and $E/s_u = 400$ for depths greater than 400 feet).
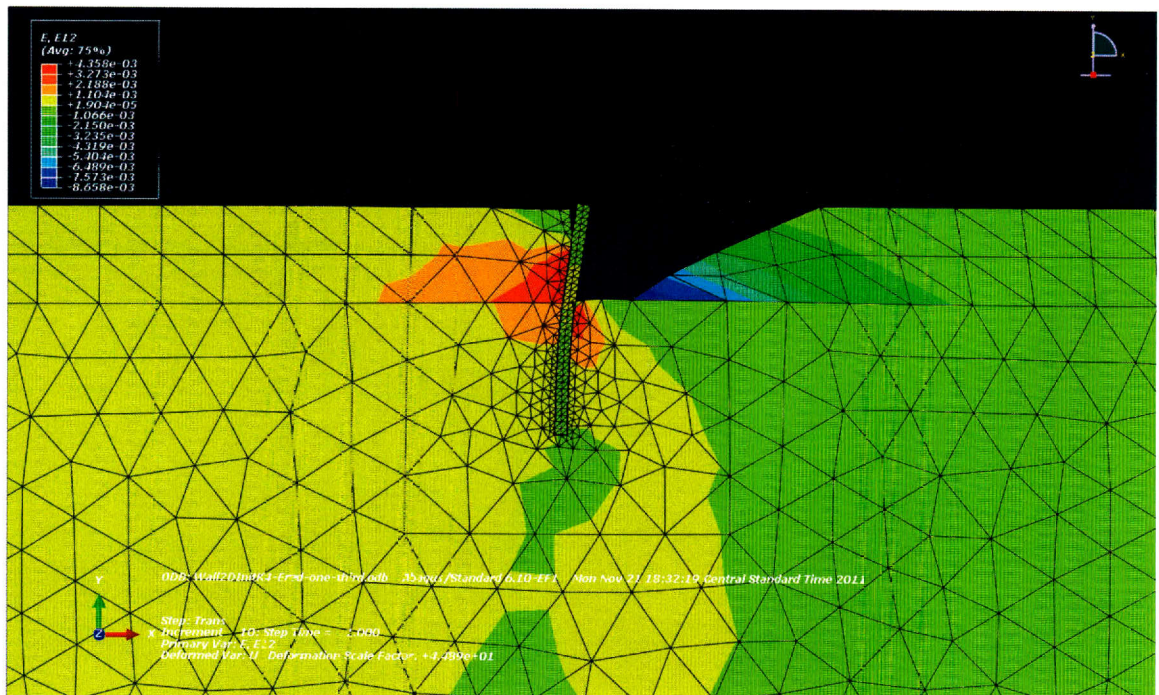
Figure 6.9: Global shear strains in soil in response to excavation in linear elastic FEM ($K_0 = 3$, $E/s_u = 180$ for depths from 0 to 15 feet and $E/s_u = 400$ for depths greater than 400 feet).

146
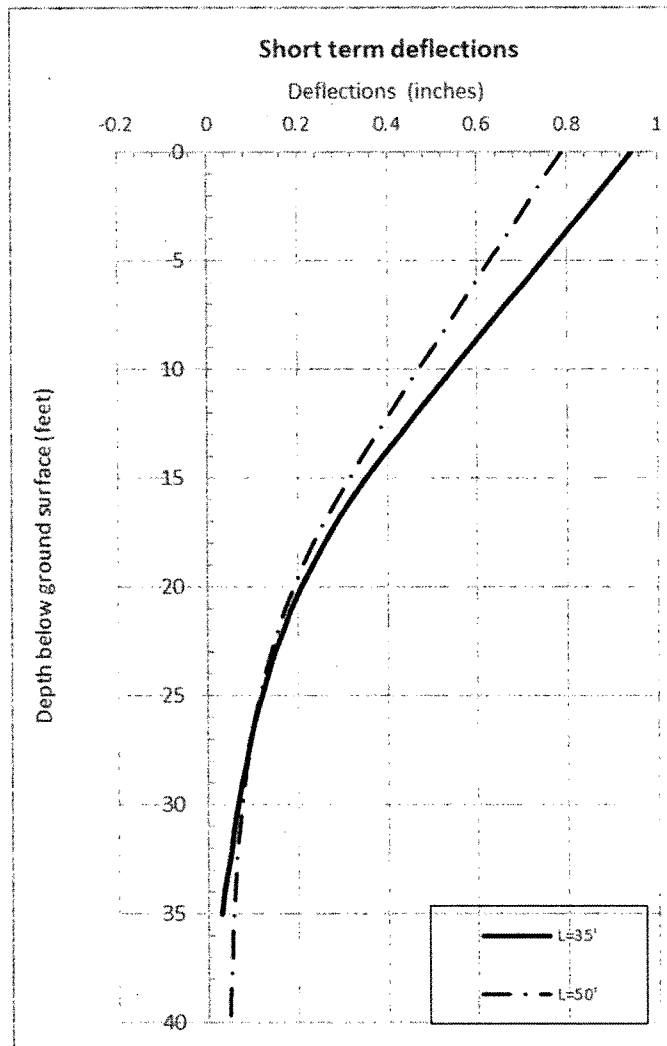
Figure 6.10: Effect of shaft length on results from linear elastic FEM ($K_0 = 3$, $E/s_u = 180$ for depths from 0 to 15 feet and $E/s_u = 400$ for depths greater than 400 feet).

6.2: Long-Term Loading

6.2.1: OBSERVED BEHAVIOR

The deflection of the wall under long-term loading with the inundation pond reached equilibrium on about June 3, 2013 (Figure 6.11); measurements from the site on this date will be used to represent the long-term loading condition. Note the depth of the excavation when the wall reached long-term equilibrium was about 13.5 feet versus 15 feet due to erosion into the excavation in the spring of 2013 (see Section 5.4.2.2.3).

The measured response of the wall at equilibrium under long-term loading is shown in Figure 6.12, Figure 6.13, and Figure 6.14. Since design calculations for the wall are not intended to account for the immediate response of the soil around the wall caused by stress relief from excavation (Figure 6.7), the inclinometer, linear potentiometer, and strain gauge measurements for the long-term condition are all referenced to the measurements at the end of excavation and facing installation (defined as 10/8/10). For comparison, the calculated deflected shape from the

147

baseline design analysis is also shown in Figure 6.12 to Figure 6.14. While the design calculations are not intended to represent this long-term condition with the inundation pond, they are shown in Figure 6.12 to Figure 6.14 to illustrate the important features of how the wall responded under the long-term loading. First, the wall deflected about 4 inches at the top, which is greater than the deflection predicted in design (Figure 6.12) because the active earth pressures in the retained soil are greater due to raising the water table in the retained soil to the top of the ground with the inundation pond. Second, the stiffness of the lateral soil resistance against the wall below the excavation is less than predicted (Figure 6.12 and Figure 6.13) since the soil presumably reached drained conditions under this long-term loading condition, dissipating negative pore water pressures and decreasing the effective stress in the foundation soil. Third, there is a curvature in the wall above the excavation back toward the retained side caused by the higher temperature on the exposed face of the wall in June; this curvature is reflected as an apparent negative bending moment above the excavation (Figure 6.14). A detailed discussion and analysis of this thermal effect is presented in Brown (2013), which is located in Appendix K.
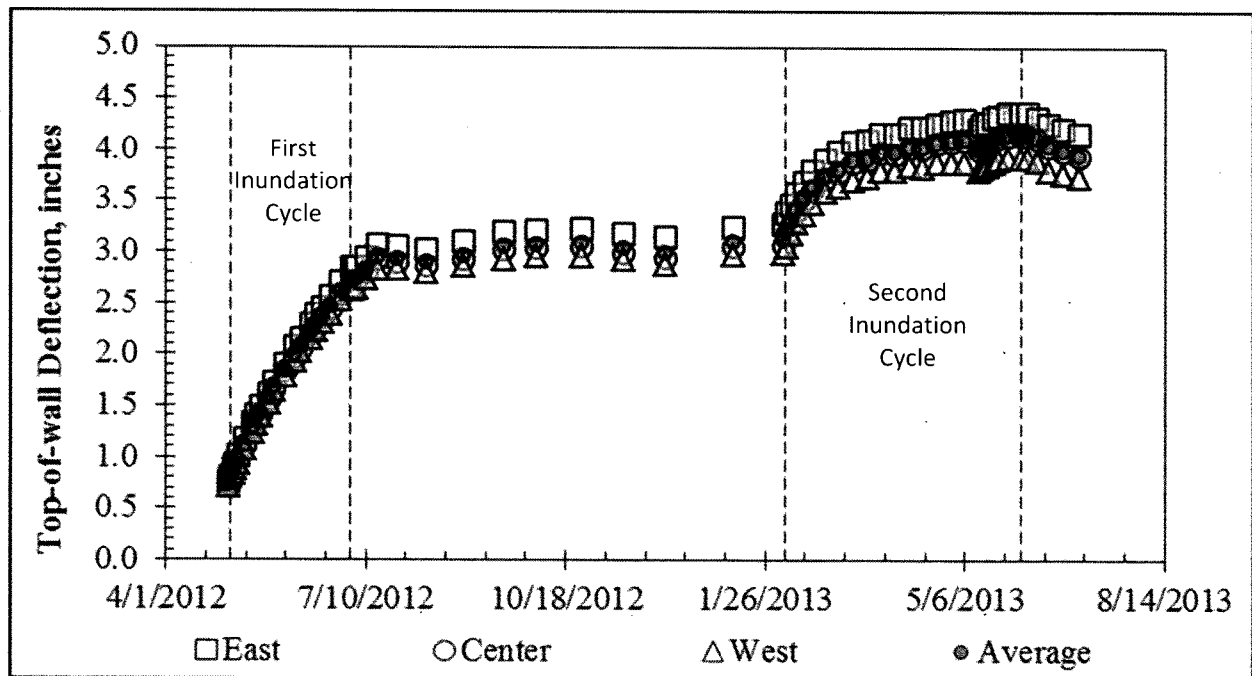
Figure 6.11: Lateral deflection at top of wall after first and second inundation cycles.

148
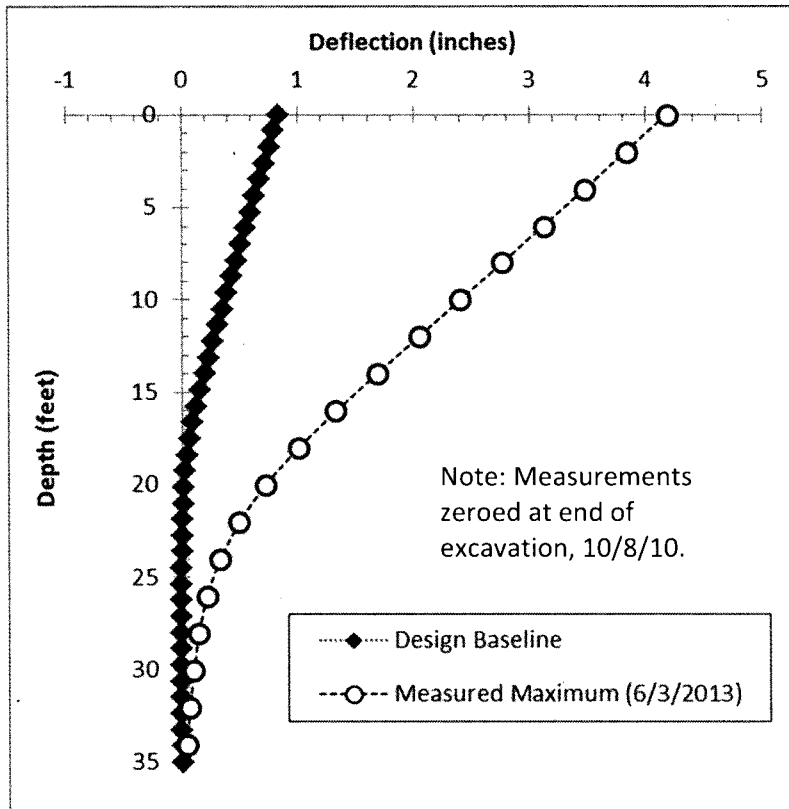
Figure 6.12: Measured deflected shape of wall at equilibrium condition under long-term loading with full inundation.
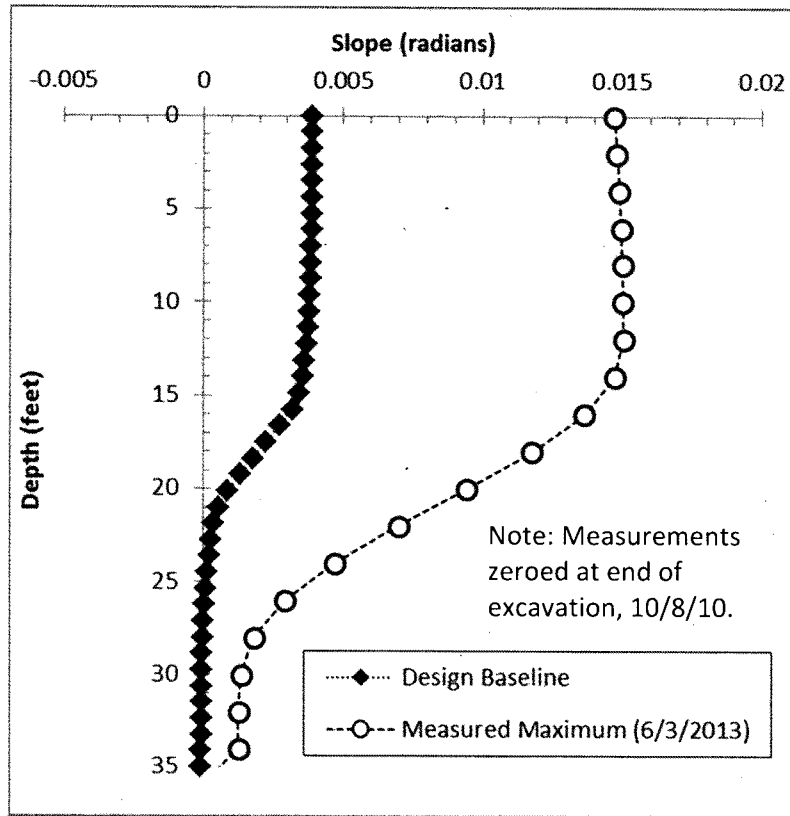
Figure 6.13: Comparison of shaft rotation profile predicted by standard design procedure with rotation profile measured at equilibrium condition under long-term loading with full inundation.
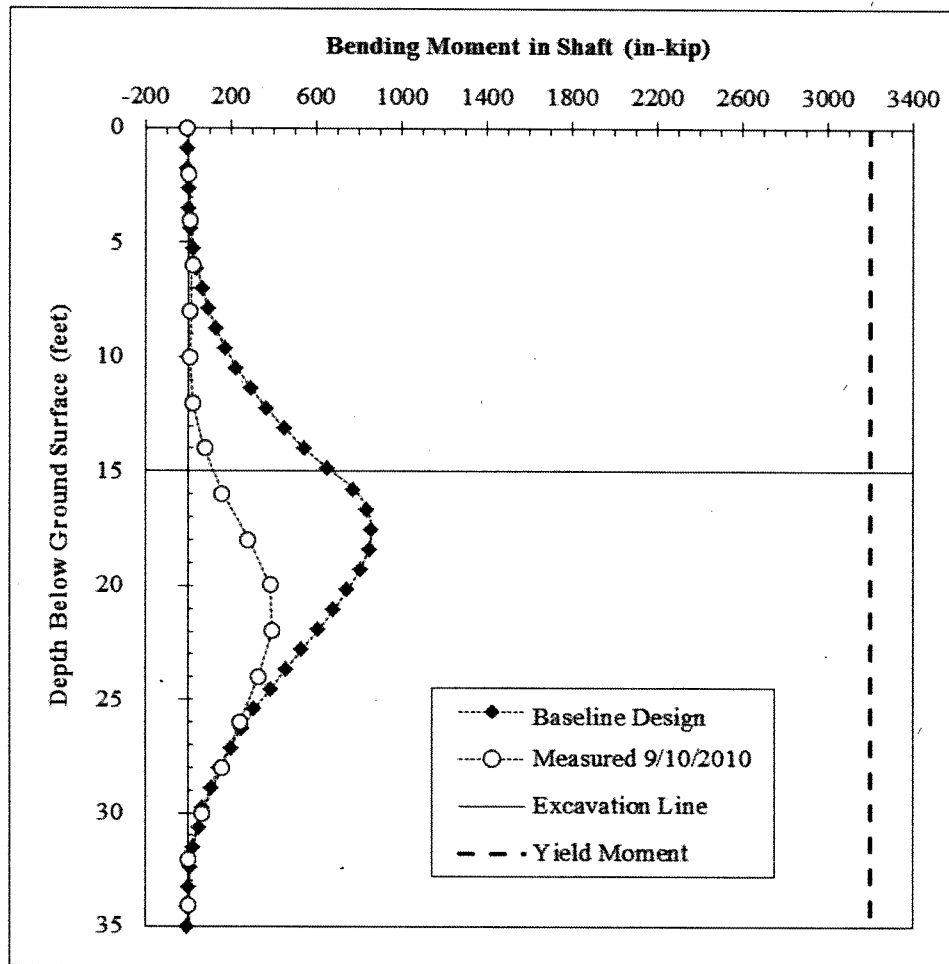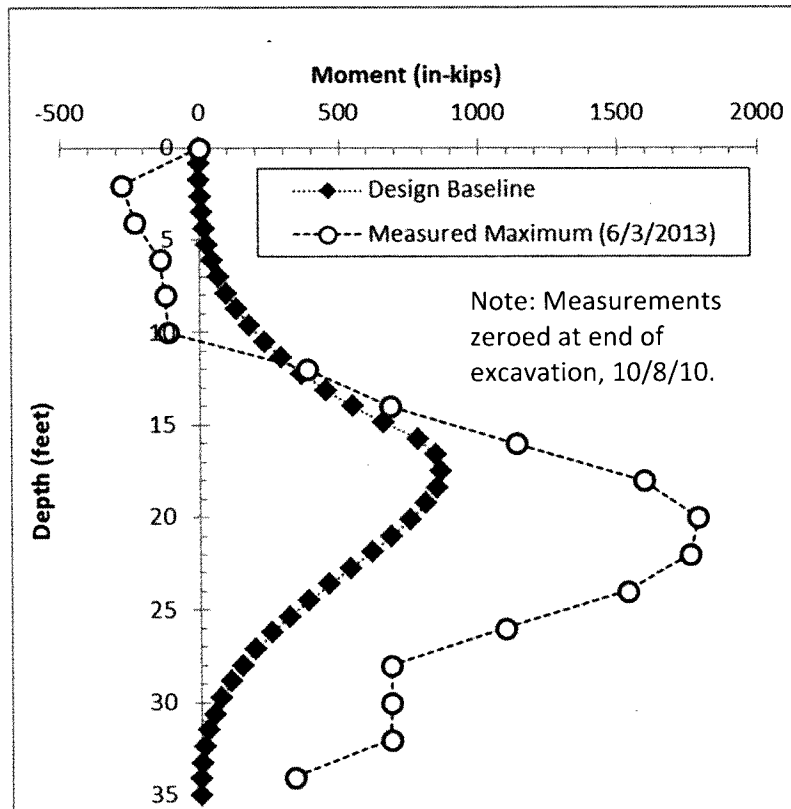
Figure 6.14: Comparison of bending moments predicted by standard design procedure with moments measured during excavation.

6.2.2: PORE WATER PRESSURES

A simplified FEM analysis was conducted to better understand the pore water pressures, and therefore the effective stresses, in the soil under the long-term equilibrium condition. ABAQUS® software was used for this analysis. This FEM model had the following attributes:

- two-dimensional flow conditions;

- isotropic soil characterized by a hydraulic conductivity equal to 3.28×10^{-8} ft/s based on information from rising head tests conducted in the piezometer and laboratory consolidation tests on samples from the soil borings (note that the soil is assumed saturated above and below the water table and the hydraulic conductivity is assumed the same above and below the water table);

- anisotropic wall with a horizontal hydraulic conductivity equal to 1/5 that for the soil (accounting for the shafts occupying 4/5 or 24 inches/30 inches of the wall face) and a vertical hydraulic conductivity equal to 1,000 times the horizontal hydraulic conductivity to model a freely draining surface due to the geocomposite drains behind the wall facing;

- a constant hydraulic head boundary condition equal to the ground elevation at the surface of the retained soil extending 23 feet back from the wall to represent the inundation pond;

151

- a constant hydraulic head boundary condition equal to the ground elevation at the surface of the excavation bottom extending the 10-foot width of the excavation away from the toe of the wall to represent the steady pumping to maintain a dry excavation; and

- freely draining boundaries along the edges of the finite element mesh, which are located 100 feet from the wall to represent the free-field conditions far away from the inundation pond and the pumped excavation (this distance was established to be far enough away so that there was approximately no flow at these boundaries), and have an imposed constant head of zero at the elevation of the free-field water table equal to 7.5 feet below the ground surface.

Three stages were used in this modeling. First, the initial flow conditions without the inundation pond and the pumped excavation were established with a water table at the depth of the excavation, 15 feet below the ground surface. Second, the constant head boundary conditions for the inundation pond and the pumped excavation and the constant head at the free-field boundaries were all imposed. Third, the simulation was progressed with time until a steady-state condition was reached.

The results of this FEM analysis are shown in Figure 6.15. The local flow conditions in the vicinity of the wall consist of horizontal flow toward the wall drain in the retained soil, vertical downward flow in the retained soil, vertical flow downward in the drain behind the wall, horizontal flow from the drain behind the wall into the excavation, vertical upward flow in the soil below the excavation, and horizontal flow toward the wall in the soil on the excavated side. Profiles of pore water pressure versus depth from the FEM results are shown in Figure 6.16 and Figure 6.17. The FEM results match very well with the piezometer measurements (Figure 6.16). While the flow is vertically downward in the retained soil (Figure 6.16) and vertically upward in the soil below the excavation (Figure 6.17), the pore water pressures are reasonably close to hydrostatic conditions for practical purposes. The simplified assumption of hydrostatic conditions will slightly overestimate the active earth pressures loading the soil on the retained side and slightly underestimate the passive earth pressures supporting the wall on the excavated side.
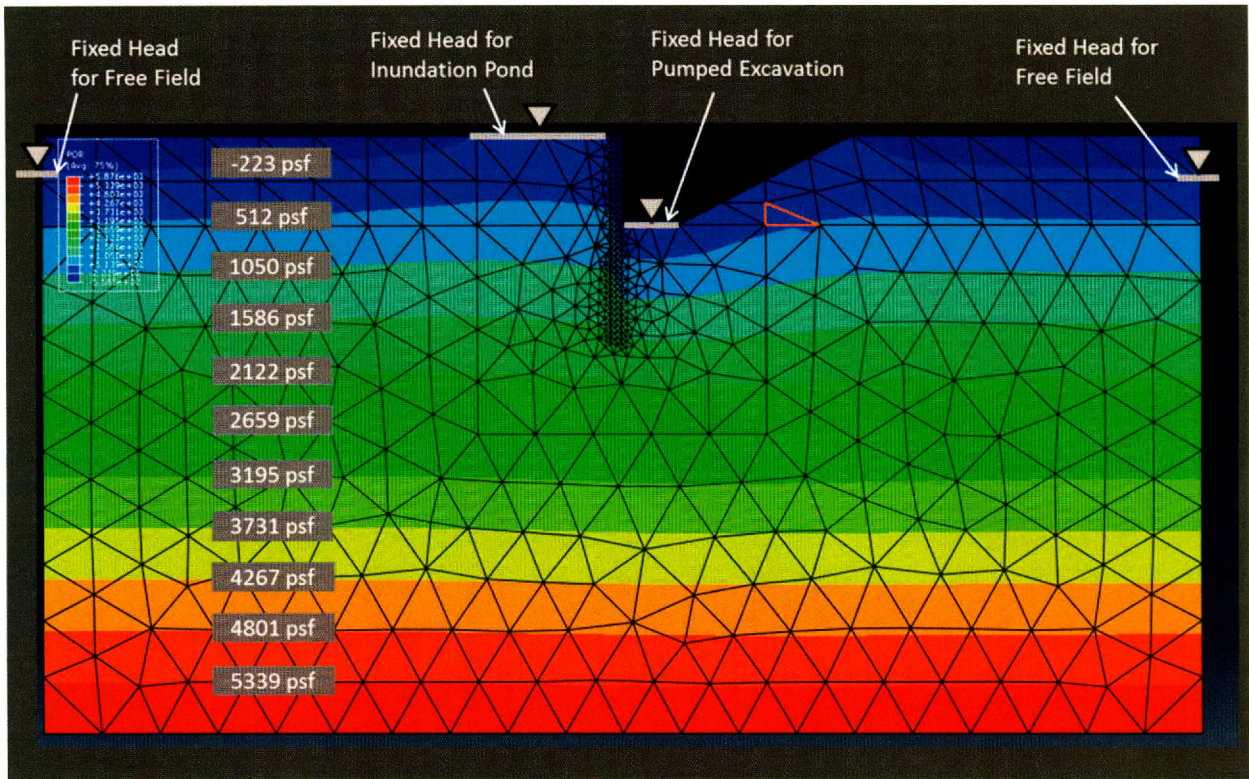
Figure 6.15: Pore-water pressure field for steady-state flow conditions under long-term inundation from FEM analysis.
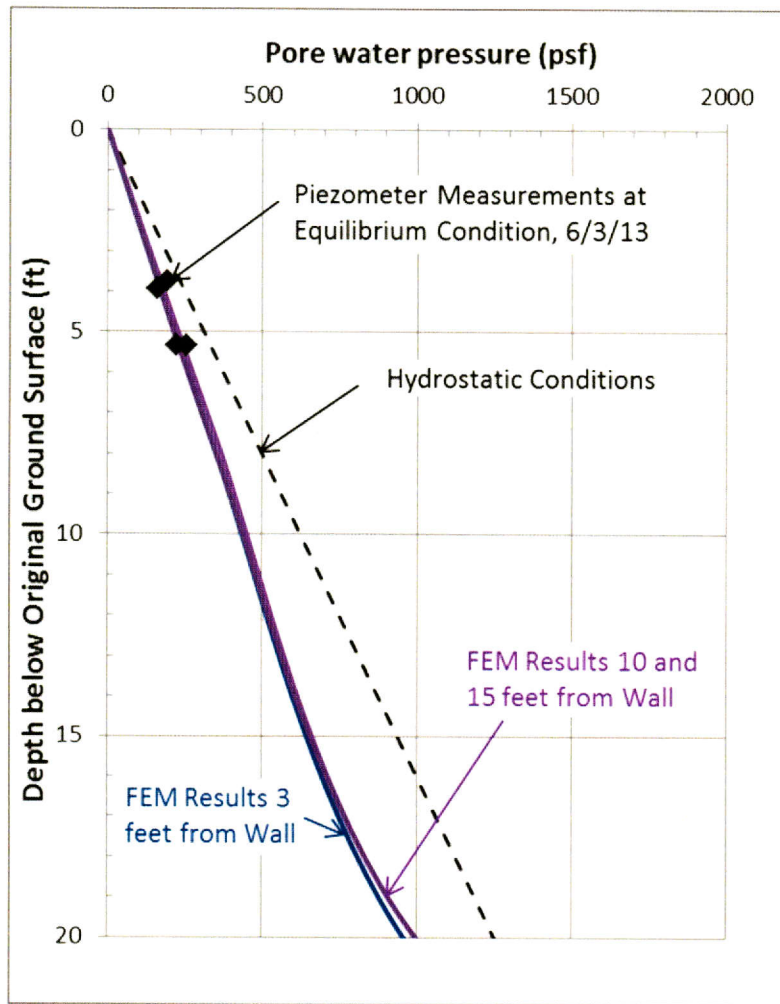
Figure 6.16: Profiles of pore water pressure versus depth in the retained soil behind the wall from FEM analysis compared with hydrostatic conditions and piezometer measurements.
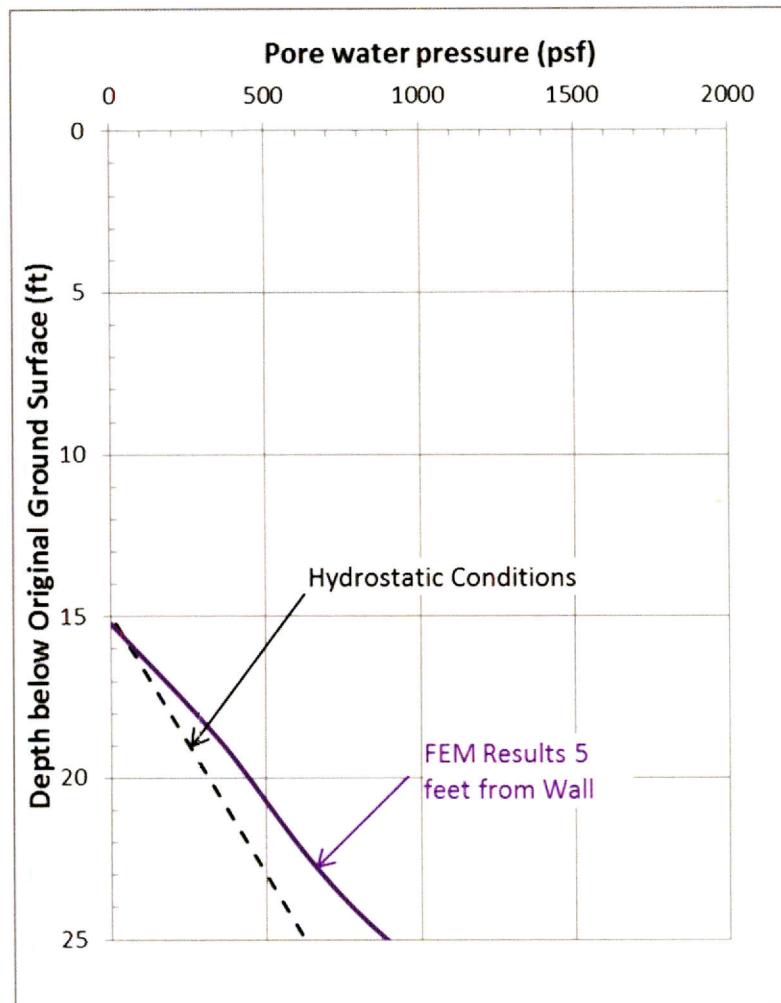
Figure 6.17: Profiles of pore water pressure versus depth in the excavated soil in front of the wall from FEM analysis compared with hydrostatic conditions.

6.2.3: ACTIVE EARTH PRESSURES

The active earth pressures applied to the wall by the retained soil were estimated for the long-term equilibrium assuming (1) hydrostatic conditions with the water table at the ground surface in the retained soil (Figure 6.16), (2) an interface friction angle between the wall and the retained soil equal to 2/3 the friction angle for the retained soil, and (3) a friction angle for the retained soil equal to the fully softened, drained shear strength (Figure 4.7). The fully softened, drained shear strength is recommended for the design of slopes and retaining walls in highly plastic clays under long-term conditions by many practitioners (e.g., Skempton 1970; Stark and Eid 1997; Duncan et al. 2011 and Gregory and Bumpas 2013), including several TxDOT research reports (Wright 2005 and Wright et al. 2007).

A comparison of calculated and measured earth pressures is shown in Figure 6.18. The assumption of a fully softened, drained shear strength and hydrostatic conditions matches the measurements reasonably well. The measured soil reactions based on the inclinometer and strain gauge measurements in the upper 6 feet are suspect because there is little bending in the shaft here and its curvature is lessened further by thermal effects. The calculated earth pressures in this

155

case are not very sensitive to the friction angle of the retained soil due to the high water table in the retained soil when it reached long-term equilibrium with the inundation pond.

For reference, a hypothesized envelope of earth pressures based on swell pressures is also shown in Figure 6.18. There is no evidence with this wall that the earth pressures in the retained soil ever exceeded the active earth pressures for a fully drained condition.
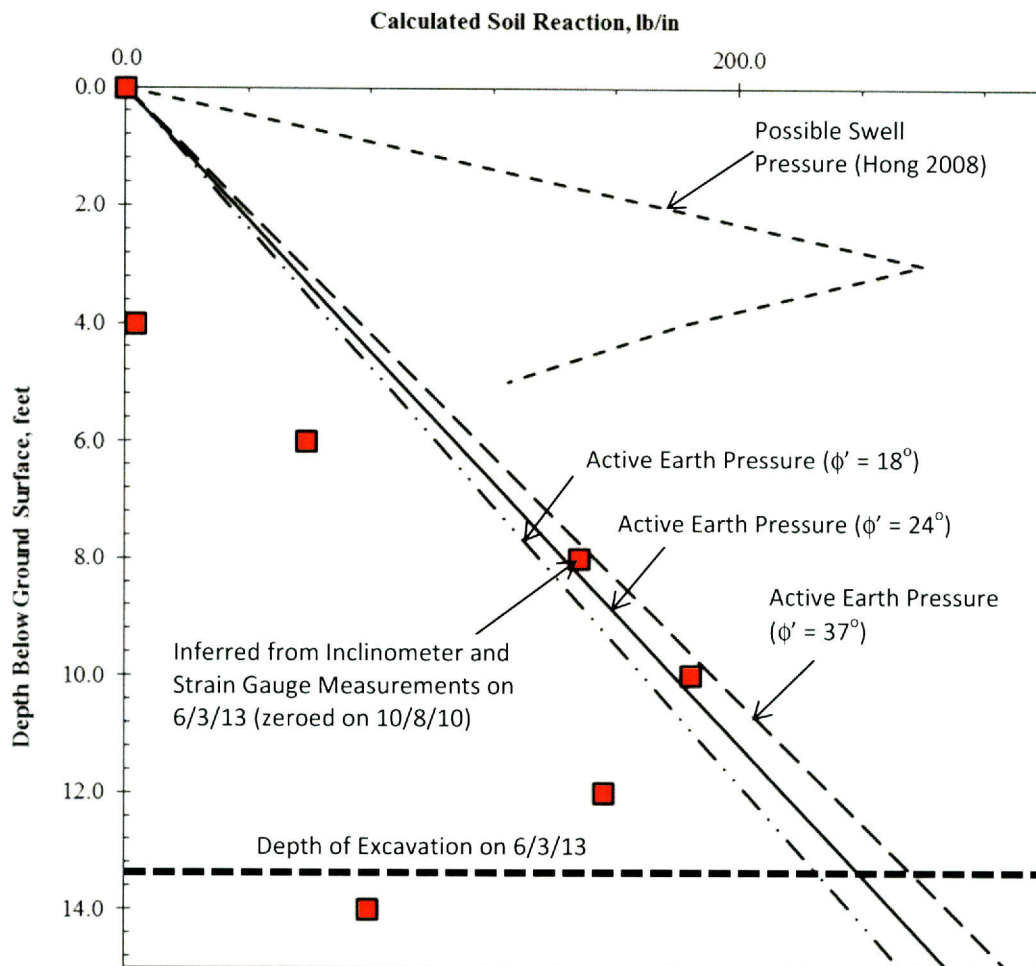
Figure 6.18: Comparison of calculated and measured active earth pressures on wall in retained soil.

6.2.4: PASSIVE EARTH PRESSURES (P-Y CURVES)

The passive soil resistance against the shafts was estimated for long-term loading conditions assuming drained conditions in the clay. Lateral soil springs were modeled using "sand" or "cohesionless" p-y curves with an initial stiffness, kpy, determined by the undrained stiffness and a group reduction factor of 0.62 to account for the close shaft spacing, as described in Section 2.6.3.

One approach to account for a group reduction is to use a p-y multiplier in LPILE, which reduces every p-value along each p-y curve. A second approach to account for the group reduction is to establish an equivalent drained friction angle that produces p-y curves similar to what would be obtained if the group reduction factor were applied directly. This approach is

156

similar to the practice of accounting for group effects for short-term loading by adjusting the undrained shear strength. A practical way to implement this approach is to determine an equivalent friction angle that gives the same ultimate p value, p_{ult}, as the actual friction angle with the group reduction factor. This approach is illustrated in Figure 6.19. For a drained friction angle of 30°, an equivalent friction angle of 24° produces a p_{ult} versus depth that is close to the desired profile (Figure 6.19). The resulting p-y curves are compared in Figure 6.20, showing that this approach produces p-y curves that are close to appropriate curves for the close shaft spacing.
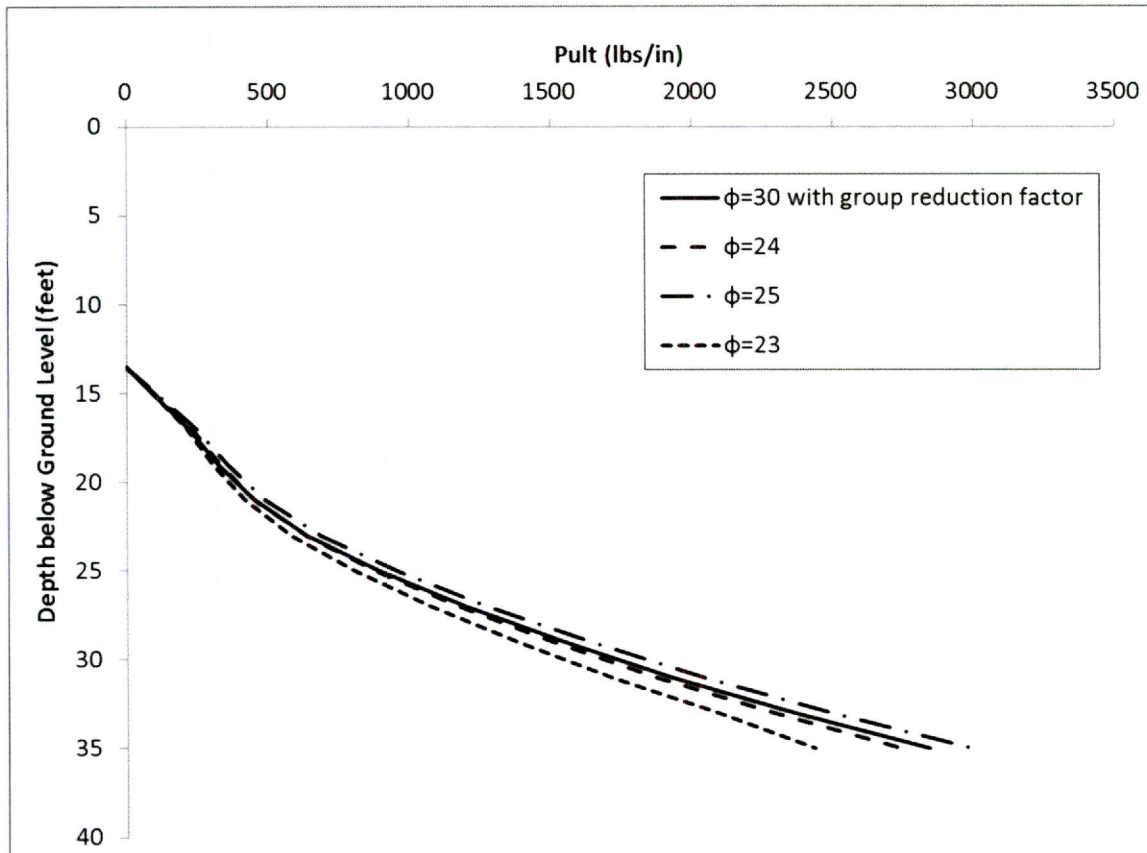
Figure 6.19: Comparison of the ultimate p for p-y curves with $\varphi=30^0$ with a group reduction factor to the ultimate p for $\varphi=24^0$, 25^0, and 23^0 without a group reduction factor.

157
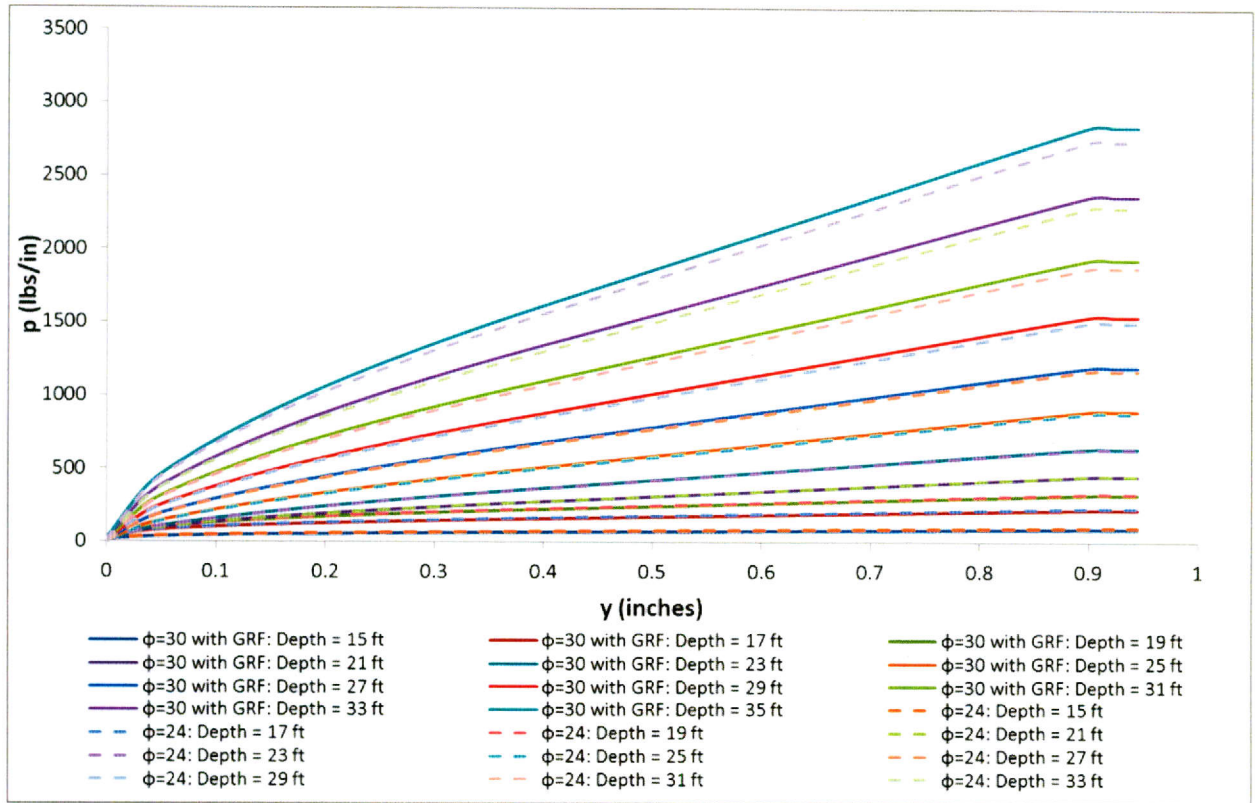
Figure 6.20: Comparison of the p-y curves with φ=30⁰ with a group reduction factor (GRF) to the p-y curves for φ=24⁰ without a group reduction factor.

Trial and error was used to find a drained soil strength that gives p-y curves similar to the measured lateral response of the wall. The result of this analysis is shown in Figure 6.21. A drained friction angle of 30° produces a reasonable match to the measured relationships between lateral soil pressure and lateral displacement at different depths, particularly at the shallowest depths that are the most important for the behavior of the wall (Figure 6.21). A drained friction angle of 30° is between the peak, drained friction angle of 37° and the fully softened, drained friction angle of 24° for this soil (Figure 4.7).
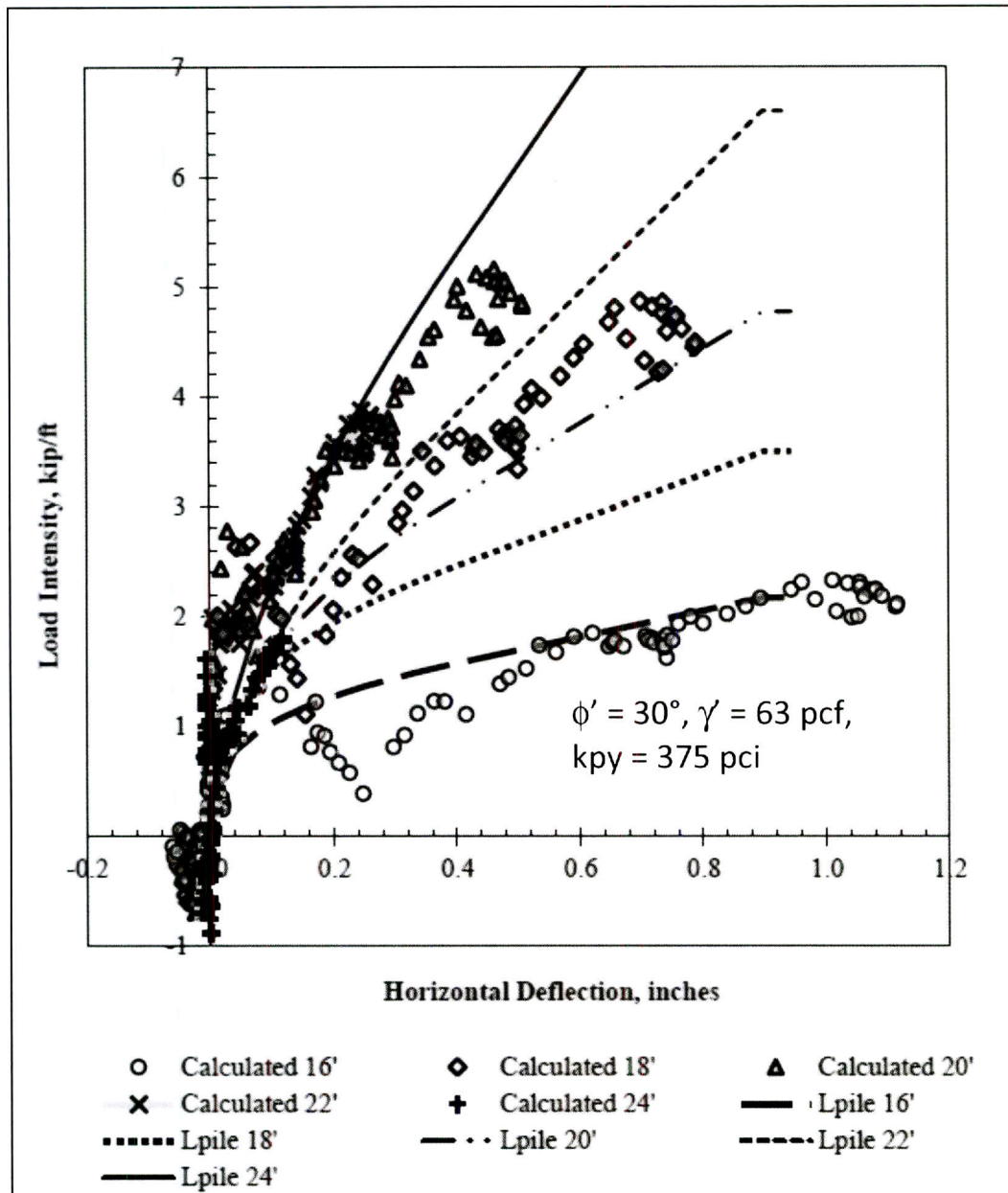
Figure 6.21: Comparison of long-term p-y curves predicted by modified LPILE analysis with p-y curves estimated from field data (reference survey is after installation of shotcrete facing on October 8, 2010).

6.2.5: LPILE ANALYSES

LPILE analyses were performed to calculate the predicted wall response in the long-term loading condition. Input parameters for these analyses are summarized in Table 6.1, and the results are shown in Figure 6.22. The deflected shape below the excavation (13.5 feet below the original ground surface) is fit best using a drained friction angle of 30° for the foundation soil (Figure 6.23). For comparison purposes, Figure 6.3 presents the results from an LPILE analysis with the conventional p-y curves used in TxDOT design practice, which are based on the profile of undrained shear strength versus depth (Figure 4.5) reduced by 50 percent in the upper 10 feet

159

to account for stress relief from the excavation; the measured response is softer than these undrained p-y curves predict.

The measured displacement profile above the excavation is reduced by the thermal effects causing a reduced curvature (the apparent negative bending moments in Figure 6.22). In order to represent these thermal effects in the analysis, a negative bending moment of 300 in-kips was imposed at the top of the wall (see Brown 2013 in Appendix K for a detailed analysis of these thermal effects). The calculated response of the wall using a drained friction angle of 30° for the foundation soil now matches the measured behavior well both above and below the excavation (Figure 6.24). Note that the friction between the wall and the soil also applies a small negative moment to the shafts above the excavation line; however, this moment is orders of magnitude smaller than the apparent negative moment due to thermal effects.

Table 6.1: Baseline assumptions and design parameters for LPILE analysis

Parameter	Value
Effective Unit Weight of Soil, γ.	62.6 pcf
Earth Pressure Loading Above Excavation	Fully Softened (ϕ = 24) + Hydrostatic
Friction Angle of Foundation Soil	24, 30, and 37°
Foundation Soil p-y Curves	Sand (Reese)
Non-Default Initial Stiffness, k_{py}	375 lb/in^3
Cracking Moment, M_{Cr}	680 k-in.
Yielding Moment, M_y	3,200 k-in.
Uncracked Bending Stiffness, EI_{uc}	67 x 10^6 k-in^2
Cracked Bending Stiffness, EI_{cr}	18 x 10^6 k-in^2
Shaft Diameter	24 in.
Height of Retained Soil, H	162 in.
Reinforcement	12 #7 bars (1.6% of gross area)
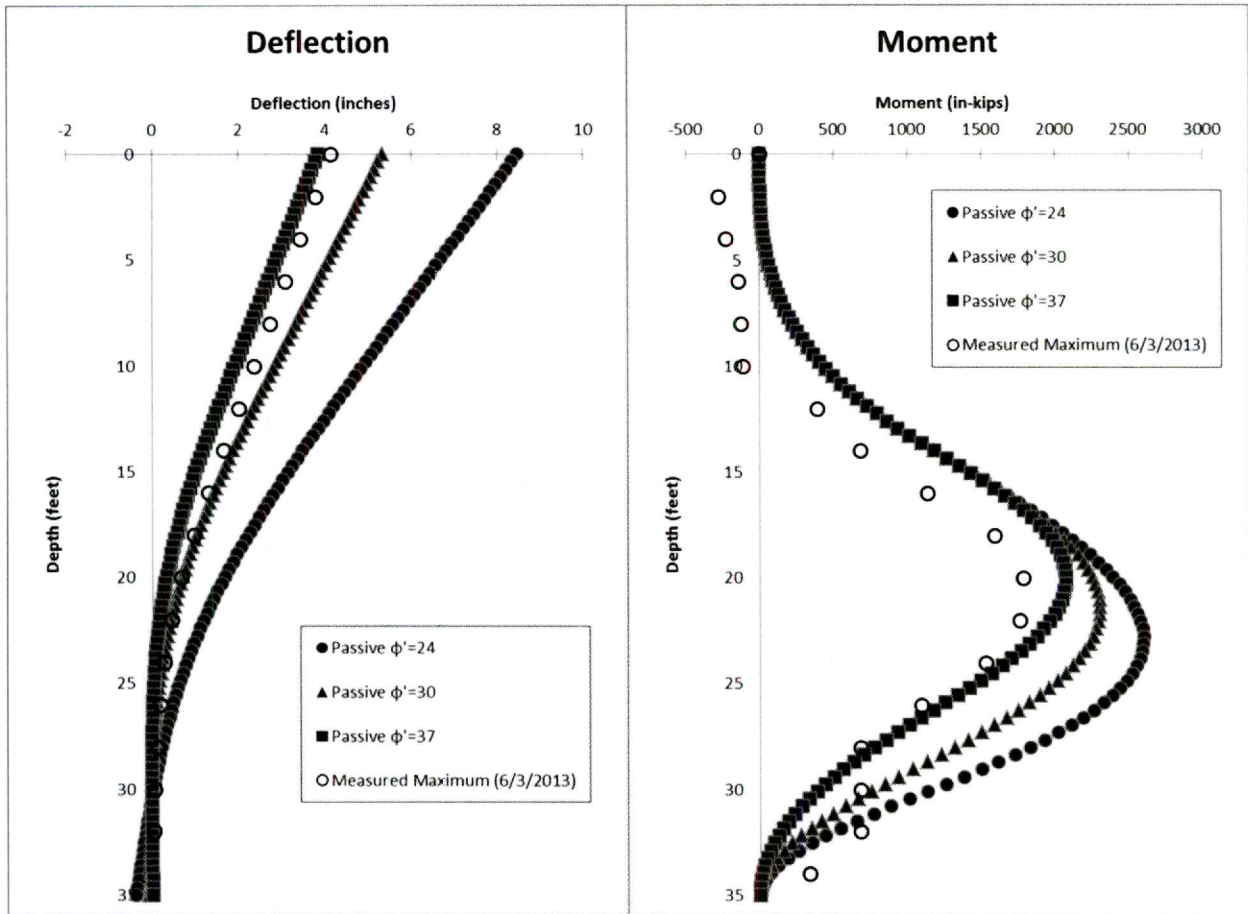
Figure 6.22: Calculated wall response from LPILE with different drained shear strengths for the foundation soil compared with measurements for long-term loading condition.
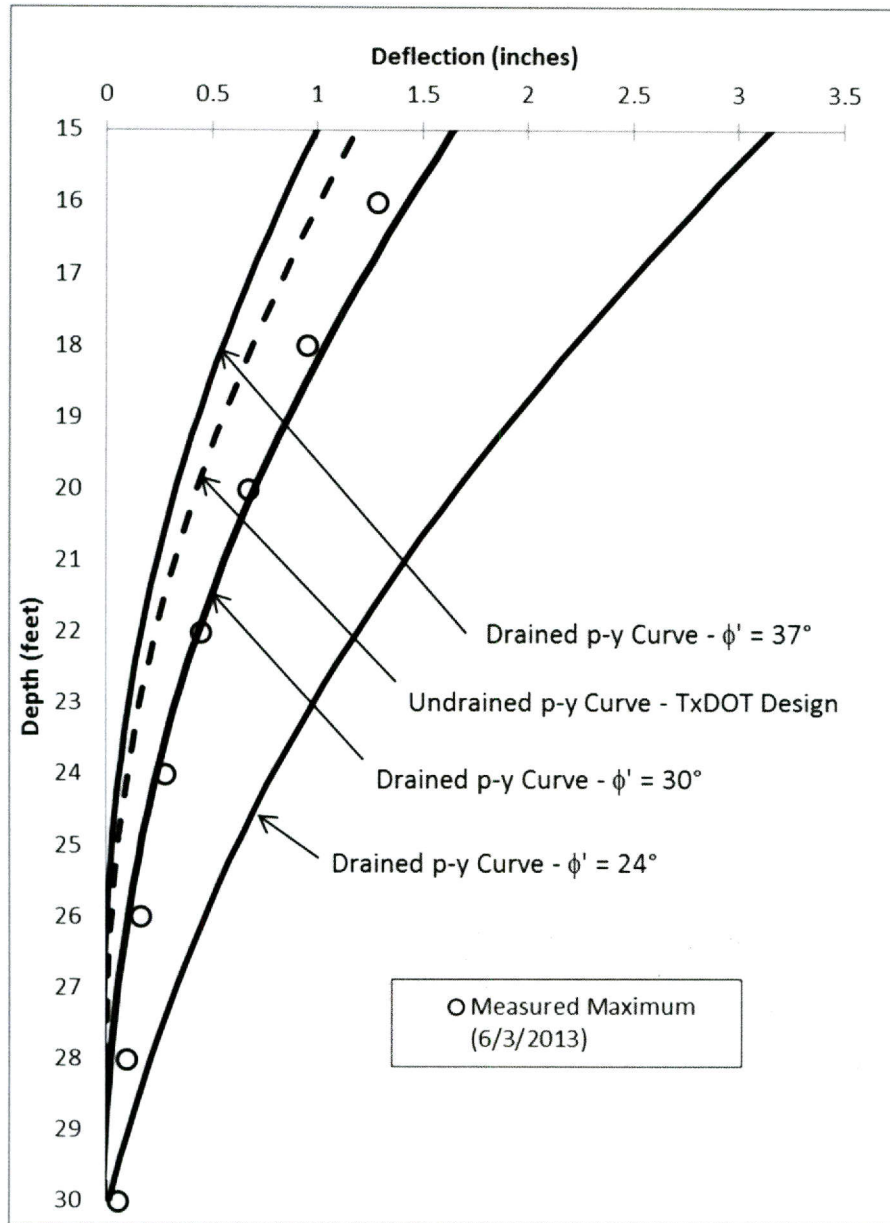
Figure 6.23: Calculated deflected shape from LPILE with different p-y curves for the foundation soil compared with measurements for long-term loading condition.
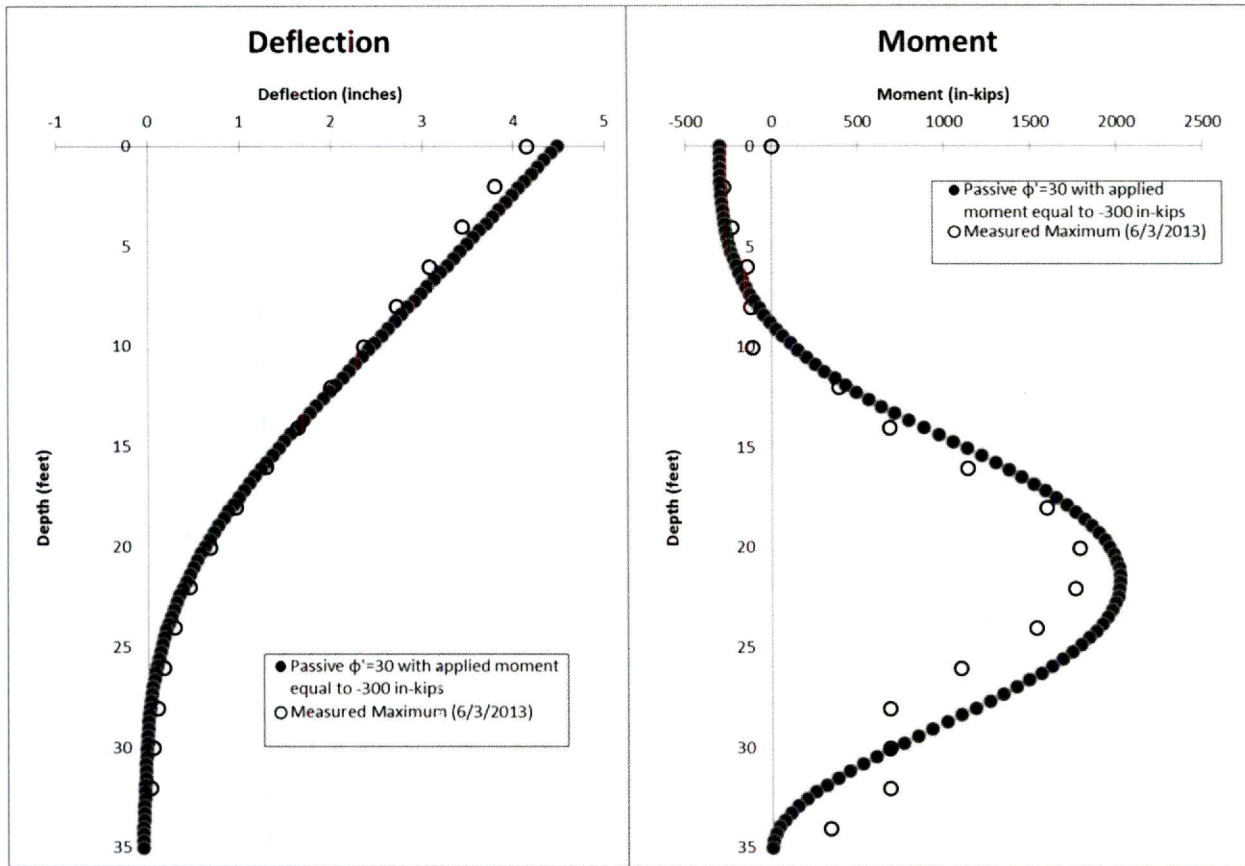
Figure 6.24: Calculated wall response from LPILE with apparent moment applied to account for thermal effects for long-term loading condition.

An analysis was performed to compare the results from PYWALL and LPILE (Figure 6.25) to explore whether the differences in these two methods (see Section 2.4) affect the calculation results. The two primary differences are that PYWALL implicitly accounts for the group reduction factor due to the close shaft spacing and accounts for the difference in overburden pressure between the back (retained) side and the front (foundation) side of the shafts. Two secondary differences are that the earth pressures in PYWALL on the active are slightly greater because it does not account for friction between the retained soil and wall and PYWALL assumes a constant bending stiffness for the shafts rather than satisfying the bending moment versus bending curvature relationship. Due to the significant bending associated with the long-term loading conditions with the water table up at the surface of the retained soil, a cracked bending stiffness was assumed in the PYWALL calculations. The LPILE and PYWALL results are very similar, with a slightly larger deflection predicted by PYWALL due to the slightly larger active earth pressures (Figure 6.25).
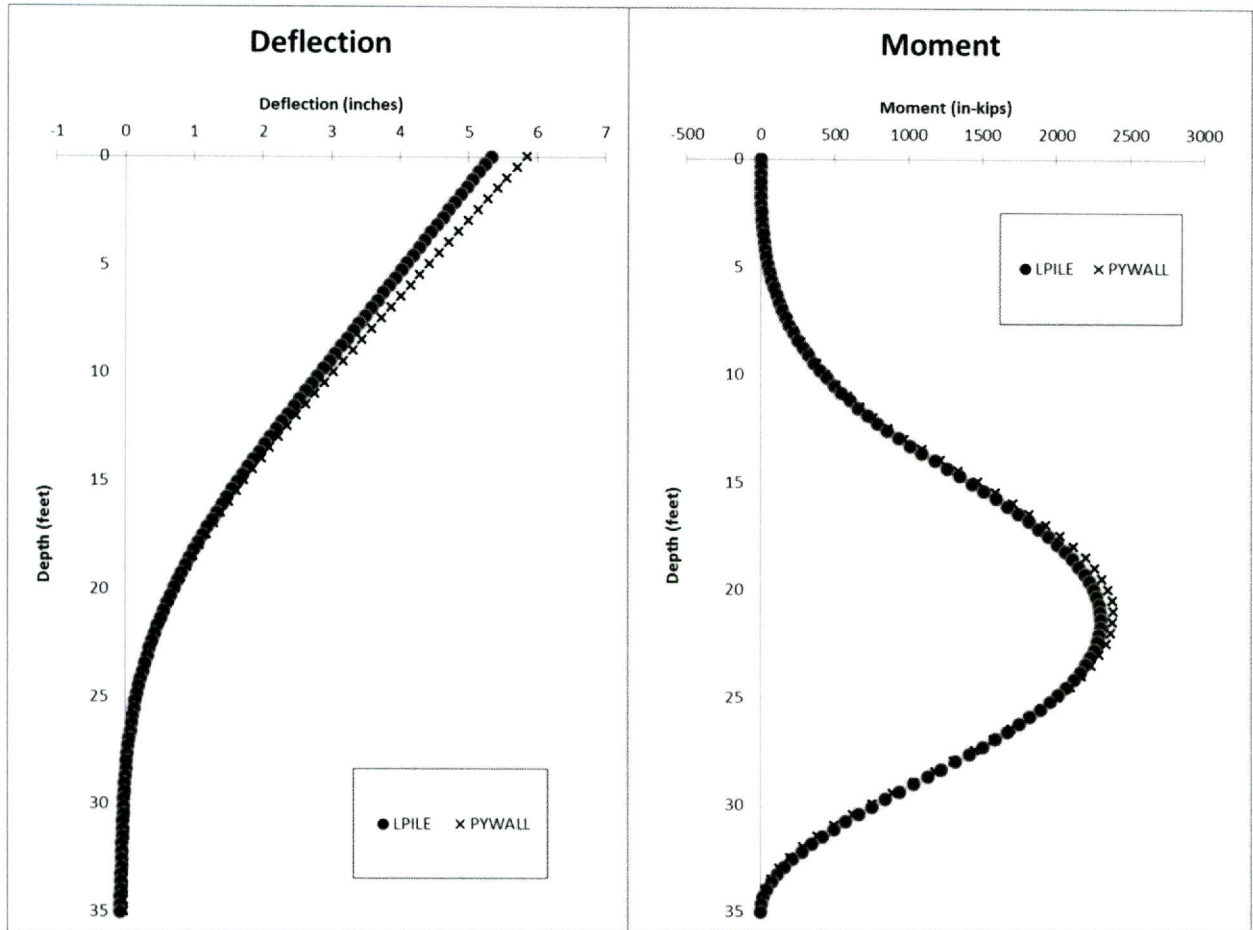
Figure 6.25: Comparison of LPILE and PYWALL for an active loading of hydrostatic conditions with a drained strength equal to 24° and passive strengths from a drained friction angle of 30°.

6.3: Summary and Conclusions

Detailed numerical analyses have been conducted for two conditions the wall experienced: the immediate response of the wall due to the excavation and the long-term response of the wall when it reached equilibrium under full inundation.

A simplified finite element method (FEM) analysis was conducted to better understand the response of the wall in the short-term. The global displacements of the soil and the shear strains in the soil show how the soil is essentially carrying the wall with it in response to the stress relief from the excavation. In order to get a more realistic representation of the soil conditions on site, the anisotropy of the soil from the large in situ lateral stresses caused by overconsolidation was considered in the analyses. Also, the stiffness estimated from small-scale and large-scale but small strain measurements was reduced based on trial and error until the calculated deflection matched the measured one.

For the long-term loading condition, the measured response of the wall was reproduced using LPILE with active earth pressures estimated from the fully softened, drained shear strength of the retained soil and passive earth pressure p-y curves estimated from a drained shear strength for the foundation soil between the peak and fully softened strengths. In addition, a numerical analysis of steady-state flow conditions shows that near hydrostatic conditions existed in the retained soil and the foundation soil under long-term loading.

CHAPTER 7: PRELIMINARY DESIGN GUIDANCE

7.1: Long-Term Design

A summary of the preliminary long-term design guidance is provided in Figure 7.1.
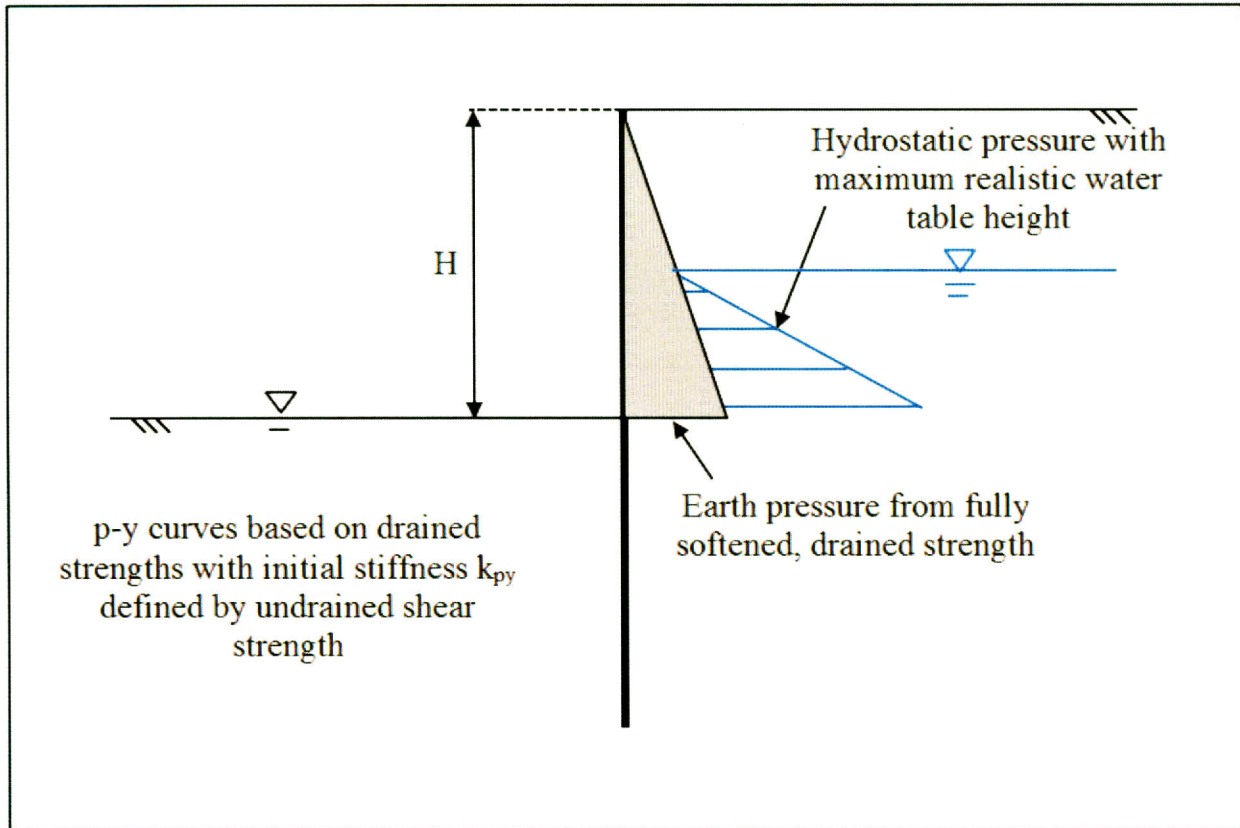
Figure 7.1: Summary of long-term design guidance

7.1.1: ACTIVE EARTH PRESSURES

An active earth pressure envelope based on the fully softened, drained shear strength of the retained soil (e.g., Wright 2005, Stark et al. 2005, Wright et al. 2007) with hydrostatic pore water pressures provides a reasonably conservative estimate of the maximum earth pressures over the long term in typical cases. A residual, drained strength may be warranted in cases where a historical slope failure is being retained. Smaller pore water pressures may be warranted if a horizontal drain system is installed into the retained soil along the potential slip surface.

7.1.2: PASSIVE EARTH PRESSURES

To model the behavior of the foundation soil, drained p-y curves based on a friction angle between the peak and fully softened drained shear strength of the soil are recommended. These curves can be obtained using the Reese et al. (1974) p-y curves developed for drained conditions (Section 2.6.3) with non-default initial stiffness values (k_{py}) defined by the undrained shear strength of the clay (Figure 7.2).

165
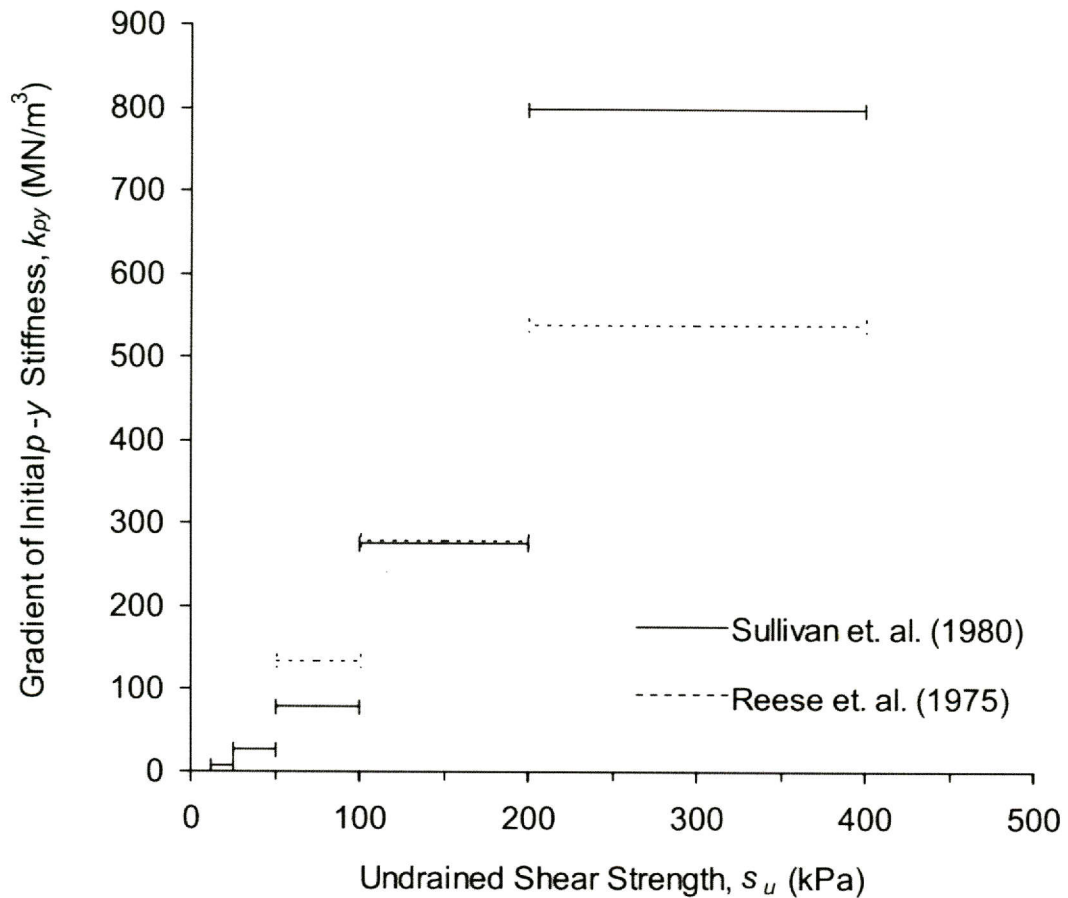
Figure 7.2: Typical k_{py} values for clays (after Dodds and Martin 2007).

7.1.3: ILLUSTRATIVE DESIGN EXAMPLES

To illustrate the preliminary design guidance for long-term conditions, the test wall and the existing wall at US59 and Hazard Street, discussed in Chapter 3, are redesigned using appropriate site properties. The purpose of these analyses is to show the changes in design that would be needed to meet TxDOT requirements.

7.1.3.1: Test Wall Redesign

To illustrate the preliminary design guidance for long-term conditions, the test wall was re-designed using a maximum water table at the ground surface to model the conditions the test wall observed. Input parameters for this analysis are summarized in Table 7.1, and the results are shown in Figure 7.3. In order to reach fixity and keep the top-of-wall deflection to 1 percent of the wall height, the diameter of the shafts was increased to 36 inches with 12 #9 reinforcement bars and the length of the shafts were increased to 50 feet (36.5 foot embedment depth below the excavation).

166

Table 7.1: Comparison of the baseline assumptions and design parameters for LPILE analysis between the as-built wall and the redesigned test wall.

Parameter	Redesign
Effective Unit Weight of Soil, γ'	62.6 pcf
Earth Pressure Loading Above Excavation	Fully Softened ($\phi = 24$) + Hydrostatic Conditions with Water Table at Ground Surface
Friction Angle of Foundation Soil	30°
Foundation Soil p-y Curves	Sand (Reese)
Non-Default Initial Stiffness, k_{py}	375 lb/in^3
Concrete Strength	4000 psi
Height of Retained Soil, H	13.5 feet
Shaft Diameter	36 in.
Shaft Clear Spacing	0 in
Reinforcement	12 #9 bars
Shaft Length	50 ft
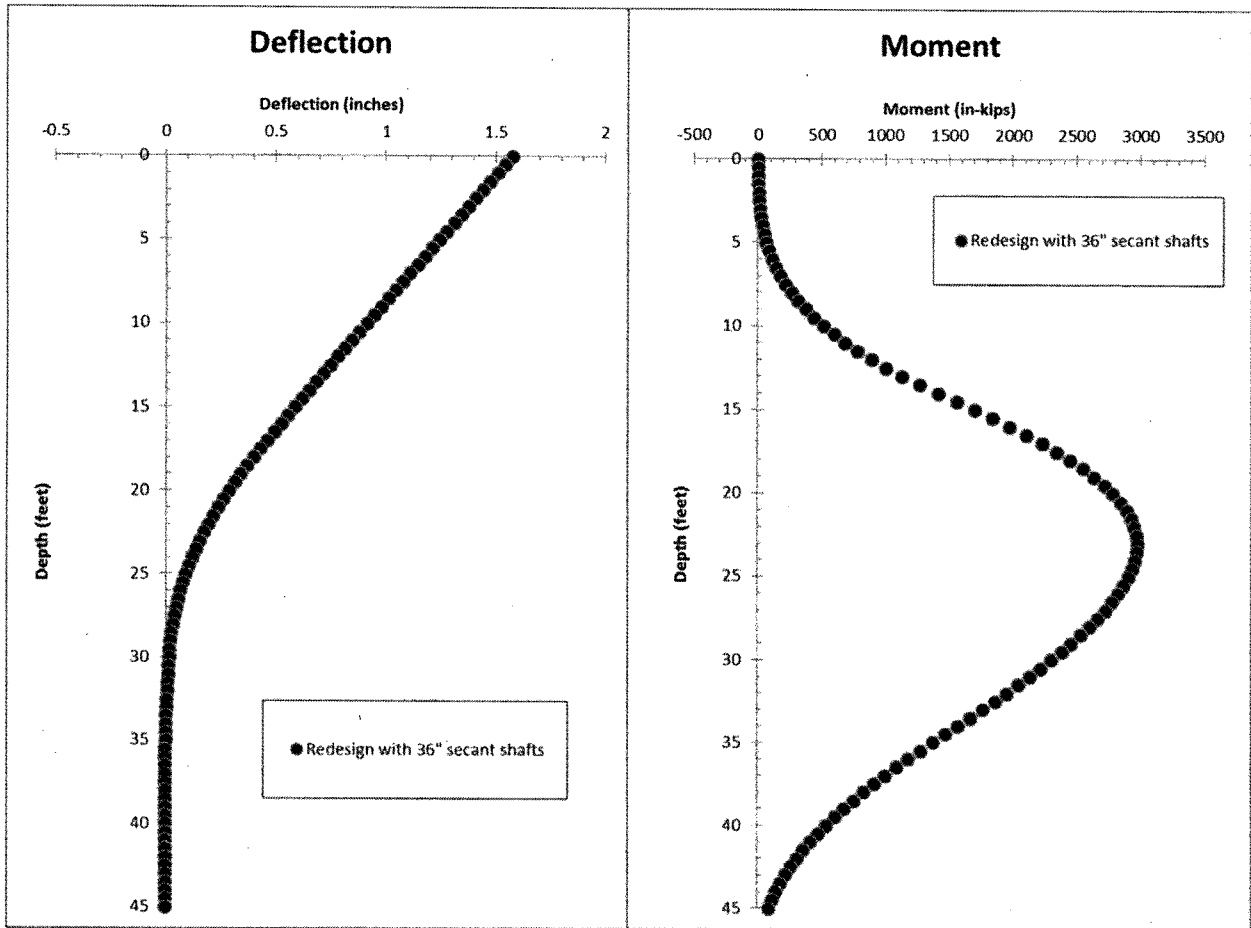
Figure 7.3: Calculated wall response from LPILE for the long-term loading condition of the redesigned wall.

7.1.3.1: US59 and Hazard Street Wall Redesign

To illustrate the preliminary design guidance for long-term conditions, the existing wall at US59 and Hazard Street was re-designed using a maximum water table at a depth of 8 feet below ground surface to model natural conditions. The design of the Hazard Street wall is described in more detail in Section 3.3.2. To simplify, the 12-inch diameter secant drilled shafts between the larger 48 inch diameter drilled shafts are neglected. The input parameters for this analysis are summarized in Table 7.2, and the results are shown in Figure 7.4. The new design still has 48-inch diameter shafts but is able to accommodate an increased clear spacing to 36 inches edge-to-edge. The shaft length is increased to 57.5 feet in order to maintain fixity.

Table 7.2: Comparison of the baseline assumptions and design parameters for LPILE analysis between the designed wall and the redesigned wall at Hazard Street.

Parameter	Redesign
Effective Unit Weight of Soil, γ	125 pcf above water table and 62.6 pcf below water table
Earth Pressure Loading Above Excavation	Fully Softened (ϕ' = 26°) + Hydrostatic Conditions with Water Table 8 ft below Ground Surface
Friction Angle of Foundation Soil	30°
Foundation Soil p-y Curves	Sand (Reese)
Non-Default Initial Stiffness, k_{py}	700 lb/in^3
Concrete Strength	4000 psi
Height of Retained Soil, H	15 feet
Shaft Diameter	48 in.
Shaft Clear Spacing	36 in
Reinforcement	12 #11 bars
Shaft Length	57.5 ft
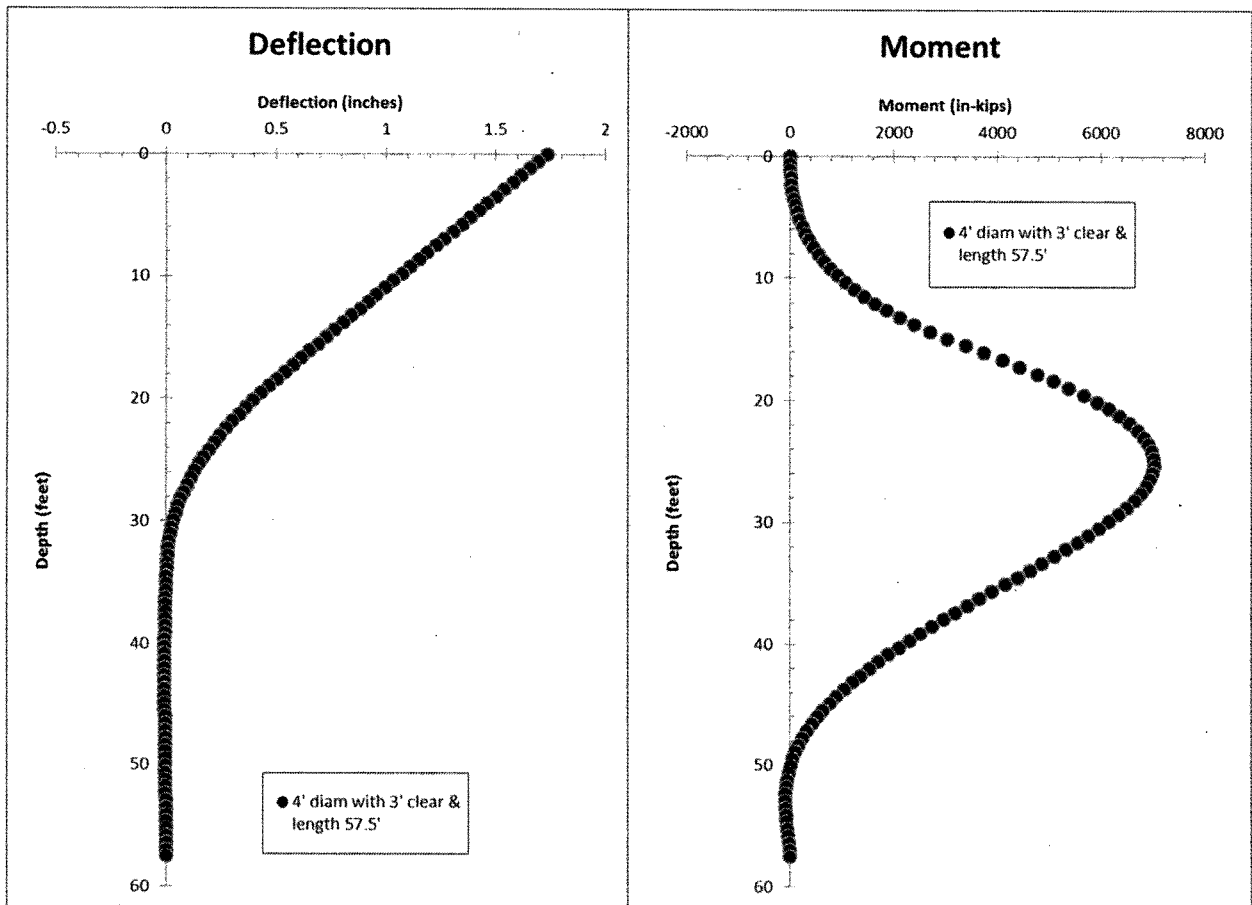
Figure 7.4: Calculated wall response from LPILE for the long-term loading condition of the redesigned wall at US59 and Hazard Street.

7.2: Short-Term Design Guidelines

The short-term behavior of the wall in response to excavation is dominated by global deformations of the soil-shaft system in response to stress relief. These global deformations cannot be easily represented with a p-y analysis. To check short-term response when the soil is excavated, the use of two-dimensional finite element modeling is recommended. At small strains, the use of simple linear elastic constitutive models is sufficient to gain an understanding of the nature of the expected global deformations.

The choice of finite element model parameters is highly dependent on local soil conditions and experience, but it is recommended that anisotropy due to high in-situ lateral stresses and stiffness reductions due to unloading be incorporated. In highly overconsolidated, stiff-fissured clays, values of K_o between 2 and 3 are commonly reported (e.g., Cripps and Taylor 1981, Smith et al. 2009). To account for the high ratio of horizontal to vertical stress, it is recommended that finite element models incorporate anisotropic conditions consistent with the expected field values of K_o. During excavation, stiffness reductions due to unloading may occur (e.g., Cripps and Taylor 1981). While in-situ values of Young's Modulus (E) are commonly estimated to be 1000 times the measured undrained shear strength, stiffness reductions of 60 to 90 percent, corresponding to E/S_u ratios of between 100 and 400, were required to approximate the behavior of the test wall.

170

7.3: Summary and Conclusions

The following preliminary design guidance for long-term conditions in drilled shaft retaining walls in high plasticity clays is developed based on the results of this research:

- Active earth pressures estimated from the fully softened, drained shear strength of the retained soil.

- Passive earth pressures represented by p-y curves based on the drained shear strength of the foundation soil.

With this preliminary design guidance, the predicted top-of-wall deflection and maximum bending moment are both slightly greater than what were measured in the test wall under the most extreme condition of full inundation. Because of the influence of pavement and drainage systems, this preliminary long-term design guidance represents a worst-case scenario that is unlikely to exist for an extended time in the field. The predicted top-of-wall deflections with this guidance are sensitive to small changes in unit weight, shear strength, pore water pressures, but the predicted maximum bending moments are not overly sensitive to these input parameters.

If immediate deflections in response to excavation during construction are a concern, then finite element method analyses that account for anisotropic in situ stresses for overconsolidated clays and stiffness reduction due to unloading are recommended.

CHAPTER 8: CONCLUSIONS AND RECOMMENDATIONS

8.1: Overview

This chapter presents brief summaries of the key findings from each chapter of this research study. The original objectives of the research study are revisited, along with summaries of the research findings for each item. Finally, brief recommendations for future research and similar projects are provided.

8.2: Conclusions

8.2.1: INSTRUMENTATION PROGRAM

8.2.1.1: Structural Performance of Drilled Shafts

In general, for monitoring the long-term effects of soil moisture on the test wall, inclinometer data was a more consistent indicator of wall behavior than strain gauge data. The direct use of strain gauge data for the determination of bending curvature generally requires more advanced data interpretation than simply taking the first derivative of rotation profiles measured from inclinometer data. Although the precision and resolution of strain gauges is vastly superior to that of an inclinometer, the strain gauges represent the behavior of individual, discrete locations in the shaft. While extrapolating the behavior of individual strain gauges to the entire pile is relatively simple for a short-term lateral load test, for long-term monitoring, inclinometer data provides a more consistent and reliable picture of what is going on in the shaft without the need for subjective data interpretation. After combining rotation profiles from the three instrumented shafts, piecewise polynomial differentiation was used with numerical smoothing methods to approximate p-y curves from inclinometer data at the test wall.

For future studies, or larger-scale studies involving several walls, inclinometer data provides a relatively inexpensive, effective, and robust method of performance monitoring. In the test wall, strain gauge data was affected by a number of factors beyond simple lateral loading of the structure, making data interpretation a complex and subjective task. While strain gauges are useful for short-term monitoring, they may not have the long-term stability and consistency of inclinometer data.

8.2.2: BEHAVIOR BEFORE EXCAVATION

Between shaft construction and excavation, a combination of concrete curing and expansive soil movement led to the development of residual stresses and strains, and evidence of tension cracks developed throughout the shafts. While no lateral loads were placed on the shafts prior to excavation, the residual stresses and strains developed during this time affected strain gauge data interpretation and the shafts' response to excavation.

8.2.3: BEHAVIOR DURING EXCAVATION

During excavation of the Lymon C. Reese research wall, the soil and wall responded immediately to the relief of stress, leading to wall deformations without the development of large earth pressures. This immediate response was a global movement of the soil-shaft system that extended beyond the shaft base. In the test wall, these global movements resulted in a top-of-wall

173

deflection of approximately 0.5 percent of the cantilever height. Because these movements represent large-scale strains in response to stress relief, they cannot be easily modeled with a traditional lateral earth pressure envelope. The use of more advanced prediction methods, such as finite element modeling, can provide estimates of the quality of these deformations.

8.2.4: BEHAVIOR DURING NATURAL MOISTURE CYCLES

8.2.4.1: Response to Moisture Fluctuations

Deformations and structural loads in the test wall were affected by moisture conditions on the project site. The test wall's deflection and structural loads were clearly affected by moisture conditions on the project site. During wetting, water infiltrated quickly through the clay fissures; as the retained soil and excavation base had access to moisture, top-of-wall deflections increased. Similarly, during prolonged periods of drying, top-of-wall deflections decreased. While this suggests volume change in expansive soil does play a part in wall deformations, no evidence of extremely high earth pressures or excessive structural loads on the shaft was observed. More importantly, access to moisture allowed negative pore pressures in the soil to dissipate, and volume change allowed the soil to approach a fully softened condition. At the conclusion of approximately 22 months of natural moisture cycles, total top-of-wall deflections since shaft construction had increased to approximately 0.09 percent of the wall height (approximately 0.04 percent since the installation of shotcrete facing in October 2010).

8.2.5: BEHAVIOR DURING CONTROLLED INUNDATION TESTING

During controlled inundation testing of the test wall, wall behavior was governed by the development of fully softened, drained conditions in both the retained soil and foundation soil. As inundation testing began, water infiltrated quickly into the soil fissures, first appearing in the excavation 30 minutes after the test began. As inundation testing continued over a period of approximately 14 months (6 months with water impounded, 8 months without), total top-of-wall deflections increased to a maximum of approximately 2.9 percent of the wall height. As wall deflections reached their maximum value, water levels in stand pipe piezometers throughout the inundation zone had stabilized near the ground surface. Moisture contents had increased by an average of 5 to 10 percentage points in the active zone above the groundwater table. Despite continued access to moisture, no evidence was observed of expansive soil damage or earth pressures greater than the envelope defined by the soil's fully softened strength with hydrostatic pressures.

The soil conditions at the conclusion of the inundation test can be approximated with a simple p-y analysis. The earth pressure envelope is defined using fully softened, drained strength parameters for the retained soil, and hydrostatic conditions with the water table at ground surface. For the foundation soil, p-y curves are defined using drained strength parameters, with initial stiffness defined by the original measured profile of undrained strength (this implicitly accounts for the transition from undrained to drained behavior with time and moisture cycles). The long-term behavior of the Manor test wall can be reasonably approximated in LPILE using these parameters with the final as-built dimensions of the wall and excavation. Predicted values of deflections, bending moments, and p-y curves are consistent with those measured in the field.

8.2.6: PRELIMINARY DESIGN GUIDANCE

The following preliminary design guidance for long-term conditions in drilled shaft retaining walls in high plasticity clays is developed based on the results of this research:

- Active earth pressures estimated from the fully softened, drained shear strength of the retained soil.

- Passive earth pressures represented by p-y curves based on the drained shear strength of the foundation soil.

If immediate deflections in response to excavation during construction are a concern, then finite element method analyses that account for anisotropic in situ stresses for overconsolidated clays and stiffness reduction due to unloading are recommended.

8.3: Recommendations for Future Work

The Lymon C. Reese research wall has provided insight into the behavior of a single drilled shaft retaining wall constructed through expansive clay. While some generalizations can be made, more thorough study of real-world walls is necessary to develop a complete understanding and framework for design. Inclinometer casings installed in future walls, with deflection profiles recorded at key dates or automated readings from an in-place unit, would provide an inexpensive and effective way to both verify the performance of existing walls and enhance the theoretical understanding of wall behavior. Additionally, a study of the behavior of a wall constructed during an extremely dry period would be of interest, to assess if initial soil moisture content at construction has any impact on wall behavior. To minimize the local effects of concrete heterogeneity and tension cracking, future instrumented walls using strain gauges could consider further isolating the gauges from direct contact with the concrete or using wall elements, like steel pipes, that respond linearly and elastically to bending.

Additional studies on the immediate response of cantilevered retaining walls in heavily overconsolidated clays and on the drained p-y curves for clays are needed.

References

Adil Haque, M. and Bryant, J. T. (2011). Failure of VERT Wall System: Forensic Evaluation and Lesson Learned. Geo-Frontiers 2011: Advances in Geotechnical Engineering , 3487–3496.

Brown, A. C., Ellis, T., Dellinger, G., El-Mohtar, C., Zornberg, J., & Gilbert, R. B. (2011). "Long-term monitoring of a drilled shaft retaining wall in expansive clay: Behavior before and during excavation." Geo-Frontiers 2011, ASCE.

Brown, A. C., Dellinger, G. F., & Gilbert, R. B. (2011). Long-Term Performance of Drilled Shaft Retaining Walls: Assessment of Existing Walls. Research Report FHWA/TX-11/0-6603-1. Center for Transportation Research. University of Texas at Austin.

Brown, Andrew. (2013). The Behavior of Drilled Shaft Retaining Walls in Expansive Clay Soils. Doctoral Dissertation, The University of Texas at Austin.

Cripps, J. C., and Taylor, R K. (1981). The Engineering Properties of Mudrocks. Quarterly Journal of Engineering Geology, Vol. 14, 325–346.

Dellinger, G. (2011). The Use of Time Domain Reflectometry Probes for Moisture Monitoring of a Drilled Shaft Retaining Wall in Expansive Clay. M.S. Thesis, The University of Texas at Austin.

Department of Army (1983). Technical Manual: Foundations in Expansive Soils.

Dodds, Andrew M. and Martin, Geoffrey R. (2007). Modeling Pile Behavior in Large Pile Groups under Lateral Loading. Technical Report MCEER-07-0004. Multidisciplinary Center for Earthquake Engineering Research.

Duncan, J. M., Brandon, T. L. and VandenBerge, D. (2011). "Report of the Workshop in Shear Strength for Stability of Slopes in Highly Plastic Clays." CGPR #67, Virginia Tech Center for Geotechnical Practice and Research.

Durham-Geo Enterprises, Inc. (2011). Digitilt Inclinometer Probe 50302599 Manual. Available www.slopeindicator.com/pdf/manuals/digitilt-probe.pdf.

Ellis, Trent. (2011). A Subsurface Investigation in Taylor Clay. Master's Thesis, The University of Texas at Austin.

Fellenius, Bengt H., Sung-Ryul Kim, Sung-Gyo Chung (2009). "Long-Term Monitoring of Strain in Instrumented Piles." Journal of Geotechnical and Geoenvironmental Engineering, Vol. 135, No. 11, November 2009, pp. 1583–1595.

Fuhr, Peter L., Dryver R. Huston, Timothy P. Ambrose, and Darrell M. Snyder. (1993). "Stress Monitoring of Concrete Using Embedded Optical Fiber Sensors." J. Struct. Engrg. 119, 2263.

Google Inc. (2011). Google Earth (Version 6.0.3.2197) [Software]. Available from http://www.google.com/earth/download/ge/agree.html.

Gregory, G. H. and Bumpas, K. K. (2013). "Post-Peak Fully-Softened Strength and Curved Strength Envelope in Shallow Slope Failure Analysis." Proceedings of ASCE GeoCongress 2013, San Diego, California. 255–268.

Hong, Gyeong Taek. (2008). Earth Pressures and Deformations in Civil Infrastructure in Expansive Soils. Ph.D. dissertation, Texas A&M University.

Isenhower, William M. and Wang, Shintower. (2013). "User's Manual for LPILE 2013" Ensoft, Inc.

Kim, Myung Hak and O'Neill, Michael W. (1998). "Side Shear Induced in Drilled Shaft by Suction Change." J. Geotech. and Geoenvir. Engrg. 124, 771.

Koutrouvelis, Iraklis. (2012). Earth Pressures Applied on Drilled Shaft Retaining Walls in Expansive Clay during Cycles of Moisture Fluctuation. Master's Thesis, The University of Texas at Austin.

Long, J. H. and Reese, L. C. (1983). An Investigation of the Behavior of Vertical Piles in Cohesive Soils Subjected to Repetitive lateral Loads. Geotechnical Engineering Report GR83-7. Geotechnical Engineering Center, the University of Texas at Austin.

Lytton, R. (2007, December 12). Design of Structures to Resist the Pressures and Movments of Expansive Soils. Texas A&M University.

Ozuna, K. "Assessment of Existing Drilled Shaft Walls for UT Study" Email to Andy Brown. August 10, 2011.

P. K. Ooi and Ramsey, T. L. (2003). "Curvature and Bending Moments from Inclinometer Data". International Journal of Geomechanics, ASCE.

Pufahl, D., Fredlund, D., and Rahardjo, H. (1983). Lateral earth pressures in expansive clay soils. Canadian Geotechnical Journal, 20, 228–241.

Puppala, A. J., Wejrungsikul, T., Willammee, R. S., Witherspoon, T. and Hoyos, L. (2011). Design of Inclined Loaded Drilled Shaft in High-Plasticity Clay Environment. Technical Report 0-6146-1. Department of Civing Engineering. University of Texas at Arlington.

Quantdec (2004). "Smoothing." Quantitative Decisions, Inc. Online resource, available from http://www.quantdec.com/Excel/smoothing.htm.

Reese, L. C., Cox, W. R., and Koop, F. D. (1974). Analysis of laterally loaded piles in sand. Sixth Annual Offshore Technology Conference, Paper No. 2080, OTC, Houston, Texas, 473–483.

Reese, L. C., Cox, W. R., and Koop, F. D. (1975). Field testing and analysis of laterally loaded piles in stiff clay. Seventh Annual Offshore Technology Conference, Paper No. 2312, OTC, Houston, Texas, 671–690.

Reese, L. C., Isenhower, W. M. & Wang, S.-T. (2006). Analysis and design of shallow and deep foundations. John Wiley & Sons, Inc.

Reese, L. C. & Van Impe, W. F. (2001). Single piles and pile groups under lateral loadings. A. A. Balkema, Rotterdam.

Reese, L. C., Wang, S.-T., Arrellaga, J.A., and Vasquez, L. (2013). "PYWALL—User's Manual" Ensoft, Inc.

Skempton, A. W. (1970). "First-Time Slides in Over-Consolidated Clays." *Géotechnique* 20, no. 3, 320–324.

Skempton, A. W. (1977). "Slope Stability of Cuttings in Brown London clay." Proceedings, Ninth International Conference on Soil Mechanics and Foundation Engineering, Tokyo, Vol. 3, pp. 261–270.

Smith, R. E., Smith, D. L., Griffin, J. A. (2009). Top-Down Construction of a Bridge in Clay Shale. American Society of Civil Engineers Conference Proceedings. 337, 76, 598–605.

Snethen, D. R., Townsend, F. C., Johnson, L. D., Patrick, D. M., Vedros, P. J. (1975). A Review of Engineering Experiences with Expansive Soils in Highway Subgrades. Soil Mechanics Division, Soils and Pavements Laboratory. U.S. Engineering Waterways Experiment Station.

Sullivan, W. R., Reese, L. C., and Fenske, C. W. (1980). "Unified Method for Analysis of Laterally Loaded Piles in Clay." Numerical Methods in Offshore Piling Conference, May 1979. Institution of Civil Engineers, London, 135–146.

Stark, T. D., Choi, H., and McCone, S. (2005). "Drained Shear Strength Parameters for Analysis of Landslides." Journal of Geotechnical and Geoenvironmental Engineering, ASCE, Vol. 131, No. 5, May, 2005, pp. 575–588.

Stark, T. D. and Eid, H. T. (1997). "Slope Stability Analyses in Stiff Fissured Clays." *Journal of Geotechnical and Geoenvironmental Engineering* 123, no. 4, 335–343.

Thomas, M. G., Puppala, A. J., Hoyos, L. R. (2009). Influence of Swell Pressure From Expansive Fill on Retaining Wall Stability. American Society of Civil Engineers Conference Proceedings. 337, 75, 590–597.

Tukey, J. W. (1977). Exploratory Data Analysis. Addison-Wesley, Reading, MA.

TxDOT (2009). Cantilver Drilled Shaft Wall Design.

TxDOT Geotechnical Manual. (2012). Texas Department of Transportation, Bridge Division, Austin, Texas.

Vipulanandan, C., Jospeh, D. (2011). Seasonal Moisture Fluctuation in the Active Zone in a Humid-Subtropical Climate. Geo-Frontiers 2011: Advances in Geotechnical Engineering, 2759–2767.

Wang, Shintower and Reese, Lymon C. (1986). Study of design method for vertical drilled shaft retaining walls. Research Report 415-2F. Center for Transportation Research, Bureau of Engineering Research. University of Texas at Austin.

Weather Underground (2013). http://www.wunderground.com/.

Welch, R. C., and Reese, L. C. (1972). Laterally loaded behavior of drilled shafts. Research Report 3-5-65-89. Center for Highway Research, University of Texas at Austin.

Wise, J. R. and Hudson, W. R.. (1971). An Examination of Expansive Clay Problems in Texas. Research Report 118-5. Center for Highway Research, University of Texas at Austin.

Wright, S. G.. (2005). "Evaluation of Soil Shear Strengths for Slope and Retaining Wall Stability Analyses with Emphasis on High Plasticity Clays." Project No. 5-1874-01. Center for Transportation Research, The University of Texas at Austin.

Wright, S. G., Zornberg, J. G., and Aguettant, J. E.. (2007). "The Fully Softened Shear Strength of High Plasticity Clays." Report No. FHWA/TX-07/0-5202-3. Center for Transportation Research, The University of Texas at Austin.

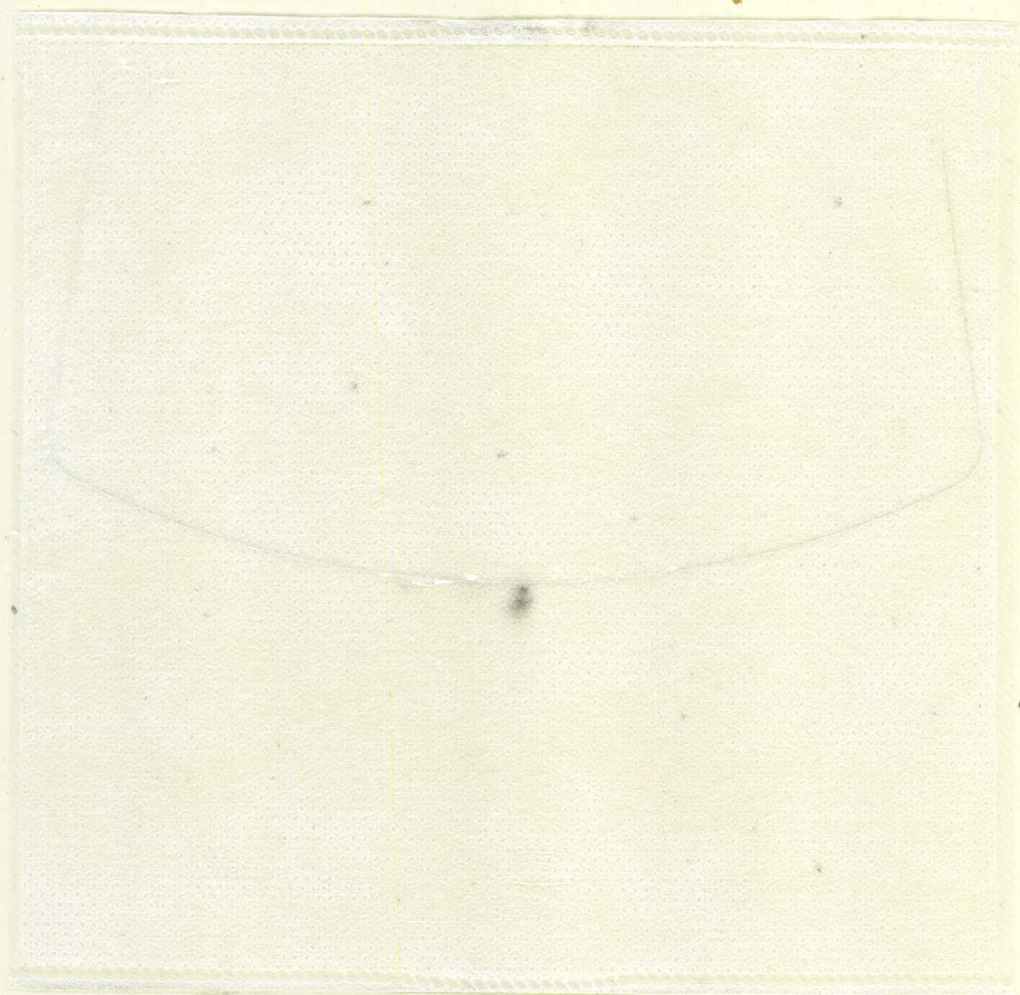CENTER FOR TRANSPORTATION RESEARCH

CTR

THE UNIVERSITY OF TEXAS AT AUSTIN
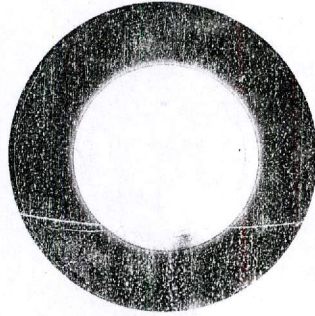
October 2013

The Long-Term Performance of a Drilled Shaft Retaining Wall in an Expansive Clay: APPENDICES

By: Robert Gilbert

0-6603-2